CSIC

UNIVERSIDAD DE SEVILLA

Función de los Antiportadores NHX1 y NHX2 de *Arabidopsis thaliana* en la Acumulación de Potasio en las Vacuolas Vegetales

Role of Ion Exchangers NHX1 and NHX2 in the Uptake of Potassium into the Cell Vacuoles of *Arabidopsis thaliana*

Memoria que presenta: **Zaida Andrés González**

para optar al título de Doctor en Bioquímica

I. INDEX

II. INTRODUCTION

I.1. Potassium

I.1. Potassium is an essential macronutrient for plants.

Potassium (K^+) is one of the most abundant inorganic cation in plant tissues, comprising up to 10% of their dry weight or concentrations of about 200 mM (Leigh and Wyn Jones, 1984; Epstein and Bloom, 2005). Potassium is concentrated in young developing tissues and reproductive organs, indicating the crucial functions of K^+ in cell metabolism, growth and stress adaptation (Amtmann et al., 2006; Römheld and Kirkby, 2010; White and Karley, 2010). Generally, these functions are classified into two groups: those that depend on stable concentrations of K^+ in specific tissues or intracellular compartments, and those that rely on K^+ movement between different compartments, cells and tissues (Amtmann et al., 2006). The former group of functions includes enzyme activation, stabilisation of protein synthesis, neutralisation of fixed negative charges and the regulation of pH homeostasis (Marschner, 1995; Amtmann et al., 2006; White and Karley, 2010). Potassium activates many enzymes including those involving energy metabolism, protein synthesis and solute transport (Leigh and Wyn Jones, 1984; Mengel et al., 2001; Amtmann et al., 2008; Römheld and Kirkby, 2010; White and Karley, 2010). To maintain the rate of K^+-dependent processes, K^+ concentrations are tightly regulated in metabolically active compartments, such as the cytosol, the nucleus, the stroma of chloroplasts and the matrix of mitochondria. These compartments contain about 100 to 150 mM of K^+ (Leigh and Wyn Jones, 1984; Walker et al., 1996). The second class of functions are linked to the high mobility of K^+ which is the driving force for osmotic changes that control, among other processes, the stomatal movements (Véry and Sentenac, 2003; Fan et al., 2004), the elongation of pollen tubes towards the fertile ovules (Mouline et al., 2002), seismonastic and circadian movements of leaves (Moran, 2007) and phloem transport (Hermans et al., 2006; Amtmann et al., 2008). Furthermore, K^+ fluxes create trans-membrane voltage gradients indipensable for supporting the transport of inorganic ions and metabolites

(e.g., sugars, amino acids and nitrate) both within and outside the cell (Marschner, 1995; Amtmann et al., 2006). The directed movement of K^+ into the vacuole is essencial for growth. The vacuole contains the major pool of K^+ in plant cells, which fulfils a biophysical function contributing to lower the sap osmotic potential to generate turgor and drive cell expansion (Leigh and Wyn Jones, 1984; Walker et al., 1996; Mengel et al., 2001). Rapid cell expansion relies on high mobility of the active osmoticum and, therefore, only a few other inorganic ions can replace K^+ in this role (e.g., Na^+) (Amtmann et al., 2006). Once cell expansion ceases the maintenance of turgor can be accomplished by less mobile osmotica, such as sugars, organic acids and compatible solutes, and K^+ ions can be partly removed from the vacuole (Leigh and Wyn Jones, 1984; Poffenroth et al., 1992; Marschner, 1995; Amtmann et al., 2006). Nevertheless, K^+ concentration in the vacuole does not decline to zero and is maintained at a limit concentration around 10-20 mM, even under K^+-starvation. This K^+ concentration is supposed to reflect equilibrium with the cytosol at a maximum trans-tonoplast voltage of about -40 to -60 mV (Leigh and Wyn Jones, 1984; Leigh, 2001). Greater concentrations of K^+ inside the vacuole could be achieved by nonelectrogenic K^+/H^+ antiporters (Walker et al., 1996).

I.1.2. The acquisition and cellular distribution of potassium.

Potassium acquisition from the soil solution takes place through root epidermal and cortical cells. Inside the root symplast K^+ can be stored in the vacuole, where it carries out osmotic functions, or transported to the aerial parts via the xylem. Potassium in the apoplast and xylem is taken up by shoot cells that also may provide stored K^+ for its redistribution via phloem. Cell membranes are not permeable to ions, water and other polar molecules, thus K^+ crosses different cells membranes through K^+-specific transport systems that regulate K^+ nutrition and functions (Aleman et al., 2011; Pardo and Rubio Muñoz, 2011).

I.1.2.1. Root K^+ acquisition in plants.

The uptake of K^+ by the roots exhibit a biphasic kinetics in response to increasing external K^+ concentrations with high- and low-affinity transport systems, operating at low (<1 mM) and high (>1 mM) rhizosphere K^+ concentrations (Epstein et al., 1963). These transport systems are not only different regarding the external K^+ concentration at which they operate but they catalyse the flux of K^+ across the plasma membrane using distinct mechanisms. High-affinity K^+ uptake is an active process mediated by H^+/K^+ symporters and involving a transmembrane H^+ gradient generated by a H^+-ATPase. By contrast, ion channels mediate low-affinity and passive K^+ uptake using the K^+ electrochemical potential gradient (Maathuis and Sanders, 1994; Britto and Kronzucker, 2008; Aleman et al., 2011).

The use of heterologous systems allowed to isolate two *Arabidopsis thaliana* cDNAs encoding the *Shaker*-like Inward-Rectifier K^+ Channels (KIRCs) AKT1 (Sentenac et al., 1992) and KAT1 (Anderson et al., 1992; Schachtman et al., 1992). The low-affinity K^+ uptake was attributed to AKT1, expressed mainly in root epidermal cells (Lagarde et al., 1996). Afterwards, the cDNA of *HvHAK1* from barley was isolated based on the homology between the *Escherichia coli* Kup K^+ transporters and the *Schwanniomyces occidentalis* high-affinity K^+ transporter SoHAK1 (Santa-María et al., 1997). HAK1-type transporters of the KT/HAK/KUP family are considered the major contributors to high-affinity K^+ uptake since they exhibit high affinity for K^+, low discrimination between K^+ and Rb^+, NH_4^+-inhibited K^+ uptake and induced expression in roots as a result of K^+ starvation, which is in agreement with the hallmarks of the high-affinity K^+ uptake observed in plant roots (Epstein et al., 1963; Glass and Dunlop, 1978; Rodríguez-Navarro and Rubio, 2006). In *Arabidopsis thaliana*, tomato and *Thellungiella halophila* root high-affinity K^+ transport is mediated by the orthologous protein HAK5 (Rodríguez-Navarro and Rubio, 2006). Even if their transport mechanism is not known in detail, HAK5 is likely to act as a H^+-K^+ symport as it was demonstrated for the *Neurospora crassa* protein NcHAK1 (Rodriguez-Navarro et al., 1986; Haro et al., 1999). On the other hand, members of the TRK-HKT family (e.g., TaHKT1) have also been associated to the high-affinity root K^+ transport (Schachtman and Schroeder, 1994). However, TaHKT1 mediates high-affinity Na^+-coupled K^+-uptake (Rubio et al., 1995) and, in most plants, HKT1-like proteins seem to be mainly related to the regulation of

Na$^+$ accumulation in roots and the recovery of Na$^+$ from the xylem (Uozumi et al., 2000; Sunarpi et al., 2005; Davenport et al., 2007; Haro et al., 2010; Aleman et al., 2011). In order to investigate the physiological relevance of the transporters HAK5 and AKT1, several works using reverse genetic have been carried out. AtHAK5 is required for K$^+$ uptake at external concentrations below 10 µM (Qi et al., 2008; Nieves-Cordones et al., 2010; Rubio et al., 2010b). Between 10 and 200 µM K$^+$, both systems contribute to K$^+$ uptake (Pyo et al., 2010; Rubio et al., 2010a). At external concentrations higher than 500 µM AKT1 is the major responsible for K$^+$ acquisition by the roots (Rubio et al., 2010a). The existence of other unidentified systems has been postulated since above an external K$^+$ concentration of 10 mM the double mutant *athak5 athkt1* did not show phenotype deficiencies compared to the wild type (Rubio et al., 2010a; Pardo and Rubio Muñoz, 2011). Candidate systems to mediate the K$^+$ transport over 10 mM of external K$^+$ are members of the cyclic nucleotide gated channels family (CNGCs) (Gobert et al., 2006; Kaplan et al., 2007), of the cation proton exchanger family (CHX) (Zhao et al., 2008) and of the glutamate receptor-like channel family (GLR) (Dietrich et al., 2010; White and Karley, 2010; Aleman et al., 2011; Pardo and Rubio Muñoz, 2011).

I.1.2.2. Potassium redistribution within the plant.

Subsequently to the uptake of K$^+$ by root epidermal and cortical cells, K$^+$ is delivered into the xylem. Up to 90% of K$^+$ entering the xylem is loaded through a symplastic route, with K$^+$ crossing different root cell layers through plasmodesmata until it reaches the stellar parenchyma cells (White and Karley, 2010). The member of the Outward-Rectifying K$^+$ Channels family (KORCs) SKOR is thought to mediate the efflux of K$^+$ from the root pericycle and stelar parechyma to the xylem, favoured by a symplast/xylem boundary voltage of around -80 mV (Gaymard et al., 1998; De Boer and Volkov, 2003; Johansson et al., 2006). The xylem K$^+$ concentration can vary from 2 to 25 mM, since several factors determine the net loading into the xylem. The presence of other ions (e.g., Na$^+$ or Ca^{2+}) in the soil solution drops down K$^+$ uptake and xylem K$^+$ concentration. Phosphate-starved plants present less K$^+$ in the xylem sap. The xylem K$^+$ concentration is also affected by the transpiration and diurnal cycles. Hence,

under drought stress, when the stomata are close and the transpirational water flux is reduced, the K$^+$ fluxes to the shoot diminish (Gaymard et al., 1998; De Boer and Volkov, 2003; White and Karley, 2010).

Potassium from mature leaves is redistributed to developing tissues via the phloem, where K$^+$ can reach concentrations of about 10 to 150 mM (White and Karley, 2010). The weakly inward-rectifying channel AKT2/3, which is expressed in phloem cells (Deeken et al., 2000), facilitates K$^+$ loading into the phloem stream (Deeken et al., 2002; Hafke et al., 2007). Aproximately 90% of the K$^+$ delivered to the shoot via the xylem is transported back to the root via the phloem (Peuke et al., 2002; White and Karley, 2010) and most of it is released again to the xylem, acting again as an osmotic driving force for xylem transport.

The fast K$^+$ recirculation within the plant via phloem participates in many physiologically processes involved in keeping a balanced distribution of nutrients and optimal photosynthate partitioning. It maintains the cation-anion inbalance within the plant, most importantly acting as the main counter anion of nitrate in the xylem sap along the repeated xylem-phloem-xylem K$^+$ circulatory cycles. Potassium flux is also essential for the loading of sugars, organic acids and amino acids into the phloem. Translocation is also important for the redistribution of K$^+$ from senescing to developing tissues, and for maintaining high K$^+$/Na$^+$ ratios in sensitive meristematic tissues (White and Karley, 2010). Recently, it has been shown that posttranslational modifications of the AKT2 channel switches on a "potassium battery" which efficiently assists the plasma membrane H$^+$-ATPase in energising the transmembrane phloem (re)loading processes. AKT2 loss-of-function mutant plants are defective in reloading assimilates leaking away from the sieve tube into the main phloem stream (Deeken et al., 2002; Gajdanowicz et al., 2011; Sandmann et al., 2011). It is also thought that phloem K$^+$ concentrations and its flux from the shoot to the root could function as a putative feedback signal for plant K$^+$ status modulating K$^+$ uptake upon plant growth demands (Amtmann et al., 2006; White and Karley, 2010).

I.1.2.3. K$^+$ transport within the vacuole.

The changes in tissue K$^+$ concentration are mostly a reflection of the dynamics of the vacuolar pool as the central vacuole of mature cells may occupy over the 80% of the intracellular volume and it is the main cellular reservoir for K$^+$. (Leigh, 2001; Martinoia et al., 2012). In K$^+$ replete plants, the vacuolar pool plays an essential role as osmoticum to generate turgor and drive cell expansion (MacRobbie, 2006). The vacuolar K$^+$ pool is also responsible of maintaining the cytosolic K$^+$ concentration within narrow limits independently of K$^+$ abundance in the growth medium. Cytosolic K$^+$ concentration is thought to decline only when the vacuolar K$^+$ reserve has been depleted below the thermodynamical equilibrium with the cytosolic pool. For that reason, the activity of vacuolar K$^+$ channels and transporters is fundamental to maintain the cellular K$^+$ homeostasis (Walker et al., 1996; Leigh, 2001; White and Karley, 2010). Due to the membrane potential difference between the vacuole and the cytosol, positive inside, it is generally accepted that K$^+$ transporters are responsible for the active uptake of K$^+$ into the vacuole, whereas K$^+$ channels chiefly mediate its efflux (Martinoia et al., 2012).

Three types of K$^+$-permeable channels have been determined in the vacuolar membrane which maintain the K$^+$ homeostasis in the cytosol: fast vacuolar (FV), slow vacuolar (SV) and vacuolar K$^+$-selective (VK) channels (Isayenkov et al., 2010b; Voelker et al., 2010; Hedrich and Marten, 2011; Martinoia et al., 2012).

The FV channel activity was first described in vacuoles isolated from sugarbeet, and subsequent studies found it also in *Vicia faba* guard cells and barley mesophyll vacuoles (Hedrich and Neher, 1987; Allen and Sanders, 1997; Tikhonova et al., 1997), but the gene(s) encoding the FV channels still remain(s) unknown. This channel presents a low selectivity for K$^+$ and Na$^+$ and other monovalent cations can permeate it. FV-type currents are quickly elicited by membrane depolarisation, and channel inactivation takes place in presence of high Ca^{2+} concentrations (> 0.1 µM) (Hedrich and Neher, 1987). The FV channel is also regulated by the K$^+$ levels both in the cytosol and in the lumen of the vacuole affecting the channel open probability. Hence it was

hypothesised that this protein could be involved in the cellular K^+ partitioning between vacuole and cytoplasm (Pottosin et al., 2009).

The slow vacuolar (SV) channels are responsible for a large outward-rectifying conductance in the presence of Ca^{2+}, and slowly activate at depolarizing potentials (more positive at the cytoplasmic side) (Hedrich and Neher, 1987). These conditions favour the K^+ release from the vacuole, although a large depolarisation can invert the K^+ flux and then K^+ is permeated into the vacuole (Ivashikina and Hedrich, 2005). This SV-type current is present in every cell type and plant species studied (Isayenkov et al., 2010b). As the FV channels, the K^+/Na^+ selectivity ratio of SV channels is around 1, and it can permeate divalent cations e.g. Ca^{2+} (Hedrich and Neher, 1987; Pottosin et al., 2009; Hedrich and Marten, 2011). SV channels are inactive at low concentrations of Ca^{2+}, whereas the channel opening requires Ca^{2+} concentrations of around 10 µM (Pottosin and Schonknecht, 2007; Pottosin et al., 2009). In addition, SV channel activity is regulated by phosphorylation, 14-3-3 proteins, redox potential and organic cations (Isayenkov et al., 2010b). The Arabidopsis SV channel is encoded by the single copy gene *AtTPC1* (two-pore channel) (Peiter et al., 2005). Albeit TPC1 is ubiquitous and shows high expression levels, loss of function mutants present only weak phenotypes. Stomatal closure in presence of high external Ca^{2+} and ABA-induced delay of germination are defective in the *tpc1-2* mutant (Peiter et al., 2005).

The vacuolar K^+-selective (VK) channel currents were originally identified in guard cells (Ward and Schroeder, 1994; Allen and Sanders, 1996) but it has been shown that these currents are present in other cell types derived from shoot and root tissues such as mesophyll or epidermal cells (Gobert et al., 2007; Voelker et al., 2010). Gobert and coworkers (2007) found that the current mediated by the AtTPK1 protein presented the hallmarks described for the guard cell VK current (Ward and Schroeder, 1994; Allen and Sanders, 1996). TPK1 is very selective for K^+ over Na^+, its channel activity is voltage-independent, and exhibits intrinsic rectification and regulation by cytoplasmic Ca^{2+} and pH (Gobert et al., 2007). TPK1 belongs to the two-pore K^+ channels gene family, which contains 5 TPK isoforms, four of them localized at the tonoplast (TPK1, 2, 3 and 5) and one (TPK4) at the plasma membrane (Becker et al.,

2004; Voelker et al., 2006; Isayenkov et al., 2010b). VK activity is also modulated by 14-3-3 proteins, but contrarily to SV channels, TPK channel activity increases after binding of 14-3-3 (Latz et al., 2007). TPK proteins are likely involved in several processes related with K^+ homeostasis as is pointed out by phenotypic analyses of *tpk1* mutant of Arabidopsis and TPK1-overexpressing plants. Seedling growth differences correlated with *TPK1* expression level at both, low (0.01 mM) and high (80 mM) K^+ concentration (Gobert et al., 2007). In guard cells TPK1 participates in K^+ release from the vacuole during stomatal closure. TPK1 loss of function mutants show slower stomatal closure kinetics in response to ABA, albeit they reach the same aperture than the wild type. However, fusicoccin-induced stomatal opening is not affected in *tpk1* plants (Ward and Schroeder, 1994; Gobert et al., 2007).

K^+ is transported into the vacuole and other endomembrane systems through members of the monovalent cation/proton-antiporter (CPA) superfamily, which is divided into two major families: CPA1 and CPA2 (Sze et al., 2004; Pardo et al., 2006; Gierth and Mäser, 2007; Chanroj et al., 2012). The family CPA1 includes eight members of the Na^+/H^+ exchanger (NHX) family, which are the focus of this work and will be thoroughly described in section I.3. CPA2 comprises three families: the putative K^+ exchange antiporters KEA, the cation/H^+ exchangers CHX and the NHD group (White and Karley, 2010; Chanroj et al., 2012). In Arabidopsis, the KEA family includes six members but little is know about their subcellular localization and physiological functions. The detection of AtKEA1 and AtKEA3 peptides in chloroplast preparations suggests a role of these proteins in ion homeostasis in plastids (Zybailov et al., 2008; Chanroj et al., 2012). The AtCHX family contains 28 isoforms localized in different cellular compartments. Most of the CHX proteins are expressed in pollen, specifically during microgametogenesis or in sporophytic tissue, indicating the importance of the K^+ homeostasis in pollen development and germination (Sze et al., 2004). The Arabidopsis CHX16-CHX20 proteins are involved in K^+ and pH homeostasis of dynamic endomembranes. AtCHX17 is preferentially expressed in roots under NaCl stress, K^+ starvation, low external pH or ABA treatment. In addition, *chx17* mutants accumulate less K^+ than the wild type under salt stress (Cellier et al., 2004) and AtCHX17 expressed in yeast is able to complement the pH sensitive phenotype of the yeast *kha1* mutant

and co-localises with Golgi markers ([Maresova and Sychrova, 2006](#)). AtCHX20 participates in stomatal opening mediating K^+ and pH regulation in the prevacuolar compartment (PVC) thus affecting the endomembranes dynamics and osmoregulation ([Padmanaban et al., 2007](#)). Another well-characterized CHX member is AtCHX23 which localises to the chloroplast envelope where it is likely involved in K^+ homeostasis and stromal pH regulation ([Song et al., 2004](#)).

I.1.3. Potassium deficiency

Plants have developed mechanisms to take up and accumulate K^+ from very low external concentrations and they can grow properly over a wide range of external K^+ supplies (from 10 µM to 10 mM). This is due to the high mobility of this cation which can be quickly redistributed within the plant among different compartments and tissues under fluctuating external K^+ conditions ([Amtmann et al., 2006](#)). It is commonly accepted that the typical K^+ concentrations in the soil solution vary between 0.1 and 1 mM ([Maathuis, 2009](#); [Aleman et al., 2011](#)). However, besides the plant's uptake mechanisms, acquisition of K^+ from the soil is dependent on several physical and chemical soil factors that can affect the K^+ availability; among others, salinity, soil compaction and drought. These factors together with an inadequate nutrient recycling turn K^+ deficiency into an agriculture issue ([Römheld and Kirkby, 2010](#)).

The response of plant growth to increasing K^+ availability follows a steep curvilinear relationship. From this relationship a "critical" concentration of K^+ can be determined, defined as the concentration at which 90% of maximum yield is obtained. Above this concentration, growth shows little response to increased K^+ content in tissues, but at lower K^+ concentrations growth declines rapidly. The "critical" concentration is around a 2% of the total dry matter, albeit tissue K^+ concentrations normally exceed those necessary for maximal growth ([Leigh and Wyn Jones, 1984](#); [White and Karley, 2010](#)).

Plants experiencing K^+ deficiency show phenotypic traits consistent with the vital role that this cation plays in plant growth and metabolism (Mengel et al., 2001; Amtmann et al., 2006; Hermans et al., 2006; White and Karley, 2010). They exhibit reduced growth, particularly of shoots, but also the roots are poorly developed. The growth of lateral roots is arrested in Arabidopsis seedlings grown under K^+ starvation on agar plates (Armengaud et al., 2004). They present scorching along the margins of older leaves, chlorosis, weak stems and small and withered seeds and fruits. In addition, they are more susceptible to different stresses, pests and diseases (Amtmann et al., 2008; Römheld and Kirkby, 2010). Physiological symptoms of K^+ deficiency include impaired phloem transport, especially of sucrose, increased leaf carbohydrate, a reduction in chlorophyll concentration and photosynthesis, decreased water content and turgor, impaired stomatal function and reduced transpiration (Cakmak et al., 1994; Hermans et al., 2006; White and Karley, 2010). The decline in photosynthesis by K^+ deficiency seems to be caused by several processes (Cakmak, 2005; Hermans et al., 2006; Amtmann et al., 2008). The lack of K^+ would hinder the establishment of a proton flux across the thylakoid membrane which is necessary to create the proton gradient that drives the ATP-synthesis via photophosphorylation (Tester and Blatt, 1989). In addition, K^+ is required for CO_2 fixation in the chloroplast (Pier and Berkowitz, 1987) and for Rubisco activity (Peoples and Koch, 1979). Potassium is also necessary to create steep pH, voltage and osmotic gradients between phloem and parenchyma cells within the sieve tubes that are essential for phloem and transport (Marschner, 1995; Amtmann et al., 2008; Römheld and Kirkby, 2010). Export and utilization of the photoassimilates within the plants maintain the photosynthesis at high rate. However a several-fold increase in sucrose accumulation in leaves, but not in roots, is observed under K^+ deficiency (Cakmak et al., 1994; Amtmann et al., 2008). This suggests a decrease in sugar export via phloem towards the sink sites or insufficient incorporation of carbon into proteins (Amtmann et al., 2008). This effect of plant K^+ status on source-sink allocation of sugars and other metabolites is related to the fact that K^+ deficiency increases the stomatal resistance, thus reducing the transpiration rate (Peoples and Koch, 1979) and the root-shoot allocation of root-born metabolites such as nitrate and amino acids (Amtmann et al., 2008). Also, K^+ deficiency has repercussions on nitrogen metabolism. Concentrations of amino acids (lysine, arginine and tyrosine), amide

nitrogen and polyaminas (e.g., putrescine) increase dramatically in K^+-deficient plants, probably for the incapacity of incorporate nitrogen into proteins by inhibition of nitrogen enzymes ([Amtmann et al., 2008](#); [White and Karley, 2010](#)).

I.1.3.1. Plant sensing of K^+-deficiency.

Plants can detect the K^+ external conditions through the root apoplast that is in contact with epidermic root cells and root hairs. In conditions of K^+-deficiency, root cells can sense the drop in external K^+ concentration and trigger a series of physiological responses ([Schachtman and Shin, 2007](#); [Wang and Wu, 2010](#)). Apoplastic K^+ concentration controls the membrane voltage of root cells in a linear relationship with the log of $[K^+]_{ext}$. Hence, the hyperpolarization of the root cell membrane potential induced by a decrease in K^+ concentration is the primary signal of K^+ deprivation ([Maathuis and Sanders, 1993](#); [Nieves-Cordones et al., 2008](#)). Membrane hyperpolarization activates the plasma membrane H^+-ATPases that generate a extracellular acidification ([Palmgren, 2001](#)). Membrane hyperpolarization and apoplast acidification enhance in turn the activities of inward K^+ channels belonging to the AKT1 subfamily and K^+/H^+ symporters ([Wang and Wu, 2010](#)).

Little is known about the molecular K^+ sensors. It has been proposed that K^+ transporters with a wide range of K^+ affinities, as in the case for AKT1, coupled to the PM-located H^+-ATPases might be the K^+ sensor ([Wang and Wu, 2010](#)). It has been reported that K^+ ions can bind to the cytoplasmic part of the H^+-ATPases and inhibit their conformational change thus abolishing the H^+ efflux. Under K^+ deprivation, AKT1-mediated K^+ influx to the cytoplasm would decrease and subsequently, the uncoupling effect of K^+ on H^+-ATPase activities would be impeded, leading to membrane hyperpolarization and extracellular acidification. Finally, K^+ channels and transporters would be activated favouring the entry of K^+ with a higher affinity ([Buch-Pedersen et al., 2006](#); [Wang and Wu, 2010](#)). The pyruvate kinase, whose activity is strongly sensitive to cytoplasmic K^+ concentrations, has been also proposed as a putative cytoplasmic K^+ sensor ([Schachtman and Shin, 2007](#); [Armengaud et al., 2009](#)). As a

central enzyme involved in plant glycolysis it is likely that the pyruvate kinase drives some of the metabolic changes induced by K^+-deficiency ([Armengaud et al., 2009](#)).

Low external K^+ concentrations can induce Ca^{2+} and ROS accumulation in Arabidopsis root cells ([Wang and Wu, 2010](#)). Ca^{2+} elevation can be mediated by hyperpolarization-activated Ca^{2+} channels as well as by ROS-activated Ca^{2+} channels, and ROS production can be caused by NADPH oxidase activation induced by Ca^{2+} magnifying the signal. Thus, a cytoplasmic Ca^{2+} signal would be generated and transduced by downstream Ca^{2+} sensors such as CaMs, CDPKs and CBLs ([Kudla et al., 1999](#); [Luan et al., 2002](#); [Wang and Wu, 2010](#)). Ethylene in also involved in relying the signal for K^+ deprivation ([Jung et al., 2009](#)).

I.1.3.2. Acclimatory responses to potassium starvation.

In order to maintain the K^+ homeostasis, the Ca^{2+} and ROS signals generated by the K^+-deficiency must be further transduced to regulate K^+ channels and transporters at both transcriptional and post-transcriptional level.

I.1.3.2.1. Transcriptional regulation.

Several Arabidopsis K^+ transporters increase their expression under K^+-starvation, such as *HAK5*, *KEA5*, *KUP3*, *CHX13* and *CHX17* ([Armengaud et al., 2004](#); [Cellier et al., 2004](#); [Gierth et al., 2005](#); [Amtmann et al., 2006](#); [Zhao et al., 2008](#); [Wang and Wu, 2010](#)). At least for HAK5, CHX13 and CHX17 their involvement in K^+ acquisition and homeostasis under K^+-starvation have been demonstrated ([Cellier et al., 2004](#); [Gierth et al., 2005](#); [Zhao et al., 2008](#)). Channels *AtSKOR1* and *AtKC1*, are transcriptionally induced in response to low K^+ conditions ([Pilot et al., 2003](#); [Shin and Schachtman, 2004](#)). As described above, Ca^{2+} channels play an important role in the K^+-deprivation signaling, and, as expected, two putative Ca^{2+} transporters show transcriptional regulation in response to K^+ deprivation: ACA1, a root plasma membrane Ca^{2+} pump, and CAX3, a vacuolar cation/H^+ antiporter ([Armengaud et al.,](#)

18

[2004](#)). A large number of non-transporter genes also show transcriptional regulation under low-K^+ stress. Among them, genes related to the plant hormones jasmonic acid (JA) and salicylic acid which are involved in pathogen defense ([Armengaud et al., 2004](#); [Amtmann et al., 2008](#)), cell wall proteins (e.g. extensins), transcription factors (e.g. bZIP), protein kinases and phosphatases (e.g. CIPK and PP2C), ROS production and detoxification proteins, enzymes involved in ethylene synthesis and enzymes of the primary metabolism (e.g. pyruvate kinase and malic enzyme) ([Armengaud et al., 2004](#); [Shin and Schachtman, 2004](#); [Amtmann et al., 2006](#)).

I.1.3.2.2. Protein modification.

Recently, new data about the post-transcriptional regulation of K^+ channels and transporters triggered by K^+-starvation have been reported, being the best characterized pathway the one comprising AKT1/CIPK23/CBL1 (and/or CBL9). The plasma membrane Ca^{2+} sensor CBL1 (and/or CBL9) detects the cytoplasmic Ca^{2+} increase induced by low-K^+ stress, interacts with the cytoplasm-located Ser/Thr kinase CIPK23 and recruits it to the plasma membrane. Here, CIPK23 phosphorylates and activates the AKT1 channel ([Li et al., 2006a](#); [Xu et al., 2006](#)). To cease the low-K^+-induced signaling, the phosphatase AIP1 deactivates the AKT1 channel via dephosphorylation ([Lee et al., 2007](#)). A similar pathway has been proposed to occur at the vacuole, where CIPK9 may interact with the tonoplast-located protein CBL3 to regulate tonoplast-located K^+ channels through phosphorylation ([Pandey et al., 2007](#); [Liu et al., 2012](#)). Also, the interaction between different subunits of heteromeric channel complexes can shift the activation threshold of the channels alone, as has been demonstrated for AtKC1 and AKT1 ([Geiger et al., 2009a](#)).

I.2. Stomata.

The leaves of land plants are covered by a waxy cuticle on their epidermis, which prevents excessive loss of water but also limits the uptake of CO_2 essential for photosynthesis. To bypass the latter limitation, stomatal pores located in the leaf epidermis enable the diffusion of gases between the plant tissues and the atmosphere. The degree of opening of these stomata result from the reversible osmotic swelling and shrinking of the two surrounding guard cells (Roelfsema and Hedrich, 2005). During stomatal opening, the uptake of solutes into guard cells decrease the water potential creating a driving force for water entry and increasing turgor and volume of guard cells. This turgor pressure causes the separation of the two guard cells, resulting in the opening of the stomatal pore. To close the stomatal pore, there is a loss of solute and water content from the two guard cells that decrease their volume and result in guard cell deflation (Pandey et al., 2007). The major solutes involved in stomatal movements are K^+, sucrose, Cl^-, $malate^{2-}$ and NO_3^-. Since mature guard cells lack plasmodesmata, solute uptake and efflux must take place through ion channels and transporters located in the plasma and vacuolar membranes (Pandey et al., 2007; Kim et al., 2010). The next section will focus in the description of these ion transporters and their roles in the stomatal movements.

I.2.1. Ion channels and transporters.

I.2.1.1. Ion transport at the plasma membrane.

H^+-ATPases

Stomatal opening is initiated by the hyperpolarisation of the guard cell plasma membrane, which is caused by the H^+-ATPase-dependent proton efflux from the cytoplasm to the apoplast (Assmann et al., 1985; Shimazaki et al., 1986). H^+-ATPases are encoded by 11 genes in Arabidopsis, all of them expressed in guard cells (Ueno et al., 2005). H^+-ATPases are regulated by auxins, ABA, Ca^{2+} and blue light and have an

autoinhibitory domain at the C-terminus, which is released from the catalytic site upon blue light illumination. Blue light perception by the receptors PHOT1 and PHOT2 trigger a signaling cascade where the phosphorylation at the C-terminus of the H^+-ATPase, and the consequent binding of a 14-3-3 protein that displaces the autoinhibitory domain, activates the proton pump and results in stomatal opening (Kinoshita and Shimazaki, 1999; Emi et al., 2001; Kinoshita et al., 2001; Kinoshita et al., 2003). Dominant mutants in the Arabidopsis gene alleles *AHA1/OST2* (*ARABIDOPSIS H$^+$-ATPASE 1/OPEN STOMATA 2*) present a constitutive H^+-ATPase activity that leads to ABA insensitivity and to permanent stomatal opening (Merlot et al., 2007b). Guard cells maintain a cytoplasmic pH of 7.5-7.8, at which the H^+-ATPase presents a low activity. H^+-ATPases become more active to acidic pH values suggesting a role in H^+ homeostasis for these proteins (Becker et al., 1993; Blatt and Armstrong, 1993; Grabov and Blatt, 1997).

K^+ transport

Plant plasma membrane has three types of K^+ channels: outward-rectifying channels (KORCs), which become more active at positive potentials; inward-rectifying channels (KIRCs), activated at more negative potentials; and voltage-independent K^+ channels. The first two types of K^+ channels have been recorded in guard cells of several species while voltage-independent K^+ channel currents have not been detected, so far, for guard cells (Roelfsema and Hedrich, 2005). Derived from their voltage dependence, at physiological conditions KORCs seem to be resposible for K^+ efflux from the guard cells to the apoplast whereas KIRCs are mainly involved in K^+ influx to the cytoplasm (Roelfsema and Hedrich, 2005). Among the K^+ channels expressed in guard cells are KIRCs KAT1, KAT2 (Pilot et al., 2001) and AKT1, the K^+ channel AKT2/3 whose voltage dependence changes with its phosphorylation status, AtKC1 that forms heteromeric channels with KAT1 and AKT1 (Szyroki et al., 2001; Michard et al., 2005), and a single outward-rectifying channel, GORK (Ache et al., 2000).

Functional K$^+$ channels likely work as homomeric or heteromeric complexes formed by four subunits ([Dreyer et al., 1997](#)). Several interactions between the K$^+$ channels have been found in heterologous systems and such interactions can change the current properties of the individual channels ([Pandey et al., 2007](#)). Although loss of function *kat1* mutant plants show normal stomatal opening and K$^+$ currents similar to those of the wild type ([Szyroki et al., 2001](#)), the overexpression of a nonfunctional *KAT1* allele decreases the inward K$^+$ conductance of guard cells by 70% and light-induced stomatal opening suggesting that the nonfunctional protein form defective tetrameric channels in combination with the other five wild-type proteins ([Kwak et al., 2001](#)). K$^+$ currents can also be regulated by K$^+$ channels relocalization. It has been shown that ABA induces specific endocytosis of KAT1 in guard cells, reducing inward K$^+$ currents at the plasma membrane and consequently stomatal opening. Endosomal KAT1 is recycled to the plasma membrane after ABA signaling in a process dependent of the SNARE protein SYP121 ([Sutter et al., 2006](#); [Sutter et al., 2007](#)). Guard cell inward K$^+$ currents are inhibited by cytoplasmic Ca^{2+} elevation. Also, membrane hyperpolarization allows Ca^{2+} permeation through the inward-rectifying channels, blocking the channel lumen ([Fairley-Grenot and Assmann, 1992](#); [Ivashikina et al., 2005](#)). Apoplastic and cytosolic pH have different effects over the inward K$^+$ channels expressed in heterologous systems. For example, KAT1 is activated by acidification of both cytosol and apoplast whereas KAT2 is activated by the apoplast acidic pH ([Hoth et al., 2001](#); [Pilot et al., 2001](#); [Pandey et al., 2007](#)). However, *in planta* measurements of the whole guard cell inward K$^+$ currents show that K$^+$ currents step up by external acidification but not by changes in cytosolic pH ([Blatt, 1992](#); [Ilan et al., 1996](#)).

GORK is the only outward-rectifying channel present in Arabidopsis guard cells ([Ache et al., 2000](#); [Hosy et al., 2003](#)). Although disruption of the GORK gene causes the complete loss of the outward-rectifying K$^+$ currents in the plasma membrane of guard cells and slowed closure of stomata, they still close in response to ABA and darkness ([Hosy et al., 2003](#)). These results indicate that guard cells possess alternative transport systems for K$^+$ releasing during stomatal closure. Outward K$^+$ currents are insensitive to Ca^{2+} regulation while are pH regulated. External acidification causes a decrease in the availability of the channel for activation by membrane depolarisation ([Blatt, 1992](#); [Ilan](#)

et al., 1996; Ache et al., 2000). Conversely, outward K^+ currents are facilitated by cytosolic alkalinization (Blatt, 1992; Blatt and Armstrong, 1993; Miedema and Assmann, 1996).

With regard to ABA signaling, it is well studied the inhibition of guard cell KIRCs by ABA (Blatt and Armstrong, 1993). It has been also reported that ABA can promote KORC activity in guard cells of isolated epidermal strips (Blatt et al., 1990) but this could not be demonstrated by measurements on guard cells in intact plants (Roelfsema et al., 2004).

Anion transport

It is well known that during stomatal opening guard cells accumulate Cl^- and malate as counterions of K^+ (Van Kirk and Raschke, 1978a). Stomatal opening in epidermal strips can be supported by both Cl^- and malate or just by malate synthesis if no plasma membrane-permeable anions are applied (Raschke and Schnabl, 1978). It has been postulated that Cl^-, due to its electrochemical gradient, might be imported by H^+/anion or OH^-/anion antiporters, but these transporters still remains to be identified.

When Cl^- is not available NO_3^- can also contribute to stomatal opening as was demonstrated using Arabidopsis plants mutated in the NO_3^- transporter CHL1/AtNRT1.1. Plants lacking CHL1 present reduced stomatal aperture when NO_3^- is supplied in the medium in the absence of Cl^-, while no differences relative to the wild type can be observed with Cl^-, supporting the hypothesis that the CHL1 transporter allows the uptake of NO_3^- into guard cells (Guo et al., 2003).

Anion channels located in the plasma membrane of guard cells mediate anion efflux during stomatal closure driving the depolarisation of the membrane that subsequently facilitates K^+ efflux across the outward-rectifying K^+ channels. They are classified as slow-activating and sustained (S-type) and rapid transient (R-type) anion channels. The R-type channels show rapid activation kinetics over a narrow voltage range while the S-type channels exhibit slow activation and deactivation kinetics over a

broader range of voltages (Schroeder and Hagiwara, 1989; Hedrich et al., 1990; Schroeder and Keller, 1992; Schroeder, 1995). Both types of channels can permeate Cl^-, NO_3^- and malate, the main anions involved in guard cell function.

It has been postulated that S-type channels play a key role in membrane depolarisation and stomatal closure (Kim et al., 2010). The first identified gene encoding a S-type anion channel has been *SLAC1* (*SLOW ANION CHANNEL-ASSOCIATED 1*), which is a distant homologue of fungal and bacterial dicarboxylate/malate transporters. *SLAC1* was isolated in two independent mutant screenings for CO_2-insensitive stomatal closure mutants (Negi et al., 2008) and ozone-sensitive mutants (Vahisalu et al., 2008). S-type currents induced by ABA and Ca^{2+} are impaired in *slac1* guard cells, indicating that SLAC1 is the main component of S-type anion channels in guard cells. However, *slac1* mutants still retain the R-type anion channel activities (Vahisalu et al., 2008). *slac1* mutants also show reduced stomatal closure in response to ABA, Ca^{2+} CO_2 and O_3 treatments (Negi et al., 2008; Vahisalu et al., 2008). Heterologous expression of AtSLAC1 in *Xenopus* oocytes demonstrated that SLAC1 functions as an anion channel with selectivity for Cl^- and NO_3^- (Geiger et al., 2009b; Lee et al., 2009). Recently, a second S-type anion channel, SLAH3 (SLAC1 homolog 3), has been identified. SLAH3 is also present in guard cells and mediates nitrate-induced anion currents in *Xenopus* oocytes. Nitrate, calcium and ABA-stimulated phosphorylation regulate SLAH3 activity (Geiger et al., 2011).

The presence of anions in the apoplast, including Cl^-, nitrate and malate, play a chief role in activating anion release during stomatal closure likely by inducing a shift in the voltage dependence of R-type anion channels, thus increasing the potency of the channel to initiate a depolarisation (Roelfsema and Hedrich, 2005). The R-type identity has remained elusive until Meyer and collegues (2010) found that the AtALMT12 transporter, which is expressed in guard cells, shows a malate-dependet R-type channel activity. Previously it was shown that *Arabidopsis almt12* mutants present impaired stomatal closure in response to ABA, Ca^{2+} and darkness but the authors related this phenotype to an anion release from the endoplasmic reticulum (ER) (Sasaki et al., 2010). Afterward, using an ALMT12:GFP fusion protein, the guard cell

plasma membrane localization of this channel was determined ([Meyer et al., 2010](#)). The ALMT12 channel is permeable not only to Cl^- and NO_3^- ([Sasaki et al., 2010](#)) but also to malate and sulphate suggesting a role in long-term anion release from guard cells ([Meyer et al., 2010](#)).

Ca^{2+} transport

External Ca^{2+} application inhibits stomatal opening and induces stomatal closure. It is believed that extracellular Ca^{2+} elicits an increase in the intracellular Ca^{2+} concentration, thus activating S- and R-type anion channels and inhibiting the inward K^+ channels ([Roelfsema and Hedrich, 2005](#); [Pandey et al., 2007](#)). Because the apoplastic Ca^{2+} concentration is ~ 100 µM ([Felle et al., 2000](#); [Roelfsema and Hedrich, 2002](#)) while the cytoplasmic concentrations vary between 100-300 nM it was thought that leak Ca^{2+} currents across the plasma membrane could sustain the rise in intracellular Ca^{2+} ([Webb et al., 2001](#); [Levchenko et al., 2005](#)). Ca^{2+} probably enters to the guard cells via nonselective Ca^{2+} channels located in the plasma membrane. This type of channels has been found in different plant cells and are permeable to monovalent and divalent cations. They have been identified in guard cell protoplasts activated by several stimuli, including hyperpolarization that induces a rise in the cytoplasmic Ca^{2+} concentration in guard cells ([Grabov and Blatt, 1998](#); [Roelfsema and Hedrich, 2005](#)). The cyclic nucleotide gated channels (CNGC) have been suggested to play a role in stomatal function since cAMP can activate a Ca^{2+} current in Arabidopsis guard cell protoplasts ([Lemtiri-Chlieh and Berkowitz, 2004](#)). In Arabidopsis roots, glutamate produces large and rapid elevations of cytoplasmic Ca^{2+} and transient membrane depolarisation. Hence, GLR3.4, a member of the glutamate receptor family (GLR) that is expressed in guard cells, is another candidate to facilitate Ca^{2+} currents ([Meyerhoff et al., 2005](#); [Qi et al., 2006](#)). Furthermore, loss-of-function mutants in the guard cell-expressed transmembrane ABC (ATP binding cassette) protein AtMRP5 (*MULTIDRUG RESISTANCE PROTEIN 5*) have impaired activation of Ca^{2+} currents, but there is no evidence that AtMRP5 functions as a Ca^{2+} permeable channel ([Gaedeke et al., 2001](#); [Suh et al., 2007](#)).

I.2.1.2. Ion transport at the vacuolar membrane.

H$^+$-ATPases and PPases

Proton fluxes across the vacuolar membrane serve to guard cells as a pH secondary messenger, regulate the tonoplast membrane potential and mediate the movements of solutes between vacuoles and cytoplasm through H$^+$-coupled antiporters (Pandey et al., 2007). Proton uptake into the Arabidopsis vacuole is carried out by the vacuolar H$^+$-ATPase (V-ATPase) and the H$^+$-translocating vacuolar pyrophosphatases (V-PPases) (Gaxiola et al., 2002). The V-ATPase consists of a multimeric complex whose subunits are encoded by at least 26 genes (Padmanaban et al., 2004). V-PPases, which use energy from pyrophosphate hydrolysis to translocate H$^+$ into the vacuole, work as homodimeric enzymes (Schumacher, 2006). The V-ATPase is involved in the control of Ca^{2+} homeostasis in guard cells since the Arabidopsis mutant in the C-subunit of the V-ATPase (*det3*) induce, prolonged Ca$^{2+}_{cyt}$ oscillations in response to external Ca^{2+} and oxidative stress, thus abolishing the stomatal closure (Allen et al., 2000). However, evidences for a role of the V-PPases in stomatal function are still lacking.

K$^+$ transport

The three types of K$^+$ permeable channels described previously in section I.1.2.3. have been found in the tonoplast of guard cells (Allen et al., 1998). All of them are likely involved in K$^+$ efflux from the vacuole during stomatal closure as the studies performed by reverse genetic and electrophysiology suggest (Ward and Schroeder, 1994; Peiter et al., 2005; Gobert et al., 2007). By contrast, K$^+$ ions are taken up into the vacuole against the vacuolar membrane potential. A recent study carried out by our group suggested that Arabidopsis NHX1 and NHX2 proteins sustain most of the accumulation of K$^+$ into plant cell vacuoles, including those of guard cells where these genes are highly expressed (Shi and Zhu, 2002; Apse et al., 2003; Barragán et al., 2012). Null double *nhx1 nhx2* mutant plants are unable to withstand osmotic stress presenting higher transpiration rates than the wild type. In addition, mutant plants

show less leaf turgor, abnormal stomata morphology and a reduction in guard cell K^+ contents (Barragán et al., 2012). The role of NHX1 and NHX2 proteins in stomatal function will be studied in depth along this work.

Anion transport

The role played by vacuolar anion channels in the stomatal movements is so far not fully characterized. In 1996, Pei and collegues identified a chloride and malate conductance in guard cell vacuoles of *Vicia faba*. This anion channel was thought to be activated by a Ca^{2+}-dependent protein kinase (Pei et al., 1996). Recently, two different vacuolar anion transporters have been characterized. AtCLCc, which localizes at the tonoplast and is expressed in guard cells, is involved in the accrual of Cl^- into the vacuole. T-DNA insertion mutants in *AtCLCc* present lower Cl^- vacuolar contents, and this fact correlates with the impaired light-induced stomatal opening and ABA-induced stomatal closure showed by these mutants (Jossier et al., 2010). The malate transporter AtALMT6 is also expressed in guard cell vacuoles and is able to mediate malate inward-rectifying currents. This activity can be modulated by cytosolic Ca^{2+}, cytosolic malate and vacuolar pH, to accumulate or release vacuolar malate at physiological membrane potentials. However, likely due to the presence in guard cells of functional redundant malate transporters, the stomatal function in *almt6* knockout mutant plants is normal, even though they show lower malate currents than the wild-type vacuoles (Meyer et al., 2011).

I.2.2. Stomatal movements.

The stomatal movements are completely dependent of the proper coupling of ion fluxes through the plasma membrane and the vacuolar membrane. Thus, H^+-pumps, ion channels and transporters must function coordinately in response to the opening and closure stimulus. The most distinctive difference between the stomatal opening and the stomatal closure are the transport mechanisms involved in both processes. Stomatal opening is based on active transport (ions symport and antiport)

whereas closure is based on passive transport (ion channels) ([Roelfsema and Hedrich, 2005](#)). Thus, stomatal closure is faster than opening. In Arabidopsis the transpiration rate increases with a velocity of 1.0 µmol m^{-2} s^{-2} in the light while it decreases with a velocity of 4.4 µmol m^{-2} s^{-2} after the application of ABA ([Langer et al., 2004](#)).

I.2.2.1. Stomatal opening.

During stomatal opening the activation of the H$^+$-ATPases generate an electrochemical gradient across the plasma membrane that can be decomposed in an electrical potential and in an H$^+$-concentration difference. This membrane hyperpolarisation drives K$^+$ uptake through inward-rectifying K$^+$ channels. Anions such as Cl$^-$ or NO$_3^-$ can enter into the cell by H$^+$-coupled symporters while malate is synthesized in the cytoplasm from phosphoenolpyruvate and CO$_2$. Most of the solutes taken up during stomatal opening, including malate, are sequestered in the vacuole. The tonoplast potential is negative at the cytoplasmic side, so anions can be transported into vacuoles through low-affinity anion channels as long as the concentration difference between the cytoplasm and the vacuole is counterbalanced by the membrane potential difference, and then the H$^+$/anion exchange systems can operate. Potassium ions are transported into the vacuole against its electrochemical gradient thus requiring a H$^+$-coupled antiport mechanism. This accumulation of solutes inside of guard cells drives the subsequent entry of water increasing cell turgor and volume that induces stomatal opening ([MacRobbie, 1998](#); [Roelfsema and Hedrich, 2005](#); [Kim et al., 2010](#)).

I.2.2.2. Stomatal closure.

When the stomata perceive the closure signalling (e.g. ABA) the rise in Ca$^{2+}_{cyt}$ activates the vacuolar K$^+$ (VK) channels that produce the K$^+$ efflux from the vacuole and vacuolar membrane depolarisation. Then, anion-permeable channels are activated and anions are released from the vacuole to the cytoplasm. Contemporarily, the increase in cytosolic Ca^{2+} concentration activates both types of plasma membrane anion channels,

S-type and R-type, driving the anion release from guard cells to the apoplast. The consequent plasma membrane depolarisation favours the efflux of K^+ through the activation of the outward-rectifying K^+ channels. This large and fast loss of ions is accompanied by the outflow of water from the guard cells that reduce their turgor and volume causing stomatal closure (Roelfsema and Hedrich, 2005; Kim et al., 2010).

I.2.3. Regulation of stomatal movements.

Guard cells constantly sense the information coming from the leaf environment, including abiotic and biotic stimuli as well as long-distance signals from the roots. Guard cells integrate all these signals and respond with appropriate changes in pressure turgor in order to balance CO_2 assimilation and water loss. Numerous important environmental factors affect stomata opening, including blue and red light, hormones, air humidity, atmospheric CO_2 concentration and biotic and abiotic stresses (Kim et al., 2010; Araujo et al., 2011). Some of the signal transduction networks that function in the response to these environmental factors will be described below, particularly those related with the ion transport regulation in guard cells.

I.2.3.1. CO_2 sensing and signaling.

Low atmospheric CO_2 concentration induces stomatal aperture in order to keep CO_2 available in the sub-stomatal chambers so the carbon fixation rate in the mesophyll cells would not be affected (Araujo et al., 2011). By contrast, elevated CO_2 concentrations decrease stomatal conductance. In the short term, CO_2 leads to stomatal closure while long-term exposure to high CO_2 concentrations decreases stomatal density in leaves (Kim et al., 2010).

In *Vicia faba* guard cells an elevation in CO_2 concentration controls the stomatal aperture by the activation of KORC and anion channels at the plasma membrane. Hence, CO_2 triggers chloride release from guard cells and membrane depolarisation (Brearley et al., 1997; Hanstein and Felle, 2002).

Recently, a few genes involved in the CO_2-mediated regulation of the stomatal movements have been identified. The Arabidopsis mutant *gca2* (*growth controlled by abscisic acid 2*) shows CO_2-induced stomatal closure impairment in response to elevated CO_2 in epidermal strips as well as in intact leaves. Furthermore, the changes in CO_2 concentration do not alter the cytoplasmic Ca^{2+} transient rate in *gca2* mutant guard cells, denoting impairment in CO_2-induced depolarisation of the plasma membrane (Young et al., 2006). The S-type anion channel SLAC1 is also a positive mediator of the CO_2-induced stomatal closure signaling network, as *slac1* mutants are strongly impaired in the high CO_2-induced stomatal closure response (Negi et al., 2008; Vahisalu et al., 2008). By contrast, HT1 (HIGH LEAF TEMPERATURE 1) protein kinase functions as a negative regulator in the high CO_2-induced stomatal closure pathway. Gas-exchange analyses performed on *ht1-2* recessive mutant show a constitutive high-[CO_2] stomatal closure (Hashimoto et al., 2006). Another negative regulator of CO_2-induced stomatal closure identified is the plasma membrane malate uptake transporter ABCB14 (ABC TRANSPORTER B FAMILY MEMBER 14). CO_2-induced stomatal closure is faster in *abcb14* detached leaves compared to the wild type, while is slower in *ABCB14* overexpressing plants. Lack of ABCB14 function may increase extracellular malate enhancing the anion channel activity (Hedrich and Marten, 1993) and reduce the intracellular malate levels, thus slightly accelerating CO_2-induced stomatal closure and reducing stomatal apertures at the same time (Lee et al., 2008).

Little is know, however, about the mechanism by which the physiological stimulus of CO_2 is transduced to regulate stomatal apertures. Albeit CO_2 is converted to carbonic acid, bicarbonate and protons, cytosolic pH does not change in response to an elevation of CO_2 concentration (Brearley et al., 1997). It has been proposed that, as a consequence of the elevated CO_2 concentrations, malate is released from mesophyll cells and that this rise in extracellular malate induces the activation of guard cell anion channels resulting in stomatal closure (Hedrich and Marten, 1993; Hedrich et al., 2001). Since guard cells release malate into the cell wall during stomatal closure (Van Kirk and Raschke, 1978b; Negi et al., 2008) and malate augments the R-type anion channel activity in guard cells (Raschke, 2003), malate released from guard cells could

generate a positive feedback by further stimulating anion channels (Lee et al., 2008). A recent report suggest that carbonic anhydrases could mediate the CO_2 response directly in guard cells, since the disruption of two of them, βCA1 and βCA4, strongly impaired the stomatal CO_2 reponses (Hu et al., 2010).

I.2.3.2. ABA sensing and signaling.

ABA is the most extensively studied hormone in relation with the stomatal movements. Under abiotic stresses such as drought and high salinity the levels of ABA increase in the roots. Next, ABA travels to the aerial parts where it is perceived by the guard cells. In guard cells, ABA triggers diverse signaling pathways that change ion fluxes leading to both stomatal closure and inhibition of stomatal opening. Hence, ABA minimize the water loss and improve the ability of plants to cope with abiotic stresses (Araujo et al., 2011).

Several candidate ABA receptors have been reported in the last few years. Among them the H subunit of the Mg-chetalase (CHLH), an ubiquitous protein involved in chlorophyll biosynthesis and plastid-to-nucleus signalling has been reported as a positive regulator of the ABA signaling (Shen et al., 2006). It has been reported that a G-protein coupled receptor 2 (GCR2) is able to bind ABA with high affinity at physiological concentration at the plasma membrane and it has been proposed that interaction of GCR2 with the G protein α-subunit GPA1 would mediate a subset of ABA responses, among them the stomatal movements (Liu et al., 2007). However, the etiology of GCR2 as an authentic ABA receptor remains controversial (Gao et al., 2007; Guo et al., 2008). More recently, it has been published that the GPCR-like proteins GTG1 and GTG2 are redundantly involved in G protein-coupled ABA signaling and that they could function as ABA receptors since they present highly specific ABA binding, and *gtg1 gtg2* mutants show ABA hyposensitive phenotype (Pandey et al., 2009). The PYR/PYL/RCAR family of proteins has been recently identified in two independent studies as ABA receptors that would function at the top of a negative regulatory pathway that controls ABA signaling by inhibiting the type 2C protein phosphatases

(PP2Cs) ABI1 and ABI2, which are themselves inhibitors of the SnRK2 protein kinases mediating most of the ABA responses (Ma et al., 2009; Park et al., 2009; Pardo, 2010).

Many second messengers regulate ABA signaling in guard cells, including reactive oxygen species (ROS), nitric oxide (NO), phosphatidic acid (PA), phosphatidyl-inositol-3-phosphate (PIP3), inositol-3-phosphate (IP3), inositol-6-phosphate (IP6), and sphingolipids (Hirayama and Shinozaki, 2007; Kim et al., 2010). ABA induces ROS production through the guard cell-expressed NADPH oxidases AtRBOHD and AtRBOHF. Mutations in both genes impair ABA-induced stomatal closing, ABA elevation of ROS production, ABA-induced cytosolic Ca^{2+} increases and ABA activation of plasma membrane Ca^{2+}-permeable channels in guard cells (Kwak et al., 2003). It has been shown that AtRBOHF directly interacts with and is phosphorylated by the OST1 protein kinase which indicates that these NADPH oxidases function in early ABA-mediated ROS signaling (Kwak et al., 2003; Sirichandra et al., 2009). Furthermore, ROS downregulate the PP2C phosphatases ABI1 and ABI2 activity *in vitro* (Meinhard and Grill, 2001). The MAP kinases 9 and 12 (MAPK9 and MAPK12) function downstream of ROS to positively regulate guard cell ABA signaling through the activation of anion channels (Jammes et al., 2009). In addition, ROS activate Ca^{2+} channels in the plasma membrane of guard cells and stimulate NO and PIP3 signaling in response to ABA, which in turn modulates the Ca^{2+}_{cyt} concentration levels in the cell (Pei et al., 2000; Neill et al., 2008).

It is known that ABA triggers an elevation in guard cell cytosolic free Ca^{2+} in *Commelina communis* and this precedes the stomatal closure (McAinsh, 1990). However, later reports show that the cytosolic Ca^{2+} elevation induced by ABA only takes place in a part of the guard cell population during stomatal closure (Kim et al., 2010). Due to the absence of a established link between ABA-induced stomatal closure and ABA-induced Ca^{2+} increases, a Ca^{2+}-independent mechanism may exist in the ABA signaling network (Allan et al., 1994).

To translate the upstream signal $[Ca^{2+}]_{cyt}$ elevations to downstream signaling events and responses, plants have several families of Ca^{2+} sensors. The most studied Ca^{2+} sensor families involved in the stomatal function are the Calcium Dependent

Protein Kinases (CDPKs or CPKs) and the Calcineurin-B Like Proteins (CBLs) together with their partners the CBL-Interacting Protein Kinases (CIPKs). From the 34 CDPK isoforms encoded by the Arabidopsis genome, 6 CDPKs have been identified with functions in guard cells positively regulating ABA signaling (Mori et al., 2006; Zhu et al., 2007; Geiger et al., 2010). CBL1 and CBL9 have been identified thus far as negative regulators of ABA signaling in guard cells by the synergistical activation of CIPK23 during the Ca^{2+}-dependent response. Double *cbl 1cbl9* and single *cipk23* mutants are hypersensitive to ABA during the stomatal movements (Cheong et al., 2007). It has been proposed that CIPK23, after its activation and recruitment to the plasma membrane by CBL1 and CBL9, activates an inward K^+ channel to promote stomatal opening. Loss-of-function *akt1* mutants present the same stomata phenotype than *cipk23* plants, thus AKT1 is the most likely target for this signaling pathway (Cheong et al., 2007; Nieves-Cordones et al., 2012).

I.2.3.3. Light sensing and signaling.

In plants, light quality and quantity is perceived by several photoreceptors, and stomatal function is regulated by both blue and red light (Shimazaki et al., 2007; Araujo et al., 2011). Blue light-induced stomatal opening is mediated by phototropins (PHOT1 and PHOT2) and cryptochromes (CRY1 and CRY2) (Mao et al., 2005). Phototropins are plant-specific Ser/Thr autophosphorylating kinases that are activated by blue light. Activated phototropins cause the phosphorylation of a Thr residue in the C-terminus of the plasma membrane H^+-ATPase provoking the binding of a 14-3-3 protein to the Thr residue and its subsequent activation (Kinoshita and Shimazaki, 1999; Emi et al., 2001; Kinoshita et al., 2001; Kinoshita et al., 2003). It has been demonstrated that the signaling between the phototropins and the H^+-ATPase is mediated by the protein phosphatase 1 (PP1) (Takemiya et al., 2006) indicating that probably ABA could be involved in the inhibition of this signaling pathway. By contrast, it has been proposed that guard cells respond indirectly to red light through a decrease of the intercellular CO_2 concentration in mesophyll cells (Roelfsema et al., 2002). Supporting this finding

guard cells in albino sections of variegated leaves do not respond to photosynthetically active radiation, but are sensitive to blue light and CO_2 (Roelfsema et al., 2006).

I.3. Plant NHX cation/proton antiporters.

I.3.1. Phylogeny and subcellular localization.

Cation/H^+ antiporters can be grouped into the CPA1 and CPA2 families (Saier et al., 1999). Proteins of the NHX group in plants and fungi belong to the intracellular NHE/NHX subfamily (IC-NHE/NHX) of the CPA1 family. These proteins, which are localized in intracelular membranes, can be found across all taxonomic groups of eukaryotes (Pardo et al., 2006; Rodriguez-Rosales et al., 2009). Plant NHXs can be divided into two main subgroups based on protein similarity and their subcellular localization. Arabidopsis class-I NHX members (AtNHX1-4) show a sequence homology of around 56-87% between them, while class-II members (AtNHX5-6) are 79% similar to each other. Class-I and class-II just share a 21-23% sequence similarity (Yokoi et al., 2002; Pardo et al., 2006). All NHX isoforms of class-I characterized to date are localized in the tonoplast and form a separate clade within the IC-NHE/NHX group that solely contains plant exchangers. On the contrary, class-II proteins are found in endosomal vesicles and other intracellular compartments in plants, animals and fungi (Pardo et al., 2006). In addition, the selectivity for ion substrate also distinguishes class-I and class-II exchangers. While the vacuolar members show similar Na^+/H^+ and K^+/H^+ exchange affinity (Venema et al., 2002; Apse et al., 2003; Barragán et al., 2012) the endosomal class-II proteins present a preference for K^+ over Na^+ as substrate (Venema et al., 2003).

I.3.2. Plant NHX protein structure.

Plant NHX exchangers are proteins of about 550 residues in length and present the typical transporter structure of 10-12 transmembrane domains with a hydrophilic C-terminal tail. To date, two different topological models have been proposed. They

will be described in section I.3.4 due to their implication in the possible mechanisms of antiporter regulation. The highest sequence homology among NHXs is found in the N-terminal part that forms the membrane pore. By contrast, the C-terminal domains sequences are more divergent (Pardo et al., 2006; Rodriguez-Rosales et al., 2009). In the animal NHE family the C-terminal domain regulates the ion translocation by the membranous region of the molecule. Hence, it is probably that variation in amino acid sequences reflects differential regulation of each isoform (Putney et al., 2002). The NHE/NHX proteins present the conserved domain of the CPA superfamily (Pfam00999) and also a small conserved stretch of 14 amino acids in the TM-4 segment, with the consensus FF(I/L) (Y/F)LFLLPPI. The drug amiloride and its derivates are able to bind to this conserved sequence and inhibit the activity of this family of exchangers (Putney et al., 2002; Brett et al., 2005a). Ion exchange by AtNHX1 was inhibited 70% by the amiloride analog ethylisopropylamiloride (Venema et al., 2002).

I.3.3. Plant NHX protein function.

Plant NHX protein activity were originally described as Na^+/H^+ exchangers at the vacuolar membrane of *Beta vulgaris* (Blumwald and Poole, 1985; Niemietz and Willenbrink, 1985). Early reports after isolation of the Arabidopsis *NHX1* genes further suggested that the encoded protein mediated Na^+/H^+ exchange in vacules (Apse et al., 1999). Because of that, historically the NHX antiporters have been considered salt tolerance determinants that control the accumulation of Na^+ into the cellular vacuole, and to prove this hypothesis many studies in different species have been conducted. Nevertheless, the results of these reports have been contradictory in many cases and the mechanisms through which NHXs improve the plants salt tolerance became a matter of controversy until recently, when it was demonstrated that Arabidopsis and tomato NHX proteins play essential physiological roles related with the accrual of K^+ into the vacuole (Rodríguez-Rosales et al., 2008; Leidi et al., 2010; Bassil et al., 2011a; Barragán et al., 2012). The roles ascribed to the NHX exchangers in salt tolerance, K^+ nutrition and pH regulation will be summarized in the next sections.

I.3.3.1. Salt tolerance.

Many plant species respond to salt stress mainly by excluding Na^+ from leaves and compartmentalizing Na^+ into the vacuole to avoid toxic concentrations within the cytoplasm (Munns and Tester, 2008). The sequestration of ions that are damaging to cellular metabolism (e.g. Na^+, Cl^-) into the vacuole while maintaining high K^+/Na^+ ratios in the cytosol provide the osmotic driving force necessary for water influx in saline environments and, at the same time, provided an efficient mechanism for ion detoxification. Hence, the storage of Na^+ inside leaf vacuoles has been suggested as a key mechanism to support growth during salt stress in most plant species (Maathuis and Amtmann, 1999; Pardo et al., 2006; Munns and Tester, 2008). The prevailing model until recently posited that NHX antiporters participate in these processes since the Na^+/H^+ antiport activity of these proteins and because the *NHX* gene expression in many plant species is induced when grown in saline environments (Rodriguez-Rosales et al., 2009). *AtNHX1* expression in mature Arabidopsis plants was shown to be upregulated in leaves but not in roots by ABA and NaCl (Quintero et al., 2000) while NaCl stress, hyper-osmotic stress and ABA induced *AtNHX1* and *AtNHX2* expression in seedlings. In addition, *AtNHX5* expression responded only to NaCl treatment (Yokoi et al., 2002). In expression pattern analyses using the AtNHX1 promoter fused to the GUS reporter gene, a higher GUS activity was obtained in response to salt stress in leaves and root hair cells (Shi and Zhu, 2002).

The role of NHX antiporters in ion accumulation and salt tolerance have been studied by overexpression or deletion of the genes, or by comparison of NHX gene expression and ion accumulation in closely related species that differ in salt tolerance (Rodriguez-Rosales et al., 2009). For instance, the salt-sensitive species *Plantago media* presented lower Na^+/H^+ antiporter activity under salt stress (50 mM NaCl) than its related salt-tolerant species *Plantago maritima* (Staal et al., 1991). The halophyte *Melilotus indicus*, which can grow up to 400 mM NaCl, accumulated less Na^+ and maintained higher levels of K^+ than its glycophytic relative *Medicago intertexta*. In this case, only the glycophytic species showed an induction of *NHX* expression under salt stress (Zahran et al., 2007).

Early studies showed that AtNHX1 T-DNA insertion mutants and tomato plants in which the antiporter LeNHX2 was silenced were more sensitive to salt stress (Rodríguez-Rosales et al., 2008). However, these reports could not explain the cause by which these mutants were more salt-sensitive due to lack of systematic data on ion accumulation. Furthermore, subsequent studies with *nhx1* and *nhx2* null single mutants did not show differences in salt tolerance compared to the wild-type line (Barragan, 2007; Bassil et al., 2011a; Barragán et al., 2012). Marginal differences in growth and in Na^+ and K^+ contents were observed between the single mutants and the wild-type, although *nhx1* and *nhx2* single mutants presented slight disturbances in germination and survival rate (Barragan, 2007).

Arabidopsis Class-II NHX5 and NHX6 seem to be functionally redundant proteins that localized to endosomal compartments associated with the TGN and Golgi. By a reverse genetic approach it has been observed that the double knockout *nhx5 nhx6* displays reduced growth, due to a smaller cell size and slowed cell proliferation, and salt sensitivity (Bassil et al., 2011b). The authors suggest that NHX5 and NHX6 could be involved in the pH regulation of the endosomal vesicles traveling from the Golgi/TGN to the vacuole. Thus, the lack of both antiporters may be affecting the sorting of vacuolar transporters necessary for Na^+ sequestration into the vacuole. In addition, nonfuntional Golgi/TGN may cause missorting of vesicles containing membrane and cell wall proteins essential for cell expansion, as well as affecting their pH-dependent posttranslational modifications (Bassil et al., 2011b).

In order to create salt-tolerant crops most of the studies have been focused in the ectopic overexpression of *NHX* genes in different species. However, the heterologuos expression approach presents several limitations. For instance, the expression of the heterologous *NHX* genes is no longer tissue-specific or stress-inducible. In addition, the cell machinery might be saturated due to the high overexpression, leading to altered cellular localization and inefficient regulation (Rodriguez-Rosales et al., 2009). For these reasons data obtained by *NHX* overexpression must be interpreted carefully. Most of the published reports on

overexpression of plant NHX isoforms in several plant species showed increased salt tolerance as improved plant survival and shoot growth over the control lines (Apse et al., 1999; Zhang and Blumwald, 2001; Zhang et al., 2001; Ohta et al., 2002; Fukuda et al., 2004; Wu et al., 2004; Li et al., 2006b; Brini et al., 2007; Liu et al., 2008; Rodríguez-Rosales et al., 2008; Zhang et al., 2008; Leidi et al., 2010; Li et al., 2011). Only one report stated that overexpression of AtNHX1 does not improve salt tolerance in transgenic Arabidopsis plants (Yang et al., 2009). In these reports salt tolerance is not always associated to the expected increment in vacuolar Na^+ accumulation, and all the combinations of changes in Na^+ and K^+ concentrations can be found in these reports in which the ion profiles were measured (e.g. higher Na^+ and lower K^+ (Apse et al., 1999); higher Na^+ and K^+ (Brini et al., 2007); higher K^+ and lower Na^+ (Rodríguez-Rosales et al., 2008; Leidi et al., 2010); only minimal differences between both ions and the control plants (Fukuda et al., 2004)). These studies demonstrate that differences in salt tolerance may be related to the regulation of NHX gene expression instead to protein efficiency since all NHX isoforms, nothwithstanding that they belong to Class-I or Class-II antiporters, present similar effects in salt tolerance.

Yeast have only one NHX isoform that belongs to the Class-II antiporters. The disruption of *ScNHX1* or the overexpression of plant antiporters in the yeast *nhx1* mutant also affects intracellular Na^+ and K^+ concentrations in yeast (Nass et al., 1997; Nass and Rao, 1998; Gaxiola et al., 1999; Quintero et al., 2000; Venema et al., 2003). Yeast cells have two different Na^+ efflux systems at the plasma membrane, the NHA1 exchanger and the Na^+-ATPases ENA1-4. Deletion of these genes causes salt sensitivity to the cells (Prior et al., 1996; Nass et al., 1997; Bañuelos et al., 1998). Disruption of *ScNHX1* in the former mutant background further decreases the Na^+ tolerance in yeast by slightly decreasing the intracellular Na^+ content and, notably, by producing a great diminution of internal K^+ (Nass et al., 1997; Quintero et al., 2000; Venema et al., 2003). Overexpression of AtNHX1 and AtNHX2 isoforms in an *ena1-4 nha1 nhx1* mutant yeast strain strongly increases intracellular K^+ and Na^+ while the overexpression of Class-II antiporters AtNHX5 and LeNHX2 increases intracellular K^+ while reducing intracellular Na^+ (Yokoi et al., 2002; Venema et al., 2003). Also, plant V-PPase (AVP1) overexpressed in yeast in association with ScNHX1 increased salt tolerance, increased K^+ contents,

and reduced intracellular Na$^+$ levels (Gaxiola et al., 1999). In addition, it has been observed that *NHX* genes are alike induced by NaCl, KCl or osmotic treatments, and that plant and yeast antiporters also confer tolerance to high KCl or hyper-osmotic shock in yeast cells (Gaxiola et al., 1999; Nass and Rao, 1999; Yokoi et al., 2002; Fukuda et al., 2004). All these observations together suggest that the mechanisms by which NHX antiporters confers salt tolerance seems to be more complex than the simple Na$^+$ accumulation into the vacuole to avoid Na$^+$ toxicity in the cytosol. According to these data, the role of these proteins in relation to salt tolerance would be mainly related to maintaining the cellular K$^+$ homeostasis.

I.3.3.2. K$^+$ nutrition.

Transgenic tomato plants overexpressing *AtNHX1* showed larger K$^+$ vacuolar pools in all growth conditions tested while their accumulation of Na$^+$ was not increased under salt stress. Indeed, these plants showed toxicity symptoms only under K$^+$-limiting conditions due to an enhanced K$^+$ compartmentation in the vacuole that occurred at the expense of the cytosolic K$^+$ pool, which was lower in transgenic tomato plants. The decreased cytoplasmic K$^+$ concentrations triggered a K$^+$-starvation response leading to higher K$^+$ uptake at the root. Hence, the capacity of transgenic tomato plants to retain intracellular K$^+$ makes them more tolerant to a salt-shock (Leidi et al., 2010). The same situation has been previously reported for Arabidopsis transgenic plants overexpressing the tomato Class-II antiporter LeNHX2 (Rodríguez-Rosales et al., 2008).

Recently, two independent reports performed with the Arabidopsis *nhx1* and *nhx2* double mutants ruled out the involvement of these antiporters in Na$^+$ accrual into the vacuole while they demonstrated that these functionally redundant proteins are essential in K$^+$ nutrition and homeostasis (Bassil et al., 2011a; Barragán et al., 2012). These mutants, that show stunted growth, are very sensitive to increasing K$^+$ concentrations in the growth media (Bassil et al., 2011a; Barragán et al., 2012). Among the phenotypic traits, these mutant plants present impaired flower development and

low fertility (Bassil et al., 2011a). In addition, *nhx1 nhx2* double mutants show a reduced water content, leaf turgor, and impaired stomatal regulation (Barragán et al., 2012). All these symptoms are linked to the fundamental role that intracellular K^+ plays as osmoticum (Mengel et al., 2001; White and Karley, 2010). Indeed, K^+ concentration analysed in leaf sap extracts and expressed on dry weight basis (i.e., percentage of content) showed a significantly lower K^+ concetrations in shoots of *nhx1 nhx2* double mutants in plants growing at various K^+ regimenes (Barragán et al., 2012). Furthermore, a great reduction in the vacuolar K^+ pool in different cell types was found by SEM-EDX measurements (Barragán et al., 2012) and by using a ratiometric K^+-sensitive dye (Bassil et al., 2011a). Albeit both Na^+/H^+ and K^+/H^+ antiporter activities were reduced in tonoplast vesicles isolated from double mutant leaves, the plants were not more sensitive to salt stress than the wild type. In fact, non-toxic Na^+ concentrations in the media improved growth, and mutant plants accumulated more Na^+ in the shoot than the wild type (Barragán et al., 2012). Together, these results indicate that NHX1 and NHX2 are resposible for the accrual of K^+ into the vacuole where it fulfils osmotic roles involved in physiological processes such as cell expansion and stomatal movements. The enhance Na^+ accumuation observed in the *nhx1 nhx2* mutant implyes that there must exist other systems involved in Na^+ uptake into the vacuole (Bassil et al., 2011a; Barragán et al., 2012).

Other results pointing out to a role for AtNHX1 in K^+ homeostasis are the enhanced expression of the high affinity K^+ uptake system KUP7/HAK7 and decreased expression of AtKEA4 in DNA array analysis of the *nhx1* null mutant (Sottosanto et al., 2004). Also, the high expression of NHX isoforms in known sinks for K^+, like guard cells (Shi and Zhu, 2002; Barragán et al., 2012), reproductive organs (Wang et al., 2007) and fruits (Hanana et al., 2007), furhter support the involvement of NHX proteins in K^+ homeostasis. Moreover, the activity of the ItNHX1 exchanger of *Ipomoea tricolor* coupled with V-ATPase, V-PPase and PM-ATPase activity induced not only a shift in vacuolar pH changing the petal color but also synchronised the uptake of K^+ into the vacuole to drive petal expansion and flower opening (Yoshida et al., 2005; Yoshida et al., 2009).

I.3.3.3. pH regulation.

Cellular pH homeostasis is a key factor for proper cellular function. Most metabolic and enzymatic processes are dependent on specific pH conditions, due both to the regulation of protein structure and function. Also, a pH gradient along the secretory pathway is important for protein modification and sorting. Proton gradients across the cellular membranes are required for active transport processes. Moreover, it has been postulated that a change in pH could act as signal (Pittman, 2012).

Involvement of plant NHX genes in vacuolar pH regulation has been extensively illustrated by the flower colour transition in *Ipomoea spp*. The colour change in flowers of *Ipomea tricolor* cv heavenly blue from red-purple to blue as the flower matures is driven by a vacuolar pH increase from 6.6 to 7.7 during flower opening, as pH determines the colour of anthocyanins inside the vacuole (Yoshida et al., 1995; Fukada-Tanaka et al., 2000; Yoshida et al., 2005). Insertion of a transposable element in the *Ipomoea nil NHX1* gene partly abolished the vacuolar pH change and flower color transition (Fukada-Tanaka et al., 2000; Yamaguchi et al., 2001). Recently, Bassil et al. (2011) demonstrated, using a ratiometric fluorescein-based pH sensitive dye, that Arabidopsis *nhx1 nhx2* root cell vacuoles are more acidic than in the wild type (Bassil et al., 2011a). Nevertheless, more investigation is needed to unravel the role of plant NHX antiporters in pH regulation.

By contrast, involvement of yeast ScNHX1 in pH homeostasis is well established. Deletion of *ScNHX1* renders the yeast cells sensitive to low pH and they show more acidic cytoplasmic and vacuolar pH (Brett et al., 2005b). Cytoplasmic acidosis linked to a reduction in activity of the yeast plasma membrane H^+-ATPase (PMA1) is thought to activate ScNHX1, thus increasing Na^+ uptake (Nass et al., 1997). In yeast, pH regulation through ScNHX1 fulfils numerous functions. On one hand, *nhx1* yeast cells show a "class E" vacuolar protein sorting (VPS) phenotype characterized by missorting of vacuolar carboxypeptidase Y (CPY) to the cell surface, late endosomal enlargement, and accumulation in endosomes of the G protein coupled receptor Ste3 or the dye FM4-64 that are delivered to the vacuole in wild-type cells (Bowers et al.,

2000; Bonangelino et al., 2002; Brett et al., 2005b). In addition, disruption of ScNHX1/VPS44 produces strong sensitivity to the drug hygromycin B that is detoxified at the vacuole, suggesting that the VPS phenotype is dependent on defective vacular biogenesis (Gaxiola et al., 1999; Bowers et al., 2000; Mukherjee et al., 2006). Addition of weak bases can suppress the VPS phenotype in *nhx1* null mutants indicating that ScNHX1-dependent endosomal alkalinisation is essential for vesicle trafficking in yeast (Mukherjee et al., 2006). ScNHX1 is localized in several endomembrane compartments such as vacuoles (Qiu and Fratti, 2010), trans-Golgi/TGN compartments, early and late endosomes in the biosynthetic, endocytic, and recycling pathways (Kojima et al., 2012) and also in the multivesicular bodies (MVBs) (Mitsui et al., 2011). ScNHX1 regulates the pH in all these compartments throught its ion exchange activity. For instance, ScNHX1 carrying point mutations in conserved acidic residues required for ion transport are not able to rescue yeast vacuolar fusion in a *nhx1Δ* mutant background (Qiu and Fratti, 2010). It is likely that such a fundamental role in pH regulation depend on the more physiologically relevant K^+ instead of the toxic ion Na^+ (Rodriguez-Rosales et al., 2009).

Both Class-I and Class-II plant NHX exchangers complement the NaCl, KCl and hygromycin sensitivity exhibited by the yeast *nhx1* disruption mutant (Quintero et al., 2000; Yokoi et al., 2002; Rodríguez-Rosales et al., 2008; Barragán et al., 2012). AtNHX1 has also been shown to suppress the VPS phenotype of *nhx1* null mutant (Hernandez et al., 2009). Thus, a role for plant NHX proteins in endosomal pH regulation and protein trafficking has been suggested, particularly for Class-II antiporters that are more closely related to yeast NHX1 (Rodriguez-Rosales et al., 2009; Bassil et al., 2011b). Still, Class-I antiporters could play a role in intracellular vesicle trafficking since DNA array analysis of the Arabidopsis *nhx1* null mutant showed expression changes in several genes encoding proteins implicated in vesicular trafficking (Sottosanto et al., 2004).

I.3.4. NHX regulation.

Although NHX proteins have been extensively studied in relation with their role in abiotic stress tolerance and plant nutrition, little is known about the signaling pathways that regulate the expression and function of NHX antiporters to regulate those processes. In animal NHE proteins, the C-terminal domain play a major role in the control of the transport activity by phosphorylation and interaction with regulatory proteins. NHE proteins interact with the Ca^{2+}-binding proteins calmodulin and CHP (calcineurin B homologous), thereby changing the affinity of the pore domain for intracellular protons (Putney et al., 2002). A similar regulatory mechanisms may operate in plant NHX antiporters. It has been reported that Arabidopsis NHX1, through its C-terminal domain, interacts with the calmodulin-like protein AtCaM15 (Yamaguchi et al., 2005). Upon binding of AtCaM15 , the antiporter reduces the rate of Na^+/H^+ but not of K^+/H^+ exchange, leading to a 46% decrease in the Na^+/K^+ selectivity ratio. This interaction is Ca^{2+}- and acidic pH-dependent (Yamaguchi et al., 2005). This study also suggested that the interaction of both proteins takes place inside the vacuolar lumen since the AtCaM15 appeared to be a vacuolar protein (Yamaguchi et al., 2005). However, the topology of AtNHX1 is still a matter of discussion. Yamaguchi et al. (2003) described that the AtNHX1 transmembrane domains (TMs) closer to the C-terminus would have the opposite orientation relative to the corresponding TMs of human NHE. Thus, the AtNHX1 C-terminal domain would be inside the vacuolar lumen instead at the cytosol as in the animal NHEs (Yamaguchi et al., 2003). However, other studies localized the AtNHX1 C-terminal domain at the cytosolic side (Sato and Sakaguchi, 2005; Hamaji et al., 2009). Sato and Sakaguchi (2005) posit that the first TM of AtNHX1 should be considered equivalent to the second TM of animal NHEs, thus discrediting the work by Yamaguchi et al. (2003). Morevoer, Hamaji et al. (2009) showed that the C-terminus of AtNHX1 was on the cytoslic side of the tonoplast by combining immunofluorescence staining with antibodies against AtNHX1 and proteinase K assays in isolated vacuoles. Several phosphoproteomic analyses of tonoplast proteins have identified phosphopeptides derived from the C-termini of NHX proteins of different species: Arabidopsis, (Sugiyama et al., 2008; Whiteman et al., 2008b); barley, (Endler et al., 2009); rice, (Whiteman et al., 2008a). This is additional

evidence supporting the cytosolic localization of the NHX C-terminal domain since ATP, as the substrate of protein kinases, has not been so far detected inside the vacuole (Farré et al., 2001; Endler et al., 2009). The protein kinases that phosphorylate the cytosolic C-termini of NHX proteins remain unknown to date. It has been reported that the NHX activity is regulated by SOS2(CIPK24) in a process that does not involve CBL4/SOS3(CBL4) and direct protein phosphorylation (Qiu et al., 2004). The tonoplast Na^+/H^+ exchange activity is significantly higher, greatly reduced, and unchanged in *sos1*, *sos2*, and *CBL4/SOS3* mutants respectively compared to the wild type. Moreover, the addition of a recombinant SOS2 protein to endosomal vesicles isolated from *sos2* plants increased the tonoplast Na^+/H^+ exchange activity (Qiu et al., 2004), although AtNHX1 phosphorylation by SOS2 was not observed. On the other hand, it has been demonstrated that SOS2 is able to stimulate the tonoplast ion exchange activity without *in vitro* protein phosphorylation through direct protein-protein interaction as is the case of CAX1 (Cheng et al., 2004) and the V-ATPase (Batelli et al., 2007). Hence, SOS2 could stimulate the NHX activity by direct protein-protein interaction, or indirectly by increasing the H^+ gradient across the tonoplast through the regulation of V-ATPase activity (Pardo and Rubio Muñoz, 2011).

III. OBJECTIVES

Considering the background exposed along the Introduction section, it is obvious the importance of K^+ not only as a macronutrient and the major ionic osmoticum in plant cells but also as an essential element involved in processes that require ion, electric potential, pH and osmotic fast changes. Stomatal aperture and closure are the paradigm of these kind of processes since are completely dependent of such K^+ movements between the apoplast and the cytosol and between the cytosol and the vacuole. As new insights about the mechanisms involved in the accumulation of K^+ into the vacuole, attributing a relevant role to cation/H^+ transporters NHX1 and NHX2 have been recently obtained, and taking the previous knowledge as starting point, this work aims to three different but related objectives:

1. Unravel the role of the proteins AtNHX1 and AtNHX2 in the cellular K^+ homeostasis.

2. Study the involvement of both antiporters in the stomatal function.

3. Investigate the posttranslational regulation of AtNHX1 and AtNHX2, particularly in relation to the importance of the phosphorylation of their C-terminal domains and search for protein-kinases interactor candidates, mainly among the members of the CIPK family.

To achieve these objectives, reverse genetic, molecular biology, plant physiology and cell biology analyses will be carried out. The well-known model organisms *Arabidopsis thaliana* and *Saccharomyces cerevisiae* will be used.

IV. MATERIALS AND METHODS

M.1. Biological material.

M.1.1. Bacteria.

Escherichia coli.

The following *E. coli* strains were used for plasmid propagation:

Strain	Genotype	Reference
One Shot® TOP10	F-, *mcrA*, (*mrr-hsd*RMS-*mcr*BC), 80*lac*ZM15, *lac*X74, *recA1*, *ara139*, (*ara-leu*)7697, *galU*, *galK*, *rpsL*, (*Str*^{R}), *endA1*, *nupG*>	Invitrogen™ Life Technologies.
BNN132	*E. coli* JM107 (λKC). *endA1*, *gyrA96*, *thi*, *hsdR17*, *supR44*, *relA1*, Δ(*lac-proAB*), (F′, *traD36*, *proAB$^+$*, *lacI^{α}lac*ZAM15)	([Yanisch-Perron et al., 1985](#))

Agrobacterium tumefaciens

Agrobacterium tumefaciens was used for transient expression in *Nicotiana benthamiana* and for stable transformation of *Arabidopsis thaliana*.

Strain	Genotype	Reference
GV3101	Rif^R, pMP90 (pTiC58DT-DNA)	([Koncz and Schell, 1986](#))
p19	pBin61-p35S:p19	([Voinnet et al., 2003](#))

M.1.1.2. Bacterial culture media and growth conditions.

Escherichia coli.

Escherichia coli strains were cultivated in Luria-Bertani medium (LB). When needed, ampicillin at 0.1 g/L, kanamycin at 0.05 g/L or streptomycin at 0.025 g/L were added into the cultures. Unless otherwise stated, *E. coli* strains were grown at 37°C.

LB medium:

Bacto^{TM} yeast extract (Difco)	0.5% (w/v)
Bacto^{TM} tryptone (Difco)	1% (w/v)
KCl	1% (w/v)

For preparing solid LB medium 1.5% (w/v) of Bacto^{TM} Agar (Difco) were added.

Super Optimal Broth medium (SOB) and Super Optimal broth with Catabolite repression medium (SOC) were used for growth and preparation of *E. coli* competent cells.

SOB medium:

Bacto^{TM} tryptone (Difco)	2% (w/v)
Bacto^{TM} yeast extract (Difco)	0.5% (w/v)
NaCl	10 mM
KCl	2.5 mM

SOC medium:

Bacto™ tryptone (Difco)	2% (w/v)
Bacto™ yeast extract (Difco)	0.5% (w/v)
NaCl	10 mM
KCl	2.5 mM
$MgCl_2$	10 mM
$MgSO_4$	10 mM
Glucose	20 mM

Agrobacterium tumefaciens.

Yeast Extract Peptone medium (YEP) was used for Agrobacterium growth. When needed, rifampicin at 0.05 g/L, gentamicin at 0.02 g/L or kanamycin at 0.05 g/L were added into the cultures. Unless otherwise stated, *A. tumefaciens* strains were grown at 30°C.

YEP medium:

Bacto™ yeast extract (Difco)	1% (w/v)
Bacto™ peptone (Difco)	1% (w/v)
KCl	0.5% (w/v)

For preparing solid YEP medium 1.5% (w/v) of Bacto™ Agar (Difco) were added.

M.1.2. Yeast.

M.1.2.1. Yeast strains.

Strain	Genotype	Use	Reference
AXT3K	*MATα, Δena1::HIS3::ena4, nha1::LEU2, nhx1::KanMX, ura3-1, trp1, ade2-1, can1-100*	**Functional studies of AtNHX proteins**	(Quintero et al., 2002)
GRF167	*MATα, ura3, his3, GAL+*	**Expression and purification of chimaeric proteins**	(Curcio and Garfinkel, 1991)
JPZN1	*MATα, Δena1::HIS3::ena4, nha1::LEU2, nhx1::KanMX, pma1::AtNHX1, ura3-1, trp1, ade2-1, can1-100*	**Functional studies of AtNHX1 in yeast.**	(Present work)
JPZN2	*MATα, Δena1::HIS3::ena4 , nha1::LEU2, nhx1::KanMX, pma1::AtNHX1, ura3-1, trp1, ade2-1, can1-100*	**Functional studies of AtNHX2 in yeast.**	(Present work)
AH109	*MATa, trp1-901, leu2-3, 112, ura3-52, his3-200, gal4Δ, gal80Δ, LYS2::GAL1$_{UAS}$GAL1$_{TATA}$-HIS3, GAL2$_{UAS}$-GAL2$_{TATA}$-ADE2, URA3::MEL1$_{UAS}$-MEL1$_{TATA}$-lacZ*	**Yeast two-hybrid**	(Clontech Laboratories, Mountain View, California, USA)

M.1.2.2. Yeast culture media and growth conditions.

Yeast manipulation techniques and growth conditions were performed as described in ([Guthrie and Fink, 1991]) and ([Ausubel et al., 1996]). Unless otherwise stated, yeast were grown at 28°C.

For routine growth and propagation of yeast cells YPD medium was used.

YPD medium:

Bacto^{TM} yeast extract (Difco)	1 % (w/v)
Bacto^{TM} peptone (Difco)	2 % (w/v)
Glucose	2 % (w/v)

For preparing solid YPD medium 2% (w/v) of Bacto^{TM} Agar (Difco) was added.

The minimal YNB medium media lacking the appropriate aminoacids, according to the strain genotype, was used as selective medium.

YNB medium:

Yeast nitrogen base w/o aminoacids	0.17% (w/v)
$(NH_4)_2SO_4$	0.5% (w/v)
Glucose	2% (w/v)

For preparing solid YNB medium 2% (w/v) of bactoagar (Difco) was added, and pH was adjusted at 6.5 with NaOH.

For yeast two-hybrid assays (section M.14.1.) an YNB medium with a modified amino acid dropout solution was prepared.

Modified 10X Dropout solution:

L-Isoleucine	300 mg/L
L-Valine	1500 mg/L
L-Adenine hemisulfate salt	200 mg/L
L-Arginine HCl	200 mg/L
L-Histidine HCl monohydrate	200 mg/L
L-Leucine	1000 mg/L
L-Lysine HCl	300 mg/L
L-Methionine	200 mg/L
L-Phenylalanine	500 mg/L
L-Threonine	2000 mg/L
L-Tryptophan	200 mg/L
L-Tyrosine	300 mg/L
L-Uracil	200 mg/L

For salt tolerance assays (section M.15.) the alkali cation-free AP medium was used (Rodriguez-Navarro and Ramos, 1984).

AP medium:

PO_4H_3	8 mM
L-arginine	10 mM
SO_4Mg	2 mM
Cl_2Ca	0.2 mM
KCl	1 mM
Glucose	2 % (w/v)
Trace elements (100X stock)	1 % (v/v)
Vitamins	1% (v/v)

pH was brought to 6.5 with L-arginine. NaCl was added as required.

Trace elements 100X stock:

H_3BO_3	50 mg/L
$CuSO_4$	4 mg/L
KI	10 mg/L
Fe_3Cl	20 mg/L
$MnSO_4.H_2O$	40 mg/L
$Na_2MoO_4.2H_2O$	20 mg/L
$ZnSO_4 .7H_2O$	4 mg/L

To avoid stock contamination, several chloroform drops were added.

Vitamins stock:

Biotin	1mL (0.2 mg/mL in ethanol)/100 mL
Nicotinic acid	4 mg/100 mL
Pyridoxine	4 mg/100 mL
Thiamine	4 mg/100 mL
Panthotenic acid	4 mg/100 mL

Vitamins solution was sterilized by filtration, and added to the autoclaved medium.

M.1.3. Plant material.

M.1.3.1. Plant species.

***Arabidopsis thaliana*.**

For the experiments where insertional T-DNA mutants in AtNHX1 and AtNHX2 genes were studied the following Arabidopsis lines were used:

Line	Source
Col-0	*Arabidopsis* Biological Resource Center (ABRC, Ohio State University, Ohio, EE.UU).
SALK_065623 (*Atnhx1-2*)	SALK Institute, San Diego CA, EE.UU.
SALK_034001 (*Atnhx1-1*)	SALK Institute, San Diego CA, EE.UU.
SALK_036114 (*Atnhx2-1*)	SALK Institute, San Diego CA, EE.UU.
L14	*Atnhx1-1 Atnhx2-1.*
KO	*Atnhx1-2 Atnhx2-1.*

***Nicotiana benthamiana*.**

Nicotiana benthamina was used for Agrobacterium mediated transient protein expression.

M.1.3.2. *Arabidopsis thaliana* growth conditions.

Plant media.

Murashige & Skoog medium (MS) ([Murashige and Skoog, 1962](#)).

Macronutrients (mM)		Micronutrients (µM)	
NH_4NO_3	20.6	H_3BO_3	100
KNO_3	18.5	$FeSO_4 .7H_2O$	100
$CaCl_2 .2H_2O$	3.0	$MnSO_4.H_2O$	100
$MgSO_4.7H_2O$	1.5	EDTA- Na_2	100
KH_2PO_4	1.2	$ZnSO_4 .7H_2O$	30
		KI	5
		$Na_2MoO_4.2H_2O$	1
		$CoCl_2 .6H_2O$	0.1
		$CuSO_4.5H_2O$	0.1

The medium solution was supplemented with 30 g/L of sucrose and buffered with MES 2.5 mM, pH was brough at 5.7 with KOH. MS solid plates were prepared by adding 0.8-1% (w/v) of bactoagar (Difco). For selection of transgenic Arabidopsis lines, kanamycin or hygromycin was added to a final concentration of 50 mg/L or 20 mg/L respectively.

LAK solution ([Barragán et al., 2012](#)):

Macronutrients (mM)		Micronutrients (µM)	
KH_2PO_4	1	H_3BO_3	30
$Ca(NO_3)_2$	2	$MnSO_4$	10
$MgSO_4$	1	$ZnSO_4$	1
		$CuSO_4$	1
		$(NH_4)_6Mo_7O_{24}$	0.03
		Fe^{2+} as *Sequestrene* 138-Fe	100

Solution was prepared with deionized water and pH was adjusted to 5.3 with KOH. In experiments with higher K^+ levels (10 and 20 mM), supplemental K^+ was added as K_2SO_4. For low (<1 mM) K medium, KH_2PO_4 was replaced by NaH_2PO_4 and K^+ was added as K_2SO_4.

M.1.3.2.1. *In vitro* plant growth conditions.

Unless otherwise indicated, plant materials were handled in a Telstar A-H laminar flow cabinet, to guarantee sterility. Mediums and solutions were sterilized by autoclaving at 120°C and 2 atm for 20 minutes. Scalpels, tweezers and needles were sterilized by heat and ethanol.

Seeds sterilization.

Seeds were surface sterilized, first immersed in 70% ethanol for two minutes, followed by a 5-minute soak in sodium hypochlorite 70%. Finally, seeds were rinsed five times with sterile deionized water. To synchronize germination, seeds were stratified at 4°C in the dark for 2-4 days prior to sowing.

M.1.3.2.2. Plant growth conditions on soil.

Seeds of *Arabidopsis thaliana* were sowed on pots with Compo® Sana Universal substrate in a Sanyo MLR-351 plant growth chamber under short day regime: 8h day/16h night, 23/19°C, 60-70% relative humidity, and 250µmol m^{-2} s^{-1} photosynthetically active radiation (PAR).

For routine plant propagation, plants grown in soil were potted in Compo® Sana Universal substrate in a greenhouse under ambient light conditions supplemented with 16 hours per day illumitation with a sodium lamp light.

Seeds harvesting and conservation.

Commercial Aracons^{TM} seed collectors (Arasystem-Betatech, Gent, Belgium) were placed soon after bolting. After pots were allowed to dry, harvesting was carried out by carefully cutting off the inflorescences over the cone device and placing the Aracon content directly onto a stainless steel tea strainer. After threshing, seeds were kept in Eppendorf tubes inside hermetic containers with Chameleon® silica gel (VWR International) at room temperature.

M.1.3.2.3. Plant hydroponic culture.

Seeds of *Arabidopsis thaliana* were stratified for 2-4 days at 4°C and then germinated at room temperature in 1.5 mL bottomless Eppendorf tubes half filled with rockwool imbibed in distilled water. Seedlings in Eppendorf tubes were transferred to 8-liter plastic containers for hydroponic culture. A modified Long Ashton mineral solution with 1 mM K$^+$ and nominally free of Na$^+$ and NH$_4^+$ (LAK solution) (Barragán et al., 2012) was used as base solution for hydroponic cultures. Hydroponic tanks were maintained in a controlled growth chamber with the day/night regime: 25/20 ±2°C, 40/60% relative humidity, 14/20 h illumination, and 250 µmol m^{-2} s^{-1} photosynthetically active radiation (PAR). Every week the solution was renewed. An

aquarium air pump was connected to the tank to provide adequate aireation to the nutrition solution.

M.1.3.3. *Nicotiana benthamiana* growth conditions.

Nicotiana benthamiana plants were grown in Compo® Sana Universal substrate at 25°C and 70% humidity under a 16-h photoperiod and an 8-h dark period in environmentally controlled growth chambers.

M.2. DNA analysis and purification.

M.2.1. DNA purification.

M.2.1.1. Bacteria.

Plasmid mini-preparations ("Minipreps").

The small scale isolation of plasmidic DNA from *E. coli* and *A. tumefaciens* for subsequent analysis was performed according to Sambrook et al. (1989). One single colony was inoculated in 3 mL of LB liquid medium containing the appropriate antibiotic and was incubated overnight al 37°C with continous shaking. Eppendorf tubes containing 1.5 mL culture aliquot were centrifuged at 13,000 rpm for 1 min. The supernatant was discarded and cells were resuspended in 100 μL of Solution I/GTE. Then, 200 μL of Solution II was added and the mixture was inverted gently 6-8 times and incubated 2-3 minutes in ice. 150 μL of Solution III was added and mixed by inversion and incubated 20 minutes in ice. The mixture was centrifuged at 13,000 rpm for 10 min, the supernatant was transferred into a new Eppendorf tube and 1 mL of ethanol 100% was added. The mixture was incubated 10 minutes in ice and centrifuged again. The pellet was resuspended in 100 μL of Solution IV and 200 μL of

ethanol 100% were added. Mixtures were incubated 10 min in ice and centrifuged at 13,000 rpm for 10 minutes. Pellet was dried and resuspended in 30 μL of T:E (1:10).

Solution I/GTE:

Tris	25 mM
EDTA pH 8	10 mM
Glucose	1% (w/v)

Solution II:

NaOH	0.2 N
SDS	10%

Solution III:

AcNa pH 4.8	3 M

Solution IV:

AcNa pH 4.8	60 mM
Tris-HCl pH 8	30 mM

For sequencing reactions (section M.3.7.) and electroporation (section M.6.1.) the NucleoSpin® Plasmid Kit from Macherey-Nagel (Düren, Germany) was used, following the manufacturer's specifications.

Plasmid maxi-preparations ("Maxipreps").

A colony of *E. coli*, containing the plasmid of interest, was inoculated in 100 mL of LB medium and grown o/n at 37°C with shaking. Culture was centrifuged at 5,000 rpm for 10 min. Cell pellet was resuspended with 5 mL of GTE buffer and 0.1 mL of 5% (w/v) lysozime (Sigma) was added. The suspension was incubated 10 min in ice. Afterwards, 10 mL of freshly prepared solution II was added and mixed by gentle inversion (8-10 times). The mixture was incubated 10 min in ice. 7.5 mL of AcK 3M pH 4.8 was added before incubating the mixture 30-60 minutes in ice to precipitate SDS, proteins and chromosomic DNA. The mixture was centrifuged at 15,000 rpm for 15 minutes at 4°C. Supernatant was filtrated using Miracloth (Calbiochem) and collected it in a new tube. DNA was precipitated with 15 mL of isopropanol and incubated 20 min in ice. Then, DNA was spinned at 10,000 rpm for 10 min at 4°C. Isopropanol was removed and the pellet resuspended, by vortexing, in 2.5 mL of T:E (1:10) pH 8. To purify the plasmid 2.5 mL of LiCl 6 M were added and the mix incubated 15 min in ice. The RNA precipitate was centrifuged at 10,000 rpm for 10 minutes and the supernatant was placed in a new tube where 5 mL of isopropanol were added before incubating for 20 min in ice. Plasmidic DNA was spinned again at 10,000 rpm for 10 min and the pellet resuspended with 0.75 mL of T:E (1:10) pH 8. Liquid was placed in a 2 mL Eppendorf tube. It was incubated 15 min at 37°C after the addition of 10 µL of 1% (v/v) RNAse. Afterward, 0.75 mL of phenol:chloroform:isoamyl alcohol (25:24:1) were added and the mixture vortexed 20 seconds and centrifuged at 13,000 rpm for 10 s. The aqueous phase was placed in a new tube, this step was repeated once more and then the aqueous phase placed in a fresh 2 mL Eppendorf tube where 75 µL of AcNa 3 M and 0.75 mL of isopropanol were added. The mixture was incubated 20 min in ice and then centrifuged at 13,000 rpm for 10 min. Isopropanol was discarted and the pellet dissolved in 0.2 mL of T:E (1:10) pH 8. Plasmid was precipitated with 0.7 mL of absolut ethanol:ammonium acetate 7.5 M (6:1) and incubated 10 min in ice. The mix was spinned and the pellet washed with 1 mL of 70% ethanol. Plasmidic DNA was dried and dissolved in 0.2 mL of T:E (1:10) pH 8.

M.2.1.2. Yeast.

Plasmidic DNA.

To extract plasmidic DNA from yeast one colony was inoculated in 10 mL of selective medium YNB and it was incubated at 30°C o/n with shaking. The culture was centrifuged at 5,000 rpm for 5 minutes. Cells were resuspended in 0.5 mL of sorbitol 1 M: EDTA 0.1 M pH 7.5 and placed in a 2 mL eppendorf tube. To lysate yeast cells 20 μl of lyticase (5 mg/mL in KH_2PO_4 pH 7.5) were added and the mixture was incubated at 37°C for 1 h. Afterwards the mixture was centrifuged at 13,000 rpm and the pellet was resuspended in 0.5 mL of Tris 50 mM pH 7.4: EDTA 20 mM. 0.2 mL of AcK 5 M were added before incubating for 1h in ice. The supernatant was placed in a new tube after centrifugation at 13,000 rpm for 5 minutes. To precipitate the DNA 1 volume of isopropanol was mixed with the supernatant and it was incubated 5 minutes at room temperature. After centrifugation at 13,000 rpm for 1 minute the pellet was dried and resuspended in TE buffer (10:1).

Genomic DNA.

To extract genomic DNA from yeast one colony was inoculated in 5 mL of YPD medium and it was incubated at 30°C o/n with shaking. The culture was centrifuged at 5,000 rpm for 5 minutes. Cells were resuspended in 0.5 mL of sorbitol 1 M: EDTA 0.1 M pH:7.5 and placed in a 2 mL eppendorf tube. To lysate yeast cells 20 μl of lyticase (5 mg/mL in KH_2PO_4 pH:7.5) were added and the mixture was incubated at 37°C for 1 h in gently shaking. Afterwards the mixture was centrifuged at 13,000 rpm and the pellet was resuspended in 0.5 mL of Tris 50 mM pH 7.4 : EDTA 20 mM. 50 μL of SDS 10% were added and the mixture was heated at 65°C for 30 min. Then, 0.2 mL of AcK 3 M were added and the sample was incubated 1 hour in ice and centrifuged at 10,000 rpm for 5 minutes. The supernatant was transferred to a new Eppendorf tube and 1 volume of isopropanol was added before centrifugation at 10,000 rpm for 10 seconds. The pellet was dried and resuspended in 0.5 mL Tris 50 mM pH 7.4 : EDTA 20 mM. The suspension was treated with RNAse at 37°C for 15 min. The sample was centrifuged at

10,000 rpm for 15 min and then the supernatant was placed in a new Eppendorf tube where 1 volume of isopropanol and 1/10 volume of AcNa 3M were added. After incubating for 5 min at room temperature, the mixture was centrifuged at 10,000 rpm for 10 seconds. The pellet was dried and diluted in 50 µL of T:E (10:1) pH 7.4.

M.2.1.3. Arabidopsis thaliana.

Isolation of Arabidopsis DNA was performed according to (Edwards et al., 1991) with modifications. Around 100 mg of fresh tissue, previously frozen with liquid nitrogen, were macerated with a plastic piston. 400 µl of extraction buffer (140 mM d-sorbitol, 220 mM Tris-HCl pH:8, 22 mM EDTA-Na2 pH:8, 800 mM NaCl, 0.8% (w/v) CTAB, 1% (w/v) n-Lauroylsarcosine) heated to 65°C and 400 µl of chloroform were added to the sample that was vortexed and heated for 5 minutes at 65°C. The cellular debris was removed by centrifugation at 13,000 rpm for 10 minutes and the supernatant transferred to a fresh Eppendorf tube. This supernatant was mixed with 1 volume of isopropanol and left at room temperature for 20 minutes, then centrifuged at 13,000 rpm for 15 minutes. The pellet was washed with ethanol 70% (v/v), air dried and dissolved in 50µl of milliQ sterile water.

M.2.2. DNA quantification.

DNA concentration was quantified using the spectrophotometer NanoDrop® ND-1000 Spectrophotometer (Thermo Fisher Scientific Inc.).

M.2.3. DNA electrophoresis in agarose gels.

Agarose gels for the electrophoresis of DNA contained 0.7-1% (w/v) agarose melted in 1x TAE buffer (40 mM Tris-acetate, 20 mM sodium acetate, 2 mM EDTA. pH 8.2). Electrophoresis was performed in 1x TAE buffer, supplemented with 0.5 µg/mL ethidium bromide, between 70-120 V. After electrophoresis the gel was photographed

with the ChemiDoc^{TM} XRS Gel documentation system (Bio-Rad). The software Quantity One® (Bio-Rad) was used for band densiometry analysis.

M.2.4. DNA fragments extraction from agarose gels.

DNA extraction from agarose gels was performed with NucleoSpin® Extract II Kit from Macherey-Nagel (Düren, Germany) following the manufacturer's instructions.

M.3. Enzymatic reactions.

M.3.1. Amplification of DNA fragments by PCR with Taq DNA polymerase.

Each reaction mix contained ~ 100 ng of DNA, 0.25 μM of both forward and reverse primers, 0.2 mM dNTPs (dATP+dCTP+dGTP+dTTP, Deoxynucleotides Set (5prime, Hamburg, Germany)), 2.5-5 μL of Taq buffer 10x (Sambrook et al., 1989) and 0.5-1 U of Taq polymerase in a volume of 25 or 50 μL. Standard conditions were: 95°C for 5 minutes followed by 25-30 cycles of: 95°C for 30 s; 50-65°C for 45 s (around 5°C below the lower primer Tm); 72°C for 90 s (1 minute for each kb to amplify) and a final 5-minutes elongation step at 72°C. Samples were used immediately or stored at –20°C.

Taq polymerase 10X buffer:

KCl	500 mM
Tris-HCl pH:8.3	100 mM
$MgCl_2$	15 mM
Gelatin	0.1% (w/v)

M.3.2. High-fidelity PCR

PCR reactions were performed with the Accuzyme^{TM} DNA polymerase kit (Bioline, London, UK) according to the manufacturer's instructions.

M.3.3. Ligation of DNA fragments.

For the ligation of DNA fragments a ratio of insert to vector of 3:1 was used. Each 20 μL ligation mix contained 1U of T4 DNA ligase (Invitrogen^{TM}, Karlsruhe, Germany) and 4 μL of the 5X ligation buffer supplied by the manufacturer. Blunt end ligations were incubated at 14°C o/n and cohesive end ligations were incubated at room temperature for 1 h. 10 μL of the ligation mix were used for bacterial transformation (section M.6.1.).

M.3.4. DNA digestions with restriction enzymes.

Restriction enzyme digestion of DNA was performed using the buffers and conditions recommended by the manufacturer. One μg of DNA was treated with at least 1 U of restriction enzyme.

For subsequent manipulations, DNA products digestion were separated by electrophoresis in agarose gels (section M.2.3.) and the DNA fragment of interest was isolated using the kit described in the section M.2.4.

M.3.5. DNA 5'end dephosphorylation.

Calf intestinal alkaline phosphatase (CIP) (Roche, Mannheim, Germany) was used to dephosphorylate linearized vector DNA prior to insert ligation, in order to avoid the recircularization of linearized plasmids during the ligation step. 1-2 U of CIP were added to the plasmid restriction mix after the digestion was completed. The mix was incubated at 37°C for 30 minutes. Then the alkaline phosphatase was inactivated

at 75°C for 10 minutes. Dephosphorylated plasmids were purified from agarose gel as described in sections M.2.3. and M.2.4.

M.3.6. Blunt ends generation.

This method was used to allow the subsequent ligation of DNA fragments generated with different restriction enzymes that produce incompatible ends. 5′ overhangs were fill-in and 3′ overhangs were removed with the activities 5′→3′ polimerase and 3′→5′ exonuclease respectivelyof the DNA Polymerase I, Large (Klenow) Fragment (New England BioLabs®) following the manufacturer's instruction.

M.3.7. Sequencing reaction.

Sequencing was done by the company Secugen (Madrid, Spain). For each sequencing reation, 15 μL of 100 ng/μL plasmidic DNA samples and specific primers at a concentration 5 μM were used.

M.4. Transcriptional analysis by RT-PCR.

M.4.1. Arabidopsis RNA extraction.

Plant tissue (~ 100 mg per sample) was collected in Eppendorf tubes and frozen in liquid nitrogen. Samples were macerated with a plastic piston and 1 mL of TRIsure reagent (Bioline, London, UK) was added. The mixture was homogenized in the vortex, incubated at 25°C for 5 minutes and centrifuged at 12,000 rpm for 10 minutes at 4°C to eliminate genomic DNA, polysaccharides and insoluble material. The supernatant was carefully collected and placed in a fresh tube where 0.2 μL of chloroform:isoamyl alcohol (24:1) were added. Samples were incubated 2-3 minutes at room temperature and centrifuged at 12,000 rpm for 15 minutes at 4°C. To precipitate the RNA 250 μL of isopropanol were added to the supernatant and the samples were incubated 10

minutes at 25°C. Next, mixtures were centrifuged at 12,000 rpm for 10 minutes at 4°C. Pellets were washed with 75 % ethanol, dried for 5 minutes at room temperature and resuspended in 10 μL of milli-Q water treated with 0.1% (v/v) of DEPC. Samples were heated at 55°C for 10 minutes to facilitate the RNA resuspension. In order to verify the RNA quality, an aliquot was run in a 0.8% (w/v) TAE gel of agarose prepared with milli-Q water treated with 0.1% (v/v) DEPC. To prevent RNA degradation the electrophoresis tank was previously cleaned with 10% (w/v) SDS and treated for 30 minutes with 3% (v/v) H_2O_2. All solutions were prepared with milli-Q water treated with 0.1% (v/v) DEPC and the material used was autoclaved twice and handled with latex gloves. RNA concentration was measured using the spectrophotometer NanoDrop® (ND-1000 Spectrophotometer). The concentration of the RNA samples was adjusted to 1 μg/μL in a final volume of 12 μL with milli-Q water treated with 0.1% (v/v) DEPC.

M.4.2. Synthesis of cDNA.

DNA was eliminated and cDNA was synthesized using the QuantiTect® Reverse Transcription Kit (Qiagen, Hilden, Germany) according to the manufacturer's instructions.

M.4.3. Amplification of cDNA fragments by PCR.

To quantify the abundance of a messenger RNA, in a given tissue, time or/and condition, PCR reactions (section M.3.1.) were performed using the same amount of cDNA (sections M.4.1. and M.4.2.) and specific primers for each gene of interest (Annex 2). To standarize the quantity and quality of cDNA samples the constitutively expressed *β-TUBULIN-4* (TB4) gene was amplified with specific primers (TUB4-F and TUB4-R, Annex 2).

M.5. Protein analysis.

M.5.1. Isolation of GST fusion proteins expressed in yeast.

M.5.1.1.The pEG(KT) system.

The pEG(KT) vector is a useful system for the expression and purification of eukaryotic proteins fused to glutathione S-transferase (GST) ([Mitchell et al., 1993](#)). The fusion gene is expressed from a CYC1 promoter under the control of a galactose inducible upstream activator sequence (GAL1-10 UAS).

Fragments of the genes *AtNHX1* and *AtNHX2* encoding the c-terminal region of their respective protein were cloned into the pEG(KT) vector in frame with the GST open reading frame. The *AtNHX1* C-terminal end (a fragment of 371 bp that includes the TGA stop codon) was amplified by high fidelity PCR (section M.3.2.) using as template the vector pAtNHX1-1 ([Quintero et al., 2000](#)) and primers NHX1ct-5′/NHX1ct-3′ (annex 2). *AtNHX1ct* fragment was first cloned in vector pCR®-Blunt (Annex 3) creating the plasmid pCB-NHX1ct. Then, AtNHX1ct was subcloned into the MCS of plasmid pEG(KT) as a *BamHI/HindIII* fragment. The resulting plasmid was called pEG(KT)-NHX1ct. To make the plasmid pEG(KT)-NHX2ct, the fragment *AtNHX2ct* was amplified by high fidelity PCR (section M.3.2.) using as template the vector pDR-AtNHX2 ([Yokoi et al., 2002](#)) and primers NHX2ct-5′/NHX2ct-3′ (annex 2). The resulting fragment was subcloned in the pCR®-Blunt vector (Annex 3) creating the plasmid pCB-NHX2ct, that was then cut with the restriction enzymes *BamHI/SalI* to clone *AtNHX2ct* in pEG(KT). pEG(KT)-SOS1ct ([Quintero et al., 2011](#)) was used as control in phosphorylation assays (section M.5.4.).

For *in vitro* phosphorylation assays, kinases were purified using the same system to create chimeric proteins fused to GST. *AtCIPK23* CDS was amplified by high fidelity PCR (section M.3.2.) using as template the vector pSPYNE(R)173-CIPK23 (kindly provided by Jörg Kudla) and primers CIPK23_pEG(KT)_F/CIPK23 R (Annex 2). *AtCIPK23*

CDS fragment was cloned into the pCR®-Blunt vector (Annex 3), creating the plasmid pCRBlunt-CIPK23, and then into pEG(KT) as a *SmaI/SalI* fragment, obtaining the plasmid pEG(KT)-CIPK23. *AtCIPK24* and its hyperactive allele *CIPK24 T168D Δ308* were subcloned in pEG(KT) as *BamHI/EcoRI* fragments from the pGEX-2TK vector described in ([Guo et al., 2001b](#))., obtaining the plasmids pEG(KT)-CIPK24 and pEG(KT)-CIPK24 T168D/Δ308.

To increase the kinase activity in phosphorylation assays (section M.5.4.), in some cases CBL proteins were added to the reaction mixes. To obtain pEG(KT)-CBL10, the vector pGEX-6P-1-SCABP8 ([Quan et al., 2007](#)) was digested with *BamHI/SalI* and a fragment containing the whole *AtCBL10* cDNA was isolated and subcloned in plasmid pEG(KT) digested with the same restriction enzymes.

M.5.1.2. GST fusion protein induction and purification from yeast.

Yeast strain GRF167 (section M.1.2.1.) was transformed with the plasmids pEG(KT) (Annex 3) containing the different GST-tagged chimeric proteins.

1 L of YNB-Ura containing 2% raffinose as source of carbon was inoculated with 5 mL of pEG(KT)-transformed yeasts grown to stationary phase in YNB-Ura dropout medium (section M.1.2.2.) and incubated at 30°C overnight. Cells were harvested by centrifugation at 5000 rpm for 5 minutes and resuspended in 1 L of YNB-Ura containing 2% galactose and 0.01% glucose as sources of carbon in order to the induce the protein expression from the promoter *CYC1*. The culture was grown for 4-5 hours at 30°C before collecting the cells by centrifugation at 5000 rpm for 5 minutes.

Pellets were resuspended in 5 mL PBS + 1% Triton (v/v) + 1 tablet of protease inhibitors (Complete Protease Inhibitor Cocktail Tablets, Roche). The resuspended yeast were transferred to a 50 mL conical Falcon tube and pre-chilled glass beads of 0.5 mm ø added until reaching the meniscus. To break the cells, samples were

subjected to three pulses of 1 minute shaking on the vortex at maximal speed separated by 1-minute incubation in ice. Then 10 mL of PBS+ 1% Triton (v/v) were added, and the mix was thoroughly shaked on the vortex. Tubes were centrifuged for 10 minutes at 3000 rpm at 4°C.

The supernatant recovered on the previous step was incubated for 45 minutes in gentle shaking at 4°C with 100 μL of the affinity chromatography medium glutathione-sepharose 4B resin (Amershan Pharmacia) washed with PBS. Then, the resin was leaving to sediment for 30 minutes and the liquid was discarded. The resin was collected with PBS, placed in a column Bio-Spin® (Bio-Rad, Richmond, California, EE.UU.) and washed with at least 5 mL of PBS. The protein concentration in the eluate was measured in the spectrophotometer NanoDrop® (ND-1000 Spectrophotometer) and when the concentration was lower than 0.01 mg/μL the resin, with our protein of interest, was collected with 200 μL of PBS + 10% glycerol (v/v) and stored at -80°C. The quality of the extraction was checked by running different amounts of the resin in a 10% acrylamide gel (section M.5.2.).

PBS:

NaCl	136.9 mM
KCl	2.7 mM
Na2HPO4	10.1 mM
KH2PO4	1.8 mM

pH was adjusted at 7.4 with HCl.

M.5.2. SDS-PAGE.

Protein electrophoresis was performed using the Mighty Small SE 250 system (GE Healthcare). PAGE gels were prepared following the instructions of Sambrook et al., (1989). Electrophoresis was performed at 20 mA/gel for approximately 1 hour.

Acrylamide gel mix:

Reagents	Running gel 10% (10 mL)	Stacking gel 5% (6 mL)
Milli-Q water	4 mL	4.1 mL
30% Bisacrylamide/Acrylamide	3.3 mL	1 mL
1.5 M Tris pH 8.8	2.5 mL	----
1 M Tris pH 6.8	----	0.75 mL
10% SDS	0.1 mL	0.06 mL
10% APS	0.1 mL	0.06 mL
TEMED	0.004 mL	0.006 mL

Electrophoresis buffer 10X

Tris Base	250 mM
Glycine	1.94 M
SDS	1% (w/v)

The pH of the 1x electrophoresis buffer must be 8.3.

4X Laemmli buffer

Tris-HCl pH 6.8	250 mM
SDS	4% (w/v)
B-mercaptoethanol	10% (v/v)
Glycerol	40% (v/v)
Bromophenol blue	100 µg/mL

Store at -20°C.

M.5.3. Coomassie staining of SDS-PAGE gels.

Proteins in acrylamide gels were stained in two steps (Bradford, 1976). First the gel was was incubated in Coomassie staining solution with gentle shaking at room temperature for at least 1 h. After removal of the staining solution, the gel was incubated in destaining solution until the protein bands appeared without background staining of the gel.

Staining solution

Glacial acetic acid	50 % (v/v)
Methanol	10 % (v/v)
Coomassie brilliant blue R-250	0.25 % (w/v)

Destaining solution

Glacial acetic acid	10 (v/v)
Methanol	10 % (v/v)

For preservation, protein gels were dried overnight using the DryEase® Mini-Gel Drying System (Invitrogen).

M.5.4. Protein *in vitro* phosphorylation.

GST:AtNHX1ct and GST:AtNHX2ct fusion proteins (section M.5.1.1.) obtained and purified from yeast (section M.5.1.2.) were used as substrate in phosphorylation reactions. GST:AtSOS1ct was used as control (Quintero et al., 2011). As protein kinases GST:AtCIPK23 and GST:AtCIPK24 were used. In order to regulate the kinase activity, GST:CBL10 was added to some reactions. To check the kinase activity and possible substrate contaminations with other kinases histone from calf thymus H4524 suitable

for substrate for protein kinase C (sigma-Aldrich) was used as control. There were mixed 100 ng of kinase protein with the indicated amount of substrate in phosphorylation buffer (20 mM Tris-HCl pH 8, 5 mM $MgCl_2$, 0.1 mM $CaCl_2$, 1 mM DTT) and the reaction was initiated by adding 0.2 mM of ATP with 1 µCi of [γ-^{32}P]ATP (1 Ci=37 GBq) in a final volume of 30 µL. The mix was incubated at 30°C for 30 minutes and the reaction was stopped by adding 10 µL of 4X LaemmLi buffer. Proteins were heated at 95°C for 1 minute before to perform SDS-PAGE (section M.5.2.) with 10 µL of each sample. Gels were stained and dried (section M.5.3.). Gels were exposed for different times on a x-ray film.

M.6. Organisms transformation.

M.6.1. Bacterial transformation.

M.6.1.1. Preparation of competent cells.

Escherichia coli.

To prepare *E. coli* One Shot® TOP10 chemically competent cells a 1 mL vial of seed stock was inoculated in 250 mL of SOB medium and grown at 20°C to an O.D.$_{600nm}$ of 0.3. Culture was centrifuged at 3000g at 4°C for 10 min in a flat bottom centrifuge bottle. The pellet was gently resuspended in 40 mL of ice-cold CCMB80 buffer and incubated on ice for 20 min. Cells were centrifuged at 3000g at 4°C for 10 min and resuspended in 5 mL of ice-cold CCMB80 buffer. The O.D.$_{600nm}$ of a mixture composed of 200 µL of SOC medium and 50 µL of the resuspended cells was measured. Chilled CCMB80 buffer was added until reaching an O.D.$_{600nm}$ of 1.0-1.5. Then, the suspension was incubated 20 minutes on ice. Aliquots of 100 µL in 1.5 mL Eppendorf tubes were immediately frozen in liquid nitrogen and stored at -80°C.

CCMB80 buffer:

KOAc pH 7.0	10 mM
$CaCl_2.2H_2O$	80 mM
$MnCl_2.4H_2O$	20 mM
$MgCl_2.6H_2O$	10 mM
Glycerol	10% (v/v)

pH was adjusted below 6.4 with HCl.

Agrobacterium tumefaciens.

In order to prepare electrocompetent *Agrobacterium tumefaciens* cells, single colonies of strain GV3101 were inoculated in 3 mL of YEP medium supplemented with rifampicin (50 μg/mL) and gentamicin (20 μg/mL) and incubated at 30°C o.n. with vigorous shaking. 100 mL of YEP medium were inoculated with 0.5 mL of this pre-inoculum. Cells were incubated to an O.D.$_{600nm}$ of 0.5-1, spun at 3,000 g for 5 minutes and washed with 1/2 volume of cold sterile 10% (v/v) glycerol. Centrifugation was repeated and cells were resuspended in 4 mL of sterile 10% (v/v) glycerol. Cells were separated into two tubes, centrifuged and resuspended in 2 mL of sterile 10% (v/v) glycerol. Both tubes were combined into one tube that was centrifuged. The pellet was finally resuspended in 1.5 mL of ice-cold 10% (v/v) glycerol. Cells were dispensed in 50 μL aliquots into 1.5 mL Eppendorf tubes and immediately frozen by adding liquid nitrogen. Aliquots were stored at -80°C.

M.6.1.2. Bacterial competent cells transformation.

Escherichia coli.

Competent cells were prepared from *E. coli* strains One Shot® TOP10 (section M.6.1.1.). For transformation, 10-100 ng of plasmidic DNA, in a maximum volume of 10 μL, were added to 100-200 μL *E. coli* competent cell aliquots. The mix was incubated for 15 minutes in ice before subjecting them to a heat shock of 42°C for 1 minute and letting to recover for 5 minutes in ice. Then, cells were incubated in 1 ml of LB medium (section M.1.1.2.) for 1 hour at 37°C. Cells were collected by centrifugation at 13,000 rpm for 1 minute and plated in LB medium supplemented with the appropriate antibiotic using sterile glass beads of 4 mm ø.

Agrobacterium tumefaciens.

A. tumefaciens strain GV3101 (section M.1.1.1.) competent cells were transform by electroporation. 50 ng of plasmidic DNA were added to 100-200 μl of *Agrobacterium* competent cells and the mix was incubated for 3 minutes in ice. The culture was placed in a Gene Pulser®/MicroPulser™ electroporation cuvette (Bio-Rad, Richmond, California, EE.UU.) and electroporation was performed with the MicroPulser™ Electroporator (Bio-Rad, Richmond, California, EE.UU.) according to the optimal conditions for *Agrobacterium* set up by the manufacturer. Cells were collected from the cuvettes and incubated in 2 mL of YEP medium (section M.1.1.2.) for 2-3 hours at 30°C. Then 100 μl of the culture were plated in YEP medium supplemented with the appropriate antibiotics using sterile glass beads of 4 mm ø.

M.6.2. Yeast transformation.

Yeast transformation was performed using the lithium acetate/PEG method, as described by (Elble, 1992) in 10 mL of YPD medium (section M.1.2.2.) and incubated o/n at 30°C. ~ 2 x 10^8 cells (D.O.$_{600}$ 0.5 is equivalent to ~ 5 x 10^6 cells/mL) were taken by centrifugation, to which 1-2 μg of plasmidic DNA and 500 μl of PLATE solution were

added. Cells were incubated for 40 minutes at 42°C or o/n at 25°C. For DNA integration into the genomic yeast DNA by homologous recombination the incubation took 48 hours at 25°C using linearized DNA. Cells were taken by centrifugation, resuspended in 100 µl of YNB and extended on selective plates using sterile glass beads of 4 mm ø.

PLATE solution:

PEG (WM 3350) 45%	40.5% (v/v)
Lithium acetate	100 mM
Tris-HCl pH:7.5	10 mM
EDTA pH:8	1 mM

M.6.3. Plant transformation.

M.6.3.1. *Agrobacterium*-mediated transformation of *Arabidopsis thaliana*.

Arabidopsis was transformed by the floral dipping method (Clough and Bent, 1998). Plants were grown under long day conditions to induce flowering. The first bolts were removed to allow proliferation of many secondary inflorescences from the axillary buds of the rosette. Completely developed flowers were eliminated during the three days previous to transformation to decrease the percentage of non-transformed siliques. Plant inflorescences were dipped during 30 seconds in an *A. tumefaciens* suspension containing 5% (w/v) sucrose and 0.02% (v/v) Silwet L-77 as surfactant. After dipping, plants were sealed in plastic bags and transferred to the greenhouse. The plastic bags were removed after two days and plants were kept in the greenhouse until seeds were harvested.

Hygromycin-resistant T_1 transgenic plants were selected on Murashige and Skoog agar medium (M.1.3.2.) supplemented with 20 µg/mL hygromycin B. Resistant plants were transferred to soil and kept in the greenhouse until seeds were harvested. T_2

transgenic plants were selected again in MS with 20 μg/mL hygromycin B. Ten hygromycin-resistant T_2 transgenic plants which showed a 3:1 segregation for the resistant marker were selected and grown on soil in the greenhouse until seeds were harvested. T_3 transgenic plants homozygous for the resistance trait were selected in MS with 20 μg/mL hygromycin B. Kanamycin-resistant transgenic plants were selected following the same process, but MS medium was supplemented with 50 μg/mL kanamycin.

M.6.3.2. *Agrobacterium*-mediated infiltration of *Nicotiana benthamiana*.

Nicotiana benthamina agroinfiltration was performed according to (Waadt and Kudla, 2008). A colony of *A. tumefaciens* carrying the construct of interest (section M.6.1.) was inoculated in 5 mL of YEP medium with antibiotics and incubated o.n. at 30°C. O.D.$_{600}$ was measured and the volume needed to get a final O.D.$_{600}$ of 0.5 was calculated in accordance to the formula $V= (V_{final} \times 0.5)/O.D._{600}$. For the p19 strain (section M.1.1.1.) the final O.D.$_{600}$ was 0.3. The calculated culture volumes of both Agrobacterium strains were put together in a Falcon tube and centrifuged at 5000 rpm for 15 minutes. The supernatant was removed and the pellet resuspended in the final volume of activation buffer, where cells were incubated at least 2 h at room temperature. 5-6-week old well-irrigated *N. Benthamiana* plants were infiltrated with the mixed cultures in their leaf abaxial side using a 5 mL syringe without a needle.

Activation buffer

MES	10 mM
MgCl$_2$	10 mM
Acetosyringone	150 µM

M.7. Obtention of *nhx1 nhx2* null double mutants by crossing.

Homozygous plants of null mutants SALK_065623 (*Atnhx1-2*) and SALK_036114 (*Atnhx2-1*) were crossed to obtain the null double mutant. Plants were grown in soil

(section M.1.3.2.2.) in individual pots. Both genotypes were used as female and male parentals. For female parental a single inflorescence per bolt was chosen, and open flowers and flower primordia which were not going to be used were eliminated. The flower primordium was carefully emasculated under the stereomicroscope SteREO Discovery.V8 (Zeiss). A stamen of the male parental was taken and rubbed over the stigma of the female parental. Once fertilized, the flower primordium was closed and covered with plastic film to maintain the humidity until the silique was formed. The mature silique was harvested when brown and placed in an Eppendorf tube until completely dried. F1 plants were sown on soil and F2 was obtained by self-pollination of F1 plants. Because the probability of appereance of double null mutants is 1/16 in the F2, we selected by PCR F2 plants with the genotype *nhx1-2/nhx1-2 NHX2/nhx2-1* to obtain a F3 enriched in double homozygous mutants (1/4 instead of 1/16). Therefore, double mutant plants carrying the null alleles *nhx1-2* and *nhx2-1* were produced by self-pollination of a plant of genotype *nhx1-2/nhx1-2 NHX2/nhx2-1* and null homozygous *nhx1-2 nhx2-1* plants were recovered under high relative humidity (above 60%) and selected by diagnostic PCR.

M.7.1. Null double mutant selection by PCR genotyping.

Insertion mutant information was obtained from the SIGnAL website (http://signal.salk.edu) and confirmed experimentally. Mutant *nhx1-2* has a T-DNA insertion at nucleotide +1246 relative to the start codon, whereas mutant *nhx2-1* carries the insertion at nucleotide +2429. To confirm the obtention of the *nhx1 nhx2* knockout double mutant line diagnostic PCR screening with allele-specific primers designed to amplify wild-type or mutated loci was performed. For *nhx1-2* allele PCR were used two combinations of primers: nhx1-5′-2/nhx1-3′ that hybridizes with the T-DNA insertion flanking regions, and nhx1-5′-2/LBa1 that hybridize upstream the T-DNA insertion point and at nucleotide +437 of the LB end, respectively. Two primer combinations were used for diagnostic PCR of the *nhx2-1* allele: nhx2-5′/nhx2-3′ that hybridize with the T-DNA insertion flanking regions, and LBa1/nhx2-3′ that hybridize inside the T-DNA and downstream the T-DNA insertion point respectively.

Homozygous knockout double mutants were selected as those that for both alleles presented DNA amplification only from the primer pair that hybridizes with the T-DNA sequence and one of the sequences flanking the T-DNA insertion and not from the primer pair that anneals with both sequences flanking the T-DNA insertion. Col-0 line was used as a control, thus wild type plants PCR showed DNA amplification from the nhx1-5′-2/nhx1-3′ and nhx2-5′/nhx2-3′ primer combinations but not by any combination that includes the LBa1 primer.

Primer sequences are described in the annex 2.

M.8. Obtention of *Arabidopsis* transgenic lines.

M.8.1. *NHX2prom:GUS* transgenic line.

A genomic DNA fragment upstream of the ATG start codon of *AtNHX2* encompassing ca. 3.1 kb of the promoter region was amplified from Arabidopsis genomic DNA with the primers PromNHX2-F and PromNHX2-R (Annex 2). The promoter region was fused with the β-glucuronidase reporter gene (*GUS*) in plasmid pBI101 (Annex 3) and the resulting construct was introduced into wild-type Arabidopsis Col-0 plants as described in section M.6.3.1. Kanamycin-resistant T_1 transgenic plants were selected as described in section M.6.3.1.

M.8.2. *γ-TIP:GFP* and *NHX2:GFP* transgenic lines.

A *γ-TIP:GFP* translational fusion was created using the GFPmut1 variant with enhanced fluorescence and optimized for translation in eukaryotic cells ([Cormack et al., 1996](#)) and the ORF of the *γ-TIP* (At2g36830) gene. The C-terminus of *γ-TIP* and the N-terminus of the GFP polypeptides were modified by PCR using oligonucleotides γ-TIP-Not and GFP-Not (Annex 2). *Not*I digestion of amplified sequences and subsequent ligation generated an in-frame fusion of GFP to the C-terminus of *γ-TIP*. The pBI321Kan-γTIP:GFP vector was constructed by cloning the γ-TIP:GFP translational fusion into the plasmid pBI321 ([Martinez-Atienza et al., 2007](#)) (annex 3) as *Xho*I-*Bam*HI

fragment. To construct the pBI321Hyg-γTIP:GFP vector, the *NOS-NPTII-NOS* expression cassette of plasmid pBI321 (Annex 3) ([Martinez-Atienza et al., 2007](#)) was replaced by a *NOS-HptII-NOS* cassette as a *Cla*I/*Eco*RV insert into the *Cla*I/*Pme*I sites of plasmid pBI321, producing plasmid pBI321Hyg; and the γ-TIP:GFP translational fusion was subcloned into the *Xho*I/*Bam*HI sites of pBI321Hyg. Plasmid pBI321Hyg-γTIP:GFP was introduced into mutant plants homozygous for the *nhx1-2* mutation and heterozygous for the *nhx2-1* mutation by *Agrobacterium tumefaciens*-mediated transformation (section M.6.3.1) whereas the plasmids pBI321Kan-γTIP:GFP and pBI321-NHX2:GFP ([Yokoi et al., 2002](#)) were introduced into Col-0 wild-type plants following the same methodology. Kanamycin or Hygromycin-resistant T_1 transgenic plants were selected as described in section M.6.3.1. In mutant transgenic lines, seeds were obtained by self-fertilization, and homozygous *nhx1-2 nhx2-1* lines expressing γTIP:GFP were identified from the T2 generation by hygromycin resistance selection combined with diagnostic PCR screening with allele-specific primers designed to amplify wild-type or mutant *NHX2* alleles (M.7.1. and annex 2).

M.9. Physiological caracterization of *nhx1 nhx2* mutant lines in hydroponic culture.

In all cases plants were cultivated as described in section M.1.3.4.

M.9.1. Growth at different K^+ concentrations.

Plants of the null *nhx1 nhx2* mutant and Col-0 lines were grown for 2 weeks in control conditions at 1 mM K^+ (M.1.3.4.). Then, 5 plants of each line were transferred to hydroponic containers with LAK solution supplemented with 0.1, 1, 10 and 20 mM of K^+ (section M.1.3.4.). After two weeks of K^+ treatments plants were collected, weighed and ionic contents were determined.

M.9.2. Phenotypic characterization.

Rosette diameter, root elongation, shoot fresh and dry weight and root fresh weight were measured after collecting plants subjected to K^+ treatments (section M.9.1.).

M.9.3. Ion contents.

Ion contents of whole shoot and roots of plants grown at different regimes of K^+ were measured by atomic absorption spectrophotometry (AAS). When ion content of a specific cellular type was measured, energy-dispersive X-ray spectroscopy couple to electronic microscopy (SEM-EDX) was used.

M.9.3.1. AAS.

For ion content analyses, plants shoots and roots were separated and their fresh weight measured. Roots were washed thoroughly with Elix water (Millipore) and blotted dry before weighing. Dry weight was also measured after drying samples at 70 °C for 48 h in a forced-air oven to obtain water contents (g water per g dry weight). Potassium was extracted by autoclaving finely ground material, and measured by atomic absorption spectrophotometry (AAS) (Perkin-Elmer 1100B, Norwalk, CT, USA).

M.9.3.2. SEM-EDX.

For SEM-EDX analysis, fragments of freshly harvested, fully expanded leaves were processed as described previously (Leidi et al., 2010). The plant pieces were mounted in slots of copper holders and fixed with optimal cutting temperature compound (BDH, http:// uk.vwr.com). The copper holder containing the samples was dipped into a bath of slush N_2 before transferring it under vacuum into the cryopreparation chamber (CT1500; Oxford Instruments, http://www.oxford-instruments.com) attached to a SEM (DSM 960, Zeiss, http://www.zeiss.com). The temperature in the chamber was left to rise from -163 to -90°C and was then set for 10 min for ice sublimation before sputter-coating with gold (2 min). The SEM was fitted with an ATW detector interfaced with a Link ISIS analyzer (http://www.oxford-instruments.com). Samples were analyzed keeping the following parameters constant: accelerating voltage, 15 kV; take-off angle 42°; collecting time of X-ray counts, 100 s; working distance between sample and detector, 24 mm. Measurements were performed by focusing on exposed vacuoles of specific cells (guard cells and subsidiary cells). The number and energy of the X-rays re-emitted from the specimen were measured by an energy-dispersive spectrometer and counts pertaining to C, O, K, Na,

Ca and Mg atoms were recorded. Results are presented as the percent of K and Na counts relative to total counts.

M.10. GUS staining.

The expression pattern of *AtNHX2* was studied using the GUS reporter system. As described in section M.8.2. a fragment of the *NHX2* promoter was fused to the beta-glucuronidase gene. This construction was transformed into Arabidopsis ecotype Col-0 (section M.6.3.1.). Histochemical GUS analyses were performed as described (Jefferson et al., 1987). The GUS expression pattern was determined in young seedlings and organs of mature plants at different stages of development, including roots, rosette leaves, young flowers and green siliques. Samples were incubated at 37 °C for 18 h in GUS staining buffer (200 mM phosphate buffer pH 7.2, 0.1% v/v Triton X-100, and 1 mM X-Gluc) and then placed for 5 hours in 90% ethanol to remove chlorophyll. Photographs of GUS-stained tissues were taken using a Zeiss Axioskop microscope equipped with Nomarski optics and the AxioVision Release 4.8.2. Zeiss software.

M.11. Stomatal aperture bioassays.

Light-induced stomatal opening bioassays were done on leaves of 4-6 week-old-plants growing as described in section M.1.3.3. Abaxial epidermal strips were harvested at the end of the night period and incubated for 2 h in darkness in stomatal incubation buffer and then for 2 h under light (250 µmol m^{-2} s^{-1}) at 22°C. Images were captured with a CCD digital camera connected to a Zeiss Axioskop microscope and stomatal apertures were measured with the AxioVision Release 4.8.2. Zeiss software. For ABA-induced stomatal closure experiments, abaxial epidermal peels were incubated for 2 h under light. Then ABA was added at a concentration of 0.1 µM, and stomatal closure was measured 2 h after treatment. Four different plants were used for each experiment, taking one leaf of each one per treatment. Stomatal apertures were determined by measuring the inner width of the stomatal pore from captured

photographs of a minimum of 40 stomata per line and condition. Stomatal aperture bioassays were performed three times as blind experiments.

Na$^+$-supported stomata opening bioassays were performed as described above but replacing KCl for NaCl (30, 50 or 75 mM) in the stomatal incubation buffer.

To monitor the vacuolar dynamics in guard cells during the stomatal movements, stomatal bioassays were performed using the transgenic lines expressing γ-TIP:GFP and AtNHX2:GFP proteins. Bioassays were done as described above but using 10 μM of ABA to promote stomatal closure and 3 μM of fusicoccin from *Fusicoccum amygdali* (Sigma) to stimulate stomatal opening. Images were taken with FluoView FV1000 Confocal Microscope (Olympus) using a 488-nm Ar/ArKr laser and 60X magnification. Images were analysed with Olympus FluoView 2.1. software (Olympus).

For time-lapse experiments leaf disc were pre-incubated in stomatal incubation buffer for 2h in dark or in light, to close and open the stomata respectively. Then, microscope samples were prepared adding the stimulus (3 μM of fusicoccin to open the closed stomata or 10 μM of ABA to close the opened stomata) and images of a single stomata were taken a different times. Interval times were the same for the wild-type and mutant lines.

Stomatal incubation buffer

MES-KOH pH:6.5	10 mM
KCl	10 mM
CaCl$_2$	50 μM

M.12. Thermal imaging.

Thermal images of 3-4 week-old plants cultivated as described in section M.1.3.3. were obtained using a ThermaCam SC5000 infrared camera (Inframetrics, FLIR Systems, http://www.flir.com/) placed in a chamber with constant humidity (70%), temperature (21°C) and light intensity (90 µmol m^{-2} s^{-1}). Images were obtained at 1-minute intervals in a 3,5/14/2,5h light/dark/light cycle. Leaf temperature was calculated as the average temperature of the pixels contained into a standard area drawn on leaves using the FLIR Altair software (Flir Systems Inc., http://www.flir.com/). Data represent the temperature moving average of two leaves per plant from three differents plants per line.

M.13. NHX1 and NHX2 circadian regulation analysis.

M.13.1. Semiquantitative RT-PCR.

To study the transcripcional regulation of *NHX1* and *NHX2* genes along a day/night cycle leaves of 6-week old Col-0 plants growing on soil in a Sanyo MLR-351 plant growth chamber under short day regime (8h day/16h night, 23/19°C, 60-70% relative humidity) (section M.1.3.2.2.) were harvested and frozen in liquid nitrogen at different points of a complete cycle: dawn, 2h light, 4h light, dusk and 4h dark. Then RNA extraction and cDNA synthesis were made as described in sections M.4.1. and M.4.2. PCR was performed with specific primers for *NHX1*, *NHX2* and *TB4* cDNA (sections M.4.3. and M.3.1.) (Annex 2). Images of the RT-PCR ethidium bromide-stained agarose gels were acquired with the ChemiDoc^{TM} XRS Gel documentation system (Bio-Rad) and the software Quantity One$^{®}$ (Bio-Rad) was used for band densiometry analysis (section M.2.3.). The ratio between the sample RNA to be determined and *TB4* was calculated to normalize for initial variations in sample concentration. Mean and standard error of two replicas were calculated after normalization to *TB4.*

M.13.2. Stomatal conductance measurements.

Leaf gas exchange was determined using the steady state porometer LI-1600 (LI-COR). Stomatal conductance rate (G_s; mmol m^{-2} s^{-1}) was measured in 7-week-old Col-0 and KO lines (section M.1.3.1.) growing on soil in a Sanyo MLR-351 plant growth chamber under short day regime (8h day/16h night, 23/19°C, 60-70% relative humidity) (section M.1.3.2.2.). Measurements were recorded at six different points of the day: dawn, 2h light, 4h light, dusk, 2h dark and 4h dark. A total of 3 measurements for each genotype (3 plants per line) were recorded and mean and standard error calculated.

M.14. Drought assay and transpiration measurements.

Col-0, L14 and KO plants (section 1.3.2.2.) were grown under short day conditions (8h day/16h night) in a growth chamber with constant temperature and humidity (section M.1.3.2.2.) during 7 weeks when they were subjected to drought. The same watering regime was applied to all the lines along the plant growth and pots were cover with plastic film to avoid water evaporation from the soil. Before to initiate the drought phase pots were well watered until their reach the field capacity of the soil and the surplus water drained away. The start of the drought tolerance assay was in coincidence with the begin of the dark period. Pots were weighed at the dusk and the onset during four consecutive days and transpiration (mL H_2O cm^{-2} min^{-1}) was calculated. At least 7 plants per line were used and their foliar area was calculated with the AxioVision Release 4.8.2 Zeiss software from pictures of their rosettes. Images of the plants were taken at different days until all plants died.

M.15. Morphology analysis.

M.15.1. Epidermal impressions using dental resin.

Impressions of the abaxial surface of 5 week-old mature rosette leaves grown as described in section M.1.3.3. were made using Genie Light Body Regular dental resin as previously described (Casson et al., 2009). Impressions were viewed on a Zeiss Axioskop microscope and imaged with the AxioVision Release 4.8.2 Zeiss software. For each line 42 images at 20X magnification were obtained (3 areas per leaf, 2 leaves per plant, 7 plants per line) and the frequency of stomatal and epidermal cells was determined with the software ImageJ (National Institutes of Health, Bethesda, Maryland). Density data and stomatal index was calculated for each area individually, and the mean was then calculated from these data. Stomatal index was calculated with the following formula: S.I. = [number of stomata/(number of other epidermal cells + number of stomata)] x 100. Cell areas were measured with the Cintiq 12WX pen display (Wacom$^{©}$) and image software AxioVision Release 4.8.2.

M.15.2. Scanning Electron Microscope (SEM).

For Scanning Electron Microscope (SEM) images, Arabidopsis leaves samples were processed as described in section M.9.3.2.

M.16. Search of AtNHX1 and AtNHX2 interacting proteins.

Two different approaches have been used for revealing NHXs interactions with other proteins: yeast two-hybrid assays (Y2H) and bimolecular fluorescence complementation (BiFC). Both will be described in detail bellow.

M.16.1. Yeast two-hybrid assays.

Yeast two-hybrid (Y2H) is a technique used to reveal physical interactions between two proteins. The two proteins of interest are fused in frame to two separate fragments of a transcription factor: the binding domain (BD) that is able to interact with its target DNA and the activation domain (AD) that activates the transcription. Thus, if two proteins interact physically, both fragments of the transcription factor come together and activate a downstream reporter gene.

To test the homo- and heteromer formation between AtNHX1ct and AtNHX2ct they were cloned in Y2H plasmid, as in those that carry the biding domain as in those that bear the activation domain. AtNHX1ct was cloned in pBD-GAL4 cam (Stratagene) (Annex 3) vector as *EcoRI/SalI* creating the plasmid pBD-NHX1ct. AtNHX2ct was cloned in pGBKT7 (Clontech) (Annex 3) as *EcoRI/SalI* fragment by PCR amplification using the primers NHX2ct-5'/NHX2ct-3'. The resulting plasmid was called pGB-NHX2ct. pGAD-NHX1ct and pGAD-NHX2ct (Clontech) (Annex 3) were kindly provided by Jörg Kudla's laboratory.

Yeast strain AH109 (section M.1.2.1.) was cotransformed with all combinations of pBD and pAD vectors containing the C-terminal fragments of NHX1 and NHX2. Each vector was also contrasformed with the corresponding empty vector as controls. Positive colonies carrying the vectors were selected in YNB/-Trp/-Leu (section M.1.2.2.). Yeast transformants were inoculated in 2 mL of YNB/-Trp/-Leu media and grown at 28°C until saturation (D.O.$_{600nm}$ ~ 2). From the saturated cultures, 1:10 serial dilutions were made and a 5 μL drop of each dilution was deposited on YNB/-Trp/-Leu and YNB/-His/-Trp/-Leu plates. Plates were incubated at 28°C during 2-3 days.

M.16.2. Bimolecular fluorescence complementation (BiFC).

This technique allows the detection of protein-protein interactions *in planta* in their native subcellular localization. This approach is based on complementation between two nonfluorescent fragments of a fluorescent protein when they are

brought together by interactions between proteins fused to each fragment (Hu et al., 2002).

BiFC was performed as described previously (Waadt et al., 2008) in order to find out interactions between AtNHX1 and AtNHX2 with AtCIPKs and to reveal the possible oligomerization of NHX proteins.

M.16.2.1. BiFC plasmid.

All vectors used were described in (Waadt et al., 2008) (Annex 3) and DNA manipulations were performed as described in section M.3.

The complete collection of the 26 AtCIPKs cloned in plasmid pSPYNE(R)173 and *AtNHX1* and *AtNHX2* cloned as in frame *SpeI/XhoI* fragments in the vector pSPYCE(M) were kindly provided by Jörg Kudla's laboratory. For oligomerization experiments *AtNHX1* and *AtNHX2* were subcloned as *XbaI/XhoI* fragments in the plasmid pSPYNE173 from pSPYCE(M)-NHX1 and pSPYCE(M)-NHX2 respectively (Annex 3).

M.16.2.2. Infiltration of transformed *Agrobacteria* in *N. benthamiana* leaves.

Agrobacterium tumefaciens strain GV3101 (section M.1.1.1.) was transformed with BiFC constructs as described in section M.6.1. These transformants were used together with the p19 strain (section M.1.1.1.) for transient expression by infiltration of 5-6-week-old *N. benthamiana* leaves as was indicated in section M.6.3.

M.16.2.3. BiFC microscopy.

Microscopy analyses were performed as in (Waadt et al., 2008). *N. Benthamiana* leaf discs were cut 3 days after infiltration. To make comparison of differents samples and fluorescence intensity quantification, the lower epidermis was analyzed in an inverted fluorescence microscope Leica DMI6000B (http://www.leica-

microsystems.com) and a Hamamatsu Orca camera (model C4742-80-12AG, Hamamatsu Photonics, http:// www.hamamatsu.com) operated with Openlab 5.0.2 software (Improvision, http://www.improvision.com) at 20X magnification. Images were obtained using constant imaging conditions: exposure time of 1ms for bright field and 1.2 s for U.V. light, gain of 100, without offset and 1 of binning. eYFPC/eYFPN complexes were visualized using a YFP filter. For BiFC quantification, 10 images were taken in random distribution and the mean fluorescence emission was measured using Openlab 5.0.2. software. Relative fluorescence was calculated after subtraction of the p19-background fluorescence.

Higher-resolution pictures were taken with a FluoView FV1000 Confocal Microscope (Olympus) using a 515-nm laser and 60X magnification. Images were analysed with the Olympus FluoView 2.1. software (Olympus).

M.17. Fuctional study of NHXs and CIPKs interactions in *Saccharomyces cerevisiae*.

M.17.1. Plasmid constructs and yeast strains generation.

The mutant alleles *nhx1*S526A, *nhx2*S532A and *nhx2*S532D were generated by PCR (section M.3.2.) using the vectors pAtNHX1-1 and pDR-NHX2 as template and the specific primers AtNHX1 Xho5′, Atnhx1SA-3′, AtNHX2 Xho5′, Atnhx2SA-3′ and Atnhx2SD-3 (Annex 2). The PCR products were cloned in plasmid pDR195 as *XhoI/BamHI* fragments creating the vectors pDR-nhx1S526A, pDR-nhx2S532A and pDR-nhx2S532D (Annex 3).

AtNHX1 and *AtNHX2* were integrated in the genome of *Saccharomyces cerevisiae* strain AXT3K (Quintero et al., 2002) (section M.1.2.1.) to produce the strains JPZN1 and JPZN2 (section M.1.2.1.). The coding sequences of *AtNHX1* and *AtNHX2* were previously cloned in the yeast expression vector pDR195 (Rentsch et al., 1995; Quintero et al., 2000; Yokoi et al., 2002). A DNA fragment containing *PMA1-AtNHX1-*

ADH coming from pAtNHX1-1 (Quintero et al., 2000) was subcloned in pCR®2.1-TOPO® (Invitrogen™) (annex 3) as a *HindIII/SphI* fragment generating pCR2.1-pDRNHX1. To create the plasmid pCR2.1-pDRNHX2, AtNHX1 cDNA was replaced from pCR2.1-pDRNHX1 by a *HindIII/BamHI* fragment encompassing the complete ORF of AtNHX2. Both plasmids were linearized by the restriction enzyme *KpnI* and *Saccharomyces cerevisiae* strain AXT3K (Quintero et al., 2002) (section M.1.2.1.) was transformed following the procedure described in M.6.2. and incubating the transformation mix for 48 hours to allow homologous recombination between *PMA1* promoter and *ADH* terminator from genomic yeast DNA and plasmid DNA to take place. Yeast containing *AtNHX1* and *AtNHX2* integrated in their genomes were selected in YPD medium (section M.1.2.2.) supplemented with 90 µg/mL of hygromycin B. The presence of both genes was confirmed by PCR with the primers AtNHX1 Xho5′, AtNHX2 Xho5′ and ADH1-R (Annex 2).

To test the yeast salt tolerance achieved by the simultaneous expression of NHX2 with its interacting CIPKs, the coding regions of CIPK23 (*SmaI/XhoI*), CIPK24 (*BamHI/EcoRI*), CIPK24T168D/Δ308 and CIPK26 (*SpeI/XhoI*) were cloned into the yeast expression vector p414GPD (Annex 3). The CBLs 1, 2, 3, 4, 6 and 10 were cloned in the yeast expression vector pYPGE15 creating the plasmids pYPGE15-CBL1, pYPGE15-CBL2, pYPGE15-CBL3, pYPGE15-CBL4, pYPGE15-CBL6, and pYPGE15-CBL10 (Annex 3).

M.17.2. Yeast drop-test.

Yeast drop-test was used to determine the tolerance of yeast transformants to different NaCl and hygromycin concentrations in AP or YPD medium respectively (section, M.1.2.2.). Yeast transformants were inoculated in 2 mL of YNB media supplemented with the corresponding amino acids and grown at 28°C until saturation (D.O.$_{600nm} \sim 2$). From the saturated cultures, 1:10 serial dilutions were made and a 5 µL drop of each dilution was deposited on AP or YPD plates supplemented with different NaCl or hygromycin concentrations. Plates were incubated at 28°C during 3-5 days.

M.18. Phosphoproteomic analysis.

The phosphoproteomic analysis of the AtNHX2ct protein purified from yeast was performed by Proteored (http://proteo.cnb.csic.es/proteomica/, Centro Nacional de Biotecnología, CSIC, Spain).

M.19. Statistical analysis.

Statistical analysis were performed using the IBM® SPSS® Statistics 19 program (IBM®, Armonk, New York, U.S.).

V. RESULTS

R.1. Construction of the null double mutant line *nhx1-2 nhx2-1.*

Previous work showed that proteins NHX1 and NHX2 are functionally redundant and that *nhx1* and *nhx2* single mutants have moderate disturbances in the germination rate, biomass production, and foliar area compared with wild-type plants (Apse et al., 2003; Bassil et al., 2011a; Barragán et al., 2012). This is in agreement with the extensive overlapping expression pattern of NHX1 and NHX2 (Shi and Zhu, 2002; Bassil et al., 2011a), identical subcellular localization of the proteins, high protein sequence similarity (87.5%), alike transcriptional regulation (Yokoi et al., 2002; Bassil et al., 2011a), and similar transport activity (Venema et al., 2002; Barragán et al., 2012). To further investigate the physiological role of vacuolar NHX proteins, we sought to produce homozygous null double mutants with alleles *nhx1-2* and *nhx2-1* carrying mutations within the coding regions of *NHX1* and *NHX2* respectively (figure R.1.) (Barragan, 2007; Bassil et al., 2011a; Barragán et al., 2012). However, early attempts to produce double knockout plants with *nhx1-2 nhx2-1* null alleles were unsuccessful. To circumvent this problem, we used for prior work another allele, *nhx1-1*, that carries a T-DNA insertion in the 5′-untranslated region of *NHX1* (at nucleotide -114 relative to the start codon). Contrary to mutant *nhx2-1*, which failed to produce detectable levels of gene transcript as determined by RNA gel blot and RT-PCR assays, mutant *nhx1-1* showed a low, yet detectable amount of *NHX1* transcript, which accumulated slightly under salt stress. Mutant *nhx2-1* produced a 5′-truncated mRNA that accumulated at greater levels than in wild-type plants (Barragán et al., 2012). Homozygous lines of genotype *nhx1-1* (leaky allele) and *nhx2-1* were crossed to generate double mutant Arabidopsis plants (from now on L2 and L14). These plants were severely stunted and failed to produce seeds. The differences in growth between L2 and L14 *nhx1 nhx2* plants and Col-0 were progressively more pronounced at increasing K^+ concentrations (from 0.1 to 20 mM K^+) in hydroponic culture, most probably due to the impossibility of the mutants to accrual the K^+ into the vacuole. The diminished size of the vacuolar K^+ pool hindered water uptake as these plants were no longer able to supply the vacuole

with sufficient amounts of K^+ to create the turgor pressure necessary for the normal expansion of leaf cells. Furthermore, *nhx1-1 nhx2-1* mutant plants could not withstand osmotic stress, suffering a significantly greater water loss than wild-type plants (Barragán et al., 2012). These data demonstrate that the absence of NHX1 and NHX2 proteins severely impaired water relations in the mutants.
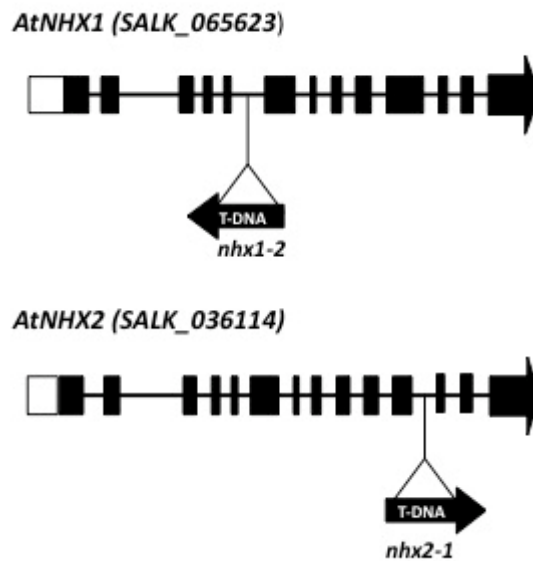
Figure R.1. T-DNA Insertion Sites in Mutant Alleles *nhx1-2* and *nhx2-1*. Black boxes and lines represent exons and introns, respectively, in the coding region. White boxes represent 5′-UTRs in cDNAs. Black arrowheads in the coding region represents the direction of transcription. Arrows labelled with T-DNA indicate the point of insertion and direction of the intervening T-DNA.
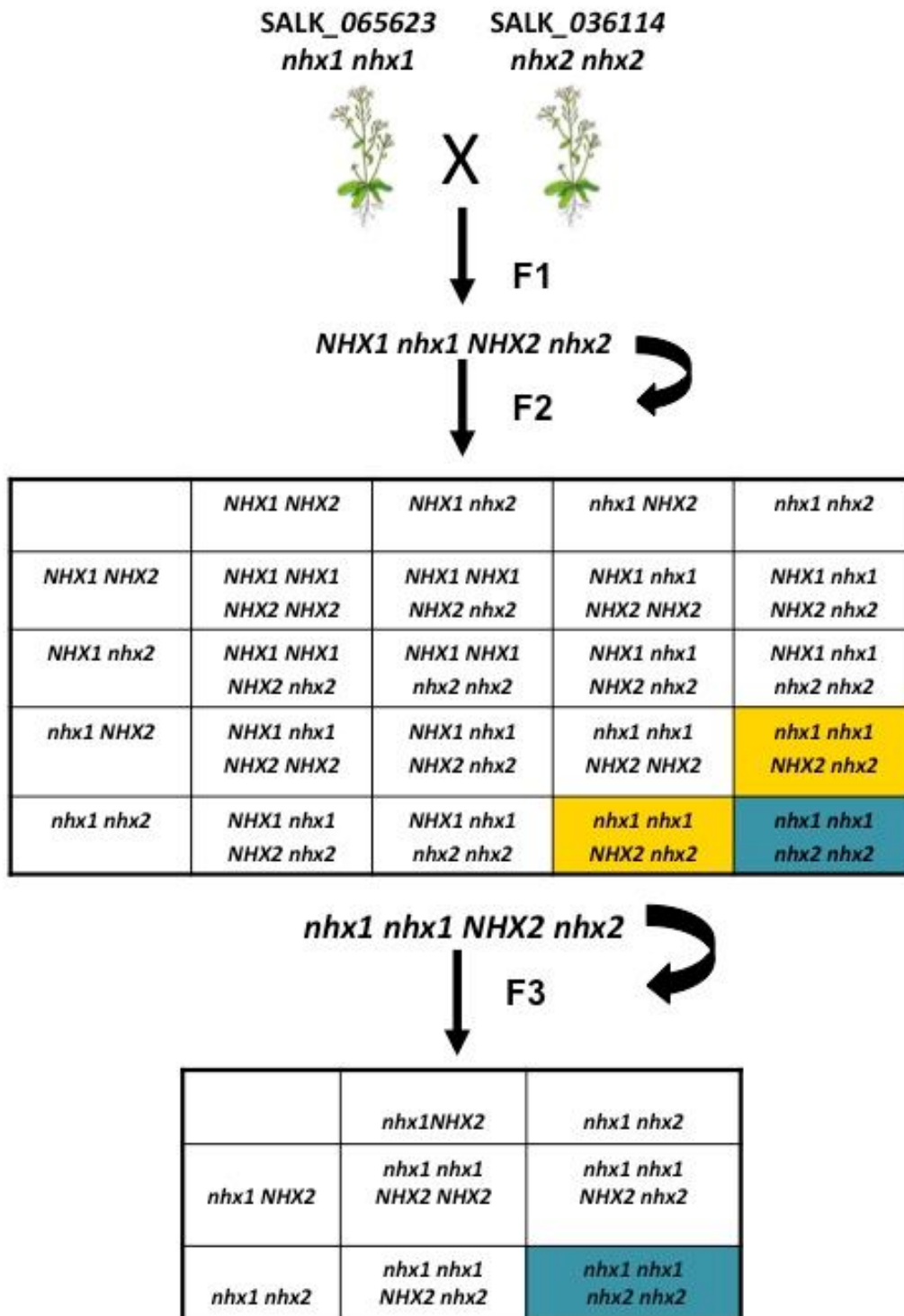
Figure R.2. Schematic description of the Null Double *nhx1-2 nhx2-1* Mutant Obtention. Yellow boxes represent the Arabidopsis genotype used to obtain the double homozygous mutant that is represented as blue boxes.

The strategy followed to obtain the double knockout mutant line *nhx1-2 nhx2-1* (from now on KO) was to grow the plants under very controlled conditions, minimizing environmental fluctuations, and maintaining relative humidity over 60%. Homozygous plants of mutants with T-DNA insertions SALK_065623 (*Atnhx1-2*) and SALK_036114 (*Atnhx2-1*) (section M.1.3.1.) were crossed as described in section M.7. Mutant *nhx1-2* has a T-DNA insertion at nucleotide +1246 relative to the start codon, whereas mutant *nhx2-1* carries the insertion at nucleotide +2429 (figures R.1. and R.2.). Plants of genotype *nhx1-2/nhx1-2 NHX2/nhx2-1* were selected from the F2 generated from the self-pollination of the F1. The self-pollination of these plants would produce the double homozygous mutants with 1/4 frequency, making easier the screening by PCR to verify the genotype (figure R.2.). PCR were performed with allele-specific primers designed to amplify from the flanking regions of the T-DNA insertion (wild-type loci) and a specific primer for the left border of the T-DNA (mutated loci) (section M.7.1. and Annex 2). Figure R.3. illustrates the position of the primers used and the PCR bands obtained from the wild type and mutated loci.
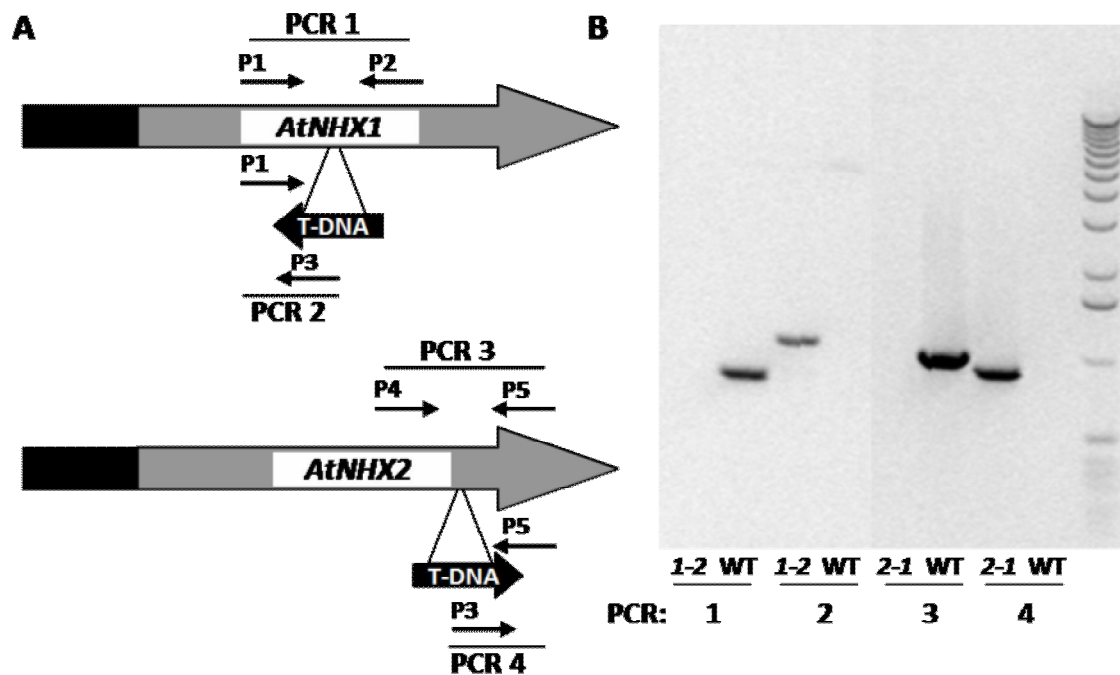
Figure R.3. PCR Genotyping of the Null Double Mutant *nhx1-2 nhx2-1*. (A) Schematic representation of the genes AtNHX1 and AtNHX2, and the annealing sites of the primers used to genotype the T-DNA insertion mutant (P1: nhx1-5′-2, P2: nhx1-3′, P3: Lba1, P4: nhx2-5′ and P5: nhx2-3′). **(B)** Example of the results obtained in a PCR using DNA from the wild type (WT) and the *nhx1-2 nhx2-1* (KO) lines as templates. The band size expected for each PCR are: PCR1→ WT: 850 pb and KO: no amplification; PCR2→ WT: no amplification and KO: 1.1 Kb; PCR3→ WT: 1 Kb and KO: no amplification; PCR4→ WT: no amplification and KO: 950 pb.

Homozygous mutants *nhx1-2 nhx2-1* were obtained with a frequency of 1/4 (16 out of 44 plants, 3:1 segregation ratio with $p<0.05$, χ^2 test). Knockout plants displayed an extremely stunted growth that allowed to single them out phenotypically prior to the PCR verification of their genotype. Although the first failed attemps to get the null double mutant made us suspect that it was a lethal genotype, these results indicate that, in fact, the simultaneous lack of both proteins is not lethal but renders these plants very sensitive to any kind of environmental stress, particularly those affecting the water status of the plant.

R.2. Phenotypic analysis of the KO mutant plants.

R.2.1. Plant growth on soil.

The most obvious phenotypic characteristic of the KO mutant plants was their extremely stunted growth along all developmental stages. Also, knockout plants produced few flowers, very small siliques and a very low number of seeds per plant (Figure R.4.).

Figure R.4. **Impaired Development of Double Null *nhx1 nhx2* Mutant**. Depicted are inflorescences and rosettes of double knockout (KO) mutant plants of genotype *nhx1-2 nhx2-1* and of wild-type Col-0 plants grown in soil. Note the diminutive siliques in the mutant plant.

In order to get enough seeds from the *nhx1-2 nhx2-1* mutant to perform statistically significant phenotypic and physiological analyses , KO mutant plants were propagated during several cycles in the same conditions used for their obtention (section M.1.3.2.2.).

R.2.2. Plant growth on hydroponic culture.

It was recently reported that *nhx1-1 nhx2-1* (L14) mutants were extremely sensitive to external K^+ and that they showed similar susceptibility to Na^+ toxicity compared to the wild type. Notably, mutant plants presented greater rates of Na^+ sequestration than the wild type suggesting that other transporters might mediate the influx of Na^+ into the vacuole (Bassil et al., 2011a; Barragán et al., 2012). Since NHX1 and NHX2 are not playing a major role in the accrual of Na^+ into the vacuolar lumen, we decided to focus on the study of the phenotype of *nhx1-2 nhx2-1* mutants under different K^+ regimes.

In order to compare the growth and development of the KO mutant line with that of the wild type (Col-0), plants of both genotypes were grown in hydroponic culture at different K^+ regimes (from 0.1 to 20 mM K^+) (section M.1.3.2.3. and M.9.1.). After germination, Col-0 and KO plants were grown for two weeks in LAK solution with 1 mM K^+ (section M.1.3.2.). Then, plants were subjected to different K^+ treatments (0.1, 1, 10 or 20 mM of K^+) for two additional weeks before harvesting (section M.1.3.2. and M.9.1.) (Figure R.5.).
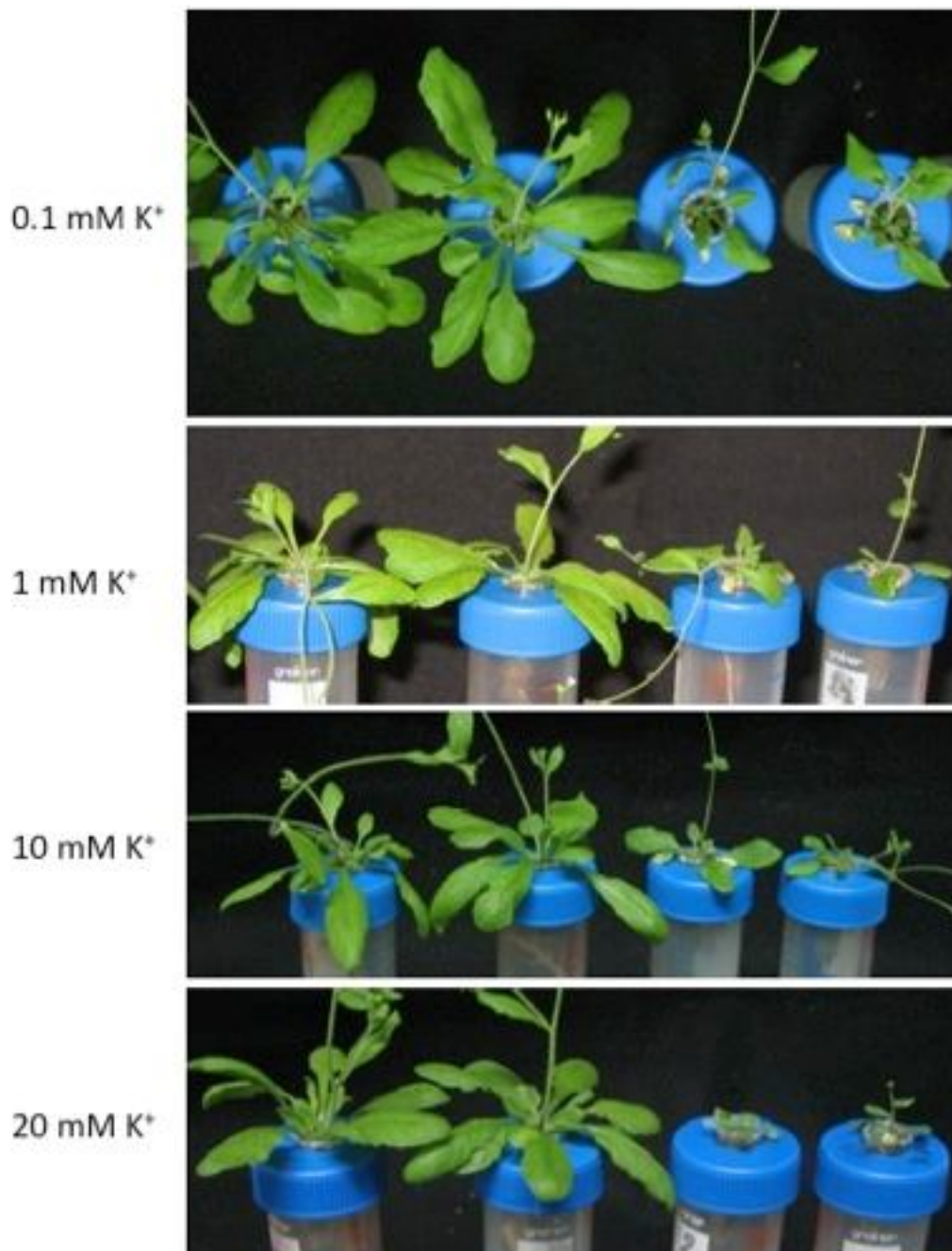
Figure R.5. Sensitivity of *nhx1 nhx2* Mutant Plants to External K⁺. Two-week-old plants of Col-0 (left) and of mutant line KO (right) grown in LAK medium with 1 mM KCl were transferred for two additional weeks to fresh hydroponic LAK medium supplemented with the indicated concentrations of K⁺.

As shown in figure R.6., the rosette diameter and root elongation of *nhx1 nhx2* KO mutant plants was significantly reduced relative to Col-0. The progressive reduction of growth at increasing K⁺ concentrations in the medium, and the increased differences

in growth with respect to the wild type were less evident in KO mutant than in the leaky L2 and L14 lines, due to the extremely small size of the former even in optimal growth conditions (Barragán et al., 2012). Nevertheless, the smallest difference in the size of the rosette among genotypes was found at the lowest K^+ concentration tested (0.1 mM K^+), whereas higher K^+ concentrations produced a striking toxicity to KO mutants that led to necrosis, leaf dessication and eventual plant death (figure R.5., R.6., R.7. and R.8.).
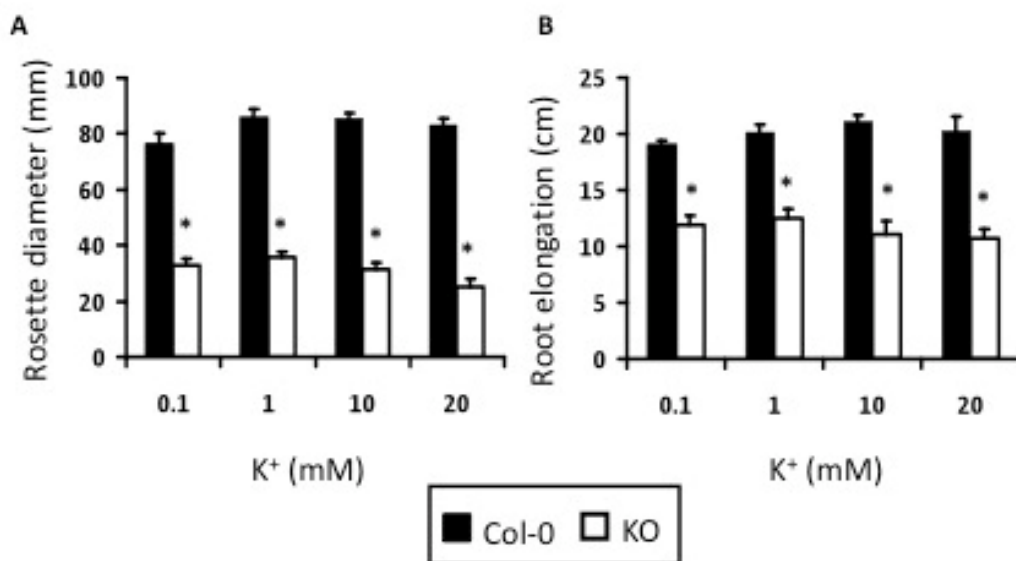
Figure R.6. Growth of Col-0 and Double Knockout Mutant *nhx1-2 nhx2-1* in Different Potassium Regimes. (A) Rosette diameter of Col-0 and KO plants treated as in figure R.5. **(B)** Root elongation of Col-0 and KO plants treated as in figure R.5. Data represent means and SE from of least three plants. Asterisks indicate statiscally significant diferences at $p < 0.05$ in pairwise comparison by the Tukey's HSD (Honestly Significant Difference) test.

There was no significant difference in the potassium concentration analyzed in leaf cell sap extracts (section M.9.3.1.) between lines when expressed on tissue water basis (i.e. molar concentration) at any K^+ concentration used in the growth medium (figure R.7.). However, when these values were expressed on a dry weight basis (i.e. percent content), the shoots of KO double mutants in plants growing at 1 mM and 20 mM of K^+ showed lower K^+ concentrations than the wild type (figure R.7.). This apparent contradiction is explained when considering that the K^+ supply affects the

98

water content of plants ([Leigh and Wyn Jones, 1984](#)). Notice that at 20 mM K$^+$ shoots of the knockout plants had only half the K$^+$ and water contents of the wild type. Plants of *nhx1-2 nxh2-1* genotype consistently accumulated less water in their shoots than the wild type, which translated into similar K$^+$ mM concentrations even though they had a lower K$^+$ content on dry matter basis (figure R.7.).
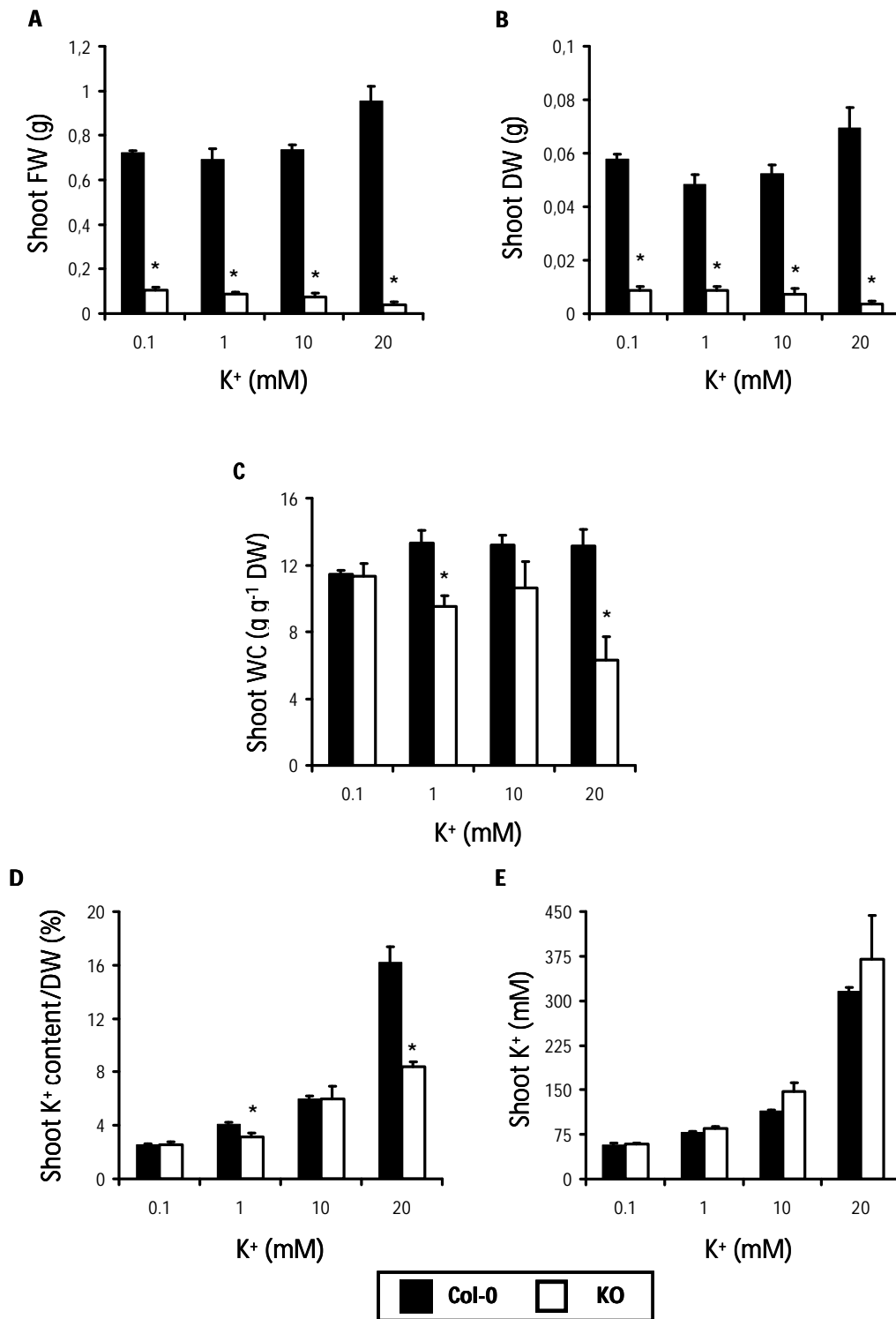
Figure R.7. Growth and K$^+$ contents of Col-0 and Double Knockout Mutant *nhx1-2 nhx2-1* Aerial Parts in Different Potassium Regimes. Phenotypic characterization of wild-type Col-0 and double mutant plants of genotype *nhx1-2 nhx2-1* grown on LAK hydroponic medium for two weeks and then transferred to 0.1, 1, 10, and 20 mM K$^+$ for an additional 2-week period. Data represent means and SE from of least three plants. Asterisks indicate statiscally significant diferences at *p*<0.05 in pairwise comparison by the Tukey's HSD (Honestly Significant Difference) test. **(A)** Shoot fresh weight (FW) **(B)** Shoot dry weight (DW)). **(C)** Shoot water content (WC). **(D)** Shoot K$^+$ content on a dry weight basis. **(E)** Shoot K$^+$ concentration.

It is a common approximation to consider most of the root weight equivalent to the cell sap, so we extracted all the liquid fraction from Col-0 and KO roots and their K^+ contents were measured by atomic absorption spectrophotometry (section M.9.3.1). In roots, K^+ concentrations were significantly lower in the double mutants compared to the wild type, being the differences between lines higher at increasing K^+ concentrations (figure R.8.).
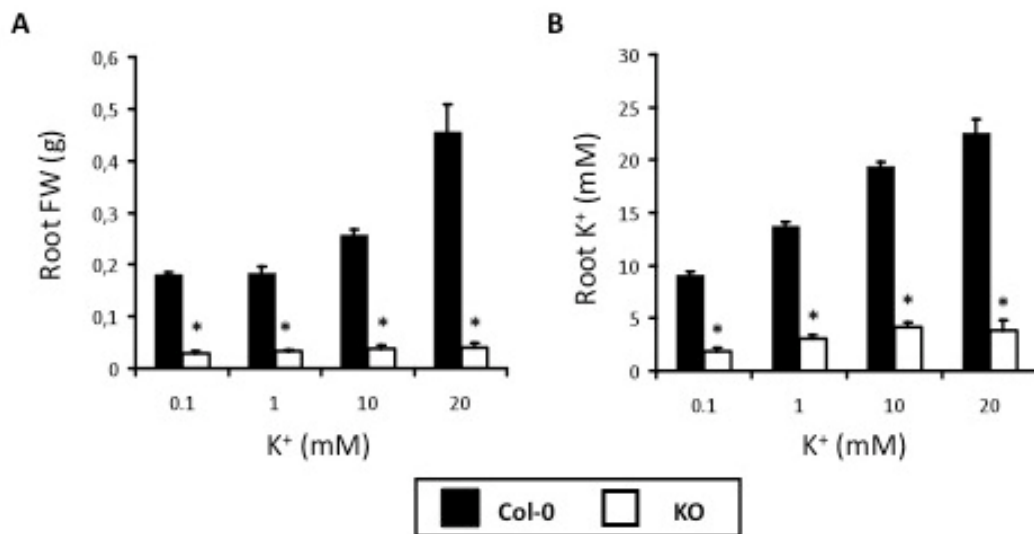
Figure R.8. Growth and K^+ contents of Double Knockout Mutant *nhx1-2 nhx2-1* Roots in Different Potassium Regimes. (**A**) Root fresh weight (FW) of wild-type Col-0 and double mutant plants of genotype *nhx1-2 nhx2-1* grown on LAK hydroponic medium for two weeks and then transferred to 0.1, 1, 10, and 20 mM K+ for an additional 2-week period. Data represent means and SE from of least three plants. Asterisks indicate statiscally significant diferences at *p*<0.05 in pairwise comparison by the Tukey's HSD (Honestly Significant Difference) test. (**B**) Root K^+ concentration. Lines analyzed and treatments as in (**A**).

Together, these results demonstrate that NHX1 and NHX2 proteins play an essential role in the accumulation of K^+ in roots and shoots of Arabidopsis and in the subsequent uptake of water by the tissues that generates the turgor pressure required for cell growth and expansion. The fact that higher K^+ concentrations in the media produce stronger toxic effects in the double mutant, instead of improving its phenotype, is most probably due to the faulty compartmentation of K^+ in the cells,

with lower than needed K$^+$ concentration into the vacuole and abnormally high values in the cytosol and in the apoplast pool.

R.2.3. Morphological analysis of *nhx1 nhx2* mutants by Scanning Electron Microscope (SEM).

The uptake of K$^+$ by plant cells, and its accumulation in vacuoles, is the primary driver for turgor generation and cell expansion (Leigh, 2001). Barragán and collaborators (2012) observed that plants of *nhx1-1 nhx2-1* genotype showed smaller leaf areas than the wild type when grown at any K$^+$ concentration. Specific leaf weight and succulence were also significantly reduced in these mutants, probably due to lower water uptake in the mutant. To further investigate the role of NHX1 and NHX2 in cell expansion we analyzed by scanning electron microscopy (SEM) the size and morphology of Col-0, L14 and KO leaves (figure R.9.). Plants were grown hidroponically and subjected to different K$^+$ regimes, as described previously, before the analysis (section M.9.1. and M.15.2.).
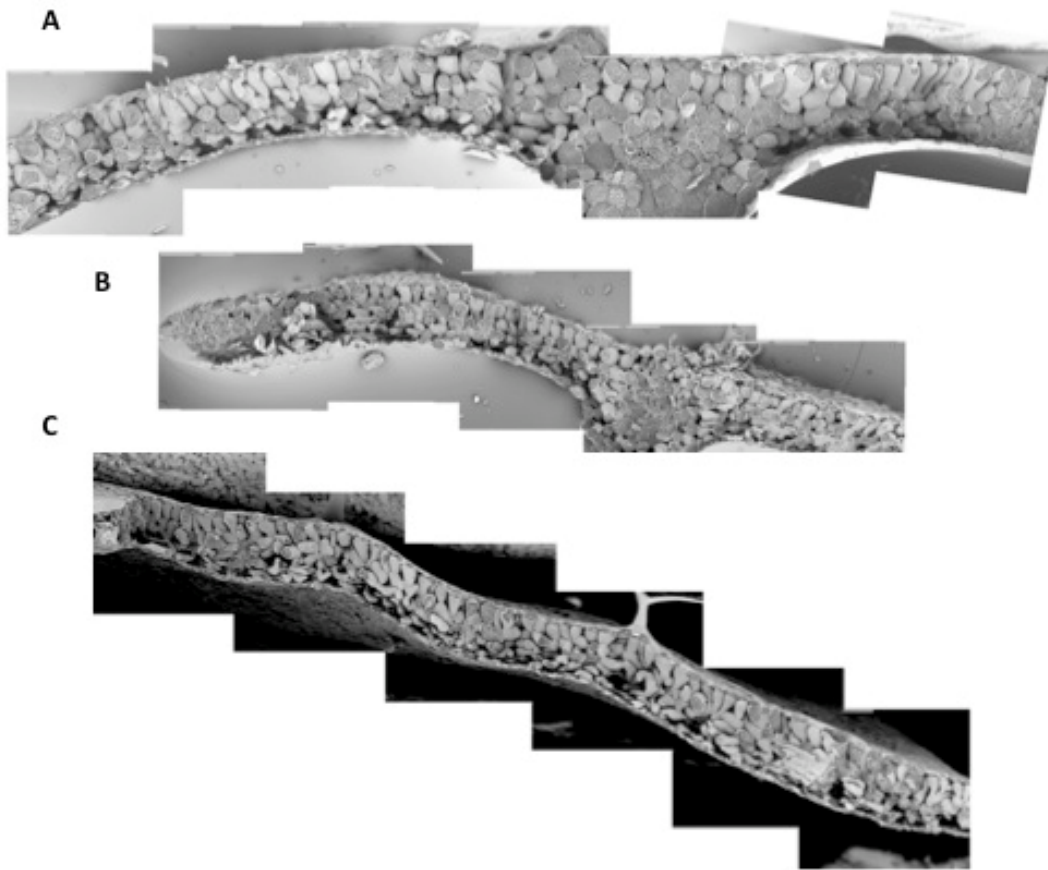
Figure R.9. Impaired Leaf Cell Expansion in *nhx1 nhx2* Mutants. Freeze-fracture sections at scanning electron microscopy from leaves of Arabidopsis Col-0 and L14 and KO mutant plants grown hydroponically in LAK medium. Bars = 200 μM. **(A)** Composition of serial pictures of a leaf from Col-0 plants grown for 2 weeks at 1 mM K$^+$ and then transferred to 20 mM K$^+$ for another 2 weeks. **(B)** Composition of an equivalent leaf from a plant of mutant line L14 treated as in **(A)**. **(C)** Composition of an equivalent leaf from a plant of mutant line KO grown for 4 weeks at 1 mM K$^+$.

In freeze-fractured sections for scanning electron microscopy, leaves from the L14 (figure R.10A.) and KO (figures R.9C. and R.10C.) lines presented a less developed spongy parenchyma when grown at 1 mM K$^+$ compared to the wild type (figures R.10A. and R.10C.). At 10 mM K$^+$, palisade cells were significantly smaller compared to the wild type and pyramidal in shape (figures R.9A. R.9B. and R.10B.). Smaller mesophyll cells resulted in a thinner leaf lamina in both mutant lines (figure R.9B. and R.9C.), what is in agreement with their smaller specific leaf weight (Barragán et al., 2012). At 20 mM K$^+$, the adaxial epidermis of the mutant line L14 presented small holes between

103

the epidermal cells (figure R.11.B.). However, the adaxial epidermis of *nhx1-2 nhx2-1* knockout mutant showed a very unusual morphology compared to L14 and Col-0 line plants. Knockout leaves presented two differentiated population of cells: epidermal cells with elongated shape instead of the normal puzzle shape, and small epidermal cells surrounding groups of stomata (figure R.11C.).
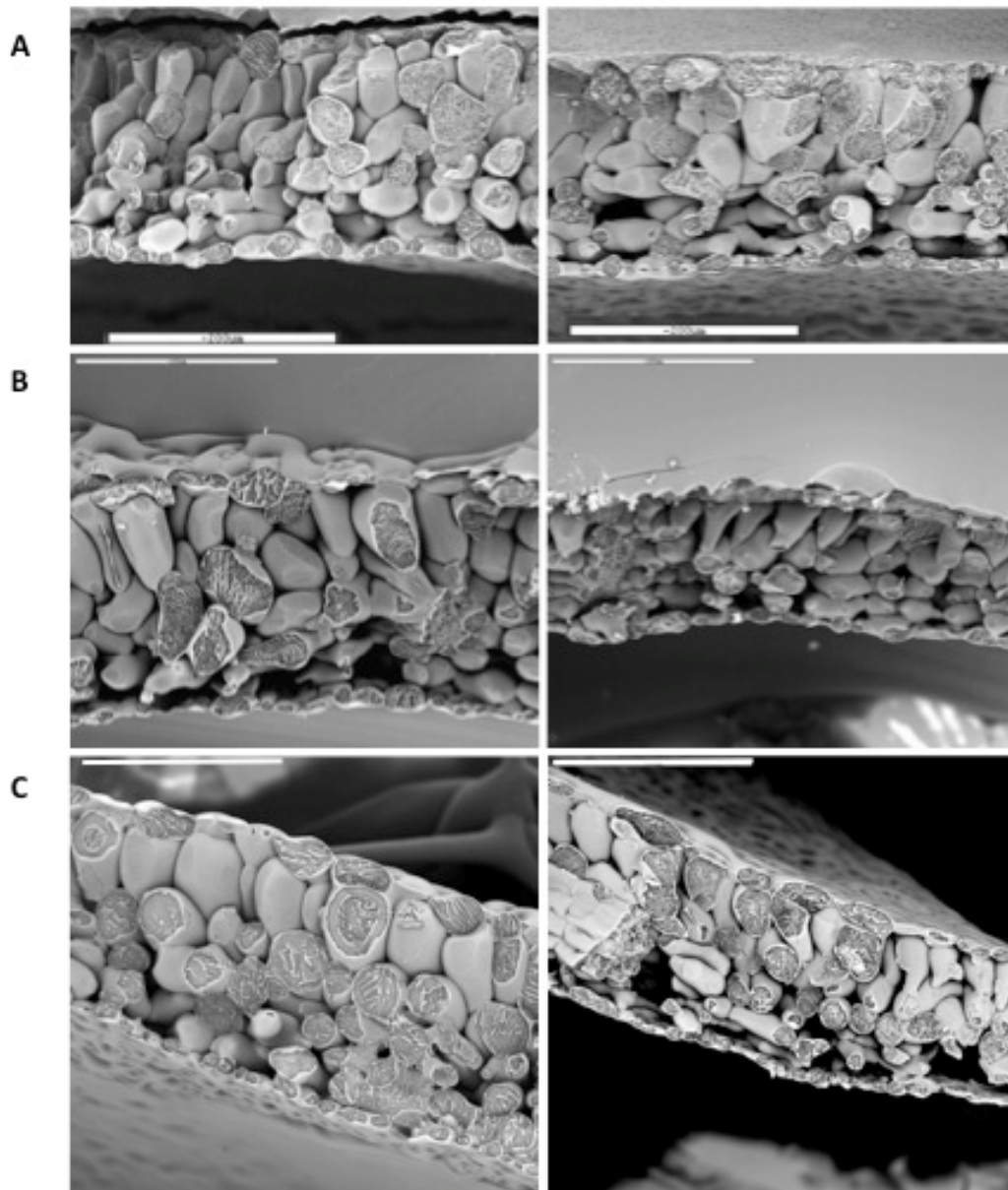
Figure R.10. Impaired Leaf Cell Expansion in *nhx1 nhx2* Mutants. Freeze-fracture sections at scanning electron microscopy from leaves of Arabidopsis Col-0 and L14 and KO mutant plants grown in LAK medium for 2 weeks and then transferred to 1 and 10mM KCl for an additional 2-week period. Equivalent leaves from each plant were processed for scanning electron microscopy. Bars = 200 µM. **(A)** Col-0 (left) and L14 (right) plants in 1 mM K$^+$. **(B)** Col-0 (left) and L14 (right) plants in 10 mM K$^+$. **(C)** Col-0 (left) and KO (right) plants in 1 mM K$^+$.
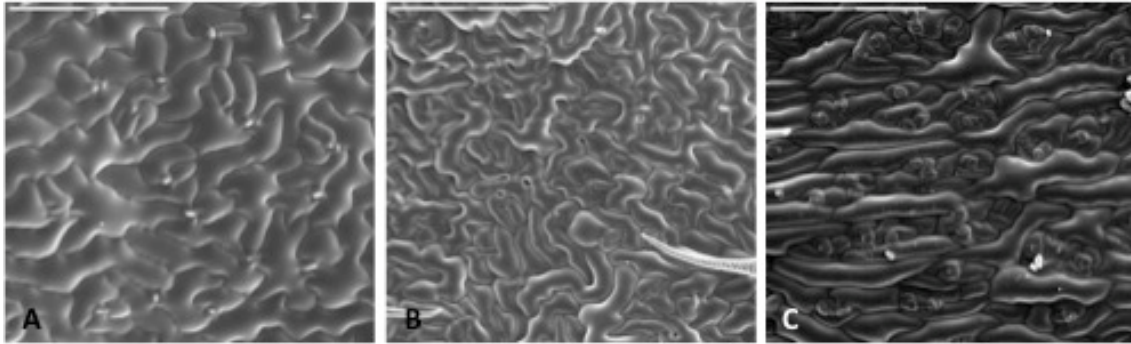
Figure R.11. Impaired Epidermal Morphology in *nhx1 nhx2* Mutants Scanning electron microscopy images from leaves of Arabidopsis Col-0 and L14 and KO mutant plants grown in LAK medium for 2 weeks and then transferred to 1, and 10mM KCl for an additional 2-week period. Equivalent leaves from each plant were processed for scanning electron microscopy. Bars = 200 µM. **(A)** Col-0 plants in 10 mM K$^+$. **(B)** L14 plants in 10 mM K$^+$. **(C)** KO plants in 1 mM K$^+$.

These data strongly suggest that the antiporters NHX1 and NHX2 are involved in cell expansion and development.

R.3. Expression Pattern of *AtNHX2*.

In previous work from other laboratories (Shi and Zhu, 2002; Apse et al., 2003) the expression pattern of *NHX1* was determined. The expression of *NHX1* was detected at all developmental stages tested and was particularly abundant in roots, stomata and pollen within anthers. To determine the tissue expression pattern of *NHX2*, a ca. 3.1 kb promoter upstream of the *NHX2* start codon was fused with the β-glucuronidase reporter gene (*GUS*) as described in section M.8.1. and the resulting construct was transformed into Col-0 wild-type Arabidopsis plants. Three independent transgenic lines were assayed for GUS expression and they produced consistent patterns. GUS expression was detected at all developmental stages tested, from seed germination to flowering and seed setting.

As depicted in figure R.12., histochemical GUS staining was detected, with varying intensity, in most tissues of Arabidopsis seedlings. In leaves and hypocotyls,

GUS staining was stronger around the vasculature, in meristems, and in guard cells of the stomata (A-D). In roots, the strongest GUS activity was detected in the vasculature, at the root tip and at the points of emergence of secondary roots, but not in root hairs and epidermis (D-F). In flowers, GUS staining was restricted to the filament of the stamens, the ovarian stigma, mature pollen grains within the anthers, and the pollen tube (G-K). A much weaker staining was seen in sepals and it was associated with vascular tissues. No significant GUS activity was detected in petals (G). Remarkably, the strongest GUS staining in flowers was also observed in stomata, including those in the anthers (J) and the ovarian stigma (H). In immature siliques, GUS staining was restricted to the septum and to the silique tip and base (L). This expression pattern strongly resembled that of *NHX1*, except at the tip of main roots, roots hairs, and meristemes, where *NHX1* and *NHX2* promoter constructs showed opposite expression levels. *NHX1* promoter showed GUS activity in root hairs but not in the main and lateral root tips, while *NHX2* promoter showed a strong GUS activity in root meristemes but it was absent in root hairs. Recently, the significant overlap of *NHX1* and *NHX2* expression patterns has also been reported ([Bassil et al., 2011a](#)) and microarray data in GENEVESTIGATOR (https://www.genevestigator.com/gv/plant.jsp) also indicates similar expression patterns of *NHX1* and *NHX2* genes and the significant greater abundance of their transcripts in guard cells of Arabidopsis. However, the various divergences regarding the expression patterns of *NHX1* and *NHX2* imply extensive overlapping but not identical physiological functions of NHX1 and NHX2.
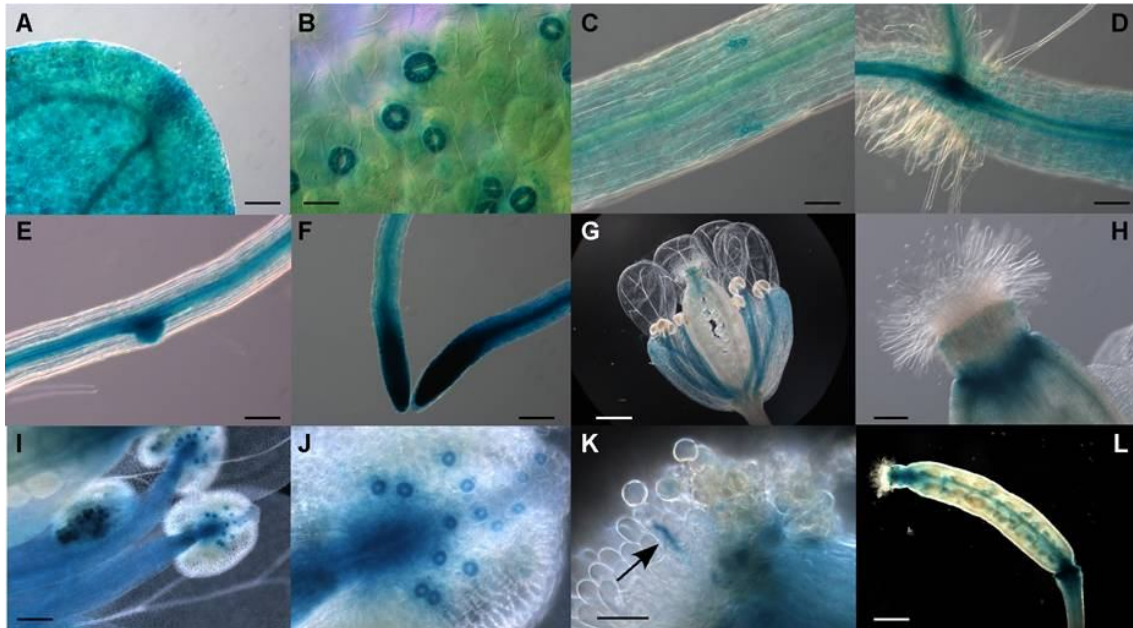
Figure R.12. **NHX2 Promoter-GUS Expression Pattern in Transgenic Arabidopsis Plants**. **(A)** GUS activity detected in cotyledons. **(B)** Strong GUS staining in guard cells of stomata in mature leaves. **(C)** to **(E)** Preferential expression in the vasculature of the main stem **(C)** and roots **(E)**. Note the strong expression in the root-shoot transition **(D)** and the point of emergence of secondary roots **(E)**. **(F)** Strong GUS staining in the root meristems. **(G)** to **(L)** Expression in reproductive organs was greater in filaments of the stamen (**[G]** and **[I]**), stigma (**[G]** and **[H]**), mature grain pollen **(I)**, and silique septum **(L)**. Note the high expression in the stomata of anthers in **(J)**, which is a close-up image of **(I)**, and in the elongating pollen tube (marked by arrow) **(K)**. Bars = 20 mm in **(K)**, 50 mm in **(B)**, 100 mm in **(A)**, **(C)**, to **(F)**, and **(I)**, and 400 mm in **(G)** and **(L)**.

R.4. Study of the role of NHX1 and NHX2 in guard cells.

In K^+-sufficient plants, the vacuolar pool plays a chief biophysical function, the lowering of osmotic potential to generate turgor and drive cell expansion. Rapid cell expansion relies on high mobility of the active osmoticum, and the highly permeant and abundant inorganic ion K^+ fits this role (MacRobbie, 2006). There are numerous examples of K^+ fluxes driving rapid cell expansion and organ movements (White and Karley, 2010), but nowhere is this critical function of the vacuolar K^+ pool more apparent than in the guard cells of the stomata. Stomatal opening and closure mainly occur in response to K^+ fluxes across the plasma membrane that allow swelling and shrinking of guard cells (Véry and Sentenac, 2003; Fan et al., 2004). In contrast to the

plasma membrane, knowledge of the changes occurring in intracellular compartments of guard cells during stomatal movements is less extensive. Guard cells use the vacuole to effect changes in their volumes, with parallel increases and decreases in vacuolar volumes during stomatal opening and closure, respectively, by more than 40% (Franks et al., 2001; Shope et al., 2003). The rapid accumulation and loss of K^+ and anionic organic acids by guard cells, mostly in the vacuolar compartment, controls the opening and closing of stomata and, thereby, gas exchange and transpiration. Among the solutes released from guard cells, more than 90% originate from vacuoles (MacRobbie, 1998). Description of the dynamic changes in vacuolar configuration during stomatal movement showed that a great number of small vacuoles are present in guard cells of closed stomata, and only a few large ones are present in guard cells of fully opened stomata (Gao et al., 2005; Tanaka et al., 2007a). Cation channel activities, which support stomatal closure, have been identified at the tonoplast, including fast vacuolar (FV), slow vacuolar (SV) and K^+-selective vacuolar (VK) cation channels (Isayenkov et al., 2010a; Hedrich and Marten, 2011). By contrast, the transporters responsible for the accrual of K^+ into vacuoles against the vacuolar membrane potential, that drive the stomatal opening, remain largely unknown.

Previous work demonstrated that NHX1 and NHX2 are involved in the accumulation of K^+ into the vacuole of plant cells, increasing their osmotic potential and forcing the uptake of water, which generates the turgor pressure necessary for cell expansion and growth (Barragán et al., 2012)(present work). We also recently postulated the involvement of NHX1 and NHX2 in the regulation of plant transpiration by demonstrating that the *nhx1 nhx2* L14 mutant showed a higher stomatal conductance and suffered a greater water loss than the wild type when plants of both genotypes were subjected to osmotic stress (Barragán et al., 2012). Furthermore, *AtNHX2* and *AtNHX1* are preferentially expressed in guard cells of the stomata (Shi and Zhu, 2002; Apse et al., 2003; Barragán et al., 2012) (present work). Together, these precedents indicate a possible malfunction of stomata in mutant plants lacking NHX1 and NHX2. Thus, to investigate further the direct role of both transporters in stomatal morphology and activity by facilitating K^+ accumulation in the vacuole of the guard cells a reverse genetics approach was applied. Stomatal responses of *nhx1-1 nhx2-1*

(L14) and *nhx1-2 nhx2-1* (KO) double mutant lines were compared with those of the wild-type line Col-0.

R.4.1. Morphological and developmental characterization of the *nhx1 nhx2* stomata.

R.4.1.1. Morphology of the stomata of *nhx1 nhx2* mutants.

Genes NHX1 and NHX2 were highly expressed in the guard cells of stomata (figure R.12.) (Shi and Zhu, 2002). To study the effect of the lack of both genes on the stomatal morphology, guard cells of Col-0, L14 and KO genotypes were visualized by SEM (section M.15.2.). Notably, stomata of mutant lines showed aberrant morphology with withered and rounded guard cells compared with the wild type, indicating that the simultaneous lack of NHX1 and NHX2 functions severely affected the turgor of guard cells, hindering their swelling capacity (figure R.13.).
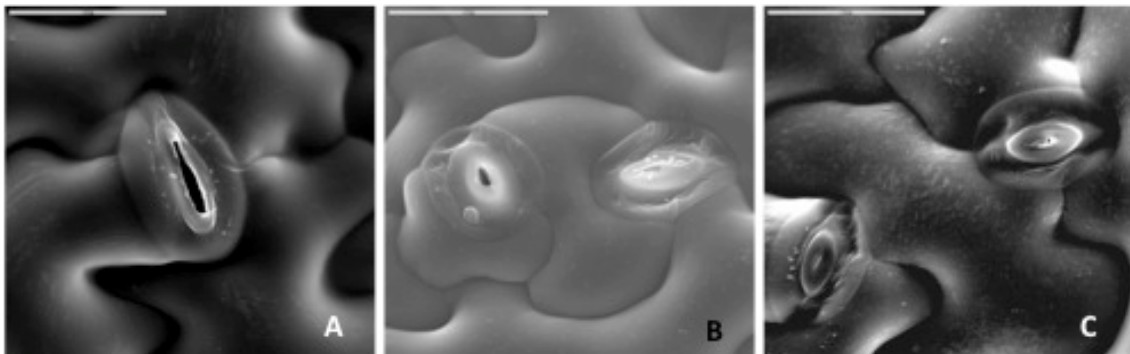
Figure R.13. Stomatal Morphology. Freeze-fracture sections at SEM from leaves of Arabidopsis Col-0 **(A)** and mutant plants from line L14 **(B)** and KO **(C)** grown hydroponically in LAK solution at 1 mM KCl. Scale bars: 20 μm.

R.4.1.2. Development of the stomata of *nhx1 nhx2* mutants.

In order to ascertain if the stomatal development in *nhx1 nhx2* mutant lines was also affected, impressions of the leaf abaxial surface using dental resin were made (section M.15.1) (figure R.14A.).
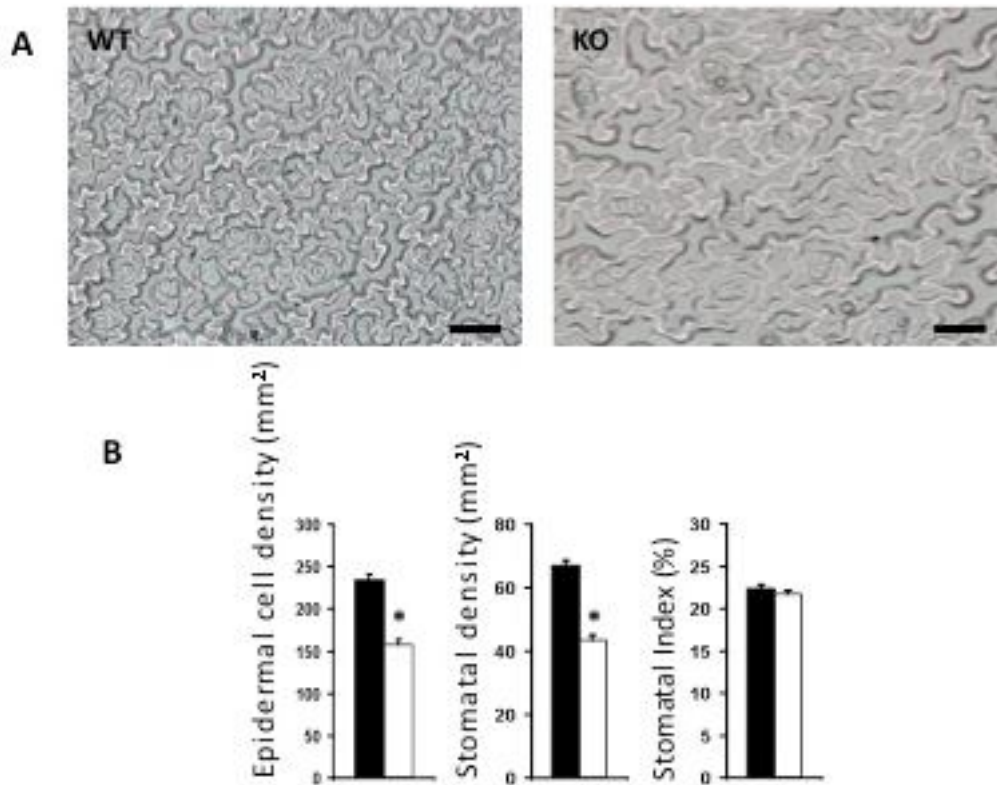
Figure R.14. Stomatal Development. **(A)** Representative images of epidermal impressions of the wild type (left panel) and the *nhx1-2 nhx2-1* mutant (right panel) Arabidopsis lines. Scale bar: 100 μm. **(B)** Epidermal cell density (left panel), stomatal density (middle panel) and stomatal index (right panel) calculated from dental resin impression images. Data represent means and SE from of least 42 images per line. Asterisks indicate statistically significant diferences at $p<0.05$ in pairwise comparison by theTukey's HSD test.

The number of epidermal cells and stomata per area was counted in KO and wild-type impressions and the stomatal index ([n° stomata/ n° epidermal cells + n° stomata]*100) was calculated. Under our growth conditions (section M.1.3.2.2.) the Col-0 line presented an average of 234 epidermal cells per mm^2, while the KO line

presented just 158 epidermal cells per mm^2 (figure R.14B.). This difference in the number of epidermal cells per area between lines is due to the presence of a heterogeneous population with disparate cell size. In our experimental conditions KO mutants presented epidermal cells larger than the wild type. Figure R.15. shows as the mode, defined as the frequency in percentage of cells included in each interval of increasing area, was displaced to higher values in the KO line (1500-2000 μm^2) compare to the Col-0 line (1000-1500 μm^2). These results are contradictory with those reported by Apse et al (2003) where they found a reduction in frequency of the very large epidermal cells in the Arabidopsis *nhx1* mutant. However, these results are coherent with the images obtained by SEM (figure R.13.). Also the number of stomata per area was lower in the mutant (43 stomata/mm^2) than in the wild type (67 stomata/mm^2) (figure R.14B.). However, both lines did not differ in the stomatal index (22.36% for the wild type and 21.71% for the KO line) (figure R.14B.), which indicates that the absence of NHX1 and NHX2 proteins do not alter the early development of guard cells.
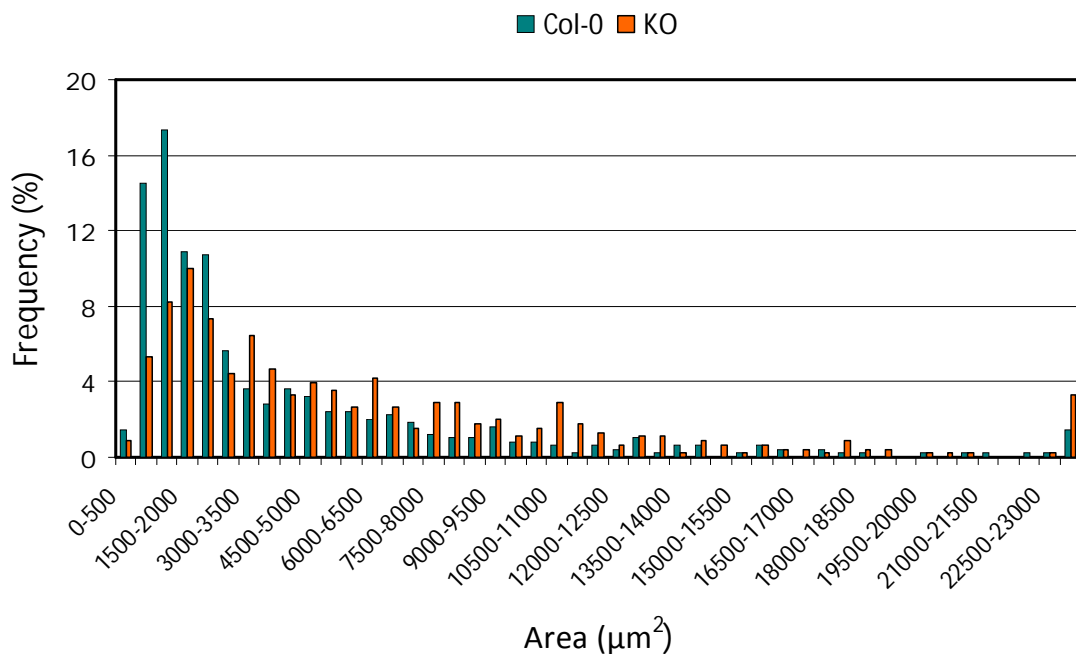
Figure R.15. Epidermal Pavement Cells Area. Frequency distribution of leaf epidermal cell size in wild type and *nhx1-2 nhx2-1* plants. Data represents the percentage of cells included in each area interval calculated from 7 epidermal impression images taken from 7 different plants per line.

R.4.2. Stomatal activity is severely impaired in *nhx1nhx2* mutant lines.

R.4.2.1. *In vitro* stomatal bioassays.

Stomatal bioassays provide a highly reliable and quantitative method for evaluating the processes of stomatal opening and closure (Merlot et al., 2007a). It has the advantage of allowing the testing, in a very controlled environment, of a wide range of effectors operating on the stomatal activity. To this end, light-induced stomatal opening and ABA-induced stomatal closure bioassays using abaxial epidermal strips of wild type and mutant lines were done following the methodology described in section M.11.

In ABA-induced stomatal closure experiments conduced with the leaky line L14 and the KO mutant line, the stomatal apertures were found to be lower by 30% in *nhx1 nhx2* mutants compared to the wild-type plants after 2 hours of illumination treatment in the absence of ABA (figure R.16A.). Furthermore, L14 and KO lines were less sensitive to ABA than wild-type plants. Col-0 epidermal peels responded to 0.1 µM ABA treatment closing their stomata around 50% compared to the control treatment without ABA. By contrast, line L14 closed their stomata a 23% in response to ABA while the KO double mutant was nearly insensitive to the hormone, closing their stomata just by 2% when ABA was applied (figures R.16B. and R.18.).
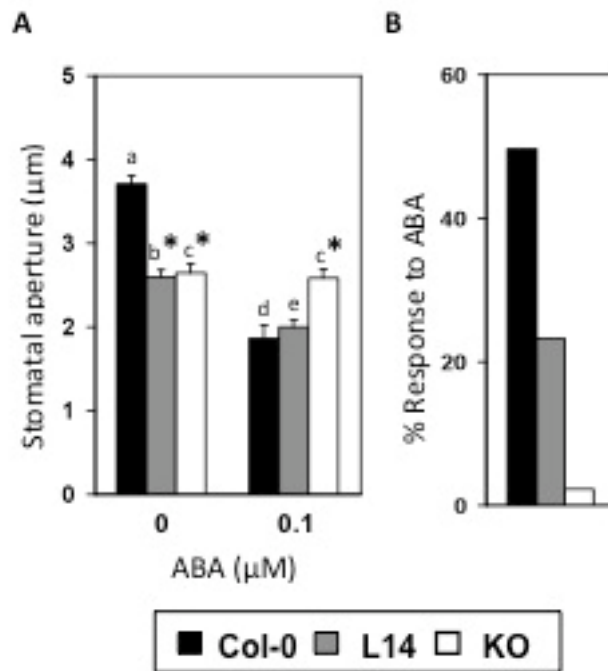
Figure R.16. ABA-Induced Stomatal Closure Bioassays. **(A)** Data represent the mean and SE of the absolute values of aperture of at least 40 stomata per line and per treatment. Asterisks indicate statistically significant diferences respect to the wild type for each treatment at $p<0.001$ in pairwise comparison by the Tukey's HSD test. Letters indicate statistically significant diferences between treatments for each line at $p<0.001$ in pairwise comparison by the Tukey's HSD test. **(B)** Data represent the mean of the response to ABA as percentage of the diminution of the maximal aperture value for each line.

In light-induced stomatal opening bioassays, after 2 hours of dark treatment to preclose the stomata, L14 and KO double mutant lines were not able to reach the same degree of closure of wild-type stomata. Stomatal apertures were found to be higher by 50% in *nhx1 nhx2* mutant plants compare to the wild type (figure R.17A.). Then, epidermal strips were incubated 2 hours under light and then stomatal apertures were measured. Under light, wild type stomata reached opening values 4.6 times higher than under dark, while L14 and KO opened their stomatas just 1.4 and 1.2 times respectively after the ligth treatment (figures R.17B. and R.18.).
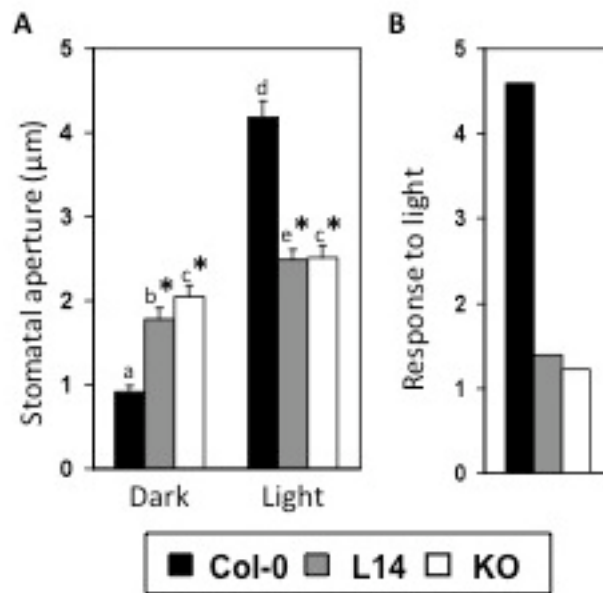
Figure R.17. Light-Induced Stomatal Aperture Bioassays. **(A)** Data represent the mean and SE of the absolute values of aperture of at least 40 stomata per line and per treatment. Asterisks indicate statistically significant diferences respect to the wild type for each treatment at $p<0.001$ in pairwise comparison by the Tukey's HSD test. Letters indicate statistically significant diferences between treatments for each line at $p<0.001$ in pairwise comparison by the Tukey's HSD test. **(B)** Data represent the mean of the increment, in x-fold units, of the stomatal aperture in response to light for each genotype.
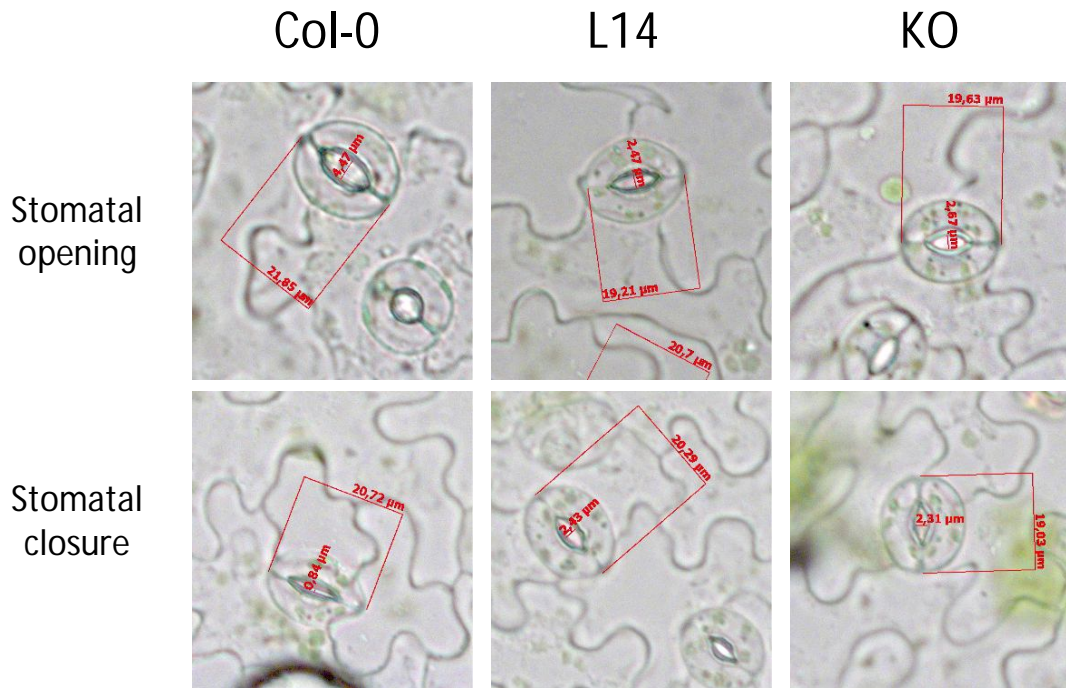
Figure R.18. *In Vitro* Stomatal Apertures. Representative images of *in vitro* stomatal bioassays after 2h of illumination treatment (upper panel) and after 2h of 0.1 µM ABA treatment (lower panel).

There are in the literature few reports on the ionic responses of stomata in detached epidermis, and these suggested that, besides K^+, other monovalent cations such as Na^+, Li^+, Rb^+ and Cs^+ could sustain stomatal opening in *Vicia faba* and *Commelina communis* L. (Humble and Hsiao, 1969; Willmer and Mansfield, 1969). Recently, two different works have shown that NHX1 and NHX2 proteins play a comparatively greater role in K^+ homeostasis than in Na^+ sequestration (Bassil et al., 2011a; Barragán et al., 2012). Arabidopsis mutant plants of genotype *nhx1 nhx2* are remarkably sensitive to moderate KCl concentrations (10 to 20 mM) but they do not show greater susceptibility to NaCl compared to the wild type. In fact, salt-related growth retardation is proportionally smaller in the *nhx1 nhx2* plants than in the wild type at 50 to 100 mM NaCl (Barragán et al., 2012) and the inclusion of moderate amounts of NaCl in the nutrient solution containing 30 mM K^+ alleviates K^+-associated toxicity symptoms (Bassil et al., 2011a). Notably, *nhx1 nhx2* mutant plants accumulated more Na^+ in their shoots than the wild type at 100 mM NaCl (Barragán et al., 2012). In order to investigate if Na^+ can support stomatal opening in the absence of

K$^+$ in Arabidopsis, and if this cation can functionally substitute K$^+$ for the stomatal opening of *nhx1 nhx2* mutant plants, light-induced stomatal opening bioassays were performed (section M.11.) incubating the epidermal strips in stomatal incubation buffer containing 10 mM K$^+$ or 10 mM of Na$^+$. Both, KCl and NaCl showed the capacity to support stomatal opening in Arabidopsis wild-type plants, although K$^+$ was significantly more efficient than Na$^+$. In contrast, stomatal aperture in the *nhx1 nhx2* mutant lines did not show significant differences between treatments, although stomatal aperture in KO mutant showed a slight increase in the presence of NaCl compared to KCl (figure R.19.).
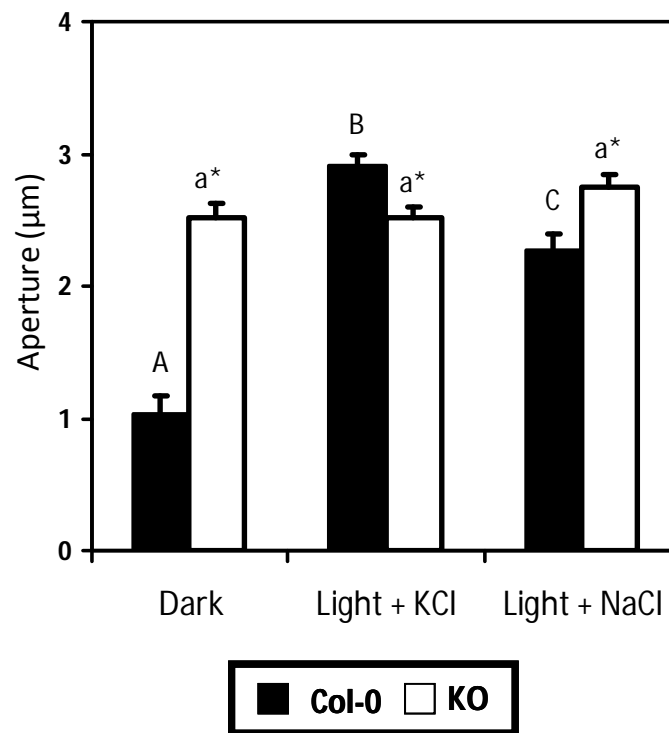
Figure R.19. Light-Induced Stomatal Aperture Bioassays in Presence of KCl or NaCl. Light-induced stomatal bioassays in presence of 10 mM KCl or 10 mM NaCl. Data represent the mean and SE of the absolute values of stomatal aperture of at least 40 stomata per treatment and per line. Asterisks indicate statistically significant diferences between lines per treatment at *p*<0.001 in pairwise comparison by the Tukey's HSD test. Different letters indicate statistically significant diferences between treatments per line at *p*<0.001 in pairwise comparison by the Tukey's HSD test.

Humble and Hsiao (1969) observed a very specific requirement for K^+ in *Vicia faba* to induce stomatal opening under light. Other cations as Na^+, Li^+ or Cs^+ could also support stomatal opening, albeit much higher concentrations were needed to reach the same outcome. Na^+ supports stomatal opening in *V. Faba* and *Commelina communis* ([Albrecht et al., 2001](#)), and in *C. communis* Na^+ is even more efficient than K^+ ([Willmer and Mansfield, 1969](#); [Robinson et al., 1997](#)). To estimate in our experimental conditions the concentration of Na^+ required for Arabidopsis stomata to reach approximately the same aperture than that achieved by 10 mM of K^+, light-induced stomatal opening bioassays were performed using 10 mM of K^+ and three different concentrations of NaCl (30, 50 and 75 mM). Wild-type stomatal aperture values were progressively higher at increasing Na^+ concentrations (from 30 to 75 mM Na^+) in the stomatal incubation buffer. In our experimental conditions, 50 mM of NaCl were necessary to obtain the same stomatal aperture than 10 mM of K^+ (figure R.20.)
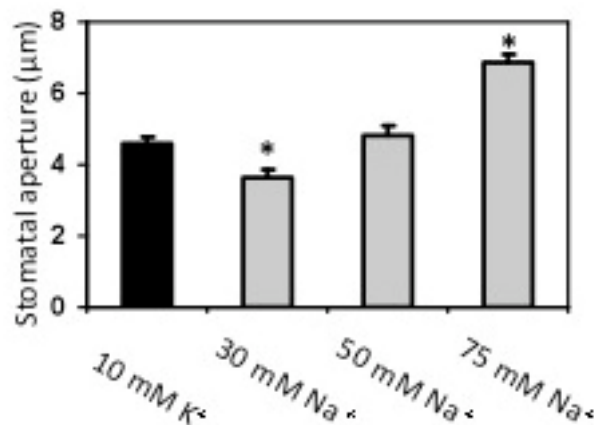
Figure R.20. Col-0 Na^+-Induced Stomatal Opening Bioassays. Stomatal opening bioassays using different buffers containing 10 mM K^+ or Na^+ at 30, 50 and 75 mM. Data represent the mean and SE of the absolute values of Col-0 stomatal aperture of at least 40 stomata per treatment. Asterisks indicate statistically significant diferences relative to the K^+ treatment at $p<0.001$ in pairwise comparison by the Tukey's HSD test.

We next examined the stomatal aperture for L14 and KO lines, incubated at 10 mM of K^+ or 50 mM of Na^+ (figure R.21.). At 10 mM K^+ only wild-type stomata responded to light-induced opening of the pore while neither mutant lines reacted to the presence of K^+ in the incubation buffer, as was shown above (figures R.17. and R.19.). By contrast, at 50 mM Na^+ lines L14 and KO showed a significant increase, of around 0.5-0.7 µm, in stomatal aperture compared to the dark and 10 mM KCl treatments. Stomatal aperture of Col-0 plants was the same in presence of 10 mM K^+ or 50 mM Na^+ (figure R.21.). Together, these results demonstrate that NHX1 and NHX2 play a major role in the stomatal movements by taking K^+ into the vacuole of guard cells in Arabidopsis, whereas they appeared to be dispensable for Na^+ accumulation. In addition, these results confirmed that Na^+ can generate cell turgor in the absence of K^+ to support stomatal opening in Arabidopsis, albeit higher amounts of this cation were required for maximum effect.
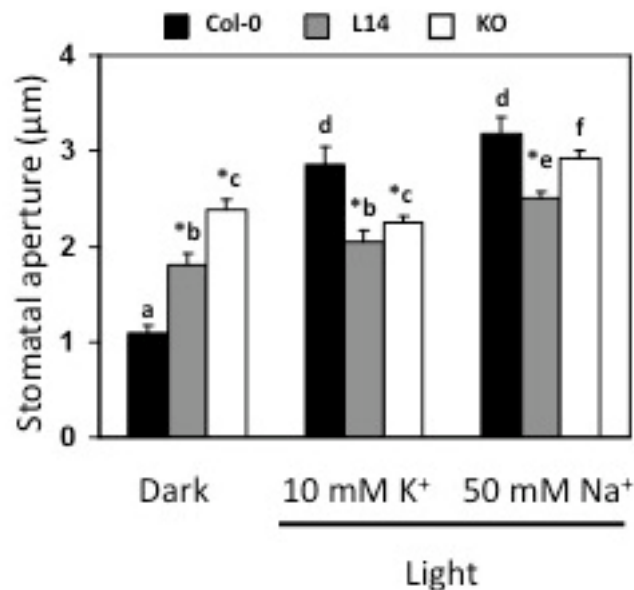
Figure R.21. Col-0, L14 and KO Na^+-Induced Stomatal Opening Bioassays. Light-induced stomatal bioassays in presence of 10 mM K+ or 50 mM Na+. Data represent the mean and SE of the absolute values of stomatal aperture of at least 40 stomata per treatment and per line. Asterisks indicate statistically significant diferences between lines per treatment at $p<0.001$ in pairwise comparison by the Tukey's HSD test. Different letters indicate statistically significant diferences between treatments per line at $p<0.001$ in pairwise comparison by the Tukey's HSD test.

R.4.2.2. Study of stomatal conductance by thermal imaging.

Infrared thermography is a non-invasive technology that correlates leaf temperature with transpiration flux, which finally represents stomatal aperture and conductance. The advantage of this method is the possibility to measure the temporal variations in stomatal aperture in intact leaves (Merlot et al., 2002; Wang et al., 2004). To further investigate the stomatal function of *nhx1 nhx2* mutants *in vivo*, infrared imaging was performed in a light-dark-light cycle.

Thermal imaging was performed as described in section M.12. Figure R.22. shows that during the first light period the leaf temperatures in L14 and KO double mutant lines were on average ~ 0.06°C and ~ 0.29°C respectively higher compared to wild type (table R.1.). These results indicate that mutant plants were transpiring less than the wild type, thus implying that their stomata were less opened than those of the control. The opposite effect was observed during the dark period. The leaves of L14 plants were approximately 0.09°C colder than wild-type leaves at the beginning of the dark period (table R.1. periods 2 and 3) but progressively reached the wild type values before the onset of the light period (table R.1. periods 4 and 5). However, the *nhx1-2 nhx2-1* mutant leaves were ~ 0.3°C colder than the wild type along all the dark period (table R.1. periods 2-5). This effect was probably due to the impossibility for the mutant to close their stomata in response to the dark, thus presenting higher transpiration rates. After the dark/light transition the values observed were similar to those of the first light period. Leaf temperatures in L14 and KO mutant lines were on average ~ 0.09°C and ~ 0.2°C higher respectively compared to the wild type at the end of the experiment (table R.1. period 6).

A

B
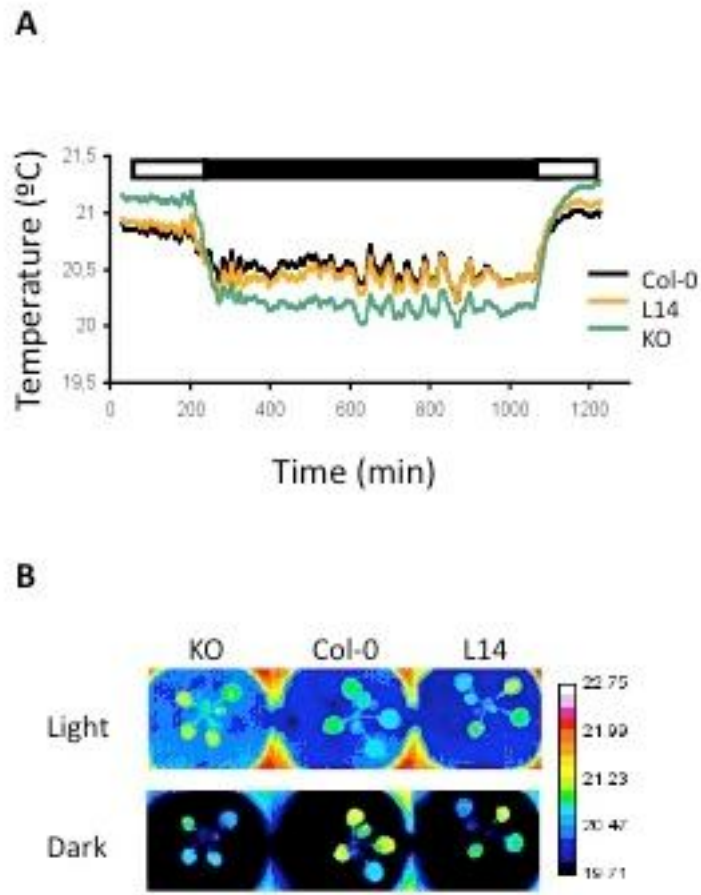
Figure R.22. Thermal imaging. (A) Data represent the moving average temperature of two leaves per plant from three differents plants of Col-0, L14 and KO lines along a light (white box)/ dark (black box)/ light cycle. **(B)** Representative infrared images of leaf temperature of Col-0, L14 and KO lines at the light and dark periods.

Period (min)	Line	Mean ± Std Dev (°C)	Paired differences Mean ± Std Dev (°C)
P1 (40-170) Day	Col-0	20.8 ± 0.27	
	L14	20.9 ± 0.25	0.06 ± 0.02[**]
	KO	21.1 ± 0.19	0.29 ± 0.08[**]
P2 (300-400) Night	Col-0	20.5 ± 0.23	
	L14	20.4 ± 0.23	0.09 ± 0.04[**]
	KO	20.2 ± 0.17	0.29 ± 0.07[**]
P3 (600-700) Night	Col-0	20.5 ± 0.36	
	L14	20.4 ± 0.35	0.09 ± 0.04[**]
	KO	20.2 ± 0.27	0.36 ± 0.11[**]
P4 (800-900) Night	Col-0	20.5 ± 0.36	
	L14	20.5 ± 0.35	0.009 ± 0.04[*]
	KO	20.2 ± 0.27	0.28 ± 0.11[**]
P5 (950-1050) Night	Col-0	20.4 ± 0.17	
	L14	20.4 ± 0.17	0.002 ± 0.03[ns]
	KO	20.1 ± 0.13	0.26 ± 0.06[**]
P6 (1100-1227) Day	Col-0	20.9 ± 0.14	
	L14	21.1 ± 0.14	0.09 ± 0.02[**]
	KO	21.2 ± 0.13	0.21 ± 0.07[**]

Table R.1. Thermal imaging dependent *t*-test between wild type plants and mutants at differents periods of the day. ** P< 0.001, * P< 0.05 and ns = no significant difference.

These *in vivo* data using complete plants are consistent which those obtained by aperture stomatal bioassays using paradermal sections of leaf abaxial epidermis. All these results together prove that the stomatal function is impaired in the *nhx1 nhx2* mutants.

R.4.3. The absence of proteins NHX1 and NHX2 affects circadian rhythm and stomatal conductance.

Daily rotation of the earth on its axis produces regular diurnal changes in light, temperature and humidity. Plants, as most organisms, couple their behavior to this daily periodicity. Most of these daily biological rhythms are controlled by the circadian clock, a 24 h timekeeper (Harmer, 2009). A self-sustaining rhythm consists in an oscillator mechanism where several genes, called clock genes, are transcriptional/translationally positive/negatively regulated producing feedback loops.

These constant rhythms are entrained by input signals coming from the environment, and by output pathways that connect the oscillator to diverse biological processes as growth, flowering, photosynthesis or stomatal opening (Webb, 2003; Yakir et al., 2007; Harmer, 2009). Circadian clocks make possible to coordinate the timing of physiology processes with environmental changes, providing adaptive advantages to the plants (Harmer, 2009). In Arabidopsis the correct matching of the periodicity of the endogenous circadian clock with the external light/dark cycles enhances chlorophyll content, photosynthetic carbon fixation, and growth (Dodd et al., 2005).

Stomatal aperture is one of the many physiological processes controlled by the circadian clock. In normal growth conditions, the circadian clock promotes stomatal preopening during the last hours of the dark period, so that the stomata be already opened at the first hours of the photoperiod when solar radiation is high but air temperature is not yet compromising the plant water status. In the middle of the photoperiod, when air temperature is high and therefore water loss from evapotranspiration increases, the circadian clock promotes stomatal closure. Stomatal closure is stimulated during the dark period because photosynthesis does not occur. This stomatal circadian rhythm would increment photosynthesis and growth while diminishing water loss (Webb, 2003). Stomatal movements are subject to fluxes of water and solutes across the cell membranes, especially K^+ and sucrose that rely on channels and transporters that are also regulated by the circadian clock. Circadian regulation of the transporters might take place at transcriptional or post-translational level, controlling the protein abundance or the transport activity (Haydon et al., 2011). Lebaudy and collaborators demonstrated that mutant plants without plasma membrane inward K^+ channel activity failed to anticipate the dawn in light/dark cycles or under extended dark conditions (Lebaudy et al., 2008). It has been reported that, among those of other ion transporters, transcrips of *AtNHX1* and *AtNHX2* present circadian regulation (Covington and Harmer, 2007; Dodd et al., 2007)(http://diurnal.cgrb.oregonstate.edu/).

In order to evaluate the differential expression of *NHX1* and *NHX2* genes in the course of a light/dark cycle transcriptional analyses by RT-PCR were performed

(section M.13.1.). Total RNA of Col-0 leaves was extracted (section M.4.1.) at 5 points of the diurnal cycle: 5 minutes before the dawn, 2 and 4 h after the onset of light, 5 minutes before the dusk and after 4 h of dark. cDNA was synthesized as described in section M.4.2. and PCR was performed using gene-specific primers for *NHX1*, *NHX2* and *β-TUBULIN-4* (section M.13.1. and annex 2). *AtNHX1* transcript abundance show a weak increment before the onset of light and then its transcription decreases progressively along the light/dark cycle whereas *AtNHX2* transcript accumulated to a maximum after 2h of light (3.5-fold induction) and declined after 4 h of light (figure R.23.). These data suggest that the expression of *AtNHX1* and *AtNHX2* are indeed responsive to the circadian clock.
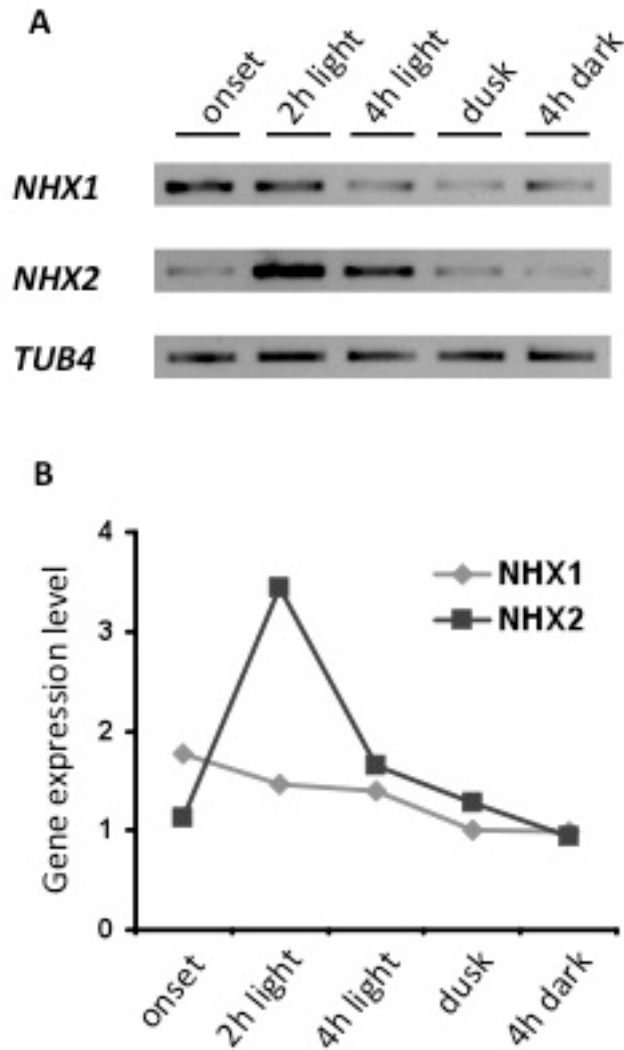
Figure R.23. Semiquantitative RT-PCR of NHX1 and NHX2. (A) RT-PCR analysis of *NHX1* and *NHX2* mRNA expression levels in wild-type line at different points of the day/night cycle. The gene *TB4* encoding β-tubulin-4 was used as loading control. **(B)** Relative *NHX1* and *NHX2* gene expression level at different points of the day/night cycle calculated by densiometry analysis of the bands obtained in **(A)**. Each point represents the mean of three different samples per line calculated after normalization to *TB4*.

We have previously reported that *nhx1-1 nhx2-1* (L14) mutant plants are unable to withstand osmotic stress. Wild-type plants responded to an osmotic challenge in hydroponic culture with a rapid closure of stomata, while *nhx1-1 nhx2-1* mutant plants responded more slowly and reached the reduced transpiration rates of the wild type only after 90 min of treatment, suggesting that the fast response mediated by rapid K⁺ fluxes was impaired in the mutant (Barragán et al., 2012). To understand the behavior

of the *nhx1 nhx2* mutant plants growing in optimal conditions, we measured stomatal conductance in leaves of intact plants at six different points in a whole nycthemeral period (8h/16h day/night) (section M.13.2.; figure R.24.). At the first measurement, which corresponds with the onset of the day photoperiod, there were not differences in stomatal conductance between the wild type and KO plants. After two hours of light, the stomatal conductance of Col-0 leaves increased from 115 ± 6.4 to 214 ± 34.8 mmol m^{-2} s^{-1} H_2O, while the stomatal conductance of KO leaves did not change significantly (from 99 ± 3.3 to 115 ± 13.0 mmol m^{-2} s^{-1} H_2O). At the middle of the photoperiod the Col-0 stomatal conductance (275 ± 15.8 m^{-2} s^{-1} H_2O) presented its maximum. By contrast, *nhx1-2 nhx2-1* stomatal conductance did not increase significantly, changing from 115 ± 13.0 to 137 ± 9.4 mmol m^{-2} s^{-1} H_2O. At dusk, stomatal conductance in the wild type decline (133 ± 16.0 mmol m^{-2} s^{-1} H_2O). At this point of the cycle the value measured in the KO plants (138 ± 3.9 mmol m^{-2} s^{-1} H_2O) coincide again with that of the wild type. After 2 h and 4 h of dark the stomatal conductance of wild type is minimal and constant (54 ± 7.6 and 51 ± 7.4 mmol m^{-2} s^{-1} H_2O). However, the knockout double mutant stomatal conductance (119 ± 8.9 and 102 ± 5.3 mmol m^{-2} s^{-1} H_2O) did not fall to the Col-0 values during the dark period, by contrast, these measurements were similar to those showed in the morning.
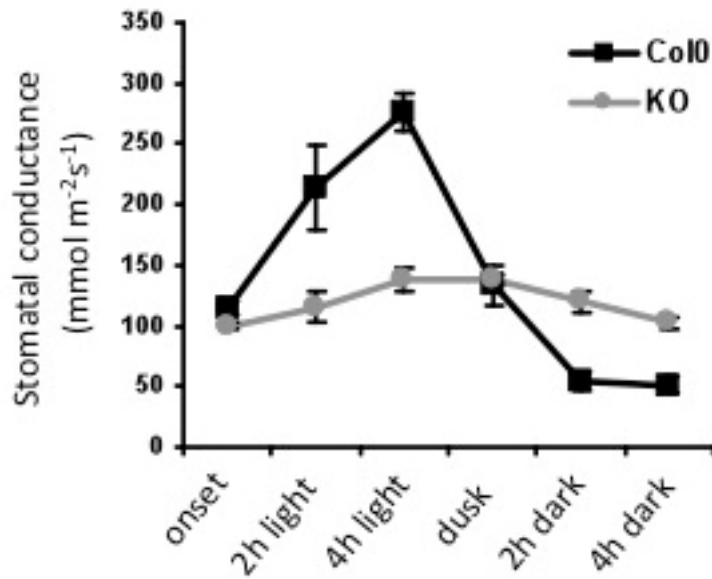
Figure R.24. Stomatal Conductance. *In planta* stomatal conductance measurements in Col-0 and KO leaves at different point of the day/night cycle. Data represent mean and SE of 3 plants per line.

Stomatal conductance data show that wild-type plants were able to anticipate the light and the dark periods preopening the stomata before the onset of the light period and preclose them before the dusk, the highest stomatal aperture occurs at midday, and stomata remain closed during the dark period. Mutant *nhx1-2 nhx2-1* plants were unable to respond to the circadian clock since their stomatal conductance, and therefore the stomatal opening, did not show significant differences between the day and the night periods (figure R.24.). Stomatal aperture of wild-type and KO lines just coincide at onset and at dusk, likely because wild-type stomata are half-open or half-closed respectively whereas KO stomata present always the same aperture around 2.5 μm (figures R.16A., R.17A. and R.18.). These results indicate that wild-type plants present a circadian regulation of the stomatal movements, thus getting a proper coupling of gas exchage and photosynthesis with the external light/dark cycles. By contrast, the *nhx1 nhx2* mutant plants did not show significant changes in the course of a light/dark cycle, which cause a lower gas exchange during the light period and a higher water loss during the night compared to the wild type.

R.4.4. *nhx1 nhx2* mutants shows high drought tolerance due to less soil water consumption.

Col-0, L14 and KO plants were grown for 7 weeks under short day conditions (8h day/16h night) in a growth chamber with constant temperature and humidity (section M.1.3.2.2.) before being subjected to drought (section M.14.). The same watering regime was applied to all the lines and pots were covered with plastic film to avoid water evaporation of the soil. Before initiating the drought phase pots were well watered until reaching the field capacity of the soil and the surplus water drained away. The start of the drought tolerance assay was in coincidence with the beginning of the dark period. Pots were weighed at dusk and at dawn during four consecutive days and transpiration was calculated as mL of water loss per foliar area and time (figure R.25A.). During the first and second day KO mutant showed higher transpiration during the dark periods than the Col-0 and L14 lines. This is in accord with the results obtained by *in vitro* closure stomata bioassays (section R.4.2.1.; figure R.16.) and thermography (section R.4.2.2.; figure R.22.) and conductance measurements (section R.4.3.; figure R.24.). By contrast, both mutant lines presented less transpiration than the wild type during the first and second light periods. These results demonstrate again that the L14 mutant is more affected in stomatal opening than in stomatal closing whereas the KO mutant is affected in both processes. At the third day the transpiratory oscillations of the wild type changed toward lower transpiration values, and as depicted in the figure R.25C. wild type plants were withered. However, the transpiratory oscillations did not change in the mutants and at the third day of drought treatment plants were still turgid. At the fourth day Col-0 transpiration continued declining while L14 and KO plants lost water at the same rate. L14 plants start to shrivel around 5-6 days after stop watering while KO mutants can survive without watering more than 25 days (figure R.25C.). Water loss measurements show that whereas the wild type consumed a 60% of the soil water in 4 days, L14 mutant consumed a 40% and the KO mutant consumed less than a 20% a value very similar to the soil water loss (figure R.25B.).

A
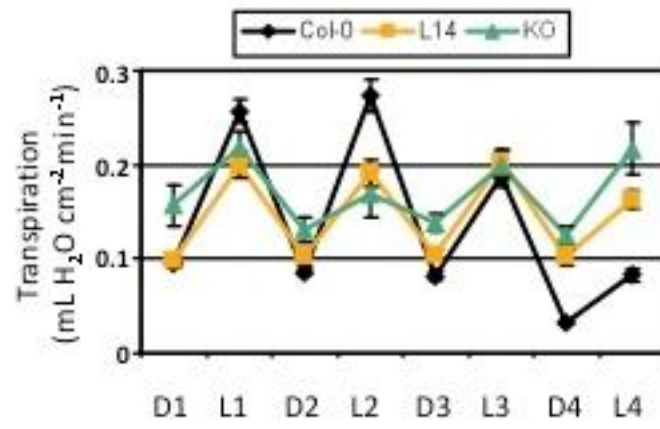
B
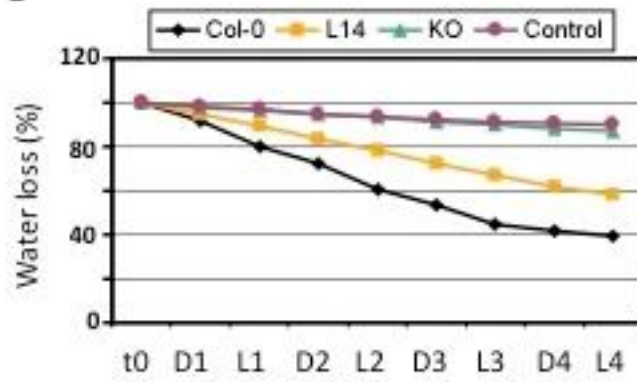
Figure R.25. Drought Assay. (A) Transpiration measurements of Col-0, L14 and KO plants during 4 days of drought stress. Pots were weighed two times per day, at the start of the dark period (D) and at the onset of the light period (L), and transpiration was calculated as mL of water lost per area in each time interval (16 h dark/ 8h light). Data represent mean and SE of at least 7 plants per genotype. **(B)** Percentage of water loss along the drought assay in Col-0, L14 and KO plants. Data represent mean and SE values from at least 7 plants per genotype and to quantify the soil evapotranspiration empty pots were used as controls. **(C)** Pictures of Col-0 (left), L14 (middle) and KO (right) plants before the drought stress (t0, upper panel) and after 2, 4, 12 and 25 days after drought.

In summary these results attest that the *nhx1 nhx2* mutants can resist long drought periods compared to the wild type because by losing less water through their stomata, they consume less water from the soil while at the same time their growth and seed production are diminished.

R.4.5. Vacuolar dynamics in guard cells.

Recent technical advances in the visualization of vacuoles and in image analysis of living cells by fluorescent dyes and fusion of tonoplast proteins with the green fluorescent protein (GFP) have revealed the highly organized and complex morphology and dynamics of vacuoles. Plant cells exhibit not only simple inflated balloon-like vacuoles but also diverse intra-vacuolar structures, as canal-like, bulb-like and sheet-like structures (Sato et al., 1997; Saito et al., 2002; Uemura et al., 2002). Guard cell vacuoles undergo several morphological changes that contribute in aperture and closure stomatal movements. Open stomata of *Vicia faba* and Arabidopsis present just a few big vacuoles that occupy nearly the entire guard cell volume. However, the vacuole of the closed stomata appears fragmented in a great number of small vacuoles and other intra-vacuolar structures as bulb-like structures and sheet-like vacuolar membrane invaginations. These vacuolar morphological changes have been shown to be essential for the stomatal function (Gao et al., 2005; Tanaka et al., 2007b).

Ir order to study if NHX-dependent vacuolar K$^+$ accumulation in guard cells affected the vacuolar dynamics, transgenic Col-0 and *nhx1 nhx2* knockout double mutant lines expressing the tonoplast intrinsic protein γ-TIP (Höfte et al., 1992) fused to GFP were created (section M.8.2.).

Stomatal opening bioassays were done on leaves of 4-6 week-old-plants as described in section M.11. Epidermal peels, where epidermal pavement cells were disrupted, were harvested at the end of the night period and incubated for 2 hours in darkness. Then stomatal opening was induced chemically by adding 3 μM of fusicoccin to the buffer and keeping the epidermal strips in dark. After 2 hours, control and

treated epidermal peels were visualized under the confocal microscope (figure R.26.). Stomata from untreated Col-0 epidermal peels were closed and their vacuoles were split up in several small vesicles. Fusicoccin-treated stomata appeared completely opened and guard cells presented just one or few big vacuoles. Fluorescence was also observed, in some cases, in the ridges of the transvacuolar strands. The stomatal opening in the KO line under fusicoccin treatment was lower compared to the wild type and a significant reduction in the fusion of vacuoles in their guard cells was found.
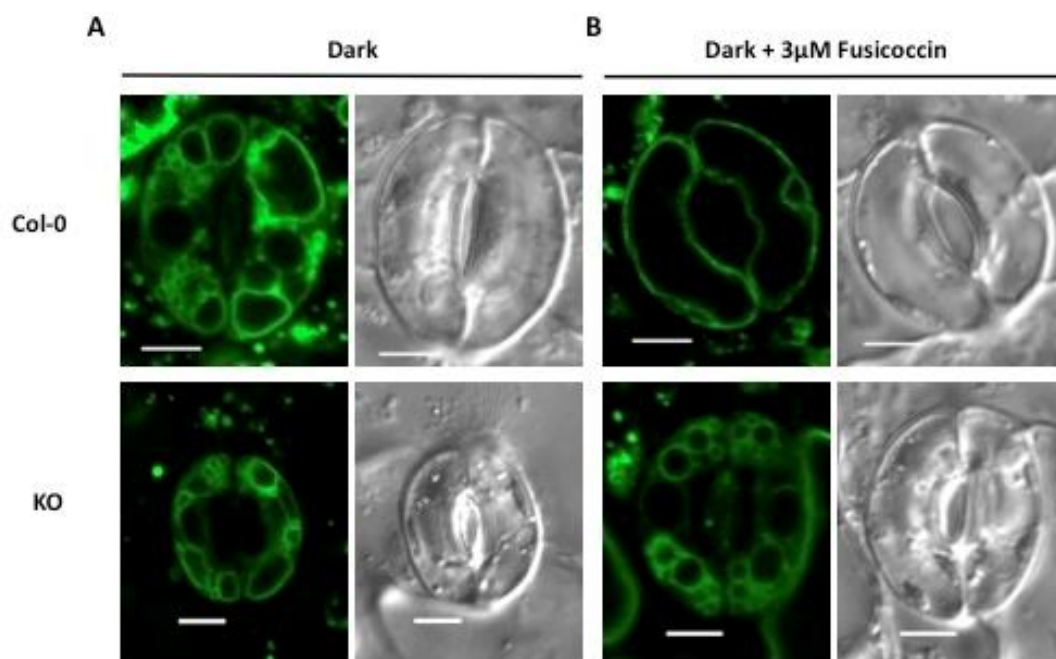
Figure R.26. Vacuolar Morphology of Col-0 and KO Guard Cells During the Stomatal Opening. Vacuolar structures of Col-0 and KO guard cells visualized with γTIP:GFP after dark incubation for 2h **(A)** and 3 μM fusicoccin treatment for 2h **(B)**. Right and left panels show bright field and fluorescence images of γTIP:GFP, respectively. Scale bar: 5 μm.

For ABA-induced stomatal closure experiments, abaxial epidermal peels were incubated for 2 hours under white light. Then ABA was added at a concentration of 10 μM and epidermal strips were incubated for 2 hours in light (section M.11.; figure R.27.). When the stomata were opened under white light illumination, γ-TIP:GFP fluorescence was mainly observed on the vacuolar membrane of wild-type guard cells while KO guard cells exhibited several vesicles instead of just a few big vacuoles. When

Col-0 stomata were closed by application of ABA, many invaginated structures, vesicles and bulb-like structures appeared in the vacuolar lumen in addition to the outer vacuolar membrane. Application of ABA did not show any effect in vacuolar morphology of *nhx1 nhx2* mutant guard cells.
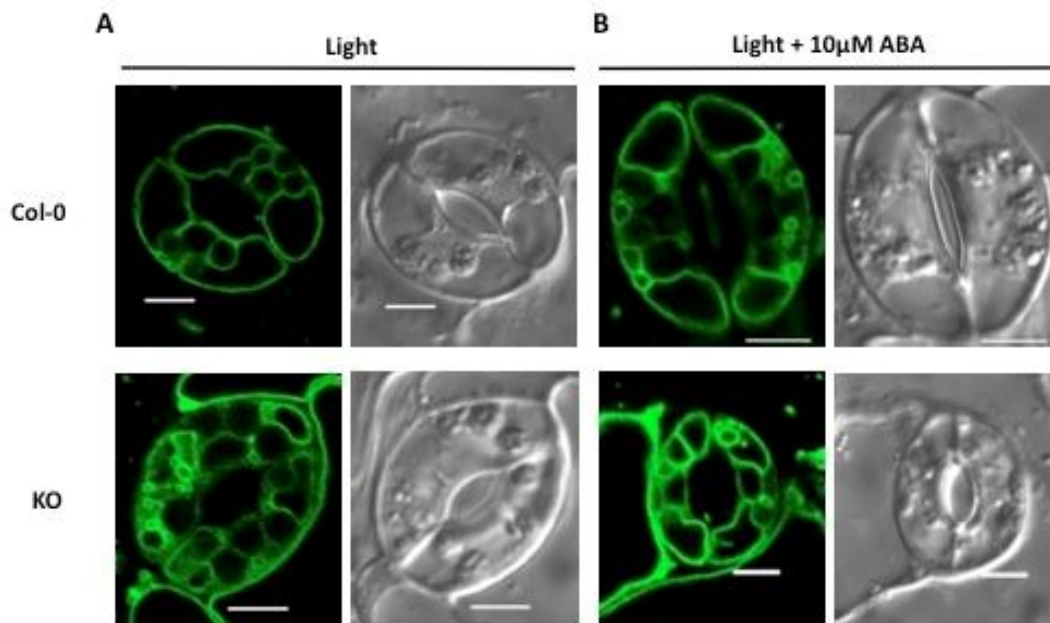
Figure R.27. Vacuolar Morphology of Col-0 and KO Guard Cells During the Stomatal Closure. Vacuolar structures of Col-0 and KO guard cells visualized with γTIP:GFP after light illumination for 2h **(A)** and 10 µM ABA treatment **(B)**. Right and left panels show bright field and GFP fluorescence images of γTIP:GFP, respectively. Scale bar: 5 µm.

As was shown in section R.4.2.1. (figure R.21.) the KO mutant exhibits some degree of stomatal aperture in the presence of 50 mM Na^+. In order to study if this increase in stomatal aperture is accompanied with vesicular fusion, KO epidermal strips were incubated 2h in light in buffer containing 10 mM K^+ or 50 mM Na^+. Figure R.28. shows that, in comparison to the stomatal opening achieved in the presence of K^+, KO stomata reached indeed higher aperture and were able to form few big vacuoles in the presence of Na^+. It is interesting to note the higher frequency of appearance of bright and spherical structures in the lumen of guard cell vacuoles (bulbs) when the stomata were opened with Na^+ (figure R.28B.).
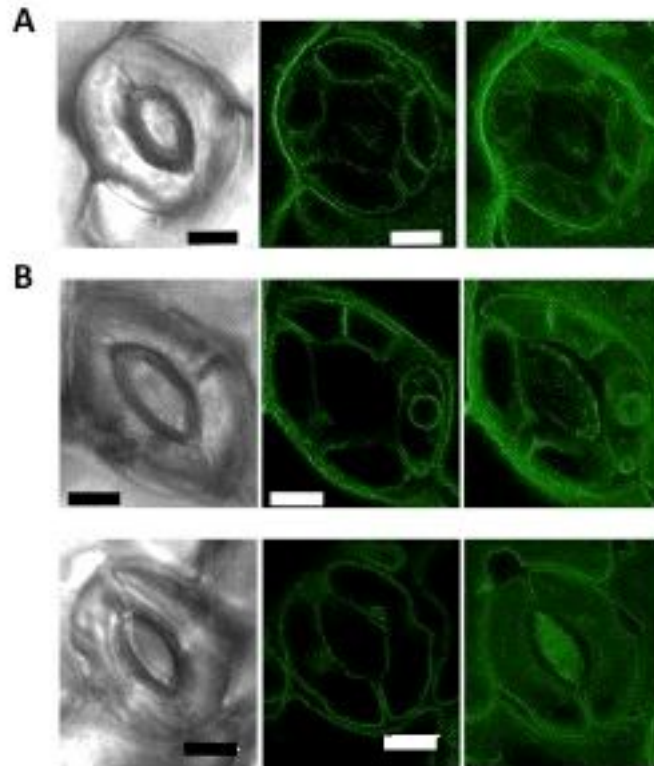
Figure R.28. KO Vacuolar Dynamics in Presence of Na⁺. Vacuolar structures of KO guard cells visualized with γTIP:GFP during the stomatal opening. Pictures were taken after light illumination for 2h in presence of 10 mM KCl **(A)** or 50 mM of NaCl **(B)**. Left, middle and right panels show bright field, GFP fluorescence images, and a 3-D reconstruction of successive Z-axis images of γTIP:GFP, respectively. Scale bar: 5 μm.

A transgenic Arabidopsis Col-0 line expressing the AtNHX2 protein fused to GFP (section M.8.2.) was used to investigate in which kind of guard cell vacuolar structures are localized the NHXs antiporters. With this purpose light-induced stomatal opening and dark-induced closure stomatal bioassays were performed and epidermal peels pictures were obtained by confocal microscopy. Figure R.29A. shows that the NHX2:GFP fluorescence was mainly observed on the vacuolar membrane when stomata were open. However, as was the case for the wild-type γ-TIP:GFP line, when stomata were closed NHX2:GFP fluorescence was observed in several tonoplast invaginations and vesicles (figure R.29B.).
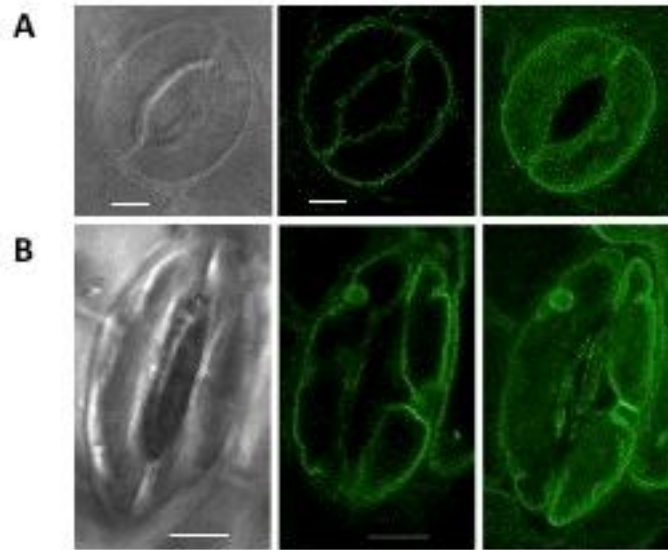
Figure R.29. Vacuolar Morphology in the NHX2:GFP Line. Stomatal vacuolar structures of the AtNHX2:GFP overexpressing line after light illumination for 2h **(A)** and after dark incubation for 2 h **(B)**. Left, middle and right panels show bright field, GFP images, and a 3-D reconstruction of successive Z-axis images of γTIP:GFP, respectively. Scale bar: 5 μm.

To monitor the vacuolar dynamics in guard cells during the stomatal movements time-lapse experiments were performed as described in section M.11. using leaf discs of the transgenic Col-0 and KO lines expressing the tonoplast intrinsic protein γ-TIP::GFP. It is worth to notice that stomatal aperture and closure were lower and greater respectively using leaf discs, where the pavement epidermal cells are viable, than using epidermal peels, where pavement epidermal cells are disrupted (Klein et al., 1996; Roelfsema and Hedrich, 2005).

Leaves of wild type and KO with viable epidermal pavement cells were harvested and incubated 2 h in light to induce stomatal opening. Then leaf discs were mounted in a stomatal buffer containing 10 μM of ABA for confocal microscopy visualization. As shown in figure R.30., wild-type stomata were completely open at time 0 (t0) of ABA application and fluorescence was just observed on the vacuolar membrane of a single big vacuole that occupied all the guard cell volume. After 5 minutes (t5) of ABA addition a 50% of stomatal closure was noted and invaginations coming from the tonoplast began to be formed. At times t10, t15 and t20 the

134

invaginations grew forming transvacuolar strands. These changes in vacuolar morphology were accompanied of stomatal closure. At t30, when the stoma was almost completely closed, the vacuole was split up in several vesicles and more vacuolar invaginations and transvacuolar strands could be observed. By contrast, in the KO mutant the stomatal aperture and the vacuolar morphology did not change at any time before or after of the ABA application (figure R.30.). The vacuole of the KO mutant, which appeared wrinkled and fragmented in several vesicles, did not occupy the entire cell volume at the start point (t0) of the experiment.
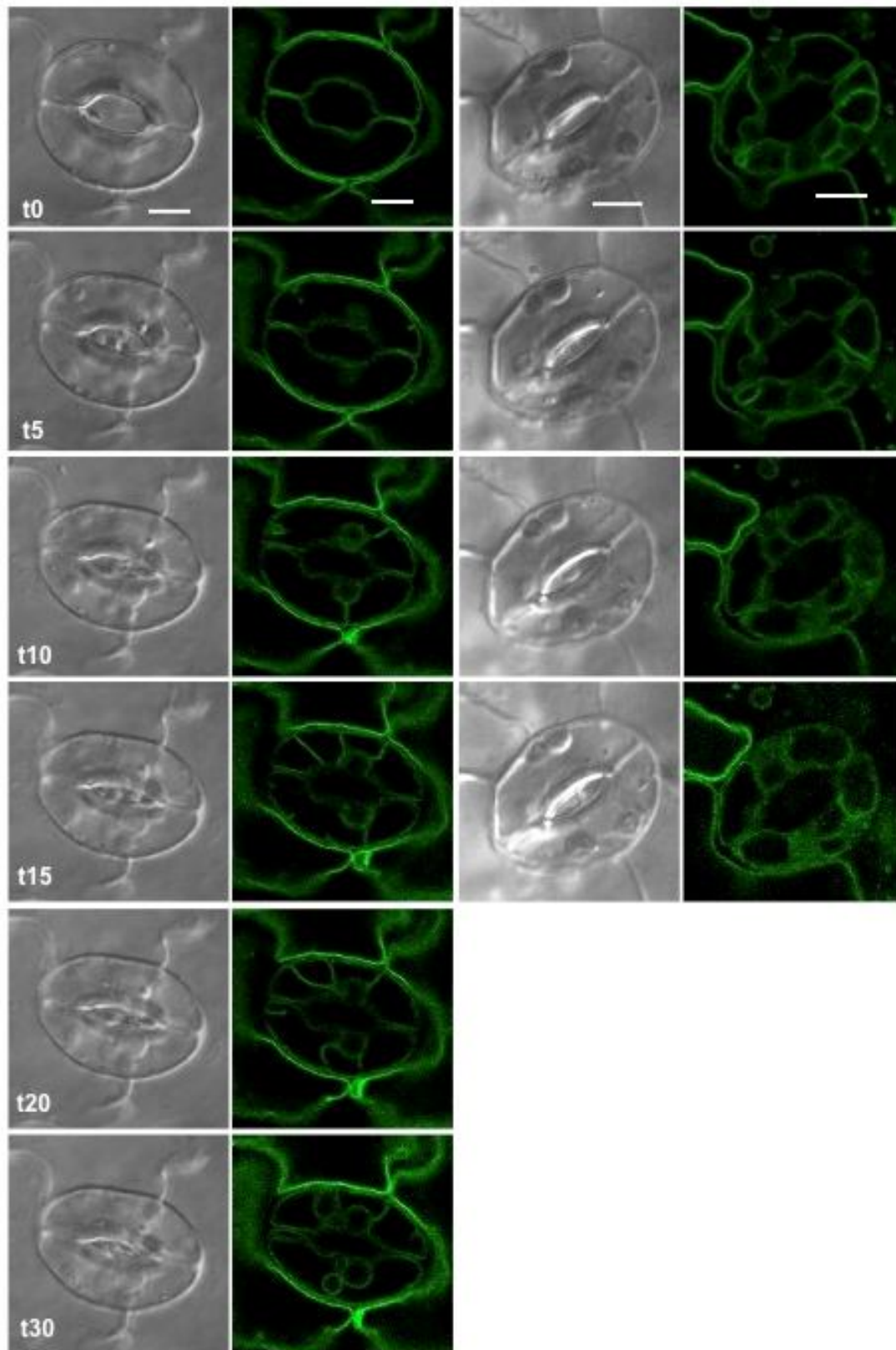
Figure R.30. Stomatal Closure Time-Lapse. Vacuolar structures of Col-0 (left columns) and KO (right columns) guard cells visualized with γTIP:GFP at different time points after 10 μM ABA treatment. Left and right panels show bright field and GFP fluorescence images of γTIP:GFP, respectively. Scale bar: 5 μm.

To study the vacuole dynamic in the stomatal opening, Col-0 and KO leaves were incubated 2 h in the dark to induce stomatal closure. Then leaf discs were mounted in a stomatal buffer containing 3 µM of fusicoccin for confocal microscopy visualization (figure R.31.). At time 0, before the fusicoccin action, wild-type stomata were completely close and the fluorescence was observed in diverse structures as vesicles, tonoplast invaginations and transvacuolar strands. Between 10 and 60 minutes after fusicoccin application the vacuolar structures were disappearing, remaining some rounded vesicles and transvacuolars strands. These vacuolar changes were linked to stomatal opening. At t90 just one large vacuole or few big vacuoles were observed in guard cells. These vacuoles swelled and occupied most of the cellular volume, leading to the stomatal opening as can be observed after 2 h (t120) of fusicoccin treatment. Stomata in leaf discs of KO line (figure R.31.) were not close prior to fusicoccin application (t0) and the vacuole presented many tonoplast invaginations and small vesicles could also be observed. At no point along the treatment a single vacuole was observed although some round-vesicle formation happened. However, these vesicle fusion events were not accompanied by an increase in stomatal opening.
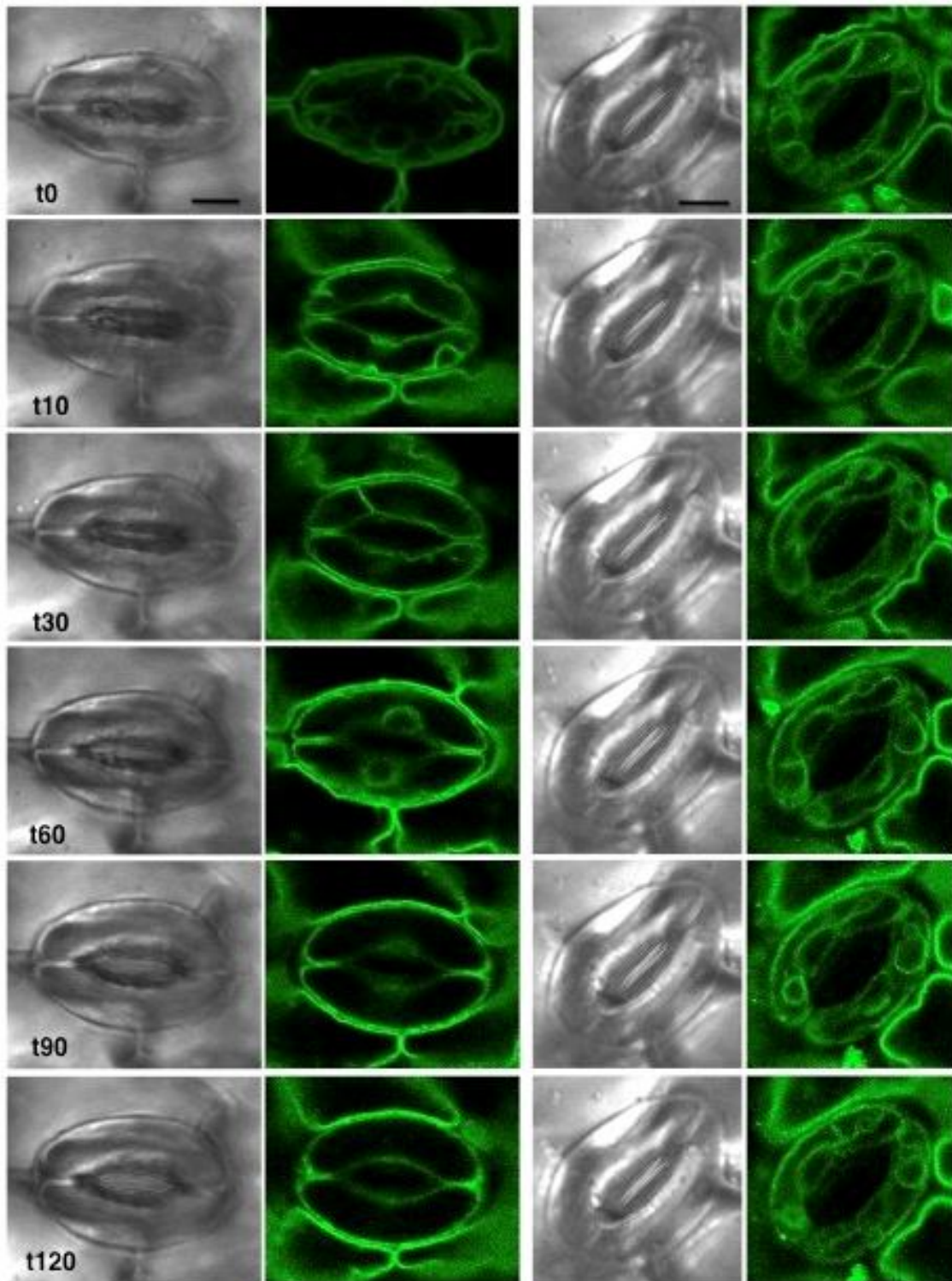
Figure R.31. Stomatal Opening Time-Lapse. Vacuolar structures of Col-0 (left columns) and KO (right columns) guard cells visualized with γTIP:GFP at different time points after 3 μM fusicoccin treatment. Left and right panels show bright field and GFP fluorescence images of γTIP:GFP, respectively. Scale bar: 5 μm.

These observations suggest that vacuolar morphology and dynamics, which is essential for the stomatal movements, are impaired in plants lacking proteins NHX1 and NHX2. In *nhx1 nhx2* mutant plants the small vacuoles do not fuse with each other to form a single big vacuole and increase the vacuolar volume, failing in stomatal opening. In general, the KO mutant present less vesicles and tonoplast structures than closed stomata of wild-type plants, likely affecting also the stomatal closure.

R.4.6. Double mutant lines presented a reduced vacuolar K^+ pool.

To estimate the size of the vacuolar K^+ pool in the *nhx1 nhx2* mutants, freeze-fractured leaves of L14 and KO plants grown in LAK medium with 1 mM K^+ were analyzed with a scanning electron microscope fitted with energy-dispersive X-ray spectroscopy (EDX) (section M.9.3.2.). This technique analyzes the elemental composition of cells and cell compartments in plant tissues by the impact of an electron beam on the sample. This produces X-rays that are characteristic for each element found in the sample. It is important notice that this technique allows to calculate the relative differences on ion contents between lines but not their absolute ion contents. The large vacuoles of mesophyll palisade cells of L14 mutant plants showed fewer K^+ counts than Col-0 (figure R.32A.) (Barragán et al., 2012). K^+ counts were also significantly lower in guard cells of stomata of mutant plants, where both NHX1 and NHX2 show high expression levels (figure R.12.; Shi & Zhu, 2002; Barragán et al, 2012), as well as in epidermal subsidiary cells neighboring the stomata. By contrast, K^+ counts were higher in guard cells of stomata of KO mutant plants (figure R.32B.). This somehow contradictory result can be explained by the fact that the vacuole of the KO mutant is always fragmented, so it is uncertain wether the X-ray beam is being aimed at the right compartment, whereas in other cellular types, such as mesophyll palisade, the size and uniformity of the vacuoles renders much more reliable ion content measures using the same technique. Further investigation using other methods would be necessary to determine the K^+ vacuolar content in *nhx1-2 nhx2-1* guard cells.
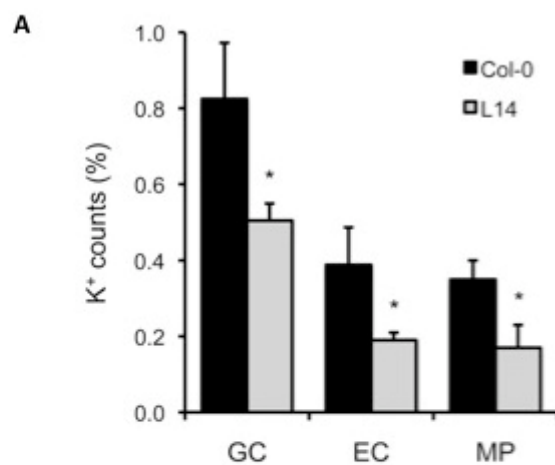
Figure R.32. Reduced Vacuolar K⁺ Content in the *nhx1 nhx2* Mutants. **(A)** K^+ content in the vacuoles of guard cells (GC), epidermal cells neighboring the stomata (EC), and in mesophyll palisade cells (MP) of L14 leaves as determined by scanning electron SEM-EDX. Shown are the average percentage and SD of K^+ counts relative to total elemental counts. A minimum of 20 cells of each cell type per line were analyzed. Significant differences between the mutant line L14 and the wild type by the LSD method ($P < 0.05$) are indicated by asterisks. **(B)** K^+, Na^+, Ca^{2+} and Cl^- contents in the vacuoles of guard cells of KO mutant leaves as determined by SEM-EDX. Shown are the average of the ion counts. A minimum of 5 cells per line were analyzed. Significant differences between the KO and the wild type lines by the LSD method ($P < 0.05$) are indicated by asterisks.

R.5. Post-translational regulation of AtNHX1 and AtNHX2.

R.5.1. NHX1 and NHX2 can form homomers and heteromers.

Oligomerization of transporter subunits seems to be a common feature of proteins involved in secondary active transport. The transporter oligomerization would

regulate their activity and function (Reinders et al., 2002; Veenhoff et al., 2002; Ludewig et al., 2003). It is known that the mammalian NHE proteins, homologous to plants and yeast NHX proteins, exist as oligomers in the membranes. NHE1 was detected as a dimer in brush-border membrane vesicles by immunoblotting under non-reducing conditions (Fliegel et al., 1993) and it was reported that the formation of NHE1 and also of NHE3 homodimers takes place via their transmembrane regions (Fafournoux et al., 1994). More recently it has been published that, in addition to the transmembrane domain, the C-terminal cytoplasmic domains of NHE1 interacs to form dimers that are essential for the proper regulation of the exchange activity in a neutral pHi range (Hisamitsu et al., 2004; Hisamitsu et al., 2006).

In order to know if the Arabidopsis NHX1 and NHX2 proteins are able to form oligomers, both genes were cloned in the BiFC vectors pSPYNE173 and pSPYCE(M) (section M.16.2.1.; Annex 3) (Waadt et al., 2008). Pairwise combinations pSPYCE(M)-NHX1/pSPYNE173-NHX1, pSPYCE(M)-NHX2/pSPYNE173-NHX2, pSPYCE(M)-NHX1/pSPYNE173-NHX2 and pSPYCE(M)-NHX2/pSPYNE173-NHX1 were co-expressed in *Nicotiana benthamiana* leaves by agroinfiltration (section M.16.2.2.) and analyzed by fluorescence microscopy 3 days after agroinfiltration (section M.16.2.3.). As shown in figure R.33. fluorescence was present in all the BiFC combinations, thus indicating that NHX1 and NHX2 can form homomers and heteromers *in planta*. As expected, all the interactions took place in the tonoplast.
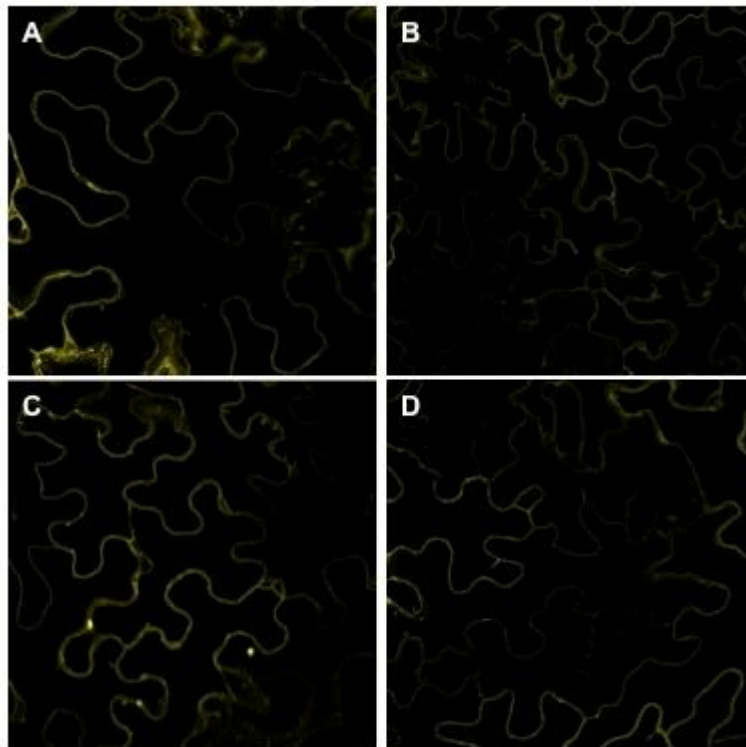
Figure R.33. NHX1 and NHX2 Oligomerization Visualized by BIFC. Epifluorescence images of *Nicotiana benthamiana* leaf sections expressing **(A)** SPYNE173-NHX1 and SPYCE(M)-NHX1, **(B)** SPYNE173-NHX2 and SPYCE(M)-NHX2, **(C)** SPYNE173-NHX1 and SPYCE(M)-NHX2, and **(D)** SPYNE173-NHX2 and SPYCE(M)-NHX1.

The oligomerization of NHX1 and NHX2 was also studied by Y2H. The C-terminal fragments of NHX1 and NHX2 were cloned in pBD and pAD vectors (section M.16.1.; annex 3). The yeast strain AH109 was transformed with different plasmid combinations as was described in section M.16.1. and the interactions were tested on YNB/-His/-Trp/-Leu. The NHXsct did not grow in selective media when they were coexpressed with the empty vectors, while the pairwise combinations pBD-NHX1ct/pGAD-NHX1ct and pBD-NHX1ct/pGAD-NHX2ct were able to grow on YNB/-His/-Trp/-Leu (figure R.34.). This result confirms that NHX1 and NHX2 proteins can form homomers and heteromers in plants and yeast, and that these interactions take place, at least, through their C-terminal domains.
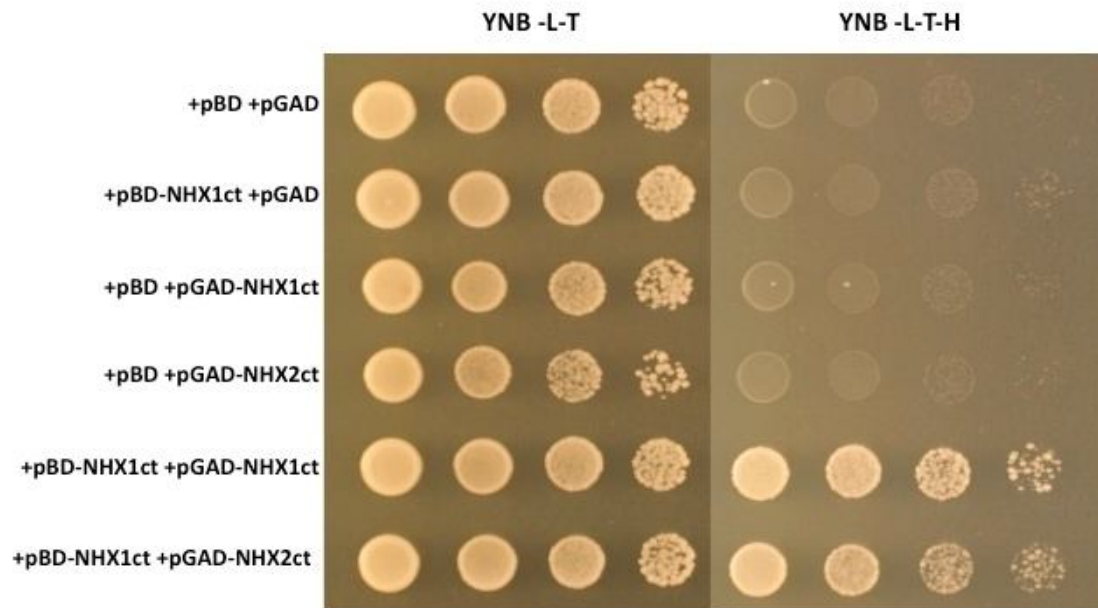
Figure R.34. NHX1ct and NHX2ct Oligomerization by Yeast Two-Hybrid.

R.5.2. The activity of AtNHX2 in yeast is dependent of phosphorylation.

The analysis of the *Arabidopsis* phosphoproteome identified the identical phosphorylated peptide GFVPFVPG[**pS**]PTER pertaining to the C-terminal end of AtNHX1 and AtNHX2, although the 100% sequence identity of both isoforms in this region did not allow to assign it to one of them, or both (Sugiyama et al., 2008; Whiteman et al., 2008b). The phosphorylated residue corresponds to Ser526 of NHX1 and Ser532 of NHX2. To evaluate the relevance of these conserved residues in the activity of AtNHX1 and AtNHX2, we generated non-phosphorylable (S to A) and phospho-mimetic (S to D) mutant alleles by substituting Ser526 of NHX1 and Ser532 of NHX2 for alanine and aspartic acid, respectively (section M.17.1. and Annex 2) (figure R.35.).

Vacuolar lumen

Cytoplasm

GFVPFVPG**S**PTER
GFVPFVPG**A**PTER
GFVPFVPG**D**PTER
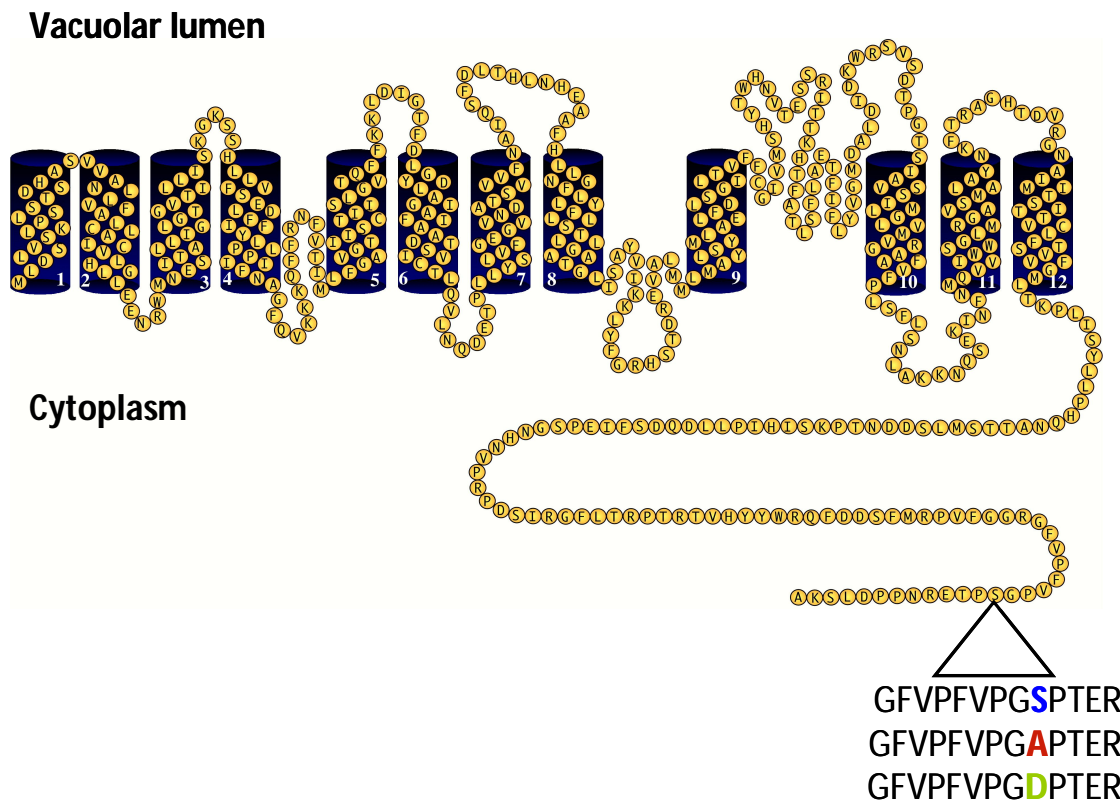
Figure R.35. Schematic Structure of NHX Proteins Indicating the Phosphorylation Site and the Mutated Alleles.

Yeast strain AXT3K lacks the plasma membrane-Na$^+$ efflux proteins ENA1-4 and NHA1, and the prevacuolar Na$^+$/H$^+$ exchanger ScNHX1, which renders these cells sensitive to NaCl and hygromycin B (Quintero et al., 2002) (section M.1.2.1.). It had previously been demonstrated that the expression in the AXT3K cells of the NHX1 and NHX2 proteins of Arabidopsis could suppress the salt- and hygromycin B-sensitive phenotypes of this strain (Quintero et al., 2000; Yokoi et al., 2002; Barragán et al., 2012). Hence, the wild type NHX1 and NHX2 and the mutant alleles *nhx1*S526A, *nhx2*S532A and *nhx2*S532D were cloned in the yeast expression vector pDR195 (section M.17.1.) and transformed in the yeast strain AXT3K (Quintero et al., 2000; Yokoi et al., 2002) to perform functional studies (sections M.1.2.1., M.6.2. and M.17.2.) (figure R.36.). Expression of wild type AtNHX1 and AtNHX2 improves AXT3K growth in the presence of 75 and 100 mM of NaCl, AtNHX2 conferring a stronger salt tolerance phenotype than AtNHX1. Cells transformed with the mutant allele *nhx1*S526A did not show any difference in growth compared to the wild-type AtNHX1,

144

suggesting that phosphorylation in the Ser526 is not important for its antiporter activity. By contrast, yeast cells bearing the mutant allele *nhx2*S532A presented a great reduction of salt tolerance at 75 and 100 mM of NaCl compared with the wild-type AtNHX2. When the Ser532 was replaced for the phosphomimetic aspartic acid, yeast growth was restored to the wild-type level. These results indicate that only phosphorylation at the C-terminal of AtNHX2 in the Ser532 is important for the exchanger function in yeast.
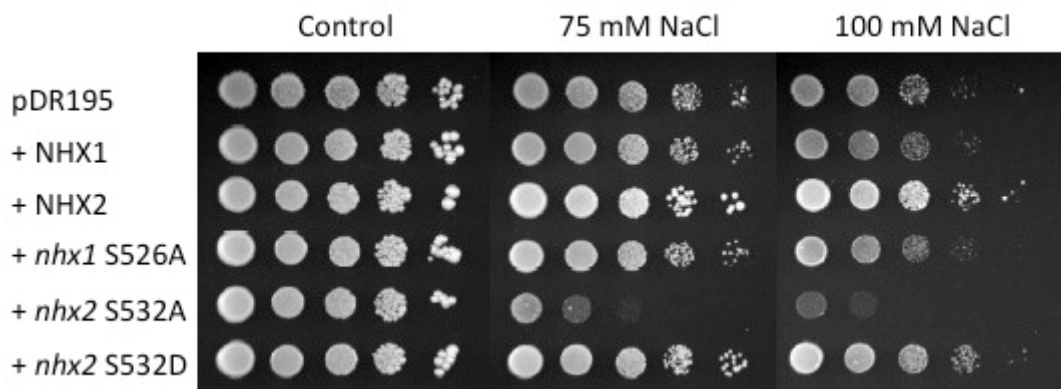
Figure R.36. NHX2 Phosphorylation is Important for its Activity in Yeast. Cells of strain AXT3K transformed with the expression vector pDR195 containing NHX1 and NHX2 wild type and mutant alleles were grown overnight in selective AP medium. Aliquots (5 μL) and 10-fold serial dilutions were spotted onto AP plates supplemented with 75 and 100 mM NaCl as indicated on each panel. Plates were photographed after 4 days at 28°C.

R.5.3. Search for AtNHX1 and AtNHX2 interacting proteins.

The Calcineurin B-Like proteins (CBLs), most likely function as sensor proteins that perceive changes in free calcium and relay these signals to target protein kinases denoted as CBL-Interacting Protein Kinases (CIPKs) (Luan et al., 2002). The Arabidopsis genome comprises 26 different genes for putative CIPK proteins. These proteins form alternative but specific complexes with some of the 10 members of the family of CBLs to regulate several physiological processes in different cell compartments by their interaction with target proteins (Albrecht et al., 2001; Kolukisaoglu et al., 2004; Weinl

and Kudla, 2009). However, just a few of these signaling pathways have been well described, as SOS1/CIPK24(SOS2)/CBL4(CBL4/SOS3), involved in Na$^+$ homeostasis (Qiu et al., 2002; Quintero et al., 2002) and AKT1/CIPK23/CBL1 (Li et al., 2006a; Xu et al., 2006) implicated in K$^+$ uptake. A number of CBL proteins are thought to recruit the interacting CIPKs to the vacuolar membrane (Waadt et al., 2008), but very little is known about the vacuolar targets of these CIPK-CBL protein kinase modules. It has been reported that the NHX activity is regulated by SOS2(CIPK24/SOS2) in a process that does not involve CBL4/SOS3(CBL4) (Qiu et al., 2004). Recently, the CIPK24(SOS2)-CBL10 complex has been suggested to regulate Na$^+$ compartmentation into the vacuole, albeit the target transporter has not been identified yet (Kim et al., 2007). In order to know if CIPKs proteins can interact and regulate the activity of AtNHX1 and AtNHX2 we performed different analysis that will be described below.

R.5.3.1. Study of the interaction between AtNHX1 and AtNHX2 with the CIPKs by BiFC.

The bimolecular fluorescence complementation (BiFC) technique allows the detection of protein-protein interactions *in planta* in their native subcellular localization. This approach is based on complementation between two nonfluorescent fragments of a fluorescent protein when they are brought together by interactions between proteins fused to each fragment (Hu et al., 2002; Walter et al., 2004; Waadt et al., 2008). In order to investigate if some CIPK proteins interact with NHX1 and/or NHX2 exchangers we performed BiFC combining each of the 26 CIPKs with NHX1 or NHX2. BiFC assays were made following the methodology described in section M.16.2. and subsections therein. Pairwise combinations of pSPYCE(M)-NHX1/NHX2 with either pSPYNE(R)173-CIPK were co-expresed in *Nicotiana benthamiana* leaves by agroinfiltration (section M.16.2.2.) and analyzed by fluorescence microscopy after 3 and 4 days (section M.16.2.3.). As positive control of a BiFC interaction at the tonoplast the combination of pSPYNE(R)173-CIPK24/SOS2 with pSPYCE(M)-CBL10 was used (Waadt et al., 2008). The efficiency of the interaction was determined by quantification of the pixel intensity of microscopic images obtained from epidermal cells as described

in section M.14.2.3. The relative fluorescence of each combination compared to the positive control was calculated for each assay (figure R.37.).
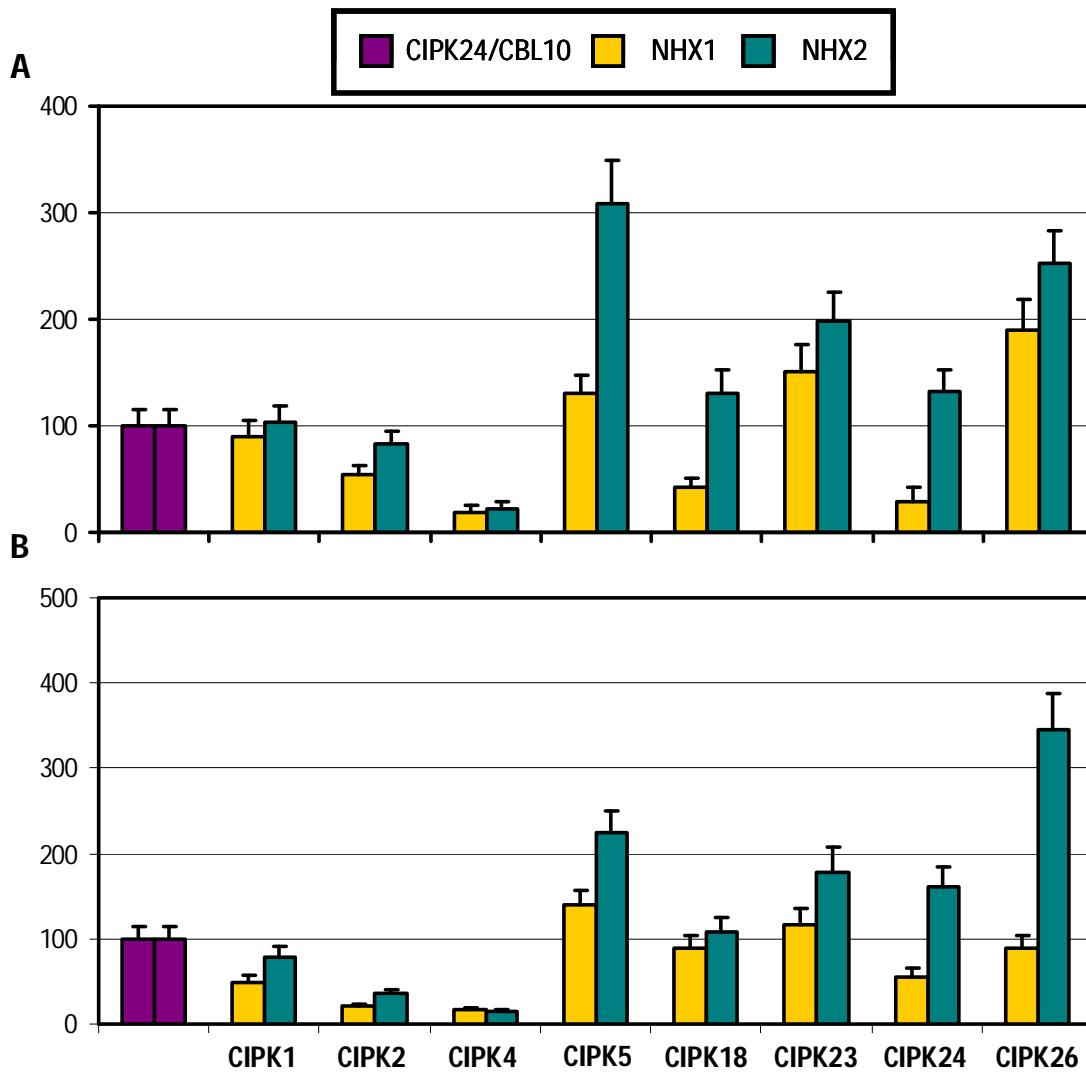
Figure R.37. Relative Fluorescence of the NHXs/CIPKs Interactions by BiFC. Data show the mean and SE (n=10) of the relative fluorescence of Nicotiana benthamiana cells expressing each NHX/CIPK combination 3 days after infiltration **(A)** and 4 days after infiltration **(B)**.

Depending of the degree of interaction, measured as relative fluorescence, each pairwise combination was classified in three differents groups: **no interaction**, a relative fluorescence lower than 50% of the positive control in all the assays was considered background signal; **weak interaction**, if the relative fluorescence was

147

higher than 50% of the positive control at least in one experiment; **strong interaction**, if the relative fluorescence measured for a pairwise combination always was higher than 50% of the positive control (table R.2. and figures R.38. and R.39.). Table R.2. shows the classification of the interactions found between the CIPKs and the NHXs antiporters. For the weak and strong interactions, in order to determine their localization, high-resolution pictures were taken by confocal microscopy (section M.14.2.3.). As shown in figures R.38. and R.39. the interactions CIPK/NHX were localized in all cases at the vacuolar membrane.

	Weak interaction	Strong interaction
NHX1	CIPKs 1,5,18,26	CIPK 23
NHX2	CIPKs 1,2,5,14,15,18	CIPKs 23,24,26

Table R.2. Classification of the Interactions Between the NHX Exchangers and the CIPKs by BIFC.

These findings demonstrate that *in planta*, NHX1 and NHX2 proteins interact at the tonoplast with some of the CIPK kinases in a specific manner. NHX1 interacts preferably with CIPK23 while NHX2 shows strong interaction with CIPK23, CIPK24/SOS2 and CIPK26, although other weak interactions can be observed for both proteins (table R.2.). These data suggest shared but not fully overlapping post-translational regulation mechanisms for NHX1 and NHX2.
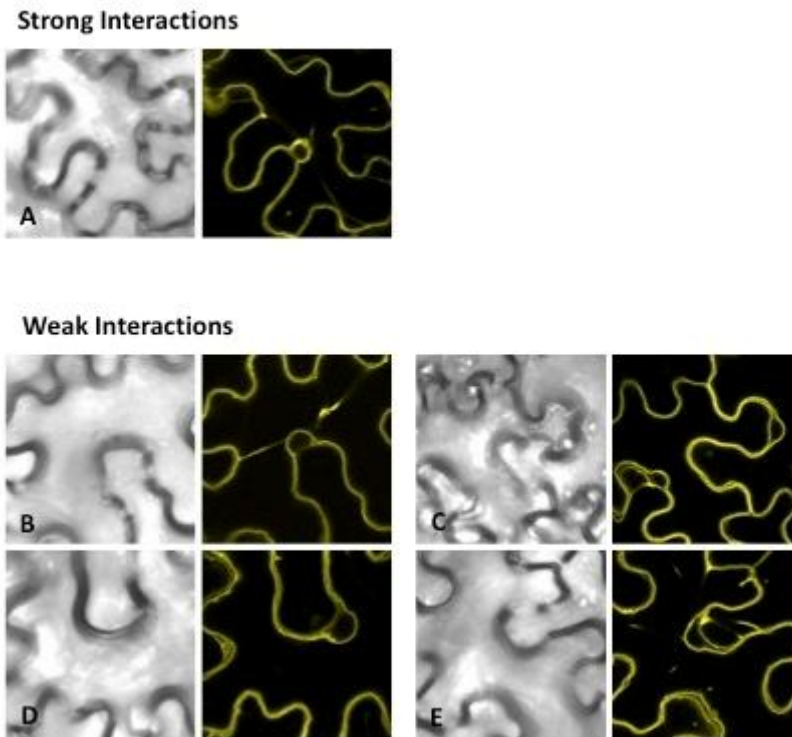
Figure R.38. NHX1/CIPK Interactions by BiFC. Epifluorescence images of *Nicotiana benthamiana* leaf sections expressing AtNHX1 in combination with **(A)** SPYNE(R)173-CIPK23, **(B)** SPYNE(R)173-CIPK1, **(C)** SPYNE(R)173-CIPK5, **(D)** SPYNE(R)173-CIPK18, and **(E)** SPYNE(R)173-CIPK26.
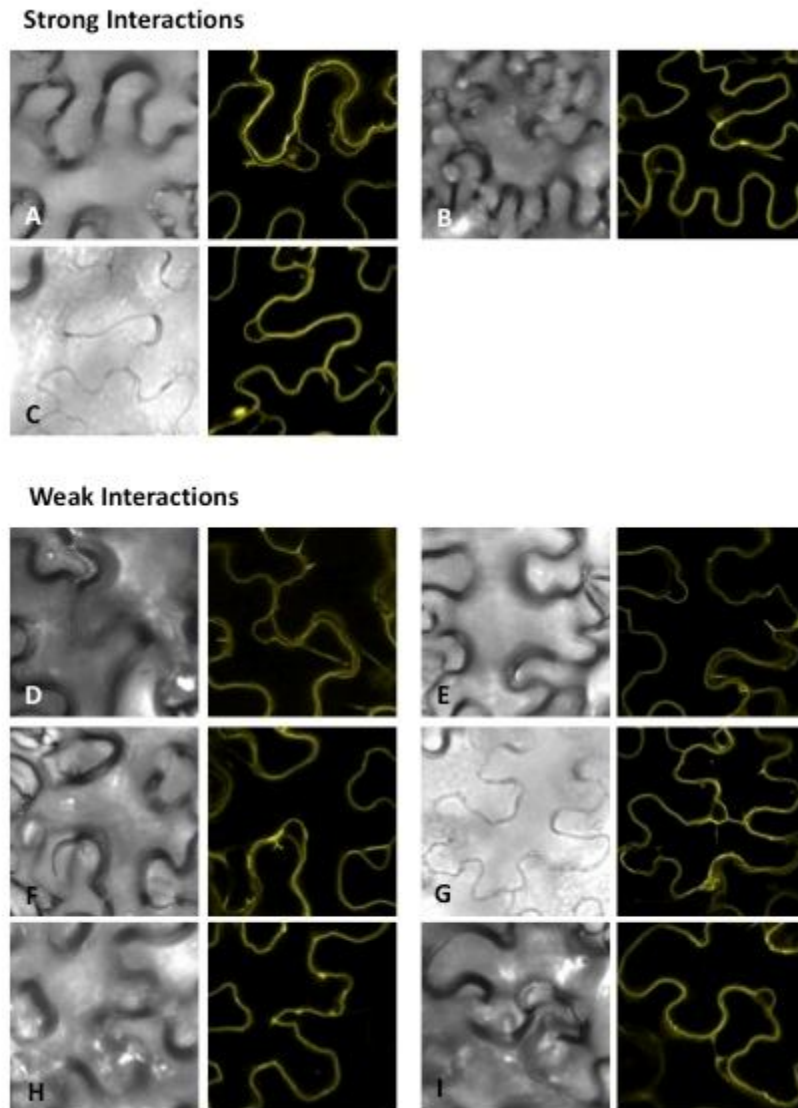
Figure R.39. NHX2/CIPK Interactions by BiFC. Epifluorescence images of *Nicotiana benthamiana* leaf sections expressing AtNHX2 in combination with **(A)** SPYNE(R)173-CIPK23, **(B)** SPYNE(R)173-CIPK24/SOS2, **(C)** SPYNE(R)173-CIPK26, **(D)** SPYNE(R)173-CIPK1, **(E)** SPYNE(R)173-CIPK2, **(F)** SPYNE(R)173-CIPK5, **(G)** SPYNE(R)173-CIPK14, **(H)** SPYNE(R)173-CIPK15, and **(I)** SPYNE(R)173-CIPK18.

R.5.3.2. Study of the NHX/CIPK/CBL signaling pathway in yeast.

To unravel the functional relevance of the interaction between the NHX exchangers and the CIPK kinases, and to identity the CBLs involved in these signaling pathways we assayed different combinations of NHXs, CIPKs and CBLs in yeast. To

facilitate the assays, *AtNHX1* and *AtNHX2* genes were integrated in the genome of the yeast strain AXT3K creating the new strains JPZN1 and JPZN2 (section M.1.2.1) following the methodology described in section M.17.1. and schematized in the figure R.40. As expected, expression of the *Arabidopsis* genes *NHX1* and *NHX2* improved the growth of the yeast strains JPZN1 and JPZN2 compared to AXT3K cells (figure R.41.).
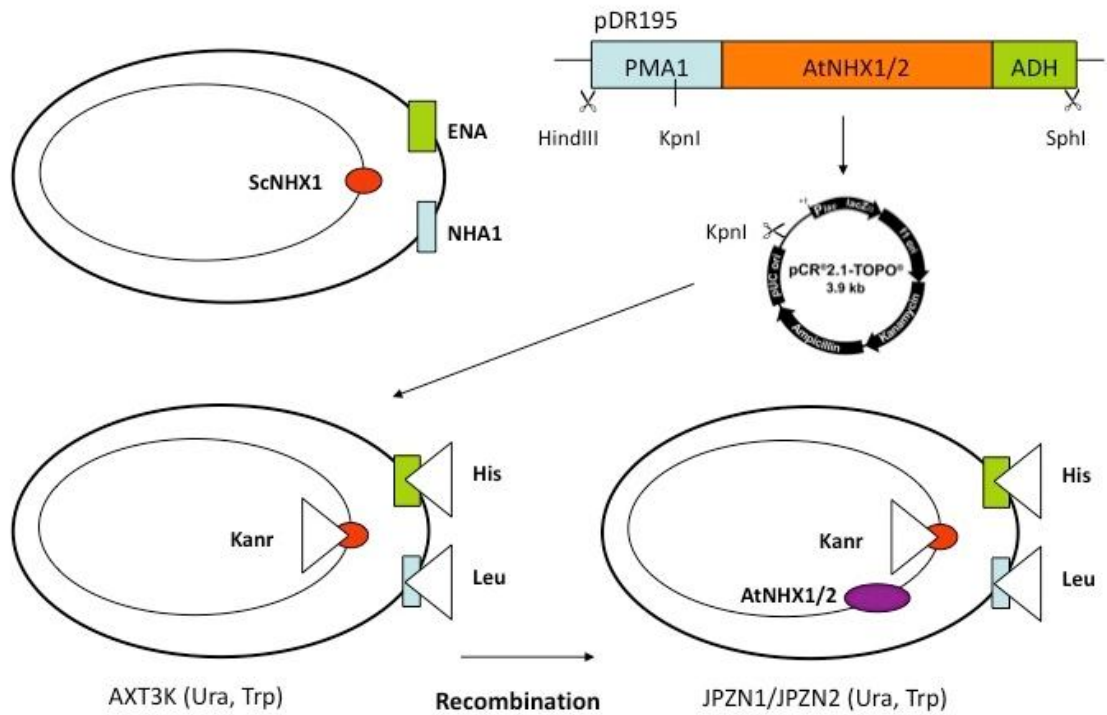
Figure R.40. Schematic Model of the *AtNHX1* and *AtNHX2* Integration into the AXT3K Yeast Genome by Homologous Recombination.
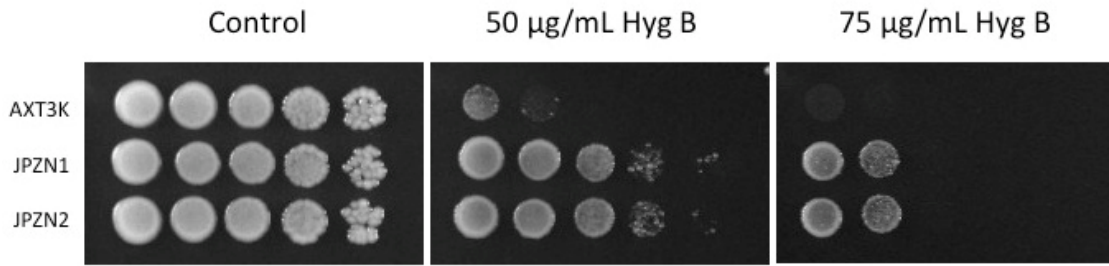
Figure R.41. The Integration of AtNHX1 and AtNHX2 in the Genome of AXT3K Yeast Strain Complement Its Hygromycin-Sensitivity Phenotype. Cells of the strains AXT3K, JPZN1 and JPZN2 were grown overnight in YPD medium. Aliquots (5 µL) and 10-fold serial dilutions were spotted onto YPD plates supplemented with 50 and 75 µg/mL hygromycin B as indicated on each panel. Plates were photographed after 2 days at 28°C.

To test their effect on JPZN2 salt tolerance (section M.17.2.), the NHX2-strong interacting CIPKs were cloned in the multi-copy plasmid p414GPD (section M.17.1. and Annex 3) and transformed into the yeast strain JPZN2. No difference in growth was observed between JPZN2 cells expressig the empty vector, CIPK23, CIPK24/SOS2 or CIPK26 in media containing up to 75 mM NaCl. However, at 100 mM NaCl the cells expressing CIPK24/SOS2 showed increased salt tolerance when compared to the other combinations (figure R.42.).
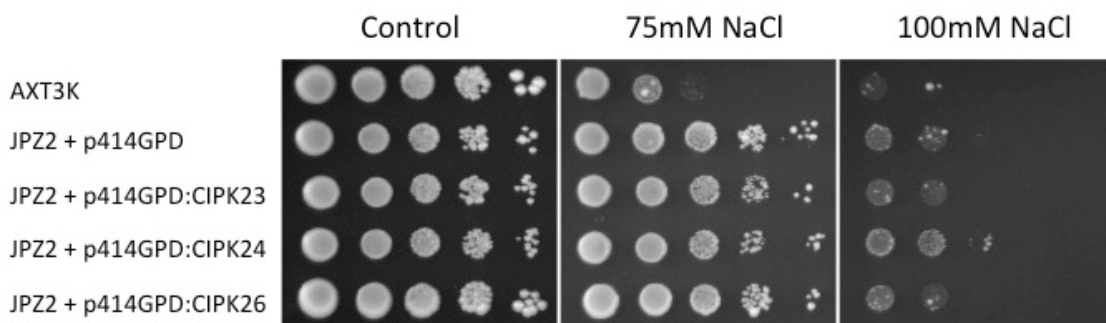
Figure R.42. AtCIPK24/SOS2 Together with AtNHX2 Improve the Salt Tolerance of the Yeast Strain AXT3K. Cells of the strain AXT3K and the strain JPZN2 expressing CIPK23, CIPK24/SOS2 and CIPK26 (in the yeast expression vector p414GPD) were grown overnight in selective AP medium. Aliquots (5 µL) and 10-fold serial dilutions were spotted onto AP plates supplemented with 75 and 100 mM NaCl as indicated on each panel. Plates were photographed after 4 days at 28°C.

The hyperactive kinase CIPK24/SOS2T168D/Δ308 is able to activate SOS1 in a CBL4/SOS3-independent manner ([Quintero et al., 2002](#)). To study if the kinase activity is sufficient for the activation of NHX2, the hyperactive allele of CIPK24/SOS2 was expressed in the yeast strain JPZN2. Due to the presence of NHX2 the Na$^+$ tolerance was the same in media containing 75 mM NaCl for cell expressing the empty vector, CIPK24/SOS2 and CIPK24/SOS2T168D/Δ308, while p141GPD-CIPK24/SOS2 was unable to complement the salt-sensitive phenotype of strain AXT3K (figure R.43.). The concurrent expression of NHX2 and the wild-type CIPK24/SOS2 improved the cellular growth in media containing up to 120 mM NaCl in comparison with the control. By contrast, the strain carrying the combination of NHX2 with the hyperactive CIPK24/SOS2 allele was unable to grow at 100 or 120 mM NaCl, suggesting that not only the kinase activity, but the complete protein is important for the regulation of NHX2 (figure R.43.).
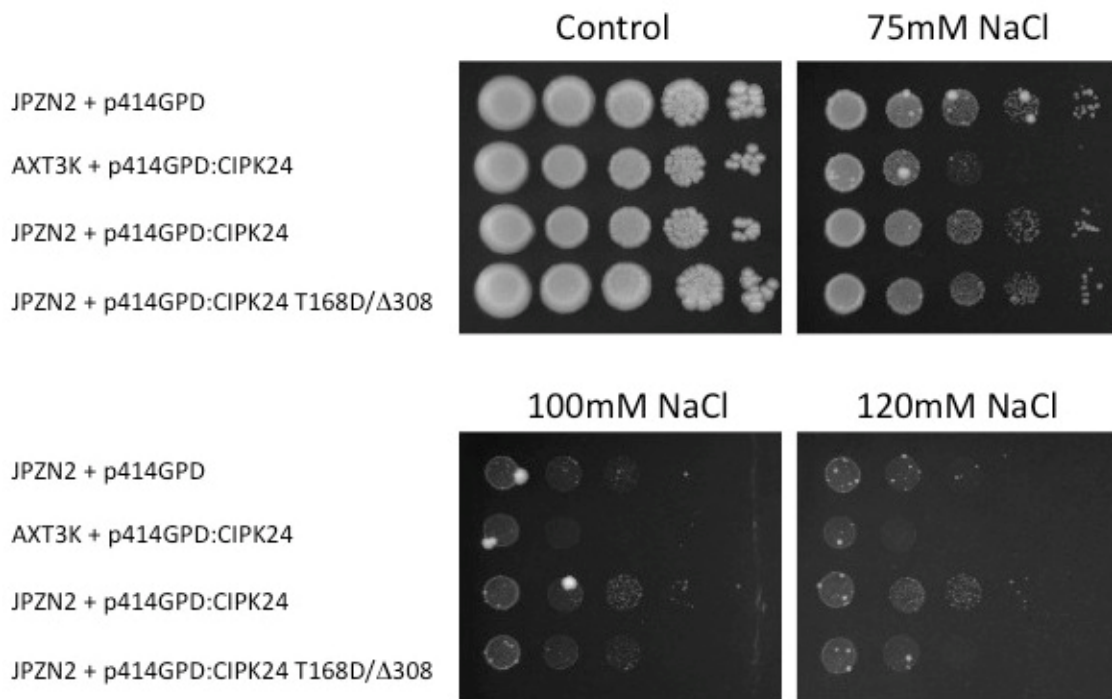
Figure R.43. Wild-Type CIPK24/SOS2 is Necessary for the Interaction with NHX2 in Yeast. Cells of the strain AXT3K expressing CIPK24/SOS2 and JPZN2 cells transformed with the wild type and the hyperactive alleles of CIPK24/SOS2 were grown overnight in selective AP medium. Aliquots (5 μL) and 10-fold serial dilutions were spotted onto AP plates supplemented with 75, 100 and 120 mM NaCl as indicated on each panel. Plates were photographed after 4 days at 28°C.

In Arabidopsis there are 10 genes encoding for CBL proteins (Albrecht et al., 2001; Kolukisaoglu et al., 2004) which are responsible for the recruitment and targeting of the CIPK kinases to specific cellular compartments (Weinl and Kudla, 2009). The purely tonoplast-localized CBL proteins are CBL2, CBL3 and CBL6. All of them share a conserved N-terminal extension that is sufficient to target these proteins to the vacuolar membrane (Batistič et al., 2010). It has been described that CBL10 recruits CIPK24/SOS2 both to the plasma membrane and to the tonoplast (Kim et al., 2007; Quan et al., 2007; Batistič et al., 2010). Furthermore, using yeast two-hybrid assays it has been found that CIPK24/SOS2 interacts strongly with CBL4/SOS3 and in a weaker manner with CBL1, CBL2 and CBL3 (Guo et al., 2001a). Hence, to identify the CBL proteins involved in the regulation of NHX2 through its interaction with CIPK24/SOS2 we performed salt tolerance assays in yeast in presence of the tonoplast-localized and the CIPK24/SOS2-interacting CBLs. For this purpose the coding sequence of *CBL1*, *CBL2*, *CBL3*, *CBL4*, *CBL6* or *CBL10* were cloned in the yeast expression vector pYPGE15 (section M.17.1. and Annex 3) and transformed into JPZN2 yeast cells expressing CIPK24/SOS2. As shown in the figure R.44., the coexpression of NHX2, CIPK24/SOS2 and CBL10 slightly increased the Na$^+$ tolerance of transformed cells compared to the coexpression of just NHX2 and CIPK24/SOS2 in media containing 100 mM NaCl. At 75 mM NaCl, also the combination NHX2-CIPK24/SOS2-CBL1 improved the yeast cell growth.
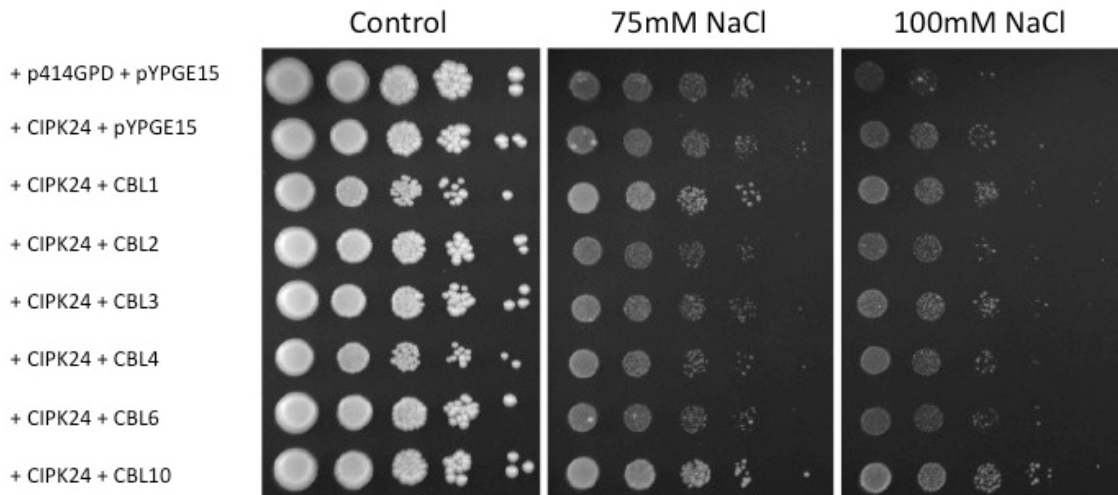
Figure R.44. CBL10 in Combination with NHX2 and CIPK24/SOS2 Further Increase the Salt Tolerance of the Yeast Strain AXT3K. Cells of the strain JPZN2 transformed with CIPK24/SOS2 (in the yeast expression vector p414GPD) and the CBLs 1, 2, 3, 4, 6 and 10 (in the yeast expression vector pYPGE15) were grown overnight in selective AP medium. Aliquots (5 µL) and 10-fold serial dilutions were spotted onto AP plates supplemented with 75 and 100 mM NaCl as indicated on each panel. Plates were photographed after 4 days at 28°C.

These results point to a possible interaction between NHX2, CIPK24/SOS2 and CBL10 that would take place at the vacuolar membrane to regulate the activity of the cation exchanger. Moreover, the results demonstrate that the wild-type CIPK24/SOS2 is necessary for the proper interaction with NHX2, since the truncated CIPK24/SOS2 fail to improve the yeast cell growth under salt treatment.

R.5.3.3. *In vitro* phosphorylation assays.

To further investigate the signaling module NHX-CIPK-CBL we performed *in vitro* phosphorylation assays of NHX1 and NHX2 with their interacting kinases following the protocol and constructions described in section M.5. and subsections therein.

Recombinant proteins GST:NHX1ct and GST:NHX2ct were purified from yeast (section M.5.1.) while CIPK23 and CIPK24/SOS2 were purified *in vitro* using the RTS 500 Wheat Germ CFCF Kit. The *in vitro* phosphorylation of NHX1ct and NHX2ct by CIPK23

155

and CIPK24/SOS2 was tested in the presence of 30 mM $MnSO_4$ and 3 mM $CaCl_2$. The C-terminus of both proteins was not phosphorylated by CIPK23 or CIPK24/SOS2 (figure R.45.). Even more, the autophosphorylation signal of both CIPKs decreased in the presence of the NHX proteins (figure R.45.). The fact that no phosphorylation was detected in the C-terminal of NHX1 and NHX2 might be due to a low kinase activity of the wild-type CIPK proteins, or to the requirement of activation by the CBL partner protein.
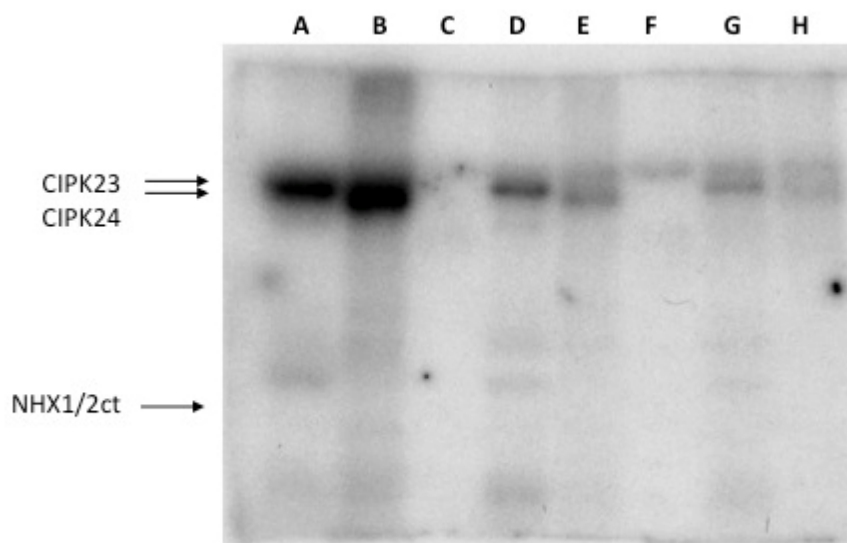
	A	B	C	D	E	F	G	H
Proteins								
NHX1ct	-	-	+	+	+	-	-	-
NHX2ct	-	-	-	-	-	+	+	+
CIPK23	+	-	-	+	-	-	+	-
CIPK24/SOS2	-	+	-	-	+	-	-	+

Figure R.45. NHX1ct and NHX2ct In vitro Phosphorylation Assay. Purified C-terminal domains of NHX1 and NHX2 were incubated with the wild type CIPK23 and CIPK24/SOS2 kinases in the presence of [γ-^{32}P]ATP, resolved in SDS/PAGE and exposed to X-ray film (upper panel). All the reactions were performed in a buffer conaining 100 mM Tris-HCl pH 8, 30 mM $MnSO_4$, 3 mM $CaCl_2$, 12 mM DTT, 60 μM ATP and 0.1 μCi/μL [γ-^{32}P]ATP. Lower panel indicates the proteins added in each reaction.

To test the first hypothesis, phosphorylation assays using the hyperactive form of CIPK24/SOS2 were performed (figure R.46.). As positive control the recombinant protein GST:SOS1ct was used. In presence of $MnCl_2$ and absence of $CaCl_2$ in the kinase reaction, phosphorylation of SOS1ct or NHXct proteins was not detected. By contrast, when the reaction buffer contained 5 mM $MgCl_2$, with or without 1 mM $CaCl_2$, SOS1ct was phosphorylated by CIPK24/SOS2T168D/Δ308. The recombinat protein GST:NHX2ct was phosphorylated when CIPK24/SOS2T168D/Δ308 was present , but also when it was alone, so we cannot clonclude that this signal is strictly dependent of the CIPK kinase. Phosphorylation of NHX1ct was not detected at any condition assayed.
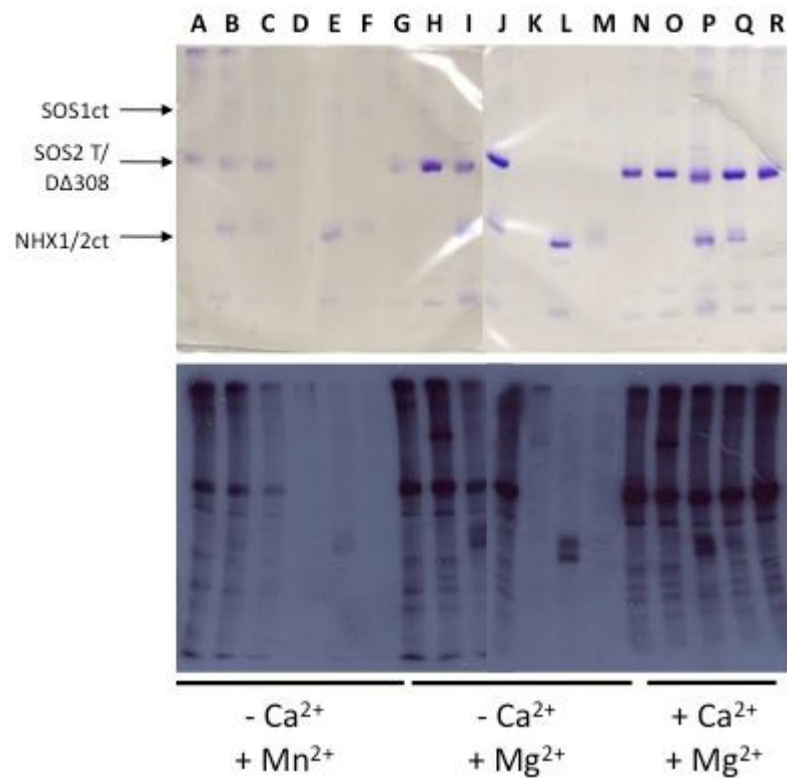
	A	B	C	D	E	F	G	H	I	J	K	L	M	N	O	P	Q	R
Proteins																		
NHX1ct	-	-	+	-	-	+	-	-	-	+	-	-	+	-	-	-	+	-
NHX2ct	-	+	-	-	+	-	-	-	+	-	-	+	-	-	-	+	-	-
CIPK24/SOS2 T168D/Δ308	+	+	+	-	-	-	+	+	+	+	-	-	-	+	+	+	+	+
SOS1ct	+	-	-	+	-	-	-	+	-	-	+	-	-	-	+	-	-	-

Figure R.46. NHX1ct and NHX2ct are not Phosphorylated by the Hyperactive CIPK24/SOS2. Purified C-terminal domains of NHX1, NHX2 and SOS1 were incubated with the CIPK24/SOS2 T168D/Δ308 in the presence of [γ-^{32}P]ATP, resolved in SDS/PAGE (upper panel) and exposed to X-ray film (lower panel). All the reactions were performed in presence of 20 mM Tris-HCl pH 8, 1 mM DTT, 10 μM ATP and 1 μCi of [γ-^{32}P]ATP. In the cases where are indicated 5 mM MgCl$_2$, 2.5 mM MnCl$_2$ and 0.1 mM of CaCl$_2$ were added to the reaction mix. Lower table indicate the proteins in each reaction.

To test if the presence of the CBLs in the reaction mix is essential for the phosphorylation of NHX proteins by the CIPKs, the phosphorylation of NHX2ct by CIPK24/SOS2 was performed in the presence of the recombinant protein GST:CBL10 (figure R.47.). As positive control the recombinant protein GST:SOS1ct was used. SOS1ct was slightly phosphorylated by the wild-type CIPK24/SOS2 independently of the presence of CBL10, indicating that CBL10 does not enhance CIPK24 activity. No phosphorylation signal was obtained for NHX2ct in the absence or presence of the CBL10 protein.
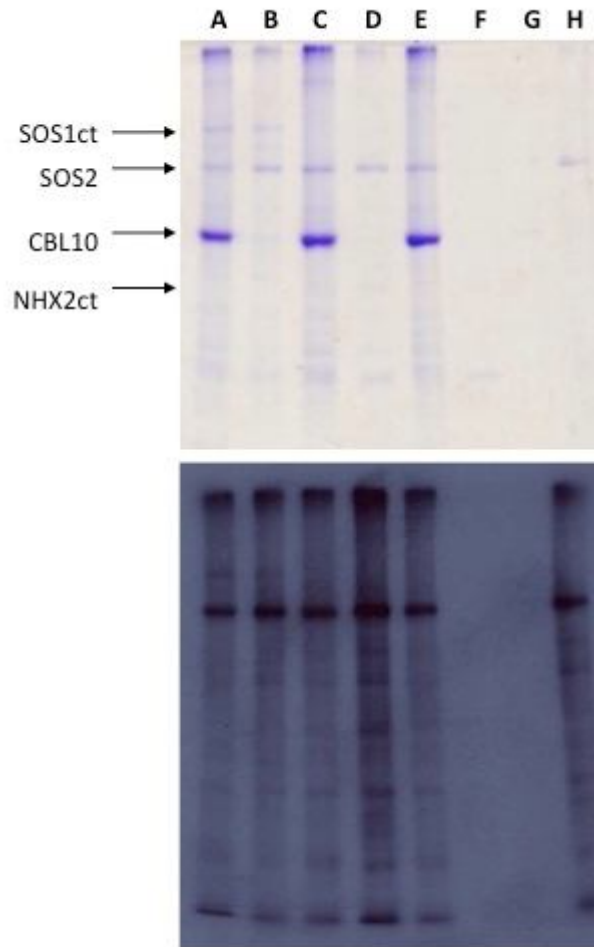
	A	B	C	D	E	F	G	H
Proteins								
NHX2ct	-	-	+	+	-	+	-	-
SOS1ct	+	+	-	-	-	-	-	-
CIPK24/SOS2	+	+	+	+	+	-	-	+
CBL10	+	-	+	-	+	-	+	-

Figure R.47. NHX2ct is not Phosphorylated by CIPK24/SOS2 in Presence of CBL10. Purified C-terminal domains of NHX2 and SOS1 were incubated with the CIPK24/SOS2 wild type and CBL10 in the presence of $[\gamma\text{-}^{32}P]ATP$, resolved in SDS/PAGE (upper panel) and exposed to X-ray film (lower panel). All the reactions were performed in presence of 20 mM Tris-HCl pH 8, 5 mM MgCl$_2$, 1 mM DTT, 0.1 mM of CaCl$_2$, 10 µM ATP and 1 µCi of $[\gamma\text{-}^{32}P]ATP$. Lower panel indicates the proteins added in each reaction.

R.5.3.4. The recombinant protein GST:NHX2ct is phosphorylated by yeast kinases.

Due to the negative results obtained in the *in vitro* phosphorylation assays together with the slight increase in salt tolerance obtained with the co-expression of NHX2-CIPK24/SOS2-CBL10 in yeast compared to the expression of NHX2 alone, we suspected that the yeast protein kinases would be able to phosphorylate the NHX proteins. To check this hypothesis the recombinant protein GST:NHX2ct was purified from yeast (section M.5.1.) and analysed by nano HPLC-ESI-MS/MS of ionic trap alternating the fragmentation techniques of CID/ETD in order to detect phosphorylated residues (section M.18.). This analysis determined the presence of a phosphorylated residue in position S9 of the peptide GFVPFVPG**pS**PTER that corresponds to the serine 532 of NHX2. The same phosphorylation event was reported to occur in planta (figure R.48.) (Sugiyama et al., 2008; Whiteman et al., 2008b). This finding shows that some yeast protein kinase can phosphorylate the ser532 of the *Arabidopsis* NHX2.
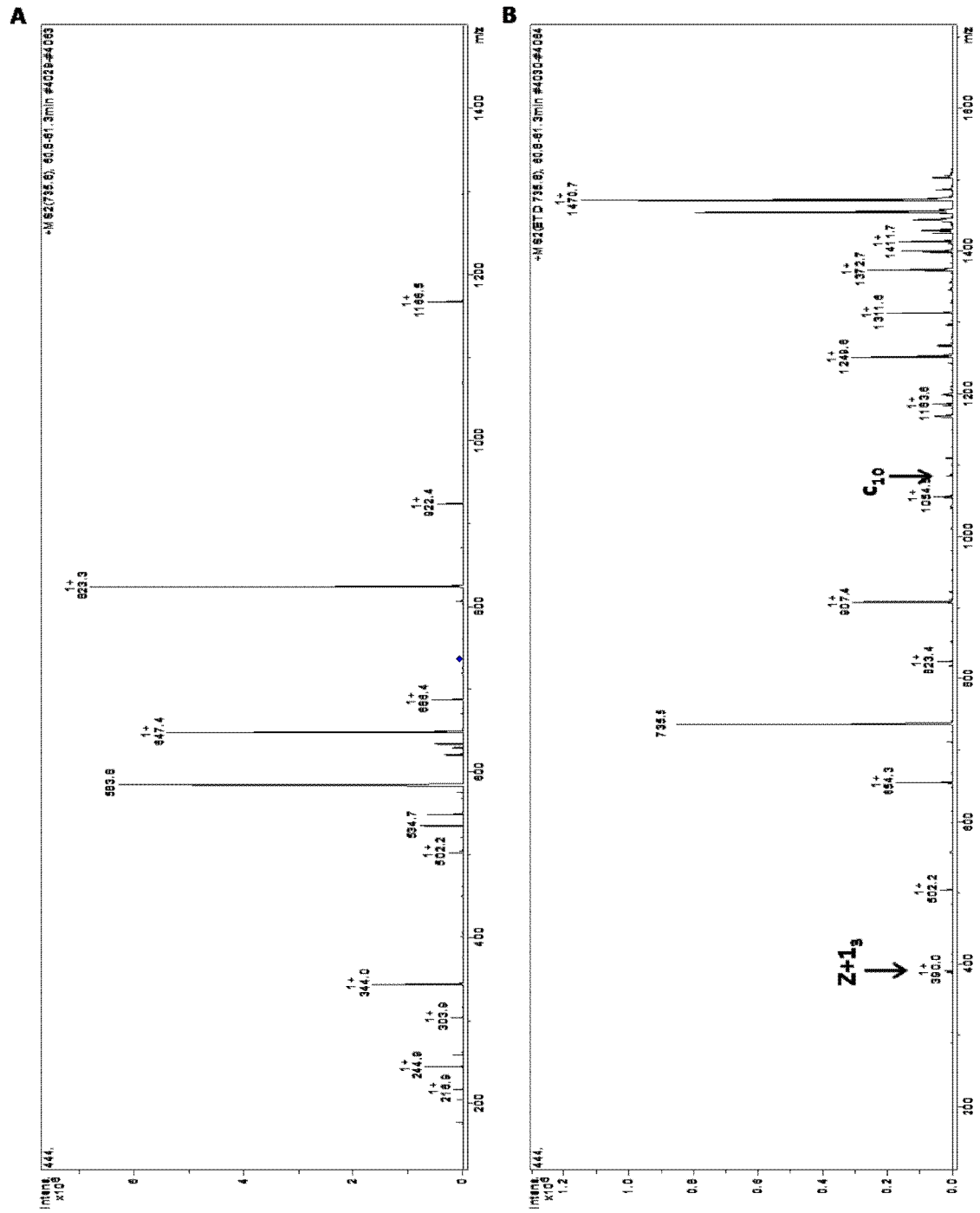
Figure R.48. Phospho-analysis of the Recombinant Protein GST:NHX2ct Purified from Yeast.
MS/MS spectra of the ion 2+ m/z 735.4 by **(A)** CID fragmentation and **(B)** ETD fragmentation of
the peptide GFVPFVPG**pS**PTER.

VI. DISCUSSION

D.1. The essential role of AtNHX1 and AtNHX2 proteins in the generation of the vacuolar K$^+$ pool and the maintenance of the cellular K$^+$ homeostasis.

K$^+$ is the major ionic osmoticum in plant cells and occurs in two major pools, in the vacuole and the cytosol. Cytosolic K$^+$ plays essential roles as activator of biochemical processes, in the regulation of cytosolic pH, and in the fine-tuning of the plasma membrane electrical potential (Amtmann et al., 2006; White and Karley, 2010). These fundamental functions demand the maintenance of the cytosolic K$^+$ concentration within narrow limits (75 to 100 mM), regardless of changes in K$^+$ supply (Walker et al., 1996; Leigh, 2001). Since vacuolar K$^+$ concentration closely follows K$^+$ availability, the vacuolar pool is the largest and most dynamic reservoir of this ion. In the vacuole K$^+$ functions as an osmoticum to generate turgor and to drive cell expansion by reducing the cell water potential and giving rise to a passive water influx, which in turn increases cell volume (Leigh and Wyn Jones, 1984). The lowest limit for vacuolar K$^+$ concentration appears to be 10 to 20 mM, which is thought to reflect equilibrium with the cytosol at a maximum trans-tonoplast voltage of -40 to -60 mV (positive in the vacuole relative to the cytoplasm) (Leigh and Wyn Jones, 1984; Walker et al., 1996; Leigh, 2001). Greater concentrations of K$^+$ inside the vacuole require active transport from the cytosol to the vacuole that could be achieved by a nonelectrogenic K$^+$/H$^+$ antiporter (Walker et al., 1996). Biochemical analyses have shown that tonoplast-localized NHX proteins catalyze the K$^+$/H$^+$ exchange with apparent affinity values (12 to 40 mM) that are below the lower limits of cytosolic K$^+$ concentrations and are thus able to translocate K$^+$ from the cytosol to the vacuole under regular physiological conditions (Venema et al., 2002; Yamaguchi et al., 2003; Hernandez et al., 2009; Barragán et al., 2012). Using a reverse genetics approach Barragán *et al.* (2012) showed that a *nhx1 nhx2* mutant had a significant 3-fold reduction in K$^+$/H$^+$ exchange in tonoplast vesicles compared with Col-0 plants and a marked reduction in the amount of K$^+$ stored in the vacuoles of leaf mesophyll cells, epidermal cells, and guard cells of stomata measured by SEM-EDX. Using a ratiometric

163

fluorescence assays, Bassil *et al.* (2011b) found a 30% reduction in vacuolar K^+ and that the vacuolar lumen was more acidic in roots of the *nhx1 nhx2* mutant than in the wild type. Together, these results indicate that proteins NHX1 and NHX2 account for the majority of the total K^+/H^+ exchange capacity in the vacuole of Arabidopsis, although the transport activity still remaining in *nhx1 nhx2* plants could be attributed to the activity of NHX3 and/or NHX4, which together with NHX1 and NHX2 constitute the class-I family of tonoplast-localized NHX proteins in Arabidopsis (Yokoi et al., 2002; Pardo et al., 2006), NHX3 is unlikely to contribute to Na^+, K^+/H^+ exchange in leaves, as ProNHX3:GUS fusions have been shown to be preferentially expressed in reproductive organs (Wang et al., 2007) By contrast, ProNHX4:GUS is expressed in roots and vascular bundles in leaves (Wang et al., 2007), partially overlapping the expression of NHX1 and NHX2. The nonvacuolar, class-II NHX proteins, NHX5 and NHX6, localize in the Golgi and trans-Golgi network, where they may regulate endosomal pH (Bassil et al., 2011b). Other cation/proton exchangers that may add to the residual Na^+, K^+/H^+ activity in the *nhx1 nhx2* plants are Cation/H^+ Exchanger (CHX) and K^+ Efflux Antiporter (KEA) proteins (Pardo et al., 2006; Chanroj et al., 2012). Arabidopsis CHX proteins (28 members), which are also thought to mediate K^+ transport and pH homeostasis, have been localized at the plasma membrane and various intracellular compartments, but not at the tonoplast (Chanroj et al., 2012). The KEA proteins (6 isoforms in Arabidopsis) are thought to regulate K^+ homeostasis in organelles (Chanroj et al., 2012). Hence, the available evidence strongly suggests that NHX1 and NHX2, the two most highly expressed members of the class-I group of NHX proteins, are also the main effectors of the active accumulation of K^+ in the vacuole. It is worth noting that disruption of active accumulation of K^+ in the vacuoles of *nhx1 nhx2* plants resulted in greater retention of K^+ in the cytosolic pool (Barragán et al., 2012). This implies that while the plasma membrane potential, that is negative inside the cell, drove the acquisition of extracellular K^+, further transit to the vacuole was impeded by the tonoplast membrane potential, which is positive in the lumen relative to the cytoplasm, in the absence of an active transport mechanism that is capable of accumulating K^+ against its electrochemical gradient. The converse situation was found in transgenic tomato expressing Arabidopsis NHX1, where enhanced recruitment of K^+ into the vacuoles

occurred at the expense of a diminishing cytosolic pool (Leidi et al., 2010; Barragán et al., 2012).

Plant cells expand by accumulating solutes, absorbing water, generating turgor pressure, and extending the cell wall. The vacuolar K^+ pool plays a fundamental biophysical role and, jointly with other vacuolar osmolytes, drives osmotic changes and water movements (Leigh, 2001; MacRobbie, 2006). This biophysical role of K^+ is required for cell expansion processes such as the growth of the root system, both in elongating roots and root hairs (Dolan and Davies, 2004), for leaf expansion, for the elongation of pollen tubes towards ovules (Mouline et al., 2002), for the enlargement of fruits and tubers (White and Karley, 2010) and for the stomatal function (Véry and Sentenac, 2003; Fan et al., 2004). Plants starved for K^+ show, among other disorders, poorly-developed root systems, smaller sizes of aerial parts, decreased water content, reduced turgor, impaired stomatal regulation, and reduced transpiration (Mengel et al., 2001; White and Karley, 2010). All these symptoms are linked to the fundamental role that intracellular K^+ plays as osmoticum. Arabidopsis *nhx1 nhx2* mutant plants presented most of these symptoms and also scorching along the margins of older leaves, thinner stems, very short filaments of the stamen, and small siliques. These phenotypic traits and their physiological consequences will be discussed in detail below.

D.1.1. The role of NHX proteins in cell expansion.

The response of plant growth to increasing K^+ availability follows a steep curvilinear relationship. From this relationship a "critical" concentration of K^+ can be determined which is defined as the concentration at which 90% of maximum yield is obtained. Above this concentration, growth shows little response to increased K^+ content in tissues, but at lower K^+ concentrations growth declines rapidly. The "critical" concentration is around a 2% of the total dry matter although K^+ may comprise up to 10% of a plant's dry weight in K^+-replete conditions (Leigh and Wyn Jones, 1984; White and Karley, 2010). Plants of *nhx1-2 nhx2-1* genotype were smaller

than control plants when their were grown on soil and in hydroponic culture at any external K$^+$ regimes (sections R.2.1 and R.2.2.; figures R.4-R.8) even if their K$^+$ content in dry matter basis exceed, in all K$^+$ treatments, the 2% required for maximal growth (figure R.7.). This could be explained as a result of the impaired compartmentation of K$^+$ in the cells, with lower than needed K$^+$ concentration into the vacuole and abnormally high values in the cytosol and in the apoplast.

In contrast with the L14 (*nhx1-2 nhx2-1*) phenotype, the stunted growth in the KO mutant was apparent for both roots and shoots (Section R.2.2.; figures R.7. and R.8.) (Barragán et al., 2012). As described in section R.3., the expression pattern of *NHX1* and *NHX2* do not overlap completely in roots. While *NHX1* promoter showed GUS activity in root hairs but not in the main and lateral root tips, *NHX2* promoter showed a strong GUS activity in root meristemes but it was absent in root hairs (figure R.12) (Shi and Zhu, 2002; Barragán et al., 2012). Thus, the protein NHX1 likely plays a more important role in the cell expansion at the elongation zone of the roots and in root hairs, which may sustain the greatest growth rates found within the root regions (van der Weele et al., 2003; Dolan and Davies, 2004). Roots of the L14 mutant probably presented less differences in growth compared to wild type because of the leaky expression of *NHX1*, which would support to some extent root elongation. To understand the differential role of both proteins it would be interesting to study the root morphology and development as well as the vacuolar morphology at different K$^+$ concentrations in *NHX1* and *NHX2* single and double mutants.

Shoot size is strictly correlated with the amount of NHX1 and NHX2 activity remaining in plants of diverse genotypes, since single mutants had near normal shoot development (Barragan, 2007), leaky double mutants of the *nhx1-1 nhx2-1* genotype were significantly smaller than the wild type, and complete knockout plants (*nhx1-2 nhx2-1*) were severely stunted (Section R.2.1. and R.2.2.; figures R.4.-R.7.) (Barragán et al., 2012). Supplemental Na$^+$ could partially recover growth of the *nhx1 nhx2* mutants, since nontoxic concentrations of Na$^+$ may substitute for K$^+$ as osmoticum (Rodríguez-Navarro and Rubio, 2006; Bassil et al., 2011a; Barragán et al., 2012). Reduced leaf size in L14 and KO mutant plants appeared to be a consequence of compromised cell

expansion and not of the reduction in the number of cells ([Bassil et al., 2011a](#); [Barragán et al., 2012](#)). The relative growth rate of plant cells is a function of the internal hydrostatic or turgor pressure and the yield threshold and extensibility of the cell wall. Tissues of the *nhx1 nhx2* mutants consistently showed reduced water contents (section R.2.2.; figure R.7.), which correlated with K^+ contents on a dry weight basis (section R.2.2.; figure R.7.) ([Barragán et al., 2012](#)). This indicates that the diminished size of the vacuolar K^+ pool hindered water uptake and that these plants were no longer able to supply the vacuole with sufficient amounts of K^+ for the normal expansion of leaf mesophyll cells (section R.2.3.; figures R.9. and R.10.) ([Barragán et al., 2012](#)). Accordingly, leaf turgor pressure measured with a leaf patch pressure probe was lower in the *nhx1 nhx2* mutant plants than in control Col-0, and this difference increased steadily over time at low (0.1 to 1 mM) external K^+ ([Barragán et al., 2012](#)). Transfer to 10 mM K^+ stabilized leaf turgor, although daily shifts in leaf turgor due to light/dark transitions and stomatal function were dampened in the mutant plants. These findings are coherent with the prevailing view that K^+ in the vacuolar pool acts as the major osmoticum driving water uptake and cell expansion. Consequently, NHX1 and NHX2, as key players in the creation of the vacuolar K^+ pool, are important determinants of plant growth. Plants with compromised K^+ acquisition also showed reduced sizes ([Hirsch et al., 1998](#)), but phenotypes under nonstarving conditions were not as dramatic as those found in the *nhx1 nhx2* mutant plants.

In contrast with the phenotype observed in the epidermis of the Col-0 and L14 mutant (section R.2.3.; figure R.11.), the leaves of the KO mutant presented two differentiated population of cells: epidermal cells with elongated shape instead of the normal puzzle shape, and small epidermal cells surrounding stomata (section R.2.3.; figure R.11.). In agreement with this results KO leaves have less epidermal cells per area (158 epidermal cells/mm^2) compared to the wild type (234 epidermal cells/mm^2), and they also present a higher percentage of larger epidermal cells than the wild type (section R.4.1.2.; figures R.14. and R.15.). These types of pavement cells have been also reported in mutants affected in the cytoskeletal dynamics ([Fu et al., 2009](#); [Ojangu et al., 2012](#)). For instance, a myosin triple mutant showed pavement cells with less extended lobes and also alterations in trichome and floral organs development

([Ojangu et al., 2012](#)) while the overexpression of the Rho-family GTPase 6 (ROP6), which enhanced the cortical microtubule ordering, turn the puzzle appearance of cells into a cylindrical shape ([Fu et al., 2009](#)). It has been demonstrated that the *S. cerevisiae* Gyp6, a GTPase-activating protein for the Ypt/Rab family of GTPases, inhibits the activity of ScNhx1 by physical interaction. The Nhx1 inhibition would render the vesicles more acidic favouring the anterograde traffic over the retrograde vesicle traffic ([Ali et al., 2004](#)). Furthermore, expression changes in genes involved in vesicular trafficking and cellular growth (e.g., MYOSIN-XI F and KINESIN-12B) have been obtained in DNA array analysis of the *Atnhx1* mutant ([Sottosanto et al., 2004](#)). Taken together the previous evidences and the results exposed in this work it can be suggested the involvement of AtNHX1 and AtNHX2 not only in cell expansion but also, in association with other proteins, in processes associated to the development of the leaf pavement cells.

D.1.2. The role of the NHX proteins in the stomatal function.

Regulation of stomatal movements relies on turgor and volume changes in the guard cells. The large central vacuole plays an essential role in the regulation of the guard cells turgor since the fluxes of K^+ and anions throught the tonoplast control the opening and closing of stomata. Among the solutes released from guard cells, more than 90% originate from vacuoles ([MacRobbie, 2006](#)). The main solutes involved in the osmoregulation process of guard cells are K^+ and sucrose and accompanying anions (chloride and malate), depending of the environmental conditions and the time of the day ([Talbott and Zeiger, 1996](#); [Talbott and Zeiger, 1998](#)). Due to the high mobility of K^+ and because it is a energetically cheap solute, guard cells accumulate K^+ salts in large amounts to open the stomata ([MacRobbie, 2006](#)). Plasma membrane K^+-channels in guard cells and their regulation and responses are well characterized ([Roelfsema and Hedrich, 2005](#); [Pandey et al., 2007](#); [Kim et al., 2010](#)). However, because of the relative inaccessibility of the tonoplast in intact cells, most of the studies on tonoplast ion movements have been obtained either by patch clamping of isolated vacuoles, or by tracer flux measurements on isolated guard cells, lacking thus most of the signalling

components ([MacRobbie, 2006](#)). The K^+ accumulation into the vacuole against the vacuolar membrane potential, necessary for stomatal opening, may be mediated by secondary active carriers, which appeared elusive ([Walker et al., 1996](#); [Leigh, 2001](#); [Roelfsema and Hedrich, 2005](#)). In this work we postulate that this function is carried out by the vacuolar antiporters NHX1 and NHX2 which are both highly expressed in guard cells (section R.3.; figure R.12.) ([Shi and Zhu, 2002](#); [Apse et al., 2003](#); [Barragán et al., 2012](#)). Light- and fusicoccin-induced stomatal opening in epidermal peels was significantly impaired in *nhx1 nhx2* mutants in the presence of KCl (sections R.4.2.1. and R.4.5.; figures R.17., R.18., R.21., R.26 and R.31.). Additionally, L14 and KO plants presented less stomatal conductance (section R.4.3.; figure R.24.) and transpiration (sections R.4.2.2. and R.4.4.; figures R.22. and R.25.) than the wild type during the day photoperiod. Barragán et al (2012) demonstrated that tonoplast vesicles of the *nhx1 nhx2* mutant had a significant threefold reduction in K^+/H^+ exchange compared with Col-0 plants. In fact, the L14 mutant presented 40% less K^+ counts in guard cells than the wild type when measured by SEM-EDX. These results could explain the ca. 40% reduction in stomatal opening observed in the L14 and KO mutants relative to the wild type (section R.4.2.1.; figure R.16.). Vacuolar K^+ contents in guard cells of KO mutant has not been properly measured by SEM-EDX because of the technical constraints exposed in section R.4.6. Although the stomatal opening is impaired in *nhx1 nhx2* mutants, they are not completly closed. It has been postulated that the lowest limit for vacuolar K^+ concentration appears to be 10 to 20 mM, which is thought to reflect equilibrium with the cytosol at a maximum trans-tonoplast voltage of about -40 to -60 mV ([Walker et al., 1996](#); [Leigh, 2001](#)). Hence, until the vacuole reaches its minimum allowable K^+ concentration, K^+ accumulation in guard cell vacuoles could be facilitated by K^+ channels that would promote a slight stomatal aperture. Sucrose, and probably other sugars, is also accumulated in the vacuole of guard cells during the stomatal opening. However, sucrose mainly accumulates during the late light period, when the vacuolar K^+ concentration already decreases ([Talbott and Zeiger, 1996](#); [Talbott and Zeiger, 1998](#)). Talbott & Zeiger (1996) demonstrated that the previous K^+ accumulation that drives the rapid stomatal opening is essential for the sucrose-dominated phase to occur, indicating that the afternoon sucrose replaces K^+ just for turgor maintenance, instead of accelerating stomatal opening. This finding is in

agreement with our results where we show that *NHX1* expression level is higher at the onset of light while *NHX2* transcript abundance has a peak after 2 hours of light, but the expression of both genes decline significantly after 2 hours of light (section R.4.3.; figure R.23). Therefore, NHX proteins are likely involved in driving the rapid stomatal opening that takes place at the start of the light period and their lack irreparably affects the succeeding phases since KO mutant do not show an increment in stomatal conductance at any point of the day (sections R.4.2.2. and R.4.3.; figures R.22. and R.24.).

In the absence of K^+, stomatal opening can be supported by other monovalent cations such as Na^+ (section R.4.2.1.) (Humble and Hsiao, 1969; Lebaudy et al., 2008) Indeed, we show an improvement on stomatal aperture of *nhx1 nhx2* mutant stomata in the presence of 50 mM of Na^+ (section R.4.2.1.; figure R.21.). It has been shown that *nhx1 nhx2* mutants are able to accumulate higher amounts of Na^+ than the wild type when this is in the nutrient solution at nontoxic concentrations, and this Na^+ accrual alleviates K^+-associated toxicity symptoms in the mutants (Bassil et al., 2011a; Barragán et al., 2012). It is important to take into account that K^+ is more efficient than Na^+ for stomatal opening since higher concentrations of Na^+ are necessary to reach the same stomatal aperture (section R.4.2.1.; figures R.19.-R.21.) (Humble and Hsiao, 1969). Thus, *in vivo*, plants would take moderate amounts of Na^+ to replace K^+ as osmoticum under K^+-deficiency conditions, but probably not in the high concentrations that are necessary to reach the maximal stomatal aperture. Lebaudy et al (2008) proved that in physiological conditions, when both K^+ and Na^+ are present in the medium, the guard cell plasma-membrane inward K^+ channels use preferentially K^+ instead of Na^+ to avoid toxicity in the cytosol. Therefore, it is likely that besides the activity of vacuolar potassium channels (see above), the uptake of Na^+ into the guard cell vacuole of *nhx1 nhx2* mutants assists the stomatal opening even if this does not support its potential maximal aperture. In the case that *nhx1 nhx2* mutants accumulated Na^+ as osmoticum to replace the lack of K^+ uptake, the stomatal closure would probably be impaired because Na^+ cannot be rapidly excreted from the cell in order to avoid toxicity in the cytosol (Lebaudy et al., 2008), as it has described in other systems. Jarvis & Mansfield (1980) showed that stomata of *C. communis* opened by

Na$^+$ presented a reduced stomatal closure in response to ABA, CO$_2$ and darkness ([Lebaudy et al., 2008](#)). Mutants affected in guard cell K$^+$ inward channel activity were unable to close the stomata in presence of Na$^+$ and presented higher transpiration rates during the darkness. In agreement, plasma membrane outward-rectifying K$^+$ channel current was reduced by cytoplasmatic Na$^+$ ([Thiel and Blatt, 1991](#)). At vacuolar level, the inability to extrude Na$^+$ may be caused by Na$^+$ blockage of slow vacuolar (SV) channels by shifting its activation potential to nonphysiological voltages ([Ivashikina and Hedrich, 2005](#)).

Interestingly, stomatal closure is also affected in *nhx1 nhx2* mutants both *in vitro* (dark- and ABA-induced stomatal closure) (sections R.4.2.1. and R.4.5.; figures R.17., R.18., R.27 and R.30.) and *in vivo* (dark-induced stomatal closure) (sections R.4.2.2. and R.4.3.; figures R.22. and R.24.). Stomatal opening derives from the active transport of solutes into the guard cells, whereas closure is based on the release of solutes along their concentration gradients. It is generally accepted that stomatal closure is dependent on the activation of ion channels in the vacuolar and plasma membranes. First, the activation of K$^+$ channels in the vacuole would cause the K$^+$ ions efflux from the vacuole to the cytoplasm with the subsequent depolarisation of the tonoplast, which in turn, would provide a driving force for anion efflux throught the activation of anion-permeable channels at the vacuolar membrane ([Roelfsema and Hedrich, 2005](#)). Next, plasma membrane depolarisation, caused by the inactivation of the H$^+$-ATPase and the activation of S-type anion channels, would activate the outward-rectifying K$^+$ channels and thus K$^+$ and anions would be extruded from the guard cells promoting stomatal closure ([Roelfsema and Hedrich, 2005](#)). Consequently, owing to the large decrease in K$^+$ content in the guard cell vacuoles of the *nhx1 nhx2* mutants, K$^+$ release from the vacuole to the cytoplasm to promote membrane depolarisation would not be favoured, and therefore the extrusion of other anions from the vacuole would be impeded, avoiding stomatal closure. Alternatively, distorted pH in the vacuoles of the *nhx1 nhx2* mutant ([Bassil et al., 2011a](#)) could in turn affect the cytosolic alkalinization in guard cells that is known to precede stomatal closure in response to ABA ([Irving et al., 1992](#); [Islam et al., 2010](#)). Changes in pHcyt of guard cells are correlated with stomatal movements, and these changes may be an

important factor in the regulation of guard cell movement (Irving et al., 1992; Islam et al., 2010).

Thermal imaging (section R.4.2.2.; figure R.22.) and stomatal bioassays (section R.4.2.1.; figures R.16.-R.18.) showed that the L14 mutant presented a less severe stomatal dysfunction than the null double mutant. Leaf temperature of L14 plants reached similar values to those of the wild type at the end of each light and dark periods (section R.4.2.2.; figure R.22.). In ABA-induced stomatal closure experiments the L14 mutant showed a 54% lower response than the wild type to ABA treatment, while the response of the KO mutant was only 4% of the Col-0 control. Presumably the remaining activity of NHX1 in the leaky mutant allowed some accumulation of K^+ into the vacuoles, thereby improving stomatal opening and particularly stomatal closure.

Other functions ascribed to NHX1 and NHX2 proteins are pH regulation, vesicle trafficking and vacuolar dynamics (Pardo et al., 2006; Hernandez et al., 2009; Bassil et al., 2011a) (section R.4.5.; figures R.26.-R.31.). The lack of both proteins then could also impair the stomatal function affecting these processes as we describe below.

Guard cell movements are dependent on cell volume and turgor pressure. In *Vicia faba* guard cells the turgor pressure has been demonstrated to increase from 1.0 to 4.5 MPa while the volume increases by 40% (Franks et al., 2001). These changes on guard cell volume are accompanied by changes of the plasma membrane and tonoplast surface area. Shope et al (2003) showed by confocal laser-scanning microscopy that guard cell volume and surface area decreased by ~ 40% during stomatal closure. This change in the surface area cannot be accounted for by the mere stretching and shrinking of the plasma membrane, as its elasticity does not allow changes of more than a 5% (Wolfe and Steponkus, 1983; Blatt, 2002). Studies in guard cell protoplast and leaf epidermis have shown that probably membrane internalization is concurrent with the decrease in surface area. Thus, endocytotic vesicles would be formed during stomatal closing and vesicle fusion with the plasma membrane would take place during stomatal opening to increase its surface area (Homann, 1998; Kubitscheck et al., 2000; Shope et al., 2003). A similar situation is found in guard cell

vacuoles, which undergo several morphological changes that contribute in aperture and closure stomatal movements. Guard cells of *Allium* presented small vacuoles that might be interconnected to form a reticulum during cell differenciation (Palevitz et al., 1981). Furthermore, guard cell vacuoles undergo several morphological changes that contribute in aperture and closure stomatal movements. Guard cells of *Vicia faba* and Arabidopsis harbor a great number of small vacuoles and other intra-vacuolar structures as bulb-like structures and sheet-like vacuolar membrane invaginations when stomata are closed but only a few large vacuoles when they are open. In this way vacuole fragmentation allows a reduction in volume while maintaining the total membrane surface area that is essential for rapid stomatal reopening (Gao et al., 2005; Tanaka et al., 2007b; Martinoia et al., 2012). Notwithstanding, Tanaka and collegues (2007) found that tonoplast surface area in fact increased by 20% during stomatal closure likely due to a fusion between endosomes and the vacuolar membrane. In this study, we have investigated the role of NHX1 and NHX2 in guard cell vacuolar dynamics during the stomatal movements using Arabidopsis Col-0 and *nhx1 nhx2* plants expressing a γ-TIP:GFP fusion (section R.4.5.). Compared to the control plants, KO mutants were not able to fuse the small vacuoles with each other to form fewer and bigger vacuoles while failing in stomatal opening (figures R.26. and R.31.). Under stomatal opening conditions, guard cells of KO plants presented several rounded small vesicles and tonoplast invaginations, and also a vacuolar wavy surface. However, the variety and number of vacuolar structures in closed stomata were higher in guard cells of the wild type than in the mutant (figures R.27. and R.30.). This effect probably correlates with the impossibility of the *nhx1 nhx2* mutants to fully close their stomata. One of the mechanisms proposed for vacuolar fusion in guard cells consist in the passive fusion due to physical contact between neighboring vesicles that increase their size accumulating ions and water (Gao et al., 2005) which would explain why the lack of NHX1 and NHX2 proteins affected the vacuolar morphology. Because the KO mutant cannot accumulate enough K^+ into the vacuole the subsequent water entry into the vesicles would be impaired and small vacuoles would not fuse to each other and enlarge.

Another mechanism, which not excludes the first one, is the vesicle fusion caused by pH changes in the lumen of the vesicles and in their surrounding cytoplasm. The K^+/H^+ antiporter activity of the NHX proteins coupled to V-ATPase and V-PPases activities would drive these pH changes. Yeast *ScNHX1* encodes a $Na^+(K^+)/H^+$ antiporter, homologue to the Arabidopsis NHX1 and NHX2 proteins, which is localized to vacuoles (Qiu and Fratti, 2010), trans-Golgi/TGN compartments, early and late endosomes in the biosynthetic, endocytic, and recycling pathways (Kojima et al., 2012) and also to the multivesicular bodies (MVBs) (Mitsui et al., 2011). ScNHX1 regulates vacuolar pH by transporting Na^+ and K^+ into the vacuole lumen in exchange for protons (Brett et al., 2005b). In consequence, ScNHX1 is involved in regulating ion homeostasis and cellular pH associated with the control of vesicular trafficking from Golgi to vacuoles (Bowers et al., 2000; Ali et al., 2004; Brett et al., 2005b). In addition to changes in vacuolar morphology, a vacuolar protein-sorting defect and the hyperacidification of the vacuolar lumen (Bonangelino et al., 2002; Seeley et al., 2002; Brett et al., 2005b), Qiu and Fratti (2010) recently found that the deletion of *ScNHX1* produced fragmented small vacuoles instead of the large single vacuole observed in wild-type yeasts. Purified vacuoles from a *nhx1Δ* yeast strain showed a 35% less fusion activity in *in vitro* assays compared to the wild type. Genetic complementation with a mutant *nhx1* gene defective in ion transport could not rescue the mutant phenotype while treating vacuoles with chloroquine (a weak base) recovered vacuole fusion activity to wild type levels. These results indicate that ScNHX1 might regulate vacuole fusion by controlling the luminal pH through its ion exchange activity (Qiu and Fratti, 2010). ScNhHX1 would be essential for priming and/or tethering stages of vesicle fusion since the addition of recombinant Vam7 proteins rescued the *nhx1* mutant fusion activity and the formation of *trans*-SNARE complexes was not affected (Qiu and Fratti, 2010). Also the mammalian Na^+/H^+ exchangers (NHEs) play fundamental roles in the regulation of the ion homeostasis and pH control because their contribution to proton efflux. Hence, overexpression of the organellar NHEs 6, 8 and 9 alkalizes the lumen of specific organelles in which they are located (Ohgaki et al., 2011). Plant NHXs proteins are also involved in regulating vacuolar pH as is best illustrated by the flower colour transition in *Ipomoea spp*. The anthocyanin pigment accumulated in vacuoles shifts from red-purple in flowers buds to blue in the open flowers. This colour change

is prompted by the alkalinization of the petal vacuoles from 6.6 to 7.7 (Yoshida et al., 1995). The insertion of a transposable element in the *Ipomoea nil NHX1* gene partly abolished the vacuolar pH change and flower color transition (Fukada-Tanaka et al., 2000; Yamaguchi et al., 2001). ItNHX1 exchanger of *Ipomoea tricolor* coupled with V-ATPase, V-PPase and PM-ATPase activity induces not only a shift in vacuolar pH changing the petal color but also the synchronized uptake of K^+ accumulation to drive cell expansion and flower opening (Yoshida et al., 2005; Yoshida et al., 2009). In the light of the results exposed above an analogous situation could be taking place during stomatal opening. After the generation of a proton gradient by the activation of the plasma membrane H^+-ATPase and the V-ATPase and V-PPase during the stomatal opening the AtNHX1 and AtNHX2 proteins would couple two simultaneous processes: the alkalinization of the small vacuoles and vesicles to initiate the vacuolar fusion which results in an increasing of vacuolar surface area and volumen, and the accumulation of the cheap osmoticum K^+ with the subsequent entry of water and rise of turgor.

D.1.3. The role of NHX proteins in reproduction and viability.

AtNHX1 and AtNHX2 play an important role in reproduction and viability. On one hand, as can be observed by GUS expression analyses both proteins are higly expressed in flowers. AtNHX1 is expressed in sepals, in pollen within anthers and in the stigma (Shi and Zhu, 2002) while AtNHX2 expression is greater in filaments of the stamen, in the stigma and also in mature pollen (section R.3.; figure R.12.) (Barragán et al., 2012). Interestingly, for NHX2, GUS staining was also detected in stomata within the anthers and the gynoecium near to the stigma (section R.3.; figure R.12.) (Barragán et al., 2012). On the other hand, *nhx1 nhx2* plants produced few flowers, very small siliques and a very low number of seeds per plant (section R.2.1. and R.2.2.; figures R.4. and R.5.) (Bassil et al., 2011a; Barragán et al., 2012). A detailed study of the *nhx1 nhx2* flowers showed two phenotypic features that are in concordance with the NHX1 and NHX2 promoter analyses. First, mature *nhx1 nhx2* stamens had notably shorter filaments that are not able to position the anthers at the height of the stigma. Since K^+

play and specific role in filament extension ([Heslop-Harrison and Heslop-Harrison, 1996](#)), it has been proposed that *nhx1 nhx2* mutants have reduced filaments due to their incapacity to accumulate K^+ in vacuoles of filament cells, where NHX proteins are highly expressed, to generate the osmotic-driven cell expansion ([Bassil et al., 2011a](#)). Anther dehiscence is a coordinated process that involve the dehydration of the endothecium and epidermal cells, which cause the locule to bend outwards, the rupture of the stomium and the release of the pollen ([Wilson et al., 2011](#)). The second feature was that only a 3% of the *nhx1 nhx2* anthers presented a normal pollen dehiscence due to impaired stomium rupture. Bassil et al. (2011) explain this mutant phenotype in base to the previous findings that demonstrate that active water movements in the anther may be due in part to localized accumulation of cations, particularly potassium. Therefore, K^+ would be accumulated in mature pollen attracting water from the surrounding regions driving the swelling of the pollen which is, to some extent, responsible for septum rupture ([Rehman and Yun, 2006](#); [Wilson et al., 2011](#)).

In this work we propose another, but non-exclusive explanation by which pollen dehyscence is affected in the *nhx1 nhx2* double mutants. It has been previously reported that the presence of stomata within the anthers in many species influences the speed of pollen dehiscence. Stomata would remain open along the stamen development promoting evaporation and thus favour anther dehiscence ([Schmid, 1976](#)). In *Gasteria verrucosa*, which has stomata on the anther, the pollen dehiscence that immediately follows anthesis seems to be caused by the presence of open stomata during all the anther dehydration process. When *G. verrucosa* stomata are closed with petroleum jelly anther dehiscence takes place very slowly compared to the untreated control. In addition, in *Allium cepa*, which does not possess stomata in its anthers, the filament tip dehydrates and shrivels slowly after anthesis and the anther dehiscence requires several days ([Keijzer et al., 1987](#)). Along this work it has been demonstrated that *nhx1 nhx2* mutants can not open properly their stomata, and this causes that mutant plants lose less water by transpiration, surviving to longer drought periods than the wild type (section R.4.4.; figure R.25.). In the light of these results, and considering the strong expression of *AtNHX2* in the anther stomata, we postulate

that *nhx1 nhx2* pollen dehiscence impairment is also produced by their incapacity to open the stomata during the anther dehydration process. In the *nhx1 nhx2* double mutants pollen dehiscence would be slower since dehydration through the anther stomata would be impeded at the same time that this water could not be used for pollen swelling, desynchronizing thus the reproductive processes.

D.1.4. The role of NHX in Na$^+$ compartmentation and stress tolerance.

Leidi et al (2010) demonstrated that that Arabidopsis NHX1 overexpression in tomato imparted tolerance to NaCl, which was related to the preemptive accrual of K$^+$ in vacuoles and improved K$^+$ retention after stress imposition, but did not enhance the ability to compartmentalize toxic Na$^+$ ions into the vacuole Similar findings were obtained by overexpression of the tomato protein NHX2 (Rodríguez-Rosales et al., 2008). The long-standing view is that, owing to the reduced volume of the apoplastic space, the principal if not the only line of defense of plant cells to avert cell injury by extracellular salt accumulation is to rely on the sequestration of salt inside the large central vacuoles, thereby preventing ion toxicity and reducing their osmotic potential to facilitate water uptake (Oertli, 1968; Flowers et al., 1991; Munns, 2002). The discovery that vacuolar NHX proteins were capable of exchanging Na$^+$ and H$^+$ across the tonoplast led to the now widespread view that NHX proteins mediate this critical process in plants faced with saline environment (Apse et al., 1999; Gaxiola et al., 1999; Blumwald, 2000; Quintero et al., 2000). However, this notion has been recently challenged based on the biochemistry of NHX proteins, which do not discriminate between Na$^+$ and K$^+$ or have a preference for K$^+$ transport (Venema et al., 2002; Rodriguez-Rosales et al., 2009; Jiang et al., 2010). The lack of correlative evidence between greater salt tolerance and the enhancement of Na$^+$ accumulation in different plant species overexpressing NHX proteins from various sources has also been pointed out (Rodriguez-Rosales et al., 2009; Jiang et al., 2010). Recently it has been shown that NHX1 and NHX2 proteins play a comparatively greater role in K$^+$ homeostasis than in Na$^+$ sequestration (Bassil et al., 2011a). In addition, mutant plants of leaky genotype were extraordinarily sensitive to moderate KCl concentrations (10 to 20 mM) but they

did not show greater susceptibility to NaCl compared with the wild type. In fact, salt-related growth retardation was proportionally less in the L14 plants than in the wild type at 50 to 100 mM NaCl (Barragán et al., 2012), and the inclusions of moderate amounts of NaCl in the nutrient solution containing 20 mM K^+ alleviated K^+-associated toxicity symptoms (Bassil et al., 2011a). Notably, *nhx1 nhx2* mutant plants accumulated more Na^+ in their shoots than the wild type at 100 mM NaCl (Barragán et al., 2012). Here, we showed that Na^+ but not K^+ can support stomatal opening in the *nhx1 nhx2* plants (section R.4.2.1. and section R.4.5.; figures R.19.-R.21. and R.28.) likely by its sequestration into the vacuoles. Together, these findings raise the question of how Na^+ gets compartimentalized into the vacuoles of Arabidopsis and which transport proteins underlie this process (Jiang et al., 2010). It is now apparent, at least in Arabidopsis, that ion transporters other than NHX1 and NHX2 mediate the influx of Na^+ into the vacuolar lumen. Biochemical analyses suggest the potential operation of NHX1 and NHX2 as Na^+/H^+ antiporters in the tonoplast (Barragán et al., 2012), but genetic evidence rules out any significant contribution of NHX1 and NHX2 in the compartmentation of Na^+ (Barragán et al., 2012). The budding yeast VNX1 protein, a member of the type II calcium exchanger family, catalyzed Na^+/H^+ and K^+/H^+ exchange, but not Ca^{2+}/H^+ exchange, in vacuole-enriched fractions with a K_m of 22.4 and 82.2 mM for Na^+ and K^+, respectively (Cagnac et al., 2007). Suggestions that members of the calcium/cation antiporter and CHX exchanger superfamilies may also mediate Na^+/H^+ exchange at the plant tonoplast have not been confirmed experimentally (Zhao et al., 2009; Chanroj et al., 2012). In this regard, it is intriguing that genetic inactivation of NHX1 and NHX2 reduced simultaneously Na^+/H^+ and K^+/H^+ exchange capacity in tonoplast vesicles and that no specific Na^+/H^+ exchange activity was unmasked by removing NHX1 and NHX2, while Na^+ accumulation still proceeded under salinity stress (Barragán et al., 2012). Electrophysiological studies have shown that nonselective FV and SV channels permeate K^+ and Na^+ into the vacuolar compartment (Hedrich and Neher, 1987; Ivashikina and Hedrich, 2005). Under salt stress plant cells accumulate Na^+ in the vacuole and release vacuolar K^+ into the cytoplasm. SV channels are thought to mediate K^+ release, but it appears that concomitant Na^+ leakage from the vacuole is impeded as luminal Na^+ blocks the SV channel in Arabidopsis (Ivashikina and Hedrich, 2005). In contrast with K^+ ions, Na^+ could not be released by SV channels even in the

presence of a 150-fold gradient (lumen to cytoplasm). This property of the SV channel guarantees that K^+ can be shuttled across the vacuolar membrane while maintaining the Na^+ stored in this organelle. However, since vacuoles of glycophytic plants may accumulate up to 80 mM Na^+, cytosolic Na^+ concentrations remain at 10 to 30 mM, and the tonoplast membrane potential is ~ 30 mV, positive in the lumen relative to the cytosol ([Carden et al., 2003](); [Tester and Davenport, 2003]()), it appears unlikely that passive permeation by SV channels would account for meaningful accumulation of Na^+ inside vacuoles. In summary, there is no likely candidate(s) yet to account for the Na^+ accumulation that occurs in the absence of NHX1 and NHX2 in Arabidopsis.

D.2. Post-translational regulation of NHX proteins.

Previously in this work the responses of plants to regulate the K^+ homeostasis have been summarized (sections I.1.3.1. and I.1.3.2.). Whereas there is a lack of transcriptional responses of K^+ transporters to external K^+ conditions, there are a large proportion of Ca^{2+}-regulated proteins (e.g., CaM2, CIPK6, CIPK9) among the K^+-regulated transcrips ([Armengaud et al., 2004](); [Amtmann et al., 2006]()), indicating that cytoplasmic Ca^{2+} is an essencial element to maintain the K^+ homeostasis. Cytoplasmic Ca^{2+} oscillations would drive post-translational and post-transcriptional responses via Ca^{2+}-dependent kinases, phosphatases, and transcription factors. At the same time they would control the tonoplast K^+ fluxes by the activation of K^+-permeable vacuolar channels ([Allen and Sanders, 1996](), [1997]()). For these reasons one of the objectives of the present work has been to acquire more knowledge about the post-translational regulation of the proteins NHX1 and NHX2 through Ca^{2+}-dependent proteins. Few phosphoproteomic analyses of Arabidopsis tonoplast proteins have identified phospho-peptides derived from the C-termini of AtNHX1 and AtNHX2 proteins ([Sugiyama et al., 2008](); [Whiteman et al., 2008b]()). However, the importance and the function of this phosphorylation event *in vivo* have not been so far investigated. In order to dissect the significance of the phosphorylation at the NHX1 and NHX2 C-terminal domain previously reported by other groups, functional analyses have been

performed using the yeast heterologous system. As it is described in the section R.5.2., NHX1 and NHX2 alleles carrying mutations in the phosphorylated residue were assayed in the yeast strain AXT3K (Quintero et al., 2002). The results show that at least the phosphorylation at the Ser532 it is important for AtNHX2 activity in yeast since the replacement from serine to alanine constrains the cell growth under salt treatment (figure R.36.). By contrast, AXT3K cells expressing the *nhx2* S532D mutant allele were able to complement the yeast salt-sensitive phenotype at the same level than the wild-type allele (figure R.36.). After the observation that AtNHX2 phosphorylation seems to be important for its activity we next investigated, by BiFC and functional assays in yeast, if AtNHX1 and AtNHX2 can interact with members of the CIPK family, especially with CIPK24.

Our results point to a possible interaction between NHX2, CIPK24 and CBL10 that takes place at the vacuolar membrane to regulate the activity of the cation exchanger (sections R.5.3.1. and R.5.3.2.; figures R.37., R.39. and R.42.-R.44.; Table R.2.). Moreover, the results demonstrate that the wild-type CIPK24 is necessary for the proper interaction with NHX2, since a truncated CIPK24 protein that retains its kinase activity failed to improve the yeast cell growth under salt treatment (section R.5.3.1.; figure R.43.). A role for the complex CIPK24/CBL10 in the vacuolar membrane has been proposed by Kim and colleagues (2007) where this complex would regulate the cation/H$^+$ antiporter NHX1 in the aerial parts of the plant. They postulate that this signaling pathway would mediate the sequestration of Na$^+$ into the vacuole under salt stress conditions. This hypothesis would be in agreement with the lower vacuolar Na$^+$/H$^+$ antiporter activity found in *cipk24* mutant plants (Qiu et al., 2004). In fact, NHX1 and NHX2 proteins catalyze K$^+$ or Na$^+$ antiport with the same affinity (Venema et al., 2002; Hernandez et al., 2009; Leidi et al., 2010; Barragán et al., 2012) and the leaky *nhx1 nhx2* double mutants exhibit much lower Na$^+$/H$^+$ and K$^+$/H$^+$ exchange activity than the wild type in tonoplast vesicles isolated from roots and leaves. However, genetic evidence rules out any significant contribution of NHX1 and NHX2 in the compartmentation of Na$^+$ into the vacuole (Barragán et al., 2012). It has been reported that CIPK24/SOS2 also interacts with the vacuolar H$^+$-ATPase and upregulates its transport activity since H$^+$ transport activity of tonoplast vesicles isolated from *sos2-2*

cells was reduced in a 30% compared to the wild type. In addition, the interaction between CIPK24 and the V-ATPase promotes salt tolerance (Batelli et al., 2007). Therefore, the role of CIPK24 in Na^+ accumulation into the vacuole would increase the transmembrane H^+ gradient that in turn can be used by cation/H^+ exchangers.

BiFC experiments also show that both NHX proteins are able to strongly interact with CIPK23 at the tonoplast (section R.5.3.2.; figures R.37.-R.39.; table R.2.). This is an interesting result due to the involvement of this kinase in the control of K^+ homeostasis at the plasma membrane. Under low-K^+ stress there is a cytoplasmic Ca^{2+} increase that is detected by the CBL1 and CBL9 proteins. These CBLs recruit the CIPK23 protein to the plasma membrane where it phosphorylates and activates the K^+ channel AKT1 (Li et al., 2006a; Xu et al., 2006) . The vacular K^+ pool is also responsible to maintain the cytosolic K^+ concentration within narrow limits, that only decline when the vacuolar K^+ reserve has been depleted below the thermodynamical equilibrium with the cytosolic pool (Walker et al., 1996; Leigh, 2001; White and Karley, 2010). For that reason it would be plausible that after a decrease in the cytosolic and vacuolar K^+ pools, the CIPK23 kinase would regulate also the K^+ homeostasis at vacuolar level by the interaction with several CBLs. Hence, CIPK23 could integrate both signals and coordinate the K^+ movements between the plasma membrane and the vacuolar membrane. In addition, as is the case for proteins NHX1 and NHX2, CIPK23 is involved in the stomatal function. CIPK23 has been described as a negative regulator of the ABA signaling in guard cells and in fact, *cipk23* mutants showed a more efficient stomatal closure in response to ABA than the wild type (Cheong et al., 2007; Nieves-Cordones et al., 2012).

Among the CIPKs that interact with the NHXs proteins, AtCIPK15, that interacts exclusively with NHX2 (section R.5.3.1.; figure R.39.; table R.2.), is involved in ABA responses through its interaction with CBL1. CIPK15 is highly expressed in guard cells and *cipk15* and *cbl1* mutants show a hypersensitive ABA stomatal response (Guo et al., 2002). It has been suggested that CIPK15 phosphorylates the APETALA2/EREBP-type transcriptional factor AtERF7 which in turn acts as a repressor of gene transcription and plays an important role in ABA responses. Indeed, stomatal closure is less sensitive

to ABA in *AtERF7* overexpression plants that showed increased transpirational water loss, while the *aterf7* RNAi lines presented the opposite ABA-related phenotype (Song et al., 2005). AtCIPK1, that interacts weakly with NHX1 and NHX2 (section R.5.3.1.; figures R.37.-R.39.; table R.2.), has been proposed to mediate the osmotic stress tolerance functioning in an ABA-dependent subpathway by its association with CBL9, and also in an ABA-independent subpathway together with CBL1 (D'Angelo et al., 2006). These CIPK1/CBLs complexes have been localised at the plasma membrane (D'Angelo et al., 2006), and thus far no role of CIPK1 at the tonoplast has been described. For CIPK14, that interacts with NHX2 but not with NHX1 (section R.5.3.1.; figure R.39.; table R.2.), it has been reported its role in ABA and salt responses in Arabidopsis. *CIPK14* is induced by ABA and salt treatments, and *cipk14* knockout mutants showed lower germination rate and less root elongation compare to the wild type under ABA and salt treatments (Qin et al., 2008). However, in the literature there is no information available yet about the roles of CIPK2, CIPK5, CIPK18 and CIPK26.

Our findings show that some yeast protein kinase can phosphorylate the ser532 of the *Arabidopsis* NHX2 (figure R.48.), which would explain some of the results obtained in the sections before. In section R.5.2. we demonstrated that the ser532 of the AtNHX2 is essential for the activity of the AtNHX2 since the mutant allele *nhx2*S532A was not able to complement the salt-sensitive phenotype of the yeast strain AXT3K. The fact that AtNHX2 by itself can confer salt tolerance in yeast indicates that one or several yeast protein kinases can recognize and phopshorylate the *Arabidopsis* protein in this specific serine, upregulating its activity (figures R.36. and R.41.). This would explain the slight increase of the tolerance to NaCl that we observed when NHX2, CIPK24 and CBL10 were co-expressed in yeast (section R.5.3.2, figures R.44.), in contrast with the strong phenotype obtained when SOS1 is specifically activated by CIPK24(SOS2)/CBL4(CBL4/SOS3) (Quintero et al., 2002). Furthermore, the inability to detect NHX phosphorylation by the CIPKs in protein kinase *in vitro* assays (section R.5.3.3.) could be due to the fact that the purified recombinant NHX proteins are already phosphorylated by the yeast kinases. The same reason would explain the apparent autophosphorylation of NHX2 found in some assays (figure R.46.). Therefore, we can conclude that yeast is not the best model to study the signaling pathway

NHX/CIPK/CBL, so it would be necessary to use alternative approaches, such as the expression and purification of the recombinant proteins from bacteria and/or to determine which yeast protein kinase is responsible for the NHX phosphorylation. Also, it is essential to investigate the role of NHX phosphorylation *in planta*.

Our data show that AtNHX1 and AtNHX2 can interact in a specific manner with several CIPK kinases at the tonoplast, but some interactions are shared by both exchangers while others are circumscribed to one of the NHX isoforms (section R.5.3.1.; figures R.37.-R.39.; table R.2.). Together with the facts that NHX1 and NHX2 can form homomers and heteromers between them (section R.5.1.; figures R.33. and R.34.), their functional redundancy in plants (Barragan, 2007; Bassil et al., 2011a; Barragán et al., 2012), the constraints to perform functional assays in yeast with these proteins (section 5.3.4.; figure R.48.), and that the NHX/CIPK interactions could be independent of phosphorylation (Batelli et al., 2007) (section R.5.3.3.; figures R.45.-R.47.), the study of the post-translational regulation of NHX1 and NHX2 in response to several stimulus becomes in an intrincated issue that needs of new approaches and studies to be resolved.

VII. CONCLUSIONS

1. The vacuolar-localized NHX1 and NHX2 proteins play a critical role in the accrual of K^+ in the vacuole, which is essencial for cell expansion, plant growth and osmotic regulation.

2. The ion exchangers NHX1 and NHX2 are essential for stomatal activity by facilitating K^+ accumulation into guard cell vacuoles.

3. No other K^+ transporter functionally substitutes their role in the tonoplast of the guard cell but Na^+ supplementation bypasses the requirement of NHX1 and NHX2.

4. The very dynamic morphological changes that vacuoles of guard cells undergo along the aperture and closure of stomata are unconditionally dependent on the instauration of K^+ uptake into the vacuolar lumen by NHX1 and NHX2 proteins.

5. There exist yeast kinases able to phosphorylate the AtNHX2 antiporter at the serine532, and this phosphorylation event is essencial for AtNHX2 activity in yeast.

6. The ion antiporters NHX1 and NHX2, which can form homomers and heteromers between them, interact *in planta* with several members of the CBL-Interacting Protein Kinases (CIPKs).

VIII. ANNEX 1

Abbreviations

AAS	Atomic absorption spectrophotometry
ABA	Abcisic acid
AD	Activation domain
AP	Arginine phosphate medium
ATP	Adenosine-5'-triphosphate
BD	Binding domain
BiFC	Bimolecular fluorescence complementation
bp	Basepair
Ca_{2+}	Calcium
cAMP	Cyclic adenosine monophosphate
cDNA	Complementary deoxyribonucleic acid
CDS	Coding sequence
CIP	Calf intestinal alkaline phosphatase
Cl^-	Chlorine
cm	Centimeter
Col-0	*Arabidopsis thaliana* cv Columbia wild type
CTAB	Hexadecyltrimethylammonium bromide
Cyt	Cytosolic
DEPC	Diethylpyrocarbonate
DNA	Deoxyribonucleic acid
dNTP	Deoxynucleotide triphosphates
DTT	Dithiothreitol
EDTA	Ethylenediaminetetraacetic acid
EDX	Energy-dispersive X-ray spectroscopy
ER	Endoplasmic reticulum
g	Gram
GBq	Gigabecquerel
GFP	Green fluorescent protein
GST	Glutathione S-transferase
GUS	Beta-glucuronidase
GTE	Glucose-Tris-EDTA
h	Hour
H+	Hydrogen or protons
His	Histidine
Hyg	Hygromycin
IC	Intracellular
JA	Jasmonic acid
K^+	Potassium
Kan	Kanamycin
kb	Kilobase
kDa	Kilodalton

KIRC	Inward-rectifier K+ channel
KO	*Arabidopsis thaliana nhx1-2 nhx2-1* mutant line
KORC	Outward-rectifier K+ channel
kV	Kilovolts
L	Litre
L14	*Arabidopsis thaliana nhx1-1 nhx2-1* mutant line
LAK	
LB	Luria-Bertani medium for bacteria growth
Leu	Leucine
m	Meter
mA	Milliampere
MES	2-(N-morpholino)ethanesulfonic acid
mg	Miligram
min	Minute
mL	Milliliter
mm	Millimeter
mM	Millimolar
mRNA	Messenger RNA
MS	Murashige & Skoog medium for plant growth
mV	Millivolts
MVBs	Multivesicular bodies
N	Normal
Na+	Sodium
NADPH	Nicotinamide adenine dinucleotide phosphate
NH_4^+	Amonium
nm	nanometer
nM	Nanomolar
NO_3^-	Nitrate
O_3	Ozone
O.D.	Optical density
o/n	overnight
PAR	Photosynthetically active radiation
PBS	Phosphate buffered saline
PCR	Polymerase chain reaction
PEG	Polyethylene glycol
PLATE	Solution for yeast transformation (PEG-lithium acetate-Tris-EDTA)
PM	Plasma membrane
Rb^+	Rubidium
RH	Relative humidity
RNA	Ribonucleic acid
rpm	Revolutions per minute
ROS	Reactive oxygen species
RT-PCR	Reverse transcription polymerase chain reaction
s	Second
SDS	sodium dodecyl sulfate

SDS-PAGE	SDS polyacrylamide gel electrophoresis
SEM	Scanning electron microscopy
Ser	Serine
S.I.	Stomatal index
SOB	Super optimal broth medium
SOC	Super optimal broth with catabolite repression medium
TAE	Tris acetate-sodium acetate-EDTA
Taq polymerase	DNA polymerase isolated from the bacterium *Thermus aquaticus*
T-DNA	Transfer DNA
TE	Tris:EDTA
TEMED	Tetramethylethylenediamine
TGN	Trans-Golgi network
Tm	Melting temperature
TM	Transmembrane domain
Thr	Threonine
Trp	Tryptophan
Ura	Uracil
U	Enzyme unit
U.V.	Ultraviolet
V	Volts
v	Volume
w	Weight
Y2H	Yeast two-hybrid
YEP	Yeast Extract Peptone medium for *Agrobacterium* growth
YFP	Yellow fluorescent protein
YNB	Yeast-nitrogen-base medium for yeast growth
YPD	Yeast-peptone-dextrose medium for yeast growth
X-Gluc	5-bromo-4-chloro-3-indolyl glucuronide
µCi	Microcurie
µL	Microliter
µM	Micromolar
µmol	Micromol
ø	Diameter

IX. ANNEX 2

Primers

1. PCR

Primer	Sequence	Gene
nhx1-5′-2	5′CACGTGCAAGTAAGTGTGGTCC3′	*AtNHX1*
nhx1-3′	5′CCAGAGCGTGCATATAGCAGCTAC3′	*AtNHX1*
nhx2-5′	5′GGTTGCAGCTATTCGCCTTGAGTGG3′	*AtNHX2*
nhx2-3′	5′CGGTATCAGGGTTCAGTGTTAGCG3′	*AtNHX2*
LBa1	5′TGGTTCACGTAGTGGGCCATCG3′	T-DNA of pROK2

2. RT-PCR

Primer	Sequence	Gene
TB4-F	5′CAGTGTCTGTGATATTGCACC3′	*AtTB4*
TB4-R	5′GACAACATCTTAAGTCTCGTA3′	*AtTB4*
NHX1rt-F	5′GTATCTATGGCTCTTGCATACAAC3′	*AtNHX1*
NHX1rt-R	5′ATCAAAGCTTTTCTTCCACGTTACCC3′	*AtNHX1*
NHX2rt-F	5′CAGGGCACACAGAATTGCGCGGGAATG3′	*AtNHX2*
NHX2rt-R	5′GTCACCATAAGAGGGAAGAGCAAG3′	*AtNHX2*

3. Cloning and mutagenesis

Primer	Sequence	Gene
NHX1ct-5′	5′GGATCCATGATCACGAGTACGATAACT3′	*AtNHX1*
NHX1ct-3′	5′AAGCTTTCAAGCCTTACTAAGATCAGG3′	*AtNHX1*
NHX2ct-5′	5′ CAGGAATTCGGATCCGGTATGCTAACCAAACCACTG3′	*AtNHX2*
NHX2ct-3′	5′ CGCGTCGACTCAAGGTTTACTAAGATCATG3′	*AtNHX2*
CIPK26-F	5′ AACCCCCGGGATGAATCGGCCAAAGGTTCAG3′	*AtCIPK26*
CIPK26_R	5′ TTTGCTCGAGTTATTTGCTTAGACCAGAGCT3′	*AtCIPK26*
CIPK23_F	5′ TCCTCCCGGGATGGCTTCTCGAACAACGCCT3′	*AtCIPK23*
CIPK23_pEG(KT)_F	5′TCCTCCCGGGAATGGCTTCTCGAACAACGCCT3′	*AtCIPK23*
CIPK23 R	5′GCCCCTCGAGTTATGTCGACTGTTTTGCAAT3′	*AtCIPK23*
γ-TIP-Not	5′CCACCGCGGCCGCCGTAGTCTGTGGTTGGGAG3′	*AtTIP1;1*
GFP-Not	5′GCTGGCGGCCGCGGTGGTGTGAGCAAGGGCGAGGAGCTG3′	*GFP*
AtNHX1 Xho5′	5′AACCTCGAGATGTTGGATTCTCTAGTGTCGAAA3′	*AtNHX1*
AtNHX2 Xho5′	5′CTCGAGATGACAATGTTCGCCTCTTTAACC3′	*AtNHX2*
Atnhx1SA-3′	5′ GGATCCTCAAGCCTTACTAAGATCAGGAGGGTTTCTCTCAGTTGGAGCAC3'	*AtNHX1*
Atnhx2SA-3′	5′ GGATCCTCAAGGTTTACTAAGATCATGGCTGCTTCTCTCAGTCGGAGCACCAGG3′	*AtNHX2*
Atnhx2SD-3′	5′ GGATCCTCAAGGTTTACTAAGATCATGGCTGCTTCTCTCAGTCGGATCACCAGG3′	*AtNHX2*

X. ANNEX 3

Vectors

1. Cloning Vectors

Vector	Organism	Selection marker	Reference
pCR®-Blunt	Bacteria	Kanamycin	Invitrogen
pCB-NHX1ct	Bacteria	Kanamycin	(Barragan, 2007)
pCB-NHX2ct	Bacteria	Kanamycin	Present work, created by Verónica Barragán
pCRBlunt-CIPK23	Bacteria	Kanamycin	Present work
pCR®2.1-TOPO®	Bacteria	Kanamycin and ampicillin	Invitrogen
pCR2.1-pDRNHX1	Bacteria	Ampicillin	Present work
pCR2.1-pDRNHX2	Bacteria	Ampicillin	Present work

2. Expression Vectors

Vector	Organism	Selection marker	Promoter/ Terminator	Reference
pEG(KT)	Yeast (multicopy) / Bacteria	URA3/ Ampicillin	CYC1/CYC1	(Mitchell et al., 1993)
pEG(KT)-NHX1ct	Yeast (multicopy) / Bacteria	URA3/ Ampicillin	CYC1/CYC1	(Barragan, 2007)
pEG(KT)-NHX2ct	Yeast (multicopy) / Bacteria	URA3/ Ampicillin	CYC1/CYC1	Present work
pEG(KT)-SOS1ct	Yeast (multicopy) / Bacteria	URA3/ Ampicillin	CYC1/CYC1	(Quintero et al., 2011)
pEG(KT)-CIPK23	Yeast (multicopy) / Bacteria	URA3/ Ampicillin	CYC1/CYC1	Present work
pEG(KT)-SOS2	Yeast (multicopy) / Bacteria	URA3/ Ampicillin	CYC1/CYC1	Present work, created by F. Javier Quintero

pEG(KT)-SOS2 HA	Yeast (multicopy) / Bacteria	URA3/ Ampicillin	CYC1/CYC1	Present work, created by F. Javier Quintero
pGEX-2TK-SOS2	Bacteria	Ampicillin	TAC/TAC	(Guo et al., 2001a)
pGEX-2TK-SOS2 HA	Bacteria	Ampicillin		(Guo et al., 2001a)
pEG(KT)-CBL10	Yeast (multicopy) / Bacteria	URA3/ Ampicillin	CYC1/CYC1	Present work, created by Imelda Mendoza
pGEX-6P-1-SCABP8	Bacteria	Ampicillin	TAC/TAC	(Quan et al., 2007)
pAtNHX1-1	Yeast (multicopy) / Bacteria	URA3/ Ampicillin	PMA1/ADH1	(Quintero et al., 2000)
pDR-AtNHX2	Yeast (multicopy) / Bacteria	URA3/ Ampicillin	PMA1/ADH1	(Yokoi et al., 2002)
pDR-nhx1S526A	Yeast (multicopy) / Bacteria	URA3/ Ampicillin	PMA1/ADH1	Present work, created by Agustín Hernández
pDR-nhx2S532A	Yeast (multicopy) / Bacteria	URA3/ Ampicillin	PMA1/ADH1	Present work
pDR-nhx2S532D	Yeast (multicopy) / Bacteria	URA3/ Ampicillin	PMA1/ADH1	Present work
pBD-GAL4 cam	Yeast	TRP1/ Chloramphenicol	ADH1/ADH1	Stratagene
pBD-NHX1ct	Yeast	TRP1/ Chloramphenicol	ADH1/ADH1	Present work, created by Verónica Barragán
pGBKT7	Yeast	TRP1/Kanamycin	ADH1/ADH1	Clontech
pGB-NHX2ct	Yeast	TRP1/Kanamycin	ADH1/ADH1	Present work
pGAD-NHX1ct	Yeast	LEU2/Ampicillin	ADH1/ADH1	Present work , created by Kudla's laboratory
pGAD-NHX2ct	Yeast	LEU2/Ampicillin	ADH1/ADH1	Present work, created by Kudla's laboratory,
p414GPD	Yeast (multicopy)	TRP1/Ampicillin	GPD/CYC1	(Mumberg et al., 1995)

	/ Bacteria			
pYPGE15	Yeast (multicopy) / Bacteria	URA3/Ampicillin	PGK1/CYC1	(Brunelli and Pall, 1993)
p414GPD-CIPK23	Yeast (multicopy) / Bacteria	TRP1/Ampicillin	GPD/CYC1	Present work, created by F. Javier Quintero
p414GPD- CIPK24 T168D/Δ308	Yeast (multicopy) / Bacteria	TRP1/Ampicillin	GPD/CYC1	(Guo et al., 2004)
p414GPD-CIPK24	Yeast (multicopy) / Bacteria	TRP1/Ampicillin	GPD/CYC1	(Guo et al., 2004)
p414GPD-CIPK26	Yeast (multicopy) / Bacteria	TRP1/Ampicillin	GPD/CYC1	Present work
pYPGE15-CBL1	Yeast (multicopy) / Bacteria	URA3/Ampicillin	PGK1/CYC1	Present work
pYPGE15-CBL2	Yeast (multicopy) / Bacteria	URA3/Ampicillin	PGK1/CYC1	Present work
pYPGE15-CBL3	Yeast (multicopy) / Bacteria	URA3/Ampicillin	PGK1/CYC1	Present work
pYPGE15-CBL4	Yeast (multicopy) / Bacteria	URA3/Ampicillin	PGK1/CYC1	(Guo et al., 2004)
pYPGE15-CBL6	Yeast (multicopy) / Bacteria	URA3/Ampicillin	PGK1/CYC1	Present work
pYPGE15-CBL10	Yeast (multicopy) / Bacteria	URA3/Ampicillin	PGK1/CYC1	Present work, created by Imelda Mendoza

3. Binary Vectors

Vector	Organism	Selection marker	Promoter/ Terminator	Reference
pBI101	Plants/Bacteria	Kanamycin	-	Clontech
pBI101-promNHX2:GUS	Plants/Bacteria	Kanamycin	NHX2/NOS	(Barragán et al., 2012)
pBI321	Plants/Bacteria	Kanamycin	CamV35S/NOS	(Martinez-Atienza et al., 2007)
pBI321Kan-γTIP:GFP	Plants/Bacteria	Kanamycin	CamV35S/NOS	Present work, created by Beatriz Cubero
pBI321Hyg-γTIP:GFP	Plants/Bacteria	Hygromycin	CamV35S/NOS	Present work, created by Javier Pérez-Hormaeche
pBI321-NHX2:GFP	Plants/Bacteria	Kanamycin	CamV35S/NOS	Present work, created by Beatriz Cubero
pSPYNE(R)173	Plants/Bacteria	Kanamycin	CamV35S/NOS	(Waadt et al., 2008)
pSPYNE173	Plants/Bacteria	Kanamycin	CamV35S/NOS	(Waadt et al., 2008)
pSPYCE(M)	Plants/Bacteria	Kanamycin	CamV35S/NOS	(Waadt et al., 2008)
pSPYCE(M)-NHX1	Plants/Bacteria	Kanamycin	CamV35S/NOS	Present work, created by Kudla's laboratory
pSPYCE(M)-NHX2	Plants/Bacteria	Kanamycin	CamV35S/NOS	Present work, created by Kudla's laboratory
pSPYNE173-NHX1	Plants/Bacteria	Kanamycin	CamV35S/NOS	Present work
pSPYNE173-NHX2	Plants/Bacteria	Kanamycin	CamV35S/NOS	Present work
pSPYNE(R)173-CIPKs (isoforms from 1 to 26)	Plants/Bacteria	Kanamycin	CamV35S/NOS	Present work, created by Kudla's laboratory

XI. BIBLIOGRAPHY

Ache, P., Becker, D., Ivashikina, N., Dietrich, P., Roelfsema, M.R.G., and Hedrich, R. (2000). GORK, a delayed outward rectifier expressed in guard cells of Arabidopsis thaliana, is a K+-selective, K+-sensing ion channel. FEBS Letters **486,** 93-98.

Albrecht, V., Ritz, O., Linder, S., Harter, K., and Kudla, J. (2001). The NAF domain defines a novel protein-protein interaction module conserved in Ca2+-regulated kinases. The EMBO journal **20,** 1051-1063.

Aleman, F., Nieves-Cordones, M., Martinez, V., and Rubio, F. (2011). Root K(+) acquisition in plants: the Arabidopsis thaliana model. Plant Cell Physiol **52,** 1603-1612.

Ali, R., Brett, C.L., Mukherjee, S., and Rao, R. (2004). Inhibition of Sodium/Proton Exchange by a Rab-GTPase-activating Protein Regulates Endosomal Traffic in Yeast. Journal of Biological Chemistry **279,** 4498-4506.

Allan, A.C., Fricker, M.D., Ward, J.L., Beale, M.H., and Trewavas, A.J. (1994). Two Transduction Pathways Mediate Rapid Effects of Abscisic Acid in Commelina Guard Cells. The Plant Cell Online **6,** 1319-1328.

Allen, G.J., and Sanders, D. (1996). Control of ionic currents in guard cell vacuoles by cytosolic and luminal calcium. The Plant journal : for cell and molecular biology **10,** 1055-1069.

Allen, G.J., and Sanders, D. (1997). Vacuolar Ion Channels of Higher Plants. In Advances in Botanical Research, D.S. R.A. Leigh and J.A. Callow, eds (Academic Press), pp. 217-252.

Allen, G.J., Amtmann, A., and Sanders, D. (1998). Calcium-dependent and calcium-independent K+ mobilization channels in Vicia faba guard cell vacuoles. Journal of experimental botany **49,** 305-318.

Allen, G.J., Chu, S.P., Schumacher, K., Shimazaki, C.T., Vafeados, D., Kemper, A., Hawke, S.D., Tallman, G., Tsien, R.Y., Harper, J.F., Chory, J., and Schroeder, J.I. (2000). Alteration of stimulus-specific guard cell calcium oscillations and stomatal closing in Arabidopsis det3 mutant. Science **289,** 2338-2342.

Amtmann, A., Troufflard, S., and Armengaud, P. (2008). The effect of potassium nutrition on pest and disease resistance in plants. Physiol Plant **133,** 682-691.

Amtmann, A., Hammond, J.P., Armengaud, P., and White, P.J. (2006). Nutrient Sensing and Signalling in Plants: Potassium and Phosphorus. In Advances in Botanical Research, J.A. Callow, ed (Academic Press), pp. 209-257.

Anderson, J.A., Huprikar, S.S., Kochian, L.V., Lucas, W.J., and Gaber, R.F. (1992). Functional expression of a probable Arabidopsis thaliana potassium channel in Saccharomyces cerevisiae. Proceedings of the National Academy of Sciences of the United States of America **89,** 3736-3740.

Apse, M.P., Sottosanto, J.B., and Blumwald, E. (2003). Vacuolar cation/H+ exchange, ion homeostasis, and leaf development are altered in a T-DNA insertional mutant of AtNHX1, the Arabidopsis vacuolar Na+/H+ antiporter. The Plant Journal **36,** 229-239.

Apse, M.P., Aharon, G.S., Snedden, W.A., and Blumwald, E. (1999). Salt tolerance conferred by overexpression of a vacuolar Na+/H+ antiport in Arabidopsis. Science **285,** 1256-1258.

Araujo, W.L., Fernie, A.R., and Nunes-Nesi, A. (2011). Control of stomatal aperture: a renaissance of the old guard. Plant signaling & behavior **6,** 1305-1311.

Armengaud, P., Breitling, R., and Amtmann, A. (2004). The potassium-dependent transcriptome of Arabidopsis reveals a prominent role of jasmonic acid in nutrient signaling. Plant physiology **136,** 2556-2576.

Armengaud, P., Sulpice, R., Miller, A.J., Stitt, M., Amtmann, A., and Gibon, Y. (2009). Multilevel analysis of primary metabolism provides new insights into the role of potassium nutrition for glycolysis and nitrogen assimilation in Arabidopsis roots. Plant physiology **150,** 772-785.

Assmann, S.M., Simoncini, L., and Schroeder, J.I. (1985). Blue light activates electrogenic ion pumping in guard cell protoplasts of Vicia faba. Nature **318,** 285-287.

Ausubel, F.M., Brent, R., Kingston, R.E., Moore, D.D., Seidman, J.G., Smith, J.A., and Struhl, K. (1996). Current Protocols in Molecular Biology. Greene Publishing and Wiley Interscience, New York.

Bañuelos, M.A., Sychrová, H., Bleykasten-Grosshans, C., Souciet, J.-L., and Potier, S. (1998). The Nhal antiporter of Saccharomyces cerevisiae mediates sodium and potassium eft: lux. Microbiology **144,** 2749-2758.

Barragan, V. (2007). Implicación de los antiportadores catión/protón NHX vacuolares de Arabidopsis thaliana en la homeostasis iónica. In Departamento de Biotecnología Vegetal (Universidad de Sevilla).

Barragán, V., Leidi, E.O., Andrés, Z., Rubio, L., De Luca, A., Fernández, J.A., Cubero, B., and Pardo, J.M. (2012). Ion Exchangers NHX1 and NHX2 Mediate Active Potassium Uptake into Vacuoles to Regulate Cell Turgor and Stomatal Function in Arabidopsis. The Plant Cell Online **24,** 1127-1142.

Bassil, E., Tajima, H., Liang, Y.-C., Ohto, M.-a., Ushijima, K., Nakano, R., Esumi, T., Coku, A., Belmonte, M., and Blumwald, E. (2011a). The Arabidopsis Na+/H+ Antiporters NHX1 and NHX2 Control Vacuolar pH and K+ Homeostasis to Regulate Growth, Flower Development, and Reproduction. The Plant cell **23,** 3482-3497.

Bassil, E., Ohto, M.A., Esumi, T., Tajima, H., Zhu, Z., Cagnac, O., Belmonte, M., Peleg, Z., Yamaguchi, T., and Blumwald, E. (2011b). The Arabidopsis intracellular Na+/H+ antiporters NHX5 and NHX6 are endosome associated and necessary for plant growth and development. The Plant cell **23,** 224-239.

Batelli, G., Verslues, P.E., Agius, F., Qiu, Q., Fujii, H., Pan, S., Schumaker, K.S., Grillo, S., and Zhu, J.K. (2007). SOS2 promotes salt tolerance in part by interacting with the vacuolar H+-ATPase and upregulating its transport activity. Molecular and cellular biology **27,** 7781-7790.

Batistič, O., Waadt, R., Steinhorst, L., Held, K., and Kudla, J. (2010). CBL-mediated targeting of CIPKs facilitates the decoding of calcium signals emanating from distinct cellular stores. The Plant Journal **61,** 211-222.

Becker, D., Zeilinger, C., Lohse, G., Depta, H., and Hedrich, R. (1993). Identification and biochemical characterization of the plasma-membrane H⁺-ATPase in guard cells of <i>Vicia faba L. Planta **190,** 44-50.

Becker, D., Geiger, D., Dunkel, M., Roller, A., Bertl, A., Latz, A., Carpaneto, A., Dietrich, P., Roelfsema, M.R., Voelker, C., Schmidt, D., Mueller-Roeber, B.,

Czempinski, K., and Hedrich, R. (2004). AtTPK4, an Arabidopsis tandem-pore K+ channel, poised to control the pollen membrane voltage in a pH- and Ca2+-dependent manner. Proceedings of the National Academy of Sciences of the United States of America **101,** 15621-15626.

Blatt, M.R. (1992). K+ channels of stomatal guard cells. Characteristics of the inward rectifier and its control by pH. The Journal of general physiology **99,** 615-644.

Blatt, M.R. (2002). Toward understanding vesicle traffic and the guard cell model. New Phytologist **153,** 405-413.

Blatt, M.R., and Armstrong, F. (1993). K<sup>+</sup> channels of stomatal guard cells: Abscisic-acid-evoked control of the outward rectifier mediated by cytoplasmic pH. Planta **191,** 330-341.

Blatt, M.R., Thiel, G., and Trentham, D.R. (1990). Reversible inactivation of K+ channels of Vcia stomatal guard cells following the photolysis of caged inositol 1,4,5-trisphosphate. Nature **346,** 766-769.

Blumwald, E. (2000). Sodium transport and salt tolerance in plants. Current Opinion in Cell Biology **12,** 431-434.

Blumwald, E., and Poole, R.J. (1985). Na+/H+ Antiport in Isolated Tonoplast Vesicles from Storage Tissue of Beta vulgaris. Plant physiology **78,** 163-167.

Bonangelino, C.J., Chavez, E.M., and Bonifacino, J.S. (2002). Genomic Screen for Vacuolar Protein Sorting Genes inSaccharomyces cerevisiae. Molecular biology of the cell **13,** 2486-2501.

Bowers, K., Levi, B.P., Patel, F.I., and Stevens, T.H. (2000). The Sodium/Proton Exchanger Nhx1p Is Required for Endosomal Protein Trafficking in the Yeast Saccharomyces cerevisiae. Molecular biology of the cell **11,** 4277-4294.

Bradford, M.M. (1976). A rapid and sensitive method for the quantitation of microgram quantities of protein utilizing the principle of protein-dye binding. Analytical biochemistry **72,** 248-254.

Brearley, J., Venis, M.A., and Blatt, M.R. (1997). The effect of elevated CO<sub>2</sub> concentrations on K<sup>+</sup> and anion channels of <i>Vicia faba L. guard cells. Planta **203,** 145-154.

Brett, C.L., Donowitz, M., and Rao, R. (2005a). Evolutionary origins of eukaryotic sodium/proton exchangers. American Journal of Physiology - Cell Physiology **288,** C223-C239.

Brett, C.L., Tukaye, D.N., Mukherjee, S., and Rao, R. (2005b). The yeast endosomal Na+K+/H+ exchanger Nhx1 regulates cellular pH to control vesicle trafficking. Molecular biology of the cell **16,** 1396-1405.

Brini, F., Hanin, M., Mezghani, I., Berkowitz, G.A., and Masmoudi, K. (2007). Overexpression of wheat Na+/H+ antiporter TNHX1 and H+-pyrophosphatase TVP1 improve salt- and drought-stress tolerance in Arabidopsis thaliana plants. Journal of experimental botany **58,** 301-308.

Britto, D.T., and Kronzucker, H.J. (2008). Cellular mechanisms of potassium transport in plants. Physiol Plant **133,** 637-650.

Buch-Pedersen, M.J., Rudashevskaya, E.L., Berner, T.S., Venema, K., and Palmgren, M.G. (2006). Potassium as an intrinsic uncoupler of the plasma membrane H+-ATPase. The Journal of biological chemistry **281,** 38285-38292.

Cagnac, O., Leterrier, M., Yeager, M., and Blumwald, E. (2007). Identification and Characterization of Vnx1p, a Novel Type of Vacuolar Monovalent Cation/H+

Antiporter of Saccharomyces cerevisiae. Journal of Biological Chemistry **282,** 24284-24293.

Cakmak, I. (2005). The role of potassium in alleviating detrimental effects of abiotic stresses in plants. Journal of Plant Nutrition and Soil Science **168,** 521-530.

Cakmak, I., Hengeler, C., and Marschner, H. (1994). Changes in phloem export of sucrose in leaves in response to phosphorus, potassium and magnesium deficiency in bean plants. Journal of experimental botany **45,** 1251-1257.

Carden, D.E., Walker, D.J., Flowers, T.J., and Miller, A.J. (2003). Single-Cell Measurements of the Contributions of Cytosolic Na+ and K+ to Salt Tolerance. Plant physiology **131,** 676-683.

Casson, S.A., Franklin, K.A., Gray, J.E., Grierson, C.S., Whitelam, G.C., and Hetherington, A.M. (2009). phytochrome B and PIF4 regulate stomatal development in response to light quantity. Current biology : CB **19,** 229-234.

Cellier, F., Conéjéro, G., Ricaud, L., Luu, D.T., Lepetit, M., Gosti, F., and Casse, F. (2004). Characterization of AtCHX17, a member of the cation/H+ exchangers, CHX family, from Arabidopsis thaliana suggests a role in K+ homeostasis. The Plant Journal **39,** 834-846.

Clough, S.J., and Bent, A.F. (1998). Floral dip: a simplified method for Agrobacterium-mediated transformation of Arabidopsis thaliana. The Plant journal : for cell and molecular biology **16,** 735-743.

Cormack, B.P., Valdivia, R.H., and Falkow, S. (1996). FACS-optimized mutants of the green fluorescent protein (GFP). Gene **173,** 33-38.

Covington, M.F., and Harmer, S.L. (2007). The Circadian Clock Regulates Auxin Signaling and Responses in <italic>Arabidopsis</italic>. PLoS Biol **5,** e222.

Curcio, M.J., and Garfinkel, D.J. (1991). Single-step selection for Ty1 element retrotransposition. Proceedings of the National Academy of Sciences of the United States of America **88,** 936-940.

Chanroj, S., Wang, G., Venema, K., Zhang, M.W., Delwiche, C.F., and Sze, H. (2012). Conserved and Diversified Gene Families of Monovalent Cation/H+ Antiporters from Algae to Flowering Plants. Frontiers in Plant Science **3**.

Cheng, N.-H., Pittman, J.K., Zhu, J.-K., and Hirschi, K.D. (2004). The Protein Kinase SOS2 Activates the Arabidopsis H+/Ca2+ Antiporter CAX1 to Integrate Calcium Transport and Salt Tolerance. Journal of Biological Chemistry **279,** 2922-2926.

Cheong, Y.H., Pandey, G.K., Grant, J.J., Batistic, O., Li, L., Kim, B.-G., Lee, S.-C., Kudla, J., and Luan, S. (2007). Two calcineurin B-like calcium sensors, interacting with protein kinase CIPK23, regulate leaf transpiration and root potassium uptake in Arabidopsis. The Plant Journal **52,** 223-239.

D'Angelo, C., Weinl, S., Batistic, O., Pandey, G.K., Cheong, Y.H., Schültke, S., Albrecht, V., Ehlert, B., Schulz, B., Harter, K., Luan, S., Bock, R., and Kudla, J. (2006). Alternative complex formation of the Ca2+-regulated protein kinase CIPK1 controls abscisic acid-dependent and independent stress responses in Arabidopsis. The Plant Journal **48,** 857-872.

Davenport, R.J., MuÑOz-Mayor, A., Jha, D., Essah, P.A., Rus, A.N.A., and Tester, M. (2007). The Na+ transporter AtHKT1;1 controls retrieval of Na+ from the xylem in Arabidopsis. Plant, Cell & Environment **30,** 497-507.

De Boer, A.H., and Volkov, V. (2003). Logistics of water and salt transport through the plant: structure and functioning of the xylem. Plant, Cell & Environment **26,** 87-101.

Deeken, R., Sanders, C., Ache, P., and Hedrich, R. (2000). Developmental and light-dependent regulation of a phloem-localised K+ channel of Arabidopsis thaliana. The Plant Journal **23,** 285-290.

Deeken, R., Geiger, D., Fromm, J., Koroleva, O., Ache, P., Langenfeld-Heyser, R., Sauer, N., May, S., and Hedrich, R. (2002). Loss of the AKT2/3 potassium channel affects sugar loading into the phloem of <SMALL>Arabidopsis</SMALL&gt. Planta **216,** 334-344.

Dietrich, P., Anschütz, U., Kugler, A., and Becker, D. (2010). Physiology and biophysics of plant ligand-gated ion channels. Plant Biology **12,** 80-93.

Dodd, A.N., Salathia, N., Hall, A., Kévei, E., Tóth, R., Nagy, F., Hibberd, J.M., Millar, A.J., and Webb, A.A.R. (2005). Plant Circadian Clocks Increase Photosynthesis, Growth, Survival, and Competitive Advantage. Science **309,** 630-633.

Dodd, A.N., Gardner, M.J., Hotta, C.T., Hubbard, K.E., Dalchau, N., Love, J., Assie, J.-M., Robertson, F.C., Jakobsen, M.K., Gonçalves, J., Sanders, D., and Webb, A.A.R. (2007). The Arabidopsis Circadian Clock Incorporates a cADPR-Based Feedback Loop. Science **318,** 1789-1792.

Dolan, L., and Davies, J. (2004). Cell expansion in roots. Current Opinion in Plant Biology **7,** 33-39.

Dreyer, I., Antunes, S., Hoshi, T., Müller-Röber, B., Palme, K., Pongs, O., Reintanz, B., and Hedrich, R. (1997). Plant K+ channel alpha-subunits assemble indiscriminately. Biophysical journal **72,** 2143-2150.

Edwards, K., Johnstone, C., and Thompson, C. (1991). A simple and rapid method for the preparation of plant genomic DNA for PCR analysis. Nucleic acids research **19,** 1349.

Elble, R. (1992). A simple and efficient procedure for transformation of yeasts. BioTechniques **13,** 18-20.

Emi, T., Kinoshita, T., and Shimazaki, K.-i. (2001). Specific Binding of vf14-3-3a Isoform to the Plasma Membrane H+-ATPase in Response to Blue Light and Fusicoccin in Guard Cells of Broad Bean. Plant physiology **125,** 1115-1125.

Endler, A., Reiland, S., Gerrits, B., Schmidt, U.G., Baginsky, S., and Martinoia, E. (2009). In vivo phosphorylation sites of barley tonoplast proteins identified by a phosphoproteomic approach. Proteomics **9,** 310-321.

Epstein, E., and Bloom, A.J. (2005). Mineral Nutrition of Plants: Principles and Perspectives. (Sinauer Associates Inc., Sunderland MA).

Epstein, E., Rains, D.W., and Elzam, O.E. (1963). Resolution of Dual Mechanisms of Potassium Absorption by Barley Roots. Proceedings of the National Academy of Sciences of the United States of America **49,** 684-692.

Fafournoux, P., Noël, J., and Pouysségur, J. (1994). Evidence that Na+/H+ exchanger isoforms NHE1 and NHE3 exist as stable dimers in membranes with a high degree of specificity for homodimers. Journal of Biological Chemistry **269,** 2589-2596.

Fairley-Grenot, K.A., and Assmann, S.M. (1992). Permeation of Ca<sup>2+</sup> through K<sup>+</sup> channels in

the plasma membrane of <i>Vicia faba guard cells. Journal of Membrane Biology **128,** 103-113.

Fan, L.M., Zhao, Z., and Assmann, S.M. (2004). Guard cells: a dynamic signaling model. Curr Opin Plant Biol **7,** 537-546.

Farré, E.M., Tiessen, A., Roessner, U., Geigenberger, P., Trethewey, R.N., and Willmitzer, L. (2001). Analysis of the Compartmentation of Glycolytic Intermediates, Nucleotides, Sugars, Organic Acids, Amino Acids, and Sugar Alcohols in Potato Tubers Using a Nonaqueous Fractionation Method. Plant physiology **127,** 685-700.

Felle, H.H., Hanstein, S., Steinmeyer, R., and Hedrich, R. (2000). Dynamics of ionic activities in the apoplast of the sub-stomatal cavity of intact Vicia faba leaves during stomatal closure evoked by ABA and darkness. The Plant Journal **24,** 297-304.

Fliegel, L., Haworth, R.S., and Dyck, J.R.B. (1993). Characterization of the placental brush border membrane $Na+/H+$ exchanger: identification of thiol-dependent transition in apparent molecular size. The Biochemical journal **289,** 101-107.

Flowers, T.J., Hajibagherp, M.A., and Yeo, A.R. (1991). Ion accumulation in the cell walls of rice plants growing under saline conditions: evidence for the Oertli hypothesis. Plant, Cell & Environment **14,** 319-325.

Franks, P.J., Buckley, T.N., Shope, J.C., and Mott, K.A. (2001). Guard Cell Volume and Pressure Measured Concurrently by Confocal Microscopy and the Cell Pressure Probe. Plant physiology **125,** 1577-1584.

Fu, Y., Xu, T., Zhu, L., Wen, M., and Yang, Z. (2009). A ROP GTPase Signaling Pathway Controls Cortical Microtubule Ordering and Cell Expansion in Arabidopsis. Current biology : CB **19,** 1827-1832.

Fukada-Tanaka, S., Inagaki, Y., Yamaguchi, T., Saito, N., and Iida, S. (2000). Colour-enhancing protein in blue petals. Nature **407,** 581-581.

Fukuda, A., Nakamura, A., Tagiri, A., Tanaka, H., Miyao, A., Hirochika, H., and Tanaka, Y. (2004). Function, intracellular localization and the importance in salt tolerance of a vacuolar $Na(+)/H(+)$ antiporter from rice. Plant Cell Physiol **45,** 146-159.

Gaedeke, N., Klein, M., Kolukisaoglu, U., Forestier, C., Müller, A., Ansorge, M., Becker, D., Mamnun, Y., Kuchler, K., Schulz, B., Mueller-Roeber, B., and Martinoia, E. (2001). The Arabidopsis thaliana ABC transporter AtMRP5 controls root development and stomata movement. The EMBO journal **20,** 1875-1887.

Gajdanowicz, P., Michard, E., Sandmann, M., Rocha, M., Corrêa, L.G.G., Ramírez-Aguilar, S.J., Gomez-Porras, J.L., González, W., Thibaud, J.-B., van Dongen, J.T., and Dreyer, I. (2011). Potassium (K+) gradients serve as a mobile energy source in plant vascular tissues. Proceedings of the National Academy of Sciences **108,** 864-869.

Gao, X.Q., Li, C.G., Wei, P.C., Zhang, X.Y., Chen, J., and Wang, X.C. (2005). The dynamic changes of tonoplasts in guard cells are important for stomatal movement in Vicia faba. Plant physiology **139,** 1207-1216.

Gao, Y., Zeng, Q., Guo, J., Cheng, J., Ellis, B.E., and Chen, J.-G. (2007). Genetic characterization reveals no role for the reported ABA receptor, GCR2, in ABA

control of seed germination and early seedling development in Arabidopsis. The Plant Journal **52,** 1001-1013.

Gaxiola, R.A., Fink, G.R., and Hirschi, K.D. (2002). Genetic Manipulation of Vacuolar Proton Pumps and Transporters. Plant physiology **129,** 967-973.

Gaxiola, R.A., Rao, R., Sherman, A., Grisafi, P., Alper, S.L., and Fink, G.R. (1999). The Arabidopsis thaliana proton transporters, AtNhx1 and Avp1, can function in cation detoxification in yeast. Proceedings of the National Academy of Sciences **96,** 1480-1485.

Gaymard, F., Pilot, G., Lacombe, B., Bouchez, D., Bruneau, D., Boucherez, J., Michaux-Ferrière, N., Thibaud, J.-B., and Sentenac, H. (1998). Identification and Disruption of a Plant Shaker-like Outward Channel Involved in K+ Release into the Xylem Sap. Cell **94,** 647-655.

Geiger, D., Becker, D., Vosloh, D., Gambale, F., Palme, K., Rehers, M., Anschuetz, U., Dreyer, I., Kudla, J., and Hedrich, R. (2009a). Heteromeric AtKC1{middle dot}AKT1 channels in Arabidopsis roots facilitate growth under K+-limiting conditions. The Journal of biological chemistry **284,** 21288-21295.

Geiger, D., Scherzer, S., Mumm, P., Stange, A., Marten, I., Bauer, H., Ache, P., Matschi, S., Liese, A., Al-Rasheid, K.A., Romeis, T., and Hedrich, R. (2009b). Activity of guard cell anion channel SLAC1 is controlled by drought-stress signaling kinase-phosphatase pair. Proceedings of the National Academy of Sciences of the United States of America **106,** 21425-21430.

Geiger, D., Scherzer, S., Mumm, P., Marten, I., Ache, P., Matschi, S., Liese, A., Wellmann, C., Al-Rasheid, K.A.S., Grill, E., Romeis, T., and Hedrich, R. (2010). Guard cell anion channel SLAC1 is regulated by CDPK protein kinases with distinct Ca2+ affinities. Proceedings of the National Academy of Sciences **107,** 8023-8028.

Geiger, D., Maierhofer, T., AL-Rasheid, K.A.S., Scherzer, S., Mumm, P., Liese, A., Ache, P., Wellmann, C., Marten, I., Grill, E., Romeis, T., and Hedrich, R. (2011). Stomatal Closure by Fast Abscisic Acid Signaling Is Mediated by the Guard Cell Anion Channel SLAH3 and the Receptor RCAR1. Sci. Signal. **4,** ra32-.

Gierth, M., and Mäser, P. (2007). Potassium transporters in plants – Involvement in K+ acquisition, redistribution and homeostasis. FEBS Letters **581,** 2348-2356.

Gierth, M., Maser, P., and Schroeder, J.I. (2005). The potassium transporter AtHAK5 functions in K(+) deprivation-induced high-affinity K(+) uptake and AKT1 K(+) channel contribution to K(+) uptake kinetics in Arabidopsis roots. Plant physiology **137,** 1105-1114.

Glass, A.D.M., and Dunlop, J. (1978). The influence of potassium content on the kinetics of potassium influx into excised ryegrass and barley roots. Planta **141,** 117-119.

Gobert, A., Park, G., Amtmann, A., Sanders, D., and Maathuis, F.J. (2006). Arabidopsis thaliana cyclic nucleotide gated channel 3 forms a non-selective ion transporter involved in germination and cation transport. Journal of experimental botany **57,** 791-800.

Gobert, A., Isayenkov, S., Voelker, C., Czempinski, K., and Maathuis, F.J. (2007). The two-pore channel TPK1 gene encodes the vacuolar K+ conductance and plays a role in K+ homeostasis. Proceedings of the National Academy of Sciences of the United States of America **104,** 10726-10731.

Grabov, A., and Blatt, M.R. (1997). Parallel control of the inward-rectifier K⁺ channel by cytosolic free Ca²⁺ and pH in *Vicia* guard cells. Planta **201,** 84-95.

Grabov, A., and Blatt, M.R. (1998). Membrane voltage initiates Ca2+ waves and potentiates Ca2+ increases with abscisic acid in stomatal guard cells. Proceedings of the National Academy of Sciences of the United States of America **95,** 4778-4783.

Guo, F.-Q., Young, J., and Crawford, N.M. (2003). The Nitrate Transporter AtNRT1.1 (CHL1) Functions in Stomatal Opening and Contributes to Drought Susceptibility in Arabidopsis. The Plant Cell Online **15,** 107-117.

Guo, J., Zeng, Q., Emami, M., Ellis, B.E., and Chen, J.-G. (2008). The *GCR2* Gene Family Is Not Required for ABA Control of Seed Germination and Early Seedling Development in Arabidopsis. PLoS ONE **3,** e2982.

Guo, Y., Halfter, U., Ishitani, M., and Zhu, J.-K. (2001a). Molecular Characterization of Functional Domains in the Protein Kinase SOS2 That Is Required for Plant Salt Tolerance. The Plant Cell Online **13,** 1383-1400.

Guo, Y., Halfter, U., Ishitani, M., and Zhu, J.K. (2001b). Molecular characterization of functional domains in the protein kinase SOS2 that is required for plant salt tolerance. The Plant cell **13,** 1383-1400.

Guo, Y., Xiong, L., Song, C.-P., Gong, D., Halfter, U., and Zhu, J.-K. (2002). A Calcium Sensor and Its Interacting Protein Kinase Are Global Regulators of Abscisic Acid Signaling in Arabidopsis. Developmental cell **3,** 233-244.

Guthrie, C., and Fink, G. (1991). Guide to yeast genetics and molecular biology. Methods Enzymology **194,** 795-823.

Hafke, J.B., Furch, A.C., Reitz, M.U., and van Bel, A.J. (2007). Functional sieve element protoplasts. Plant physiology **145,** 703-711.

Hamaji, K., Nagira, M., Yoshida, K., Ohnishi, M., Oda, Y., Uemura, T., Goh, T., Sato, M.H., Morita, M.T., Tasaka, M., Hasezawa, S., Nakano, A., Hara-Nishimura, I., Maeshima, M., Fukaki, H., and Mimura, T. (2009). Dynamic aspects of ion accumulation by vesicle traffic under salt stress in Arabidopsis. Plant Cell Physiol **50,** 2023-2033.

Hanana, M., Cagnac, O., Yamaguchi, T., Hamdi, S., Ghorbel, A., and Blumwald, E. (2007). A Grape Berry (Vitis vinifera L.) Cation/Proton Antiporter is Associated with Berry Ripening. Plant and Cell Physiology **48,** 804-811.

Hanstein, S.M., and Felle, H.H. (2002). CO2-Triggered Chloride Release from Guard Cells in Intact Fava Bean Leaves. Kinetics of the Onset of Stomatal Closure. Plant physiology **130,** 940-950.

Harmer, S.L. (2009). The Circadian System in Higher Plants. Annual Review of Plant Biology **60,** 357-377.

Haro, R., Bañuelos, M.A., and Rodríguez-Navarro, A. (2010). High-affinity sodium uptake in land plants. Plant and Cell Physiology **51,** 68-79.

Haro, R., Sainz, L., Rubio, F., and Rodríguez-Navarro, A. (1999). Cloning of two genes encoding potassium transporters in Neurospora crassa and expression of the corresponding cDNAs in Saccharomyces cerevisiae. Molecular microbiology **31,** 511-520.

Hashimoto, M., Negi, J., Young, J., Israelsson, M., Schroeder, J.I., and Iba, K. (2006). Arabidopsis HT1 kinase controls stomatal movements in response to CO2. Nature cell biology **8,** 391-397.

Haydon, M.J., Bell, L.J., and Webb, A.A. (2011). Interactions between plant circadian clocks and solute transport. Journal of experimental botany **62,** 2333-2348.

Hedrich, R., and Neher, E. (1987). Cytoplasmic calcium regulates voltage-dependent ion channels in plant vacuoles. Nature **329,** 833-836.

Hedrich, R., and Marten, I. (1993). Malate-induced feedback regulation of plasma membrane anion channels could provide a CO2 sensor to guard cells. The EMBO journal **12,** 897-901.

Hedrich, R., and Marten, I. (2011). TPC1-SV channels gain shape. Molecular plant **4,** 428-441.

Hedrich, R., Busch, H., and Raschke, K. (1990). Ca2+ and nucleotide dependent regulation of voltage dependent anion channels in the plasma membrane of guard cells. The EMBO journal **9,** 3889-3892.

Hedrich, R., Neimanis, S., Savchenko, G., Felle, H.H., Kaiser, W.M., and Heber, U. (2001). Changes in apoplastic pH and membrane potential in leaves in relation to stomatal responses to CO<SUB>2</SUB>, malate, abscisic acid or interruption of water supply. Planta **213,** 594-601.

Hermans, C., Hammond, J.P., White, P.J., and Verbruggen, N. (2006). How do plants respond to nutrient shortage by biomass allocation? Trends in plant science **11,** 610-617.

Hernandez, A., Jiang, X., Cubero, B., Nieto, P.M., Bressan, R.A., Hasegawa, P.M., and Pardo, J.M. (2009). Mutants of the Arabidopsis thaliana cation/H+ antiporter AtNHX1 conferring increased salt tolerance in yeast: the endosome/prevacuolar compartment is a target for salt toxicity. The Journal of biological chemistry **284,** 14276-14285.

Heslop-Harrison, Y., and Heslop-Harrison, J.S. (1996). Lodicule Function and Filament Extension in the Grasses: Potassium Ion Movement and Tissue Specialization. Annals of Botany **77,** 573-582.

Hirayama, T., and Shinozaki, K. (2007). Perception and transduction of abscisic acid signals: keys to the function of the versatile plant hormone ABA. Trends in plant science **12,** 343-351.

Hirsch, R.E., Lewis, B.D., Spalding, E.P., and Sussman, M.R. (1998). A Role for the AKT1 Potassium Channel in Plant Nutrition. Science **280,** 918-921.

Hisamitsu, T., Pang, T., Shigekawa, M., and Wakabayashi, S. (2004). Dimeric Interaction between the Cytoplasmic Domains of the Na+/H+ Exchanger NHE1 Revealed by Symmetrical Intermolecular Cross-Linking and Selective Co-immunoprecipitation†. Biochemistry **43,** 11135-11143.

Hisamitsu, T., Ammar, Y.B., Nakamura, T.Y., and Wakabayashi, S. (2006). Dimerization Is Crucial for the Function of the Na+/H+ Exchanger NHE1†. Biochemistry **45,** 13346-13355.

Höfte, H., Hubbard, L., Reizer, J., Ludevid, D., Herman, E.M., and Chrispeels, M.J. (1992). Vegetative and Seed-Specific Forms of Tonoplast Intrinsic Protein in the Vacuolar Membrane of Arabidopsis thaliana. Plant physiology **99,** 561-570.

Homann, U. (1998). Fusion and fission of plasma-membrane material accommodates for osmotically induced changes in the surface area of guard-cell protoplasts. Planta **206,** 329-333.

Hosy, E., Vavasseur, A., Mouline, K., Dreyer, I., Gaymard, F., Porée, F., Boucherez, J., Lebaudy, A., Bouchez, D., Véry, A.-A., Simonneau, T., Thibaud, J.-B., and Sentenac, H. (2003). The Arabidopsis outward K+ channel GORK is involved in regulation of stomatal movements and plant transpiration. Proceedings of the National Academy of Sciences **100,** 5549-5554.

Hoth, S., Geiger, D., Becker, D., and Hedrich, R. (2001). The Pore of Plant K+ Channels Is Involved in Voltage and pH Sensing: Domain-Swapping between Different K+ Channel α-Subunits. The Plant Cell Online **13,** 943-952.

Hu, C.D., Chinenov, Y., and Kerppola, T.K. (2002). Visualization of interactions among bZIP and Rel family proteins in living cells using bimolecular fluorescence complementation. Molecular cell **9,** 789-798.

Hu, H., Boisson-Dernier, A., Israelsson-Nordstrom, M., Bohmer, M., Xue, S., Ries, A., Godoski, J., Kuhn, J.M., and Schroeder, J.I. (2010). Carbonic anhydrases are upstream regulators of CO_2-controlled stomatal movements in guard cells. Nature cell biology **12,** 87-93; sup pp 81-18.

Humble, G.D., and Hsiao, T.C. (1969). Specific requirement of potassium for light-activated opening of stomata in epidermal strips. Plant physiology **44,** 230-234.

Ilan, N., Schwartz, A., and Moran, N. (1996). External Protons Enhance the Activity of the Hyperpolarization-activated K Channels in Guard Cell Protoplasts of <b><i>Vicia faba </b&gt. Journal of Membrane Biology **154,** 169-181.

Irving, H.R., Gehring, C.A., and Parish, R.W. (1992). Changes in cytosolic pH and calcium of guard cells precede stomatal movements. Proceedings of the National Academy of Sciences of the United States of America **89,** 1790-1794.

Isayenkov, S., Isner, J.C., and Maathuis, F.J. (2010a). Vacuolar ion channels: Roles in plant nutrition and signalling. Febs Letters **584,** 1982-1988.

Isayenkov, S., Isner, J.C., and Maathuis, F.J. (2010b). Vacuolar ion channels: Roles in plant nutrition and signalling. FEBS Lett **584,** 1982-1988.

Islam, M.M., Hossain, M.A., Jannat, R., Munemasa, S., Nakamura, Y., Mori, I.C., and Murata, Y. (2010). Cytosolic Alkalization and Cytosolic Calcium Oscillation in Arabidopsis Guard Cells Response to ABA and MeJA. Plant and Cell Physiology **51,** 1721-1730.

Ivashikina, N., and Hedrich, R. (2005). K+ currents through SV-type vacuolar channels are sensitive to elevated luminal sodium levels. The Plant journal : for cell and molecular biology **41,** 606-614.

Ivashikina, N., Deeken, R., Fischer, S., Ache, P., and Hedrich, R. (2005). AKT2/3 Subunits Render Guard Cell K+ Channels Ca2+ Sensitive. The Journal of general physiology **125,** 483-492.

Jammes, F., Song, C., Shin, D., Munemasa, S., Takeda, K., Gu, D., Cho, D., Lee, S., Giordo, R., Sritubtim, S., Leonhardt, N., Ellis, B.E., Murata, Y., and Kwak, J.M. (2009). MAP kinases MPK9 and MPK12 are preferentially expressed in guard cells and positively regulate ROS-mediated ABA signaling. Proceedings of the National Academy of Sciences **106,** 20520-20525.

Jefferson, R.A., Kavanagh, T.A., and Bevan, M.W. (1987). GUS fusions: beta-glucuronidase as a sensitive and versatile gene fusion marker in higher plants. The EMBO journal **6,** 3901-3907.

Jiang, X., Leidi, E.O., and Pardo, J.M. (2010). How do vacuolar NHX exchangers function in plant salt tolerance? Plant signaling & behavior **5,** 792-795.

Johansson, I., Wulfetange, K., Porée, F., Michard, E., Gajdanowicz, P., Lacombe, B., Sentenac, H., Thibaud, J.-B., Mueller-Roeber, B., Blatt, M.R., and Dreyer, I. (2006). External K+ modulates the activity of the Arabidopsis potassium channel SKOR via an unusual mechanism. The Plant Journal **46,** 269-281.

Jossier, M., Kroniewicz, L., Dalmas, F., Le Thiec, D., Ephritikhine, G., Thomine, S., Barbier-Brygoo, H., Vavasseur, A., Filleur, S., and Leonhardt, N. (2010). The Arabidopsis vacuolar anion transporter, AtCLCc, is involved in the regulation of stomatal movements and contributes to salt tolerance. The Plant journal : for cell and molecular biology **64,** 563-576.

Jung, J.-Y., Shin, R., and Schachtman, D.P. (2009). Ethylene Mediates Response and Tolerance to Potassium Deprivation in Arabidopsis. The Plant Cell Online **21,** 607-621.

Kaplan, B., Sherman, T., and Fromm, H. (2007). Cyclic nucleotide-gated channels in plants. FEBS Letters **581,** 2237-2246.

Keijzer, C.J., Hoek, I.H.S., and Willeemse, M.T.M. (1987). THE PROCESSES OF ANTHER DEHISCENCE AND POLLEN DISPERSAL III. THE DEHYDRATION OF THE FILAMENT TIP AND THE ANTHER IN THREE MONOCOTYLEDONOUS SPECIES. New Phytologist **106,** 281-287.

Kim, B.-G., Waadt, R., Cheong, Y.H., Pandey, G.K., Dominguez-Solis, J.R., Schültke, S., Lee, S.C., Kudla, J., and Luan, S. (2007). The calcium sensor CBL10 mediates salt tolerance by regulating ion homeostasis in Arabidopsis. The Plant Journal **52,** 473-484.

Kim, T.H., Bohmer, M., Hu, H., Nishimura, N., and Schroeder, J.I. (2010). Guard cell signal transduction network: advances in understanding abscisic acid, CO2, and Ca2+ signaling. Annu Rev Plant Biol **61,** 561-591.

Kinoshita, T., and Shimazaki, K. (1999). Blue light activates the plasma membrane H(+)-ATPase by phosphorylation of the C-terminus in stomatal guard cells. The EMBO journal **18,** 5548-5558.

Kinoshita, T., Doi, M., Suetsugu, N., Kagawa, T., Wada, M., and Shimazaki, K.-i. (2001). phot1 and phot2 mediate blue light regulation of stomatal opening. Nature **414,** 656-660.

Kinoshita, T., Emi, T., Tominaga, M., Sakamoto, K., Shigenaga, A., Doi, M., and Shimazaki, K.-i. (2003). Blue-Light- and Phosphorylation-Dependent Binding of a 14-3-3 Protein to Phototropins in Stomatal Guard Cells of Broad Bean. Plant physiology **133,** 1453-1463.

Klein, M., Cheng, G., Chung, M., and Tallman, G. (1996). Effects of turgor potentials of epidermal cells neighbouring guard cells on stomatal opening in detached leaf epidermis and intact leaflets of Vicia faba L. (faba bean). Plant, Cell & Environment **19,** 1399-1407.

Kojima, A., Toshima, J.Y., Kanno, C., Kawata, C., and Toshima, J. (2012). Localization and functional requirement of yeast Na+/H+ exchanger, Nhx1p, in the

endocytic and protein recycling pathway. Biochimica et biophysica acta **1823,** 534-543.

Kolukisaoglu, Ü., Weinl, S., Blazevic, D., Batistic, O., and Kudla, J. (2004). Calcium Sensors and Their Interacting Protein Kinases: Genomics of the Arabidopsis and Rice CBL-CIPK Signaling Networks. Plant physiology **134,** 43-58.

Koncz, C., and Schell, J. (1986). The promoter of TL-DNA gene 5 controls the tissue specific expression of chimaeric genes carried by a novel type of *Agrobacterium* binary vector. Molecular & general genetics : MGG **204,** 383-396.

Kubitscheck, U., Homann, U., and Thiel, G. (2000). Osmotically evoked shrinking of guard-cell protoplasts causes vesicular retrieval of plasma membrane into the cytoplasm. Planta **210,** 423-431.

Kudla, J., Xu, Q., Harter, K., Gruissem, W., and Luan, S. (1999). Genes for calcineurin B-like proteins in Arabidopsis are differentially regulated by stress signals. Proceedings of the National Academy of Sciences of the United States of America **96,** 4718-4723.

Kwak, J.M., Murata, Y., Baizabal-Aguirre, V.M., Merrill, J., Wang, M., Kemper, A., Hawke, S.D., Tallman, G., and Schroeder, J.I. (2001). Dominant Negative Guard Cell K+ Channel Mutants Reduce Inward-Rectifying K+ Currents and Light-Induced Stomatal Opening in Arabidopsis. Plant physiology **127,** 473-485.

Kwak, J.M., Mori, I.C., Pei, Z.-M., Leonhardt, N., Torres, M.A., Dangl, J.L., Bloom, R.E., Bodde, S., Jones, J.D.G., and Schroeder, J.I. (2003). NADPH oxidase AtrbohD and AtrbohF genes function in ROS-dependent ABA signaling in Arabidopsis. The EMBO journal **22,** 2623-2633.

Lagarde, D., Basset, M., Lepetit, M., Conejero, G., Gaymard, F., Astruc, S., and Grignon, C. (1996). Tissue-specific expression of Arabidopsis AKT1 gene is consistent with a role in K+ nutrition. The Plant journal : for cell and molecular biology **9,** 195-203.

Langer, K., Levchenko, V., Fromm, J., Geiger, D., Steinmeyer, R., Lautner, S., Ache, P., and Hedrich, R. (2004). The poplar K+ channel KPT1 is associated with K+ uptake during stomatal opening and bud development. The Plant Journal **37,** 828-838.

Latz, A., Becker, D., Hekman, M., Müller, T., Beyhl, D., Marten, I., Eing, C., Fischer, A., Dunkel, M., Bertl, A., Rapp, U.R., and Hedrich, R. (2007). TPK1, a Ca2+-regulated Arabidopsis vacuole two-pore K+ channel is activated by 14-3-3 proteins. The Plant Journal **52,** 449-459.

Lebaudy, A., Vavasseur, A., Hosy, E., Dreyer, I., Leonhardt, N., Thibaud, J.B., Very, A.A., Simonneau, T., and Sentenac, H. (2008). Plant adaptation to fluctuating environment and biomass production are strongly dependent on guard cell potassium channels. Proceedings of the National Academy of Sciences of the United States of America **105,** 5271-5276.

Lee, M., Choi, Y., Burla, B., Kim, Y.Y., Jeon, B., Maeshima, M., Yoo, J.Y., Martinoia, E., and Lee, Y. (2008). The ABC transporter AtABCB14 is a malate importer and modulates stomatal response to CO2. Nature cell biology **10,** 1217-1223.

Lee, S.C., Lan, W., Buchanan, B.B., and Luan, S. (2009). A protein kinase-phosphatase pair interacts with an ion channel to regulate ABA signaling in plant guard cells. Proceedings of the National Academy of Sciences of the United States of America **106,** 21419-21424.

Lee, S.C., Lan, W.Z., Kim, B.G., Li, L., Cheong, Y.H., Pandey, G.K., Lu, G., Buchanan, B.B., and Luan, S. (2007). A protein phosphorylation/dephosphorylation network regulates a plant potassium channel. Proceedings of the National Academy of Sciences of the United States of America **104,** 15959-15964.

Leidi, E.O., Barragan, V., Rubio, L., El-Hamdaoui, A., Ruiz, M.T., Cubero, B., Fernandez, J.A., Bressan, R.A., Hasegawa, P.M., Quintero, F.J., and Pardo, J.M. (2010). The AtNHX1 exchanger mediates potassium compartmentation in vacuoles of transgenic tomato. The Plant journal : for cell and molecular biology **61,** 495-506.

Leigh, R.A. (2001). Potassium homeostasis and membrane transport. Journal of Plant Nutrition and Soil Science **164,** 193-198.

Leigh, R.A., and Wyn Jones, R.G. (1984). A HYPOTHESIS RELATING CRITICAL POTASSIUM CONCENTRATIONS FOR GROWTH TO THE DISTRIBUTION AND FUNCTIONS OF THIS ION IN THE PLANT CELL. New Phytologist **97,** 1-13.

Lemtiri-Chlieh, F., and Berkowitz, G.A. (2004). Cyclic Adenosine Monophosphate Regulates Calcium Channels in the Plasma Membrane of Arabidopsis Leaf Guard and Mesophyll Cells. Journal of Biological Chemistry **279,** 35306-35312.

Levchenko, V., Konrad, K.R., Dietrich, P., Roelfsema, M.R.G., and Hedrich, R. (2005). Cytosolic abscisic acid activates guard cell anion channels without preceding Ca2+ signals. Proceedings of the National Academy of Sciences of the United States of America **102,** 4203-4208.

Li, L., Kim, B.-G., Cheong, Y.H., Pandey, G.K., and Luan, S. (2006a). A Ca2+ signaling pathway regulates a K+ channel for low-K response in Arabidopsis. Proceedings of the National Academy of Sciences **103,** 12625-12630.

Li, M., Lin, X., Li, H., Pan, X., and Wu, G. (2011). Overexpression of AtNHX5 improves tolerance to both salt and water stress in rice (Oryza sativa L.). Plant Cell Tiss Organ Cult **107,** 283-293.

Li, W.Y., Wong, F.L., Tsai, S.N., Phang, T.H., Shao, G., and Lam, H.M. (2006b). Tonoplast-located GmCLC1 and GmNHX1 from soybean enhance NaCl tolerance in transgenic bright yellow (BY)-2 cells. Plant Cell Environ **29,** 1122-1137.

Liu, H., Wang, Q., Yu, M., Zhang, Y., Wu, Y., and Zhang, H. (2008). Transgenic salt-tolerant sugar beet (Beta vulgaris L.) constitutively expressing an Arabidopsis thaliana vacuolar Na/H antiporter gene, AtNHX3, accumulates more soluble sugar but less salt in storage roots. Plant Cell Environ **31,** 1325-1334.

Liu, L.-L., Ren, H.-M., Chen, L.-Q., Wang, Y., and Wu, W.-H. (2012). A protein kinase CIPK9 interacts with calcium sensor CBL3 and regulates K+ homeostasis under low-K+ stress in Arabidopsis. Plant physiology.

Liu, X., Yue, Y., Li, B., Nie, Y., Li, W., Wu, W.-H., and Ma, L. (2007). A G Protein-Coupled Receptor Is a Plasma Membrane Receptor for the Plant Hormone Abscisic Acid. Science **315,** 1712-1716.

Luan, S., Kudla, J., Rodriguez-Concepcion, M., Yalovsky, S., and Gruissem, W. (2002). Calmodulins and Calcineurin B–like Proteins: Calcium Sensors for Specific Signal Response Coupling in Plants. The Plant Cell Online **14,** S389-S400.

Ludewig, U., Wilken, S., Wu, B., Jost, W., Obrdlik, P., El Bakkoury, M., Marini, A.-M., André, B., Hamacher, T., Boles, E., von Wirén, N., and Frommer, W.B. (2003).

Homo- and Hetero-oligomerization of Ammonium Transporter-1 Uniporters. Journal of Biological Chemistry **278,** 45603-45610.

Ma, Y., Szostkiewicz, I., Korte, A., Moes, D., Yang, Y., Christmann, A., and Grill, E. (2009). Regulators of PP2C phosphatase activity function as abscisic acid sensors. Science **324,** 1064-1068.

Maathuis, F.J. (2009). Physiological functions of mineral macronutrients. Curr Opin Plant Biol **12,** 250-258.

Maathuis, F.J., and Sanders, D. (1994). Mechanism of high-affinity potassium uptake in roots of Arabidopsis thaliana. Proceedings of the National Academy of Sciences of the United States of America **91,** 9272-9276.

Maathuis, F.J.M., and Sanders, D. (1993). Energization of potassium uptake in <i>Arabidopsis thaliana</i>. Planta **191,** 302-307.

Maathuis, F.J.M., and Amtmann, A. (1999). K+Nutrition and Na+Toxicity: The Basis of Cellular K+/Na+Ratios. Annals of Botany **84,** 123-133.

MacRobbie, E.A.C. (1998). Signal transduction and ion channels in guard cells. Philosophical Transactions of the Royal Society of London. Series B: Biological Sciences **353,** 1475-1488.

MacRobbie, E.A.C. (2006). Osmotic effects on vacuolar ion release in guard cells. Proceedings of the National Academy of Sciences of the United States of America **103,** 1135-1140.

Mao, J., Zhang, Y.-C., Sang, Y., Li, Q.-H., and Yang, H.-Q. (2005). A role for Arabidopsis cryptochromes and COP1 in the regulation of stomatal opening. Proceedings of the National Academy of Sciences of the United States of America **102,** 12270-12275.

Maresova, L., and Sychrova, H. (2006). Arabidopsis thaliana CHX17 gene complements the kha1 deletion phenotypes in Saccharomyces cerevisiae. Yeast **23,** 1167-1171.

Marschner, H. (1995). Mineral Nutrition of Higher Plants. (London: Academic Press).

Martinez-Atienza, J., Jiang, X., Garciadeblas, B., Mendoza, I., Zhu, J.K., Pardo, J.M., and Quintero, F.J. (2007). Conservation of the salt overly sensitive pathway in rice. Plant physiology **143,** 1001-1012.

Martinoia, E., Meyer, S., De Angeli, A., and Nagy, R. (2012). Vacuolar transporters in their physiological context. Annu Rev Plant Biol **63,** 183-213.

McAinsh, B.H.M.R.C.A.M. (1990). Abscisic acid-induced elevation of guard cell cytosolic Ca2+ precedes stomatal closure. Nature **343,** 186-188.

Meinhard, M., and Grill, E. (2001). Hydrogen peroxide is a regulator of ABI1, a protein phosphatase 2C from Arabidopsis. FEBS Letters **508,** 443-446.

Mengel, K., Kirkby, E., Kosegarten, H., and Appel, T. (2001). Principles of Plant Nutrition. (Dordrecht: Kluwer Academic Publishers).

Merlot, S., Mustilli, A.C., Genty, B., North, H., Lefebvre, V., Sotta, B., Vavasseur, A., and Giraudat, J. (2002). Use of infrared thermal imaging to isolate Arabidopsis mutants defective in stomatal regulation. The Plant journal : for cell and molecular biology **30,** 601-609.

Merlot, S., Leonhardt, N., Fenzi, F., Valon, C., Costa, M., Piette, L., Vavasseur, A., Genty, B., Boivin, K., and Mѵ°ller, A. (2007a). Constitutive activation of a plasma membrane H+-ATPase prevents abscisic acid-mediated stomatal closure. The EMBO Journal **26,** 3216-3226.

Merlot, S., Leonhardt, N., Fenzi, F., Valon, C., Costa, M., Piette, L., Vavasseur, A., Genty, B., Boivin, K., Muller, A., Giraudat, J., and Leung, J. (2007b). Constitutive activation of a plasma membrane H+-ATPase prevents abscisic acid-mediated stomatal closure. The EMBO journal **26,** 3216-3226.

Meyer, S., Scholz-Starke, J., De Angeli, A., Kovermann, P., Burla, B., Gambale, F., and Martinoia, E. (2011). Malate transport by the vacuolar AtALMT6 channel in guard cells is subject to multiple regulation. The Plant journal : for cell and molecular biology **67,** 247-257.

Meyer, S., Mumm, P., Imes, D., Endler, A., Weder, B., Al-Rasheid, K.A.S., Geiger, D., Marten, I., Martinoia, E., and Hedrich, R. (2010). AtALMT12 represents an R-type anion channel required for stomatal movement in Arabidopsis guard cells. The Plant Journal **63,** 1054-1062.

Meyerhoff, O., Müller, K., Roelfsema, M., Latz, A., Lacombe, B., Hedrich, R., Dietrich, P., and Becker, D. (2005). <i>AtGLR3.4 , a glutamate receptor channel-like gene is sensitive to touch and cold. Planta **222,** 418-427.

Michard, E., Lacombe, B., Porée, F., Mueller-Roeber, B., Sentenac, H., Thibaud, J.-B., and Dreyer, I. (2005). A Unique Voltage Sensor Sensitizes the Potassium Channel AKT2 to Phosphoregulation. The Journal of general physiology **126,** 605-617.

Miedema, H., and Assmann, S.M. (1996). A Membrane-delimited Effect of Internal pH on the K<sup>+</sup> Outward Rectifier of <i>Vicia Faba Guard Cells. Journal of Membrane Biology **154,** 227-237.

Mitchell, D.A., Marshall, T.K., and Deschenes, R.J. (1993). Vectors for the inducible overexpression of glutathione S-transferase fusion proteins in yeast. Yeast **9,** 715-722.

Mitsui, K., Koshimura, Y., Yoshikawa, Y., Matsushita, M., and Kanazawa, H. (2011). The endosomal Na(+)/H(+) exchanger contributes to multivesicular body formation by regulating the recruitment of ESCRT-0 Vps27p to the endosomal membrane. The Journal of biological chemistry **286,** 37625-37638.

Moran, N. (2007). Osmoregulation of leaf motor cells. FEBS Lett **581,** 2337-2347.

Mori, I.C., Murata, Y., Yang, Y., Munemasa, S., Wang, Y.-F., Andreoli, S., Tiriac, H., Alonso, J.M., Harper, J.F., Ecker, J.R., Kwak, J.M., and Schroeder, J.I. (2006). CDPKs CPK6 and CPK3 Function in ABA Regulation of Guard Cell S-Type Anion- and Ca^{2+}- Permeable Channels and Stomatal Closure. PLoS Biol **4,** e327.

Mouline, K., Very, A.A., Gaymard, F., Boucherez, J., Pilot, G., Devic, M., Bouchez, D., Thibaud, J.B., and Sentenac, H. (2002). Pollen tube development and competitive ability are impaired by disruption of a Shaker K(+) channel in Arabidopsis. Genes & development **16,** 339-350.

Mukherjee, S., Kallay, L., Brett, C.L., and Rao, R. (2006). Mutational analysis of the intramembranous H10 loop of yeast Nhx1 reveals a critical role in ion homoeostasis and vesicle trafficking. The Biochemical journal **398,** 97-105.

Munns, R. (2002). Comparative physiology of salt and water stress. Plant Cell Environ **25,** 239-250.

Munns, R., and Tester, M. (2008). Mechanisms of salinity tolerance. Annu Rev Plant Biol **59,** 651-681.

Murashige, T., and Skoog, F. (1962). A Revised Medium for Rapid Growth and Bio Assays with Tobacco Tissue Cultures. Physiologia Plantarum **15,** 473-497.

Nass, R., and Rao, R. (1998). Novel Localization of a Na+/H+ Exchanger in a Late Endosomal Compartment of Yeast. Journal of Biological Chemistry **273,** 21054-21060.

Nass, R., and Rao, R. (1999). The yeast endosomal Na+/H+ exchanger, Nhx1, confers osmotolerance following acute hypertonic shock. Microbiology **145,** 3221-3228.

Nass, R., Cunningham, K.W., and Rao, R. (1997). Intracellular Sequestration of Sodium by a Novel Na+/H+ Exchanger in Yeast Is Enhanced by Mutations in the Plasma Membrane H+-ATPase. Journal of Biological Chemistry **272,** 26145-26152.

Negi, J., Matsuda, O., Nagasawa, T., Oba, Y., Takahashi, H., Kawai-Yamada, M., Uchimiya, H., Hashimoto, M., and Iba, K. (2008). CO2 regulator SLAC1 and its homologues are essential for anion homeostasis in plant cells. Nature **452,** 483-486.

Neill, S., Barros, R., Bright, J., Desikan, R., Hancock, J., Harrison, J., Morris, P., Ribeiro, D., and Wilson, I. (2008). Nitric oxide, stomatal closure, and abiotic stress. Journal of experimental botany **59,** 165-176.

Niemietz, C., and Willenbrink, J. (1985). The function of tonoplast ATPase in intact vacuoles of red beet is governed by direct and indirect ion effects. Planta **166,** 545-549.

Nieves-Cordones, M., Aleman, F., Martinez, V., and Rubio, F. (2010). The Arabidopsis thaliana HAK5 K+ transporter is required for plant growth and K+ acquisition from low K+ solutions under saline conditions. Molecular plant **3,** 326-333.

Nieves-Cordones, M., Caballero, F., Martinez, V., and Rubio, F. (2012). Disruption of the Arabidopsis thaliana inward-rectifier K+ channel AKT1 improves plant responses to water stress. Plant Cell Physiol **53,** 423-432.

Nieves-Cordones, M., Miller, A., Alemán, F., Martínez, V., and Rubio, F. (2008). A putative role for the plasma membrane potential in the control of the expression of the gene encoding the tomato high-affinity potassium transporter HAK5. Plant Molecular Biology **68,** 521-532.

Oertli, J. (1968). Extracellular salt accumulation, a possible mechanism of salt injury in plants. Agrochimica **12,** 461-469.

Ohgaki, R., van, I.S.C., Matsushita, M., Hoekstra, D., and Kanazawa, H. (2011). Organellar Na+/H+ exchangers: novel players in organelle pH regulation and their emerging functions. Biochemistry **50,** 443-450.

Ohta, M., Hayashi, Y., Nakashima, A., Hamada, A., Tanaka, A., Nakamura, T., and Hayakawa, T. (2002). Introduction of a Na+/H+ antiporter gene from Atriplex gmelini confers salt tolerance to rice. FEBS Lett **532,** 279-282.

Ojangu, E.-L., Tanner, K., Pata, P., Jarve, K., Holweg, C., Truve, E., and Paves, H. (2012). Myosins XI-K, XI-1, and XI-2 are required for development of pavement cells, trichomes, and stigmatic papillae in Arabidopsis. BMC Plant Biology **12,** 81.

Padmanaban, S., Lin, X., Perera, I., Kawamura, Y., and Sze, H. (2004). Differential Expression of Vacuolar H+-ATPase Subunit c Genes in Tissues Active in Membrane Trafficking and Their Roles in Plant Growth as Revealed by RNAi. Plant physiology **134,** 1514-1526.

Padmanaban, S., Chanroj, S., Kwak, J.M., Li, X., Ward, J.M., and Sze, H. (2007). Participation of Endomembrane Cation/H+ Exchanger AtCHX20 in Osmoregulation of Guard Cells. Plant physiology **144,** 82-93.

Palevitz, B.A., O'Kane, D.J., Kobres, R.E., and Raikhel, N.V. (1981). The vacuole system in stomatal cells of<i>Allium. vacuole movements and changes in morphology in differentiating cells as revealed by epifluorescence, video and electron microscopy. Protoplasma **109,** 23-55.

Palmgren, M.G. (2001). PLANT PLASMA MEMBRANE H+-ATPases: Powerhouses for Nutrient Uptake. Annual review of plant physiology and plant molecular biology **52,** 817-845.

Pandey, S., Zhang, W., and Assmann, S.M. (2007). Roles of ion channels and transporters in guard cell signal transduction. FEBS Letters **581,** 2325-2336.

Pandey, S., Nelson, D.C., and Assmann, S.M. (2009). Two novel GPCR-type G proteins are abscisic acid receptors in Arabidopsis. Cell **136,** 136-148.

Pardo, J.M. (2010). Biotechnology of water and salinity stress tolerance. Current Opinion in Biotechnology **21,** 185-196.

Pardo, J.M., and Rubio Muñoz, F. (2011). Na+ and K+ transporters in plant signaling (Springer), pp. 65-98.

Pardo, J.M., Cubero, B., Leidi, E.O., and Quintero, F.J. (2006). Alkali cation exchangers: roles in cellular homeostasis and stress tolerance. Journal of experimental botany **57,** 1181-1199.

Park, S.Y., Fung, P., Nishimura, N., Jensen, D.R., Fujii, H., Zhao, Y., Lumba, S., Santiago, J., Rodrigues, A., Chow, T.F., Alfred, S.E., Bonetta, D., Finkelstein, R., Provart, N.J., Desveaux, D., Rodriguez, P.L., McCourt, P., Zhu, J.K., Schroeder, J.I., Volkman, B.F., and Cutler, S.R. (2009). Abscisic acid inhibits type 2C protein phosphatases via the PYR/PYL family of START proteins. Science **324,** 1068-1071.

Pei, Z.-M., Murata, Y., Benning, G., Thomine, S., Klusener, B., Allen, G.J., Grill, E., and Schroeder, J.I. (2000). Calcium channels activated by hydrogen peroxide mediate abscisic acid signalling in guard cells. Nature **406,** 731-734.

Pei, Z.M., Ward, J.M., Harper, J.F., and Schroeder, J.I. (1996). A novel chloride channel in Vicia faba guard cell vacuoles activated by the serine/threonine kinase, CDPK. The EMBO journal **15,** 6564-6574.

Peiter, E., Maathuis, F.J.M., Mills, L.N., Knight, H., Pelloux, J., Hetherington, A.M., and Sanders, D. (2005). The vacuolar Ca2+-activated channel TPC1 regulates germination and stomatal movement. Nature **434,** 404-408.

Peoples, T.R., and Koch, D.W. (1979). Role of Potassium in Carbon Dioxide Assimilation in Medicago sativa L. Plant physiology **63,** 878-881.

Peuke, A.D., Jeschke, W.D., and Hartung, W. (2002). Flows of elements, ions and abscisic acid in Ricinus communis and site of nitrate reduction under potassium limitation. Journal of experimental botany **53,** 241-250.

Pier, P.A., and Berkowitz, G.A. (1987). Modulation of water stress effects on photosynthesis by altered leaf k. Plant physiology **85,** 655-661.

Pilot, G., Gaymard, F., Mouline, K., Cherel, I., and Sentenac, H. (2003). Regulated expression of Arabidopsis shaker K+ channel genes involved in K+ uptake and distribution in the plant. Plant Mol Biol **51,** 773-787.

Pilot, G., Lacombe, B., Gaymard, F., Cherel, I., Boucherez, J., Thibaud, J.B., and Sentenac, H. (2001). Guard cell inward K+ channel activity in arabidopsis involves expression of the twin channel subunits KAT1 and KAT2. The Journal of biological chemistry **276,** 3215-3221.

Pittman, J.K. (2012). Multiple Transport Pathways for Mediating Intracellular pH Homeostasis: The Contribution of H(+)/ion Exchangers. Front Plant Sci **3,** 11.

Poffenroth, M., Green, D.B., and Tallman, G. (1992). Sugar Concentrations in Guard Cells of Vicia faba Illuminated with Red or Blue Light : Analysis by High Performance Liquid Chromatography. Plant physiology **98,** 1460-1471.

Pottosin, II, and Schonknecht, G. (2007). Vacuolar calcium channels. Journal of experimental botany **58,** 1559-1569.

Pottosin, I., Wherrett, T., and Shabala, S. (2009). SV channels dominate the vacuolar Ca2+ release during intracellular signaling. FEBS Letters **583,** 921-926.

Prior, C., Potier, S., Souciet, J.-L., and Sychrova, H. (1996). Characterization of the NHA1 gene encoding a Na+/H+-antiporter of the yeast Saccharomyces cerevisiae. FEBS Letters **387,** 89-93.

Putney, L.K., Denker, S.P., and Barber, D.L. (2002). THE CHANGING FACE OF THE Na+/H+ EXCHANGER, NHE1: Structure, Regulation, and Cellular Actions. Annual Review of Pharmacology and Toxicology **42,** 527-552.

Pyo, Y.J., Gierth, M., Schroeder, J.I., and Cho, M.H. (2010). High-affinity K(+) transport in Arabidopsis: AtHAK5 and AKT1 are vital for seedling establishment and postgermination growth under low-potassium conditions. Plant physiology **153,** 863-875.

Qi, Z., Stephens, N.R., and Spalding, E.P. (2006). Calcium Entry Mediated by GLR3.3, an Arabidopsis Glutamate Receptor with a Broad Agonist Profile. Plant physiology **142,** 963-971.

Qi, Z., Hampton, C.R., Shin, R., Barkla, B.J., White, P.J., and Schachtman, D.P. (2008). The high affinity K+ transporter AtHAK5 plays a physiological role in planta at very low K+ concentrations and provides a caesium uptake pathway in Arabidopsis. Journal of experimental botany **59,** 595-607.

Qin, Y., Li, X., Guo, M., Deng, K., Lin, J., Tang, D., Guo, X., and Liu, X. (2008). Regulation of salt and ABA responses by CIPK14, a calcium sensor interacting protein kinase in Arabidopsis. Sci. China Ser. C-Life Sci. **51,** 391-401.

Qiu, Q.S., and Fratti, R.A. (2010). The Na+/H+ exchanger Nhx1p regulates the initiation of Saccharomyces cerevisiae vacuole fusion. Journal of cell science **123,** 3266-3275.

Qiu, Q.S., Guo, Y., Dietrich, M.A., Schumaker, K.S., and Zhu, J.K. (2002). Regulation of SOS1, a plasma membrane Na+/H+ exchanger in Arabidopsis thaliana, by SOS2 and CBL4/SOS3. Proceedings of the National Academy of Sciences of the United States of America **99,** 8436-8441.

Qiu, Q.S., Guo, Y., Quintero, F.J., Pardo, J.M., Schumaker, K.S., and Zhu, J.K. (2004). Regulation of vacuolar Na+/H+ exchange in Arabidopsis thaliana by the salt-overly-sensitive (SOS) pathway. The Journal of biological chemistry **279,** 207-215.

Quan, R., Lin, H., Mendoza, I., Zhang, Y., Cao, W., Yang, Y., Shang, M., Chen, S., Pardo, J.M., and Guo, Y. (2007). SCABP8/CBL10, a putative calcium sensor, interacts

with the protein kinase SOS2 to protect Arabidopsis shoots from salt stress. The Plant cell **19,** 1415-1431.

Quintero, F.J., Blatt, M.R., and Pardo, J.M. (2000). Functional conservation between yeast and plant endosomal Na+/H+ antiporters. FEBS Letters **471,** 224-228.

Quintero, F.J., Ohta, M., Shi, H., Zhu, J.K., and Pardo, J.M. (2002). Reconstitution in yeast of the Arabidopsis SOS signaling pathway for Na+ homeostasis. Proceedings of the National Academy of Sciences of the United States of America **99,** 9061-9066.

Quintero, F.J., Martinez-Atienza, J., Villalta, I., Jiang, X., Kim, W.Y., Ali, Z., Fujii, H., Mendoza, I., Yun, D.J., Zhu, J.K., and Pardo, J.M. (2011). Activation of the plasma membrane Na/H antiporter Salt-Overly-Sensitive 1 (SOS1) by phosphorylation of an auto-inhibitory C-terminal domain. Proceedings of the National Academy of Sciences of the United States of America **108,** 2611-2616.

Raschke, K. (2003). Alternation of the slow with the quick anion conductance in whole guard cells effected by external malate. Planta **217,** 651-657.

Raschke, K., and Schnabl, H. (1978). Availability of Chloride Affects the Balance between Potassium Chloride and Potassium Malate in Guard Cells of Vicia faba L. Plant physiology **62,** 84-87.

Rehman, S., and Yun, S.J. (2006). Developmental regulation of K accumulation in pollen, anthers, and papillae: are anther dehiscence, papillae hydration, and pollen swelling leading to pollination and fertilization in barley (Hordeum vulgare L.) regulated by changes in K concentration? Journal of experimental botany **57,** 1315-1321.

Reinders, A., Schulze, W., Kühn, C., Barker, L., Schulz, A., Ward, J.M., and Frommer, W.B. (2002). Protein–Protein Interactions between Sucrose Transporters of Different Affinities Colocalized in the Same Enucleate Sieve Element. The Plant Cell Online **14,** 1567-1577.

Rentsch, D., Laloi, M., Rouhara, I., Schmelzer, E., Delrot, S., and Frommer, W.B. (1995). NTR1 encodes a high affinity oligopeptide transporter in Arabidopsis. FEBS Letters **370,** 264-268.

Robinson, M.F., Véry, A.-A., Sanders, D., and Mansfield, T.A. (1997). How Can Stomata Contribute to Salt Tolerance? Annals of Botany **80,** 387-393.

Rodriguez-Navarro, A., and Ramos, J. (1984). Dual system for potassium transport in Saccharomyces cerevisiae. Journal of bacteriology **159,** 940-945.

Rodriguez-Navarro, A., Blatt, M.R., and Slayman, C.L. (1986). A potassium-proton symport in Neurospora crassa. The Journal of general physiology **87,** 649-674.

Rodríguez-Navarro, A., and Rubio, F. (2006). High-affinity potassium and sodium transport systems in plants. Journal of experimental botany **57,** 1149-1160.

Rodriguez-Rosales, M.P., Galvez, F.J., Huertas, R., Aranda, M.N., Baghour, M., Cagnac, O., and Venema, K. (2009). Plant NHX cation/proton antiporters. Plant signaling & behavior **4,** 265-276.

Rodríguez-Rosales, M.P., Jiang, X., Gálvez, F.J., Aranda, M.N., Cubero, B., and Venema, K. (2008). Overexpression of the tomato K+/H+ antiporter LeNHX2 confers salt tolerance by improving potassium compartmentalization. New Phytologist **179,** 366-377.

Roelfsema, M.R., and Hedrich, R. (2005). In the light of stomatal opening: new insights into 'the Watergate'. The New phytologist **167,** 665-691.

Roelfsema, M.R.G., and Hedrich, R. (2002). Studying guard cells in the intact plant: modulation of stomatal movement by apoplastic factors. New Phytologist **153,** 425-431.

Roelfsema, M.R.G., Levchenko, V., and Hedrich, R. (2004). ABA depolarizes guard cells in intact plants, through a transient activation of R- and S-type anion channels. The Plant Journal **37,** 578-588.

Roelfsema, M.R.G., Hanstein, S., Felle, H.H., and Hedrich, R. (2002). CO_2 provides an intermediate link in the red light response of guard cells. The Plant Journal **32,** 65-75.

Roelfsema, M.R.G., Konrad, K.R., Marten, H., Psaras, G.K., Hartung, W., and Hedrich, R. (2006). Guard cells in albino leaf patches do not respond to photosynthetically active radiation, but are sensitive to blue light, CO_2 and abscisic acid. Plant, Cell & Environment **29,** 1595-1605.

Römheld, V., and Kirkby, E. (2010). Research on potassium in agriculture: needs and prospects. Plant and Soil **335,** 155-180.

Rubio, F., Gassmann, W., and Schroeder, J.I. (1995). Sodium-Driven Potassium Uptake by the Plant Potassium Transporter HKT1 and Mutations Conferring Salt Tolerance. Science **270,** 1660-1663.

Rubio, F., Alemán, F., Nieves-Cordones, M., and Martínez, V. (2010a). Studies on Arabidopsis athak5, atakt1 double mutants disclose the range of concentrations at which AtHAK5, AtAKT1 and unknown systems mediate K+ uptake. Physiologia Plantarum **139,** 220-228.

Rubio, F., Arevalo, L., Caballero, F., Botella, M.A., Rubio, J.S., Garcia-Sanchez, F., and Martinez, V. (2010b). Systems involved in K+ uptake from diluted solutions in pepper plants as revealed by the use of specific inhibitors. Journal of plant physiology **167,** 1494-1499.

Saier, M.H., Jr., Eng, B.H., Fard, S., Garg, J., Haggerty, D.A., Hutchinson, W.J., Jack, D.L., Lai, E.C., Liu, H.J., Nusinew, D.P., Omar, A.M., Pao, S.S., Paulsen, I.T., Quan, J.A., Sliwinski, M., Tseng, T.T., Wachi, S., and Young, G.B. (1999). Phylogenetic characterization of novel transport protein families revealed by genome analyses. Biochimica et biophysica acta **1422,** 1-56.

Saito, C., Ueda, T., Abe, H., Wada, Y., Kuroiwa, T., Hisada, A., Furuya, M., and Nakano, A. (2002). A complex and mobile structure forms a distinct subregion within the continuous vacuolar membrane in young cotyledons of Arabidopsis. The Plant Journal **29,** 245-255.

Sandmann, M., Sklodowski, K., Gajdanowicz, P., Michard, E., Rocha, M., Gomez-Porras, J.L., Gonzalez, W., Correa, L.G., Ramirez-Aguilar, S.J., Cuin, T.A., van Dongen, J.T., Thibaud, J.B., and Dreyer, I. (2011). The K (+) battery-regulating Arabidopsis K (+) channel AKT2 is under the control of multiple post-translational steps. Plant signaling & behavior **6,** 558-562.

Santa-María, G.E., Rubio, F., Dubcovsky, J., and Rodríguez-Navarro, A. (1997). The HAK1 gene of barley is a member of a large gene family and encodes a high-affinity potassium transporter. The Plant Cell Online **9,** 2281-2289.

Sasaki, T., Mori, I.C., Furuichi, T., Munemasa, S., Toyooka, K., Matsuoka, K., Murata, Y., and Yamamoto, Y. (2010). Closing Plant Stomata Requires a Homolog of an Aluminum-Activated Malate Transporter. Plant and Cell Physiology **51,** 354-365.

Sato, M.H., Nakamura, N., Ohsumi, Y., Kouchi, H., Kondo, M., Hara-Nishimura, I., Nishimura, M., and Wada, Y. (1997). The AtVAM3 Encodes a Syntaxin-related Molecule Implicated in the Vacuolar Assembly in Arabidopsis thaliana. Journal of Biological Chemistry **272,** 24530-24535.

Sato, Y., and Sakaguchi, M. (2005). Topogenic Properties of Transmembrane Segments of Arabidopsis thaliana NHX1 Reveal a Common Topology Model of the Na+/H+ Exchanger Family. Journal of Biochemistry **138,** 425-431.

Schachtman, D.P., and Schroeder, J.I. (1994). Structure and transport mechanism of a high-affinity potassium uptake transporter from higher plants. Nature **370,** 655-658.

Schachtman, D.P., and Shin, R. (2007). Nutrient Sensing and Signaling: NPKS. Annual Review of Plant Biology **58,** 47-69.

Schachtman, D.P., Schroeder, J.I., Lucas, W.J., Anderson, J.A., and Gaber, R.F. (1992). Expression of an inward-rectifying potassium channel by the Arabidopsis KAT1 cDNA. Science **258,** 1654-1658.

Schmid, R. (1976). Filament histology and anther dehiscence. Botanical Journal of the Linnean Society **73,** 303-315.

Schroeder, J.I. (1995). Anion channels as central mechanisms for signal transduction in guard cells and putative functions in roots for plant-soil interactions. Plant Molecular Biology **28,** 353-361.

Schroeder, J.I., and Hagiwara, S. (1989). Cytosolic calcium regulates ion channels in the plasma membrane of Vicia faba guard cells. Nature **338,** 427-430.

Schroeder, J.I., and Keller, B.U. (1992). Two types of anion channel currents in guard cells with distinct voltage regulation. Proceedings of the National Academy of Sciences of the United States of America **89,** 5025-5029.

Schumacher, K. (2006). Endomembrane proton pumps: connecting membrane and vesicle transport. Current Opinion in Plant Biology **9,** 595-600.

Seeley, E.S., Kato, M., Margolis, N., Wickner, W., and Eitzen, G. (2002). Genomic Analysis of Homotypic Vacuole Fusion. Molecular biology of the cell **13,** 782-794.

Sentenac, H., Bonneaud, N., Minet, M., Lacroute, F., Salmon, J., Gaymard, F., and Grignon, C. (1992). Cloning and expression in yeast of a plant potassium ion transport system. Science **256,** 663-665.

Shen, Y.-Y., Wang, X.-F., Wu, F.-Q., Du, S.-Y., Cao, Z., Shang, Y., Wang, X.-L., Peng, C.-C., Yu, X.-C., Zhu, S.-Y., Fan, R.-C., Xu, Y.-H., and Zhang, D.-P. (2006). The Mg-chelatase H subunit is an abscisic acid receptor. Nature **443,** 823-826.

Shi, H., and Zhu, J.-K. (2002). Regulation of expression of the vacuolar Na<sup>+</sup>/H<sup>+</sup> antiporter gene <i>AtNHX1 by salt stress and abscisic acid. Plant Molecular Biology **50,** 543-550.

Shimazaki, K., Iino, M., and Zeiger, E. (1986). Blue light-dependent proton extrusion by guard-cell protoplasts of Vicia faba. Nature **319,** 324-326.

Shimazaki, K., Doi, M., Assmann, S.M., and Kinoshita, T. (2007). Light regulation of stomatal movement. Annu Rev Plant Biol **58,** 219-247.

Shin, R., and Schachtman, D.P. (2004). Hydrogen peroxide mediates plant root cell response to nutrient deprivation. Proceedings of the National Academy of Sciences of the United States of America **101,** 8827-8832.

Shope, J.C., DeWald, D.B., and Mott, K.A. (2003). Changes in Surface Area of Intact Guard Cells Are Correlated with Membrane Internalization. Plant physiology **133,** 1314-1321.

Sirichandra, C., Gu, D., Hu, H.-C., Davanture, M., Lee, S., Djaoui, M., Valot, B., Zivy, M., Leung, J., Merlot, S., and Kwak, J.M. (2009). Phosphorylation of the Arabidopsis AtrbohF NADPH oxidase by OST1 protein kinase. FEBS Letters **583,** 2982-2986.

Song, C.-P., Guo, Y., Qiu, Q., Lambert, G., Galbraith, D.W., Jagendorf, A., and Zhu, J.-K. (2004). A probable Na+(K+)/H+ exchanger on the chloroplast envelope functions in pH homeostasis and chloroplast development in Arabidopsis thaliana. Proceedings of the National Academy of Sciences of the United States of America **101,** 10211-10216.

Song, C.-P., Agarwal, M., Ohta, M., Guo, Y., Halfter, U., Wang, P., and Zhu, J.-K. (2005). Role of an Arabidopsis AP2/EREBP-Type Transcriptional Repressor in Abscisic Acid and Drought Stress Responses. The Plant Cell Online **17,** 2384-2396.

Sottosanto, J.B., Gelli, A., and Blumwald, E. (2004). DNA array analyses of Arabidopsis thaliana lacking a vacuolar Na+/H+ antiporter: impact of AtNHX1 on gene expression. The Plant journal : for cell and molecular biology **40,** 752-771.

Staal, M., Maathuis, F.J.M., Elzenga, J.T.M., Overbeek, J.H.M., and Prins, H.B.A. (1991). Na+/H+ antiport activity in tonoplast vesicles from roots of the salt-tolerant Plantago maritima and the salt-sensitive Plantago media. Physiologia Plantarum **82,** 179-184.

Sugiyama, N., Nakagami, H., Mochida, K., Daudi, A., Tomita, M., Shirasu, K., and Ishihama, Y. (2008). Large-scale phosphorylation mapping reveals the extent of tyrosine phosphorylation in Arabidopsis. Molecular systems biology **4,** 193.

Suh, S.J., Wang, Y.-F., Frelet, A., Leonhardt, N., Klein, M., Forestier, C., Mueller-Roeber, B., Cho, M.H., Martinoia, E., and Schroeder, J.I. (2007). The ATP Binding Cassette Transporter AtMRP5 Modulates Anion and Calcium Channel Activities in Arabidopsis Guard Cells. Journal of Biological Chemistry **282,** 1916-1924.

Sunarpi, Horie, T., Motoda, J., Kubo, M., Yang, H., Yoda, K., Horie, R., Chan, W.-Y., Leung, H.-Y., Hattori, K., Konomi, M., Osumi, M., Yamagami, M., Schroeder, J.I., and Uozumi, N. (2005). Enhanced salt tolerance mediated by AtHKT1 transporter-induced Na+ unloading from xylem vessels to xylem parenchyma cells. The Plant Journal **44,** 928-938.

Sutter, J.U., Campanoni, P., Tyrrell, M., and Blatt, M.R. (2006). Selective mobility and sensitivity to SNAREs is exhibited by the Arabidopsis KAT1 K+ channel at the plasma membrane. The Plant cell **18,** 935-954.

Sutter, J.U., Sieben, C., Hartel, A., Eisenach, C., Thiel, G., and Blatt, M.R. (2007). Abscisic acid triggers the endocytosis of the arabidopsis KAT1 K+ channel and its recycling to the plasma membrane. Current biology : CB **17,** 1396-1402.

Sze, H., Padmanaban, S., Cellier, F., Honys, D., Cheng, N.-H., Bock, K.W., Conéjéro, G., Li, X., Twell, D., Ward, J.M., and Hirschi, K.D. (2004). Expression Patterns of a Novel AtCHX Gene Family Highlight Potential Roles in Osmotic Adjustment and K+ Homeostasis in Pollen Development. Plant physiology **136,** 2532-2547.

Szyroki, A., Ivashikina, N., Dietrich, P., Roelfsema, M.R.G., Ache, P., Reintanz, B., Deeken, R., Godde, M., Felle, H., Steinmeyer, R., Palme, K., and Hedrich, R. (2001). KAT1 is not essential for stomatal opening. Proceedings of the National Academy of Sciences **98,** 2917-2921.

Takemiya, A., Kinoshita, T., Asanuma, M., and Shimazaki, K.-i. (2006). Protein phosphatase 1 positively regulates stomatal opening in response to blue light in Vicia faba. Proceedings of the National Academy of Sciences **103,** 13549-13554.

Talbott, L.D., and Zeiger, E. (1996). Central Roles for Potassium and Sucrose in Guard-Cell Osmoregulation. Plant physiology **111,** 1051-1057.

Talbott, L.D., and Zeiger, E. (1998). The role of sucrose in guard cell osmoregulation. Journal of experimental botany **49,** 329-337.

Tanaka, Y., Kutsuna, N., Kanazawa, Y., Kondo, N., Hasezawa, S., and Sano, T. (2007a). Intra-vacuolar reserves of membranes during stomatal closure: the possible role of guard cell vacuoles estimated by 3-D reconstruction. Plant and Cell Physiology **48,** 1159-1169.

Tanaka, Y., Kutsuna, N., Kanazawa, Y., Kondo, N., Hasezawa, S., and Sano, T. (2007b). Intra-vacuolar reserves of membranes during stomatal closure: the possible role of guard cell vacuoles estimated by 3-D reconstruction. Plant Cell Physiol **48,** 1159-1169.

Tester, M., and Blatt, M.R. (1989). Direct measurement of k channels in thylakoid membranes by incorporation of vesicles into planar lipid bilayers. Plant physiology **91,** 249-252.

Tester, M., and Davenport, R. (2003). Na+ Tolerance and Na+ Transport in Higher Plants. Annals of Botany **91,** 503-527.

Thiel, G., and Blatt, M.R. (1991). The Mechanism of Ion Permeation through K+ Channels of Stomatal Guard Cells: Voltage-Dependent Block by Na+. Journal of plant physiology **138,** 326-334.

Tikhonova, L.I., Pottosin, I.I., Dietz, K.-J., and Schönknecht, G. (1997). Fast-activating cation channel in barley mesophyll vacuoles. Inhibition by calcium. The Plant Journal **11,** 1059-1070.

Uemura, T., Yoshimura, S.H., Takeyasu, K., and Sato, M.H. (2002). Vacuolar membrane dynamics revealed by GFP-AtVam3 fusion protein. Genes to Cells **7,** 743-753.

Ueno, K., Kinoshita, T., Inoue, S.-i., Emi, T., and Shimazaki, K.-i. (2005). Biochemical Characterization of Plasma Membrane H+-ATPase Activation in Guard Cell Protoplasts of Arabidopsis thaliana in Response to Blue Light. Plant and Cell Physiology **46,** 955-963.

Uozumi, N., Kim, E.J., Rubio, F., Yamaguchi, T., Muto, S., Tsuboi, A., Bakker, E.P., Nakamura, T., and Schroeder, J.I. (2000). The Arabidopsis HKT1 gene homolog mediates inward Na(+) currents in xenopus laevis oocytes and Na(+) uptake in Saccharomyces cerevisiae. Plant physiology **122,** 1249-1259.

Vahisalu, T., Kollist, H., Wang, Y.F., Nishimura, N., Chan, W.Y., Valerio, G., Lamminmaki, A., Brosche, M., Moldau, H., Desikan, R., Schroeder, J.I., and Kangasjarvi, J. (2008). SLAC1 is required for plant guard cell S-type anion channel function in stomatal signalling. Nature **452,** 487-491.

van der Weele, C.M., Jiang, H.S., Palaniappan, K.K., Ivanov, V.B., Palaniappan, K., and Baskin, T.I. (2003). A New Algorithm for Computational Image Analysis of

Deformable Motion at High Spatial and Temporal Resolution Applied to Root Growth. Roughly Uniform Elongation in the Meristem and Also, after an Abrupt Acceleration, in the Elongation Zone. Plant physiology **132,** 1138-1148.

Van Kirk, C.A., and Raschke, K. (1978a). Presence of Chloride Reduces Malate Production in Epidermis during Stomatal Opening. Plant physiology **61,** 361-364.

Van Kirk, C.A., and Raschke, K. (1978b). Release of Malate from Epidermal Strips during Stomatal Closure. Plant physiology **61,** 474-475.

Veenhoff, L.M., Heuberger, E.H.M.L., and Poolman, B. (2002). Quaternary structure and function of transport proteins. Trends in Biochemical Sciences **27,** 242-249.

Venema, K., Quintero, F.J., Pardo, J.M., and Donaire, J.P. (2002). The Arabidopsis Na+/H+Exchanger AtNHX1 Catalyzes Low Affinity Na+ and K+ Transport in Reconstituted Liposomes. Journal of Biological Chemistry **277,** 2413-2418.

Venema, K., Belver, A., Marín-Manzano, M.C., Rodríguez-Rosales, M.P., and Donaire, J.P. (2003). A Novel Intracellular K+/H+ Antiporter Related to Na+/H+ Antiporters Is Important for K+ Ion Homeostasis in Plants. Journal of Biological Chemistry **278,** 22453-22459.

Véry, A.-A., and Sentenac, H. (2003). MOLECULAR MECHANISMS AND REGULATION OF K+ TRANSPORT IN HIGHER PLANTS. Annual Review of Plant Biology **54,** 575-603.

Voelker, C., Schmidt, D., Mueller-Roeber, B., and Czempinski, K. (2006). Members of the Arabidopsis AtTPK/KCO family form homomeric vacuolar channels in planta. The Plant journal : for cell and molecular biology **48,** 296-306.

Voelker, C., Gomez-Porras, J.L., Becker, D., Hamamoto, S., Uozumi, N., Gambale, F., Mueller-Roeber, B., Czempinski, K., and Dreyer, I. (2010). Roles of tandem-pore K+ channels in plants – a puzzle still to be solved*. Plant Biology **12,** 56-63.

Voinnet, O., Rivas, S., Mestre, P., and Baulcombe, D. (2003). An enhanced transient expression system in plants based on suppression of gene silencing by the p19 protein of tomato bushy stunt virus. The Plant journal : for cell and molecular biology **33,** 949-956.

Waadt, R., and Kudla, J. (2008). In Planta Visualization of Protein Interactions Using Bimolecular Fluorescence Complementation (BiFC). CSH protocols **2008,** pdb prot4995.

Waadt, R., Schmidt, L.K., Lohse, M., Hashimoto, K., Bock, R., and Kudla, J. (2008). Multicolor bimolecular fluorescence complementation reveals simultaneous formation of alternative CBL/CIPK complexes in planta. The Plant journal : for cell and molecular biology **56,** 505-516.

Walker, D.J., Leigh, R.A., and Miller, A.J. (1996). Potassium homeostasis in vacuolate plant cells. Proceedings of the National Academy of Sciences of the United States of America **93,** 10510-10514.

Walter, M., Chaban, C., Schutze, K., Batistic, O., Weckermann, K., Nake, C., Blazevic, D., Grefen, C., Schumacher, K., Oecking, C., Harter, K., and Kudla, J. (2004). Visualization of protein interactions in living plant cells using bimolecular fluorescence complementation. The Plant journal : for cell and molecular biology **40,** 428-438.

Wang, W., Li, Y., Zhang, Y., Yang, C., Zheng, N., and Xie, Q. (2007). Comparative expression analysis of three genes from the <i>Arabidopsis vacuolar

Na^+/H^+ antiporter (AtNHX) family in relation to abiotic stresses. Chinese Science Bulletin **52,** 1754-1763.

Wang, Y., and Wu, W.H. (2010). Plant sensing and signaling in response to K+-deficiency. Molecular plant **3,** 280-287.

Wang, Y., Holroyd, G., Hetherington, A.M., and Ng, C.K. (2004). Seeing 'cool' and 'hot'--infrared thermography as a tool for non-invasive, high-throughput screening of Arabidopsis guard cell signalling mutants. Journal of experimental botany **55,** 1187-1193.

Ward, J.M., and Schroeder, J.I. (1994). Calcium-Activated K+ Channels and Calcium-Induced Calcium Release by Slow Vacuolar Ion Channels in Guard Cell Vacuoles Implicated in the Control of Stomatal Closure. The Plant cell **6,** 669-683.

Webb, A.A.R. (2003). The physiology of circadian rhythms in plants. New Phytologist **160,** 281-303.

Webb, A.A.R., Larman, M.G., Montgomery, L.T., Taylor, J.E., and Hetherington, A.M. (2001). The role of calcium in ABA-induced gene expression and stomatal movements. The Plant Journal **26,** 351-362.

Weinl, S., and Kudla, J. (2009). The CBL-CIPK Ca(2+)-decoding signaling network: function and perspectives. The New phytologist **184,** 517-528.

White, P., and Karley, A. (2010). Potassium. In Cell Biology of Metals and Nutrients, R. Hell and R.-R. Mendel, eds (Springer Berlin Heidelberg), pp. 199-224.

Whiteman, S.-A., Nühse, T.S., Ashford, D.A., Sanders, D., and Maathuis, F.J.M. (2008a). A proteomic and phosphoproteomic analysis of Oryza sativa plasma membrane and vacuolar membrane. The Plant Journal **56,** 146-156.

Whiteman, S.A., Serazetdinova, L., Jones, A.M., Sanders, D., Rathjen, J., Peck, S.C., and Maathuis, F.J. (2008b). Identification of novel proteins and phosphorylation sites in a tonoplast enriched membrane fraction of Arabidopsis thaliana. Proteomics **8,** 3536-3547.

Wilson, Z.A., Song, J., Taylor, B., and Yang, C. (2011). The final split: the regulation of anther dehiscence. Journal of experimental botany **62,** 1633-1649.

Willmer, C.M., and Mansfield, T.A. (1969). A Critical Examination of the Use of Detached Epidermis in Studies of Stomatal Physiology. New Phytologist **68,** 363-375.

Wolfe, J., and Steponkus, P.L. (1983). Mechanical Properties of the Plasma Membrane of Isolated Plant Protoplasts. Plant physiology **71,** 276-285.

Wu, C.A., Yang, G.D., Meng, Q.W., and Zheng, C.C. (2004). The cotton GhNHX1 gene encoding a novel putative tonoplast Na(+)/H(+) antiporter plays an important role in salt stress. Plant Cell Physiol **45,** 600-607.

Xu, J., Li, H.-D., Chen, L.-Q., Wang, Y., Liu, L.-L., He, L., and Wu, W.-H. (2006). A Protein Kinase, Interacting with Two Calcineurin B-like Proteins, Regulates K+ Transporter AKT1 in Arabidopsis. Cell **125,** 1347-1360.

Yakir, E., Hilman, D., Harir, Y., and Green, R.M. (2007). Regulation of output from the plant circadian clock. FEBS Journal **274,** 335-345.

Yamaguchi, T., Apse, M.P., Shi, H., and Blumwald, E. (2003). Topological analysis of a plant vacuolar Na+/H+ antiporter reveals a luminal C terminus that regulates antiporter cation selectivity. Proceedings of the National Academy of Sciences of the United States of America **100,** 12510-12515.

Yamaguchi, T., Aharon, G.S., Sottosanto, J.B., and Blumwald, E. (2005). Vacuolar Na+/H+ antiporter cation selectivity is regulated by calmodulin from within the vacuole in a Ca2+- and pH-dependent manner. Proceedings of the National Academy of Sciences of the United States of America **102,** 16107-16112.

Yamaguchi, T., Fukada-Tanaka, S., Inagaki, Y., Saito, N., Yonekura-Sakakibara, K., Tanaka, Y., Kusumi, T., and Iida, S. (2001). Genes Encoding the Vacuolar Na+/H+ Exchanger and Flower Coloration. Plant and Cell Physiology **42,** 451-461.

Yang, Q., Chen, Z.-Z., Zhou, X.-F., Yin, H.-B., Li, X., Xin, X.-F., Hong, X.-H., Zhu, J.-K., and Gong, Z. (2009). Overexpression of SOS (Salt Overly Sensitive) Genes Increases Salt Tolerance in Transgenic Arabidopsis. Molecular plant **2,** 22-31.

Yanisch-Perron, C., Vieira, J., and Messing, J. (1985). Improved M13 phage cloning vectors and host strains: nucleotide sequences of the M13mpl8 and pUC19 vectors. Gene **33,** 103-119.

Yokoi, S., Quintero, F.J., Cubero, B., Ruiz, M.T., Bressan, R.A., Hasegawa, P.M., and Pardo, J.M. (2002). Differential expression and function of Arabidopsis thaliana NHX Na+/H+ antiporters in the salt stress response. The Plant Journal **30,** 529-539.

Yoshida, K., Kondo, T., Okazaki, Y., and Katou, K. (1995). Cause of blue petal colour. Nature **373,** 291-291.

Yoshida, K., Kawachi, M., Mori, M., Maeshima, M., Kondo, M., Nishimura, M., and Kondo, T. (2005). The Involvement of Tonoplast Proton Pumps and Na+(K+)/H+ Exchangers in the Change of Petal Color During Flower Opening of Morning Glory, Ipomoea tricolor cv. Heavenly Blue. Plant and Cell Physiology **46,** 407-415.

Yoshida, K., Miki, N., Momonoi, K., Kawachi, M., Katou, K., Okazaki, Y., Uozumi, N., Maeshima, M., and Kondo, T. (2009). Synchrony between flower opening and petal-color change from red to blue in morning glory, Ipomoea tricolor cv. Heavenly Blue. Proceedings of the Japan Academy. Series B, Physical and biological sciences **85,** 187-197.

Young, J.J., Mehta, S., Israelsson, M., Godoski, J., Grill, E., and Schroeder, J.I. (2006). CO2 signaling in guard cells: Calcium sensitivity response modulation, a Ca2+-independent phase, and CO2 insensitivity of the gca2 mutant. Proceedings of the National Academy of Sciences **103,** 7506-7511.

Zahran, H.H., Marín-Manzano, M.C., Sánchez-Raya, A.J., Bedmar, E.J., Venema, K., and Rodríguez-Rosales, M.P. (2007). Effect of salt stress on the expression of NHX-type ion transporters in Medicago intertexta and Melilotus indicus plants. Physiologia Plantarum **131,** 122-130.

Zhang, G.H., Su, Q., An, L.J., and Wu, S. (2008). Characterization and expression of a vacuolar Na(+)/H(+) antiporter gene from the monocot halophyte Aeluropus littoralis. Plant physiology and biochemistry : PPB / Societe francaise de physiologie vegetale **46,** 117-126.

Zhang, H.X., and Blumwald, E. (2001). Transgenic salt-tolerant tomato plants accumulate salt in foliage but not in fruit. Nature biotechnology **19,** 765-768.

Zhang, H.X., Hodson, J.N., Williams, J.P., and Blumwald, E. (2001). Engineering salt-tolerant Brassica plants: characterization of yield and seed oil quality in transgenic plants with increased vacuolar sodium accumulation. Proceedings of

the National Academy of Sciences of the United States of America **98,** 12832-12836.

Zhao, J., Connorton, J.M., Guo, Y., Li, X., Shigaki, T., Hirschi, K.D., and Pittman, J.K. (2009). Functional Studies of Split Arabidopsis Ca2+/H+ Exchangers. Journal of Biological Chemistry **284,** 34075-34083.

Zhao, J., Cheng, N.H., Motes, C.M., Blancaflor, E.B., Moore, M., Gonzales, N., Padmanaban, S., Sze, H., Ward, J.M., and Hirschi, K.D. (2008). AtCHX13 is a plasma membrane K+ transporter. Plant physiology **148,** 796-807.

Zhu, S.-Y., Yu, X.-C., Wang, X.-J., Zhao, R., Li, Y., Fan, R.-C., Shang, Y., Du, S.-Y., Wang, X.-F., Wu, F.-Q., Xu, Y.-H., Zhang, X.-Y., and Zhang, D.-P. (2007). Two Calcium-Dependent Protein Kinases, CPK4 and CPK11, Regulate Abscisic Acid Signal Transduction in Arabidopsis. The Plant Cell Online **19,** 3019-3036.

Zybailov, B., Rutschow, H., Friso, G., Rudella, A., Emanuelsson, O., Sun, Q., and van Wijk, K.J. (2008). Sorting Signals, N-Terminal Modifications and Abundance of the Chloroplast Proteome. PLoS ONE **3,** e1994.